UNIVERSITÄT DUISBURG ESSEN

Open-Minded

Ureteral Tissue Engineering: Development of a Bioreactor System and Subsequent Characterization of the Generated Biohybrids

Dissertation

Zur Erlangung des akademischen Grades eines Doktors der Naturwissenschaften

– Doctor rerum naturalium –

vorgelegt von

Volker Seifarth

geboren in Köln

Fakultät für Chemie der Universität Duisburg-Essen

2014

Die vorliegende Arbeit wurde im Zeitraum von Juli 2011 bis Juli 2014 im Arbeitskreis von Prof. Dr. rer. nat. Matthias Epple angefertigt.

Tag der Disputation: 25. Februar 2015

Gutachter: Herr Prof. Dr. Matthias Epple
Frau Prof. Dr. Dr. Aysegül (Temiz) Artmann

Vorsitzende: Frau Prof. Dr. Bettina Siebers

This dissertation is dedicated to

my beloved wife, Anna Seifarth,

for her love and encouragement.

Content

1 Abstract

Today, 1-2.5% of all genitourinary tract trauma affect the ureters, leading to severe impairments of the urine's drainage. Till now, classical reconstructive surgery has the possibility to bridge up to 15 cm of damaged tissue, depending on the location. Even the "gold standard", with intestine interposition, where longer distances can be overcome, can lead to postoperative side effects like stricture formation, calcification or excessive mucous production.

This thesis presents a new attempt for the replacement of damaged ureters by the use of tissue engineering technologies. A bioreactor system is developed for the generation of tubular biohybrids consisting of a natural and a composite biomaterial (pure collagen or fibrin and PVDF) in combination with different cell types (Urotsa, C2C12, fibroblasts and primary smooth muscle cells). A mechanotransduction is established for a mechanical stimulation and orientation of the applied cells.

The bioreactor system allows a reliable incubation of a modularly constructed bioreactor for the cultivation of mammalian cells for up to two weeks. Incubation parameters are kept in defined ranges with deviations of ≤1 °C (temperature), ≤0.2 (pH value) and ≤0.3% (CO_2 concentration). Cocultivations of Urotsa and C2C12 cells are possible in combination with a porous OPTIMAIX 3D, which has radially oriented pores with varying diameters. Mechanical stimulation that is based on a kyphoplasty catheter is applied on primary smooth muscle cells that are embedded in a PVDF-supported fibrin matrix. Biochemical and mechanical evaluations reveal that there is no significant difference between a mechanically stimulated and an unstimulated prosthesis with respect to the diffusion of urea/creatinine or the rupture pressure. Histological analysis shows two distinguishable cell layers with a longitudinal alignment on the outer surface and a circular orientation in the matrix of the stimulated fibrin-based prosthesis.

It can be concluded that biohybrids can be generated in this bioreactor system with at least two different cellular orientations. These biohybrids need to be characterised in further (animal) experiments.

2 Introduction

Life expectancy is constantly increasing in modern, industrial countries like Germany, France, Spain, Japan or the USA. The rise in the last 40 years is in the range of 5 to 10 years, depending on the country and sex.[1] It has to be concluded, that factors like social, political and economical changes, as well as biomedical developments lead to people living longer than only decades ago.[1] This, in turn, often results in multimorbid patients i.e. people developing more than one chronic disease. This trend requires individual, personalised medical care.[2] Furthermore, it can be observed that the demand for organ transplants cannot be satisfied adequately. In 2012, 6337 patients were registered on German waiting lists for organ transplantations, while 1024 persons were listed as donors. The total demand for organ transplants was 6711 whereas 2625 organs were transplanted.[3] Figure 1 shows an illustration of deceased organ donors in Germany from 1998 to 2013.

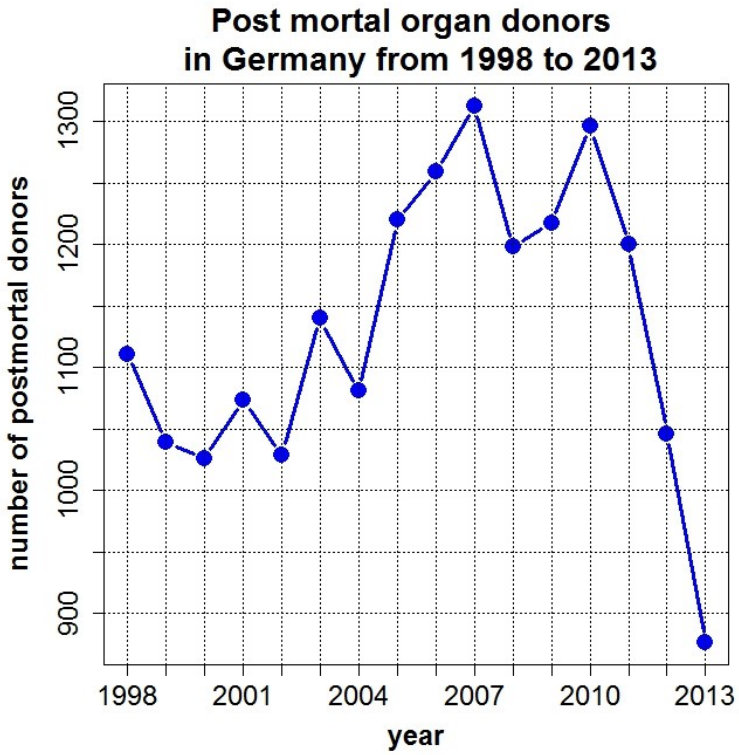

Figure 1: Progression of post mortal organ donators from 1998-2013 in Germany. Data investigated by the German Organ Transplantation Foundation and „statista“.[4–6]

This figure illustrates that there was a dramatic decrease in donors between 2011 and 2013. The lack of donor organs got worse due to scandals caused by manipulated waiting lists.

In regenerative medicine, the developing scientific field of tissue engineering (TE) may help counteract this lack. Tissue Engineering is a modern, multidisciplinary field of engineering sciences and medicine. Its purpose is to understand organ function in general and devise methods to grow functionalised organs that maintain or enhance.[7,8]

Biologists, physicians, engineers, material scientists and many more work on this interdisciplinary perspective. It is necessary to consider all demands on an organ's function and its generation to be successful in TE.[9–11]

The engineering part includes the development of devices and (bio) materials, for tissue cultivation and functionalisation. All materials, including bioreactor components and liquids, that are in contact with the tissue equivalent need to mimic nature. Tissue Engineering has to be biomimetic.[12]

The aim of this study was to develop a bioreactor system with the ability to functionalize biohybrids that may serve as tissue equivalents for the replacement of damaged tubular organs of the genitourinary tract, especially the ureters. To achieve this, a first bioreactor prototype had to be further developed, cell culture technologies had to be refined, a peristaltic stimulation procedure had to be established and a suitable biohybrids composition had to found.

3 Background

3.1 The genitourinary tract

The genitourinary tract is a central group of organs, keeping the biochemical balance, producing signal molecules, excreting metabolic wastes and controlling the body's water household.[13,14]

Figure 2 gives an overview of the revulsive organ network, disregarding sex specific genitalia. On the left side of the figure, each organ is symbolised by mechanical components in order to illustrate its function in a simplified manner and convey an engineer's point of view.

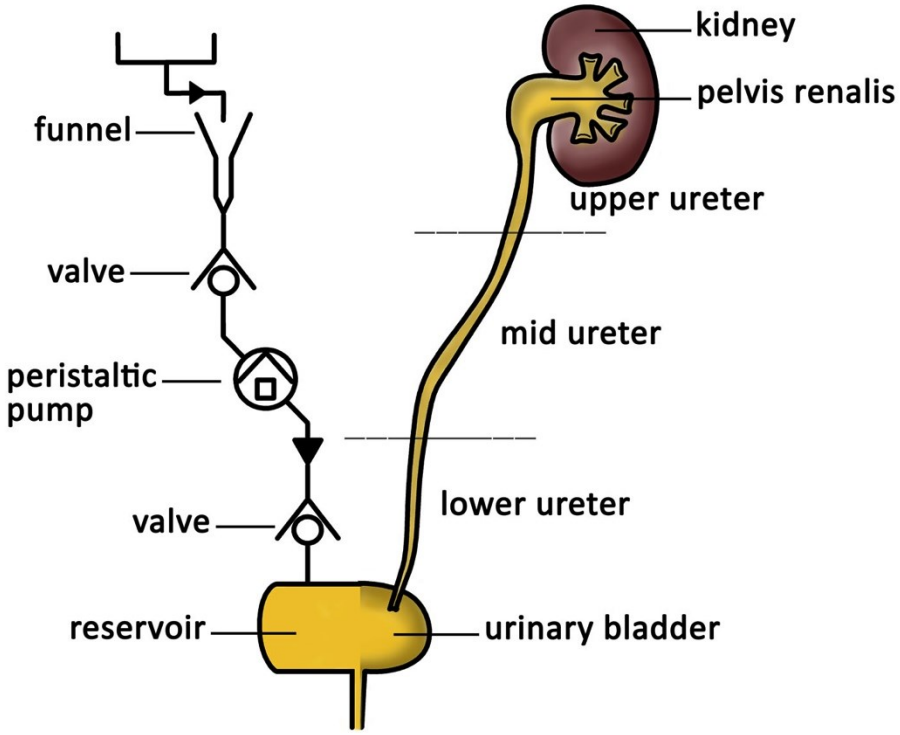

Figure 2: Schematic illustration of the genitourinary tract from the urine producing kidneys down to the urine storing bladder. Organs and their function are symbolised by equivalent mechanical components.[6]

As Figure 2 shows, the "simplified" urinary tract (left side of the schematic illustration) consists of a funnel, which is comparable to the renal pelvis. The attached tube that represents the ureter is equipped with a peristaltic pump and valves. The peristaltic pump is a self-occluding pump and simulates the physiologic peristaltic effect of the natural ureter. Attached redundant and

unidirectional valves represent a closed tubular structure, which prevents a backflow of fluid. A reservoir is connected at the end of the system to store the urine. Under normal conditions, the urine storage capacity is in the range of 350 ± 150 mL.[15]

3.1.1 Anatomy and physiology of the ureters

The ureters are bilateral tubes that connect the kidneys with the urinary bladder. Their length is in the range of 22 to 30 cm. Urine that is collected in the renal pelvis is transferred actively towards of the urinary tract.[13,14] The intravenous urogram in Figure 3 shows the abdominal region with bones and the urinary system that is made visible by means of a contrast agent.

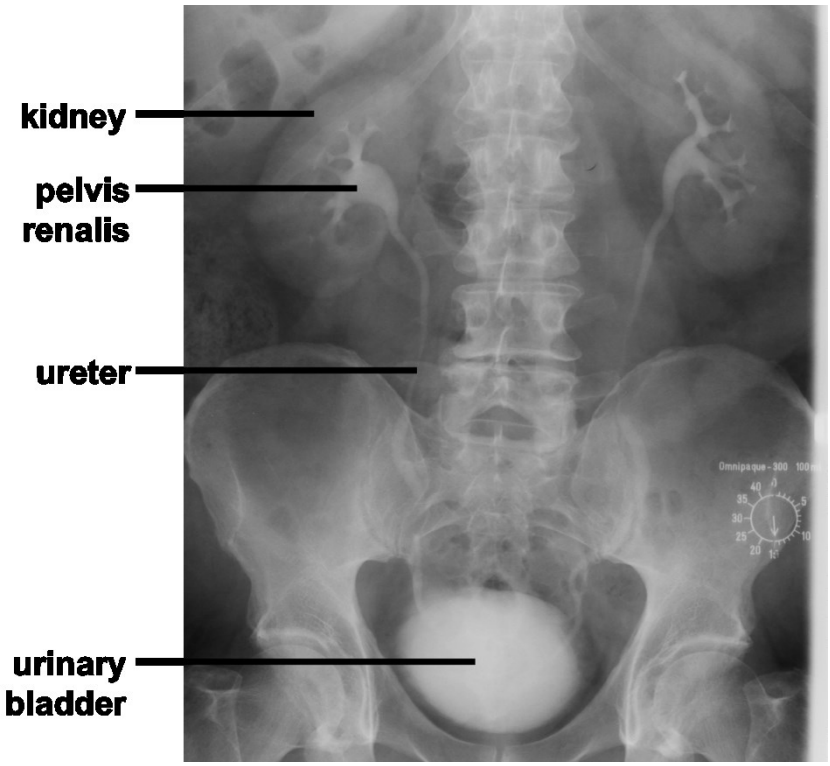

Figure 3: X-ray urography for the illustration of the urinary tract with the renal pelvis, ureter and urinary bladder.[16]

It can be seen that the right kidney is compressed and shifted caudally. The upper kidney and adrenal gland are protected by ribs 11 and 12.[14] As depicted in Figure 3, the renal pelvis is directed medially, so that pressures which are applied from the outer abdomen cannot lead to obstructions. This medial/parasagittal location in close proximity to large blood vessels shows the importance of these organs with respect to their function. Waste excretion is a vital necessity. A damage of this

system can lead to crucial consequences like the loss of a the kidney(s).[17] Thick muscles and bones shield this sensitive tubular structure. The pars abdominalis (cranial) is protected by the vertebral column and the musculus psoas, the pars pelvic (caudal) by the bony pelvic girdle.[13,14,18] The ureters are embedded in loose connective tissue, which makes them highly mobile. This mobility has to be ensured for the systematical transport of urine as well as for the protection against hyperextension.

Figure 4 shows a cross-section of porcine ureter. The structure is comparable to a human ureter.

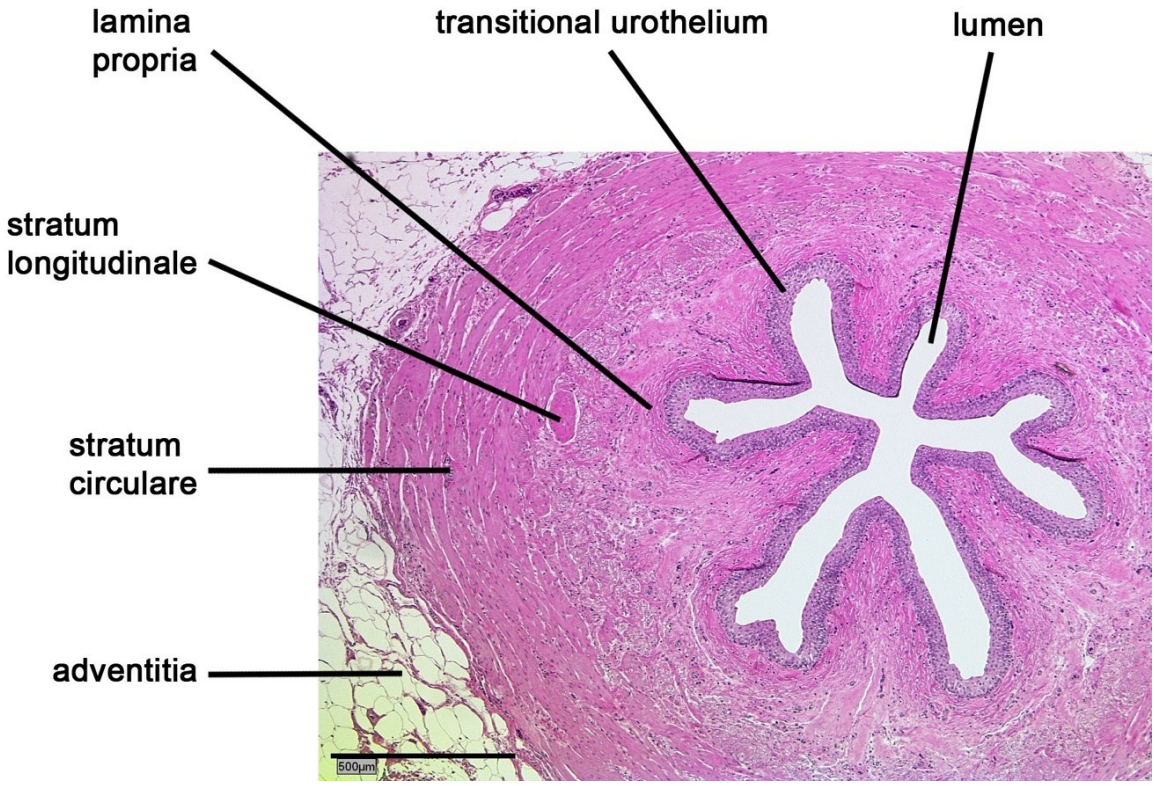

Figure 4: Histological haematoxylin & eosin (HE) overview staining of a porcine ureteral cross-section. Starting at the top, Figure 4 shows (in counterclockwise direction) the lumen, the transitional urothelium, the underlying lamina propria, followed by longitudinally smooth muscles, the circularly smooth muscles and finally the serosa adventitia. Scale bar: 500 µm.[6]

The human ureter is about 1-10 mm thick.[19] As in Figure 4, five to seven physiological mucosal (transitional urothelium) wrinkles can be seen at the closed ureteral lumen; they are arranged longitudinally throughout the ureter. This shape can be observed under normal, relaxed conditions. The luminal surface is covered by a transitional epithelium, which consists of 4 to 6 cell layers.[13,18] The thickness of this layer is reduced during peristalsis due to expansion of the luminal cross-section. Urothelial cells have an important protective function; they control immune responses, cell-cell signalling as well as the tissue permeability. Yet, the urothelium is one of the most impermeable tissues due to numerous tight junctions between the cells. This tight intercellular space allows to hold up strong concentration gradients between the urine and the plasma and to resist shifting pH values.[14,18,20–23] Urine osmolality varies over a broad range from 50 to 1200 mosmole L^{-1}. Fluid uptake, medications, renal performance, general health, blood pressure and osmolality as well as other factors influence the urine osmolality and volume.[14,19,24,25] In contrast to that, the physiological plasma osmolality range is 290 ± 10 mosmole L^{-1}.[13,26] The physiological pH value of urine varies between 4.5 and 8, the average lies between 5.5 and 6.5.[14,19] Friedlander et al. (2014) found out that increasing age leads to a pH shift towards acidic values.[27]

An elastic lamina (lamina propria) lies beneath the transitional urothelium. This lamina contains elastic proteins that ensure the distension of the luminal cross-section while a urine bolus passes the ureter.[13,14,19]

The lamina propria is covered by the tunica muscularis, which is necessary for the peristaltic effect that forwards the urine into the direction of the vesica urinaria (urinary bladder). The tunica muscularis can be divided into two smooth muscle layers: an inner (stratum longitudinale) and an outer circular layer (stratum circulare).[13,14,18] Additionally, the last third of the proximal ureter is equipped with a longitudinally arranged smooth layer on the outer surface.[18,19]

An adventitia, made up of loose connective tissue, integrates the ureters into the surrounding tissue, ensures the blood supply and provides the elastic support.[13,14,19]

The peristaltic effect of the ureter is required for an active transport of urine from the kidney towards the most caudal part of the system described, the urinary bladder. This is due to the fact that the force of gravity alone is not sufficient for draining. The resulting contraction of the smooth muscle is similar to the

contraction that is found in all other tubular hollow organs like the oesophagus, bowel, fallopian tube and many more. A schematic illustration in Figure 5 depicts the epithelium with its smooth muscle layers arranged longitudinally and circularly. The highlighted regions are contracting one after another to forward the urine.

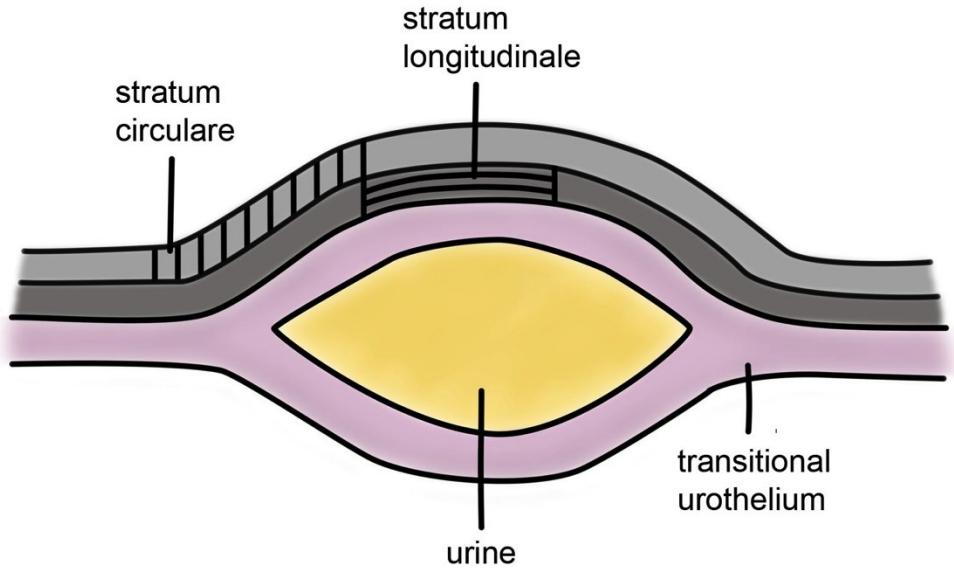

Figure 5: Schematic illustration of the peristaltic forwarding of a urine bolus induced by a contraction of the longitudinal smooth muscle layer, followed by a contraction of the circularly arranged smooth muscle layer.[6]

Peristaltic forwarding of a droplet starts with the opening of the luminal cross-section. This opening is a consequence of contracting longitudinally directed smooth muscle cells (SMC). Subsequently, the circular SMCs contract, preventing a reflux of urine, and press the urine bolus towards the urinary bladder. As a result of mechanical stress on the SMCs, the same procedure repeat itself.

The contraction waves are assumed to start in the calix renalis region, in the deep renal pelvis.[28–30] The stimulus is transmitted myogenically in the smooth muscle cell membranes.[28,31] The contraction frequencies vary depending on the location in the urinary tract. Table 1 gives an overview about the sites and related frequencies.

Table 1: Contraction frequencies decrease with the distance to the renal pelvis.[28]

Location	Frequency [Hz]
Calix renalis	0.190
Pelvis renalis	0.150
Pyleureteral junction	0.133
Ureter	0.067

Under normal conditions, there is a laminar flow of urine inside the ureterand the urine bolus passes the ureter together with the contraction stimulus in the transmission phase. In the relaxed phase, the ureter is occluded to prevent a reflux of urine towards the kidneys.[31,32] At a certain, critical frequency and flow rate, the urine nevertheless begins to flow back.[32]

Table 2 shows the pressures inside the upper urinary tract and the urinary bladder. It can be seen that Shafik et al. (1998)[33] measured different pressures at different positions in the urinary system. The pressures range from 3 to 33 cm H_2O and is highest in the ureters during peristalsis.[33]

Table 2: Pressures in the upper urinary tract and the urinary bladder.[33]

	Pressure [Pa]	
	Mean	Range
Renal pelvis	450 ± 140	300-700
Ureteropelvic junction	1460 ± 380	1100-1800
(Ureter-) Basal	460 ± 110	300-600
(Ureter-) During peristalsis	2660 ± 630	1800-3200
Ureterovesical junction	1060 ± 1240	900-1400
Bladder	510 ± 150	300-700

3.1.2 Ureteral injuries

The ureter is protected from other abdominal tissues, so that there is just a relatively small amount of ureteric injuries (1-2.5%) compared to all urogenital trauma.[34]

Figure 6 shows a classification of ureteric injuries by cause, location and classification of the American Association for Surgery of Trauma (AAST).

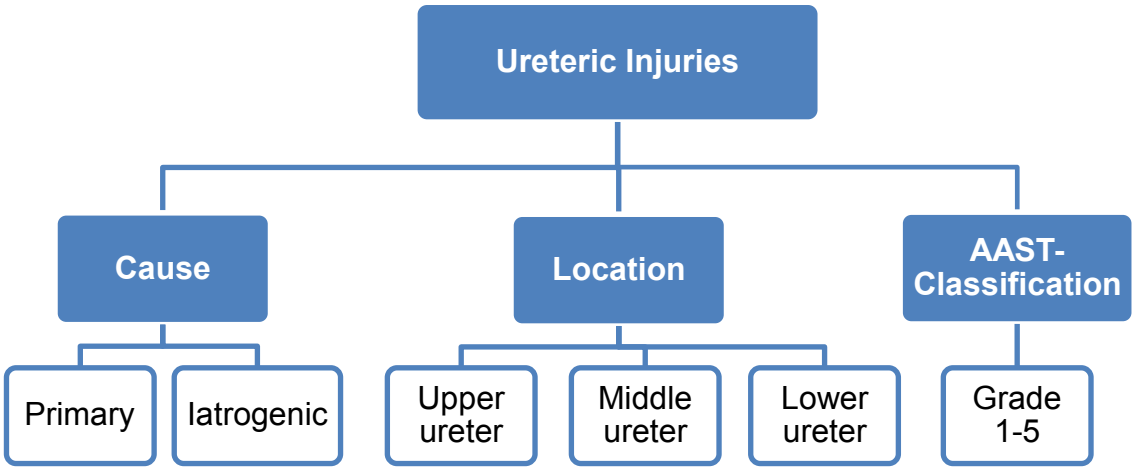

Figure 6: Classification of ureteric injuries according to their cause, location and AAST grading.[6]

Traumas can be assigned to primary (direct) or iatrogenic (caused by medical interventions) injuries. Direct injuries include accidents, gunshots, malformations or diseases that affect the ureters. Iatrogenic injuries often occur during medical interventions like ureteroscopic, gynaecological, colorectal and vascular medical procedures.[35–37]

A summary of two American studies about primary injuries inflicted by gunshots, stab wounds and blunt trauma included 761 cases. This summary shows that the upper ureter is affected more often (38.9%) than the mid (31.9%) and lower ureter (29.2%).[35,38]

Taking a look at the causes of ureteral trauma, a European study revealed that as many as 75% of all cases of ureteric traumas are related to iatrogenic injuries. Furthermore, this retrospective study with 450 patients revealed that 74% of the ureteric trauma were located in the lower, 13% in the middle and 13% in the upper ureter.[39]

The same trend for primary and iatrogenic injuries was observed by D.J. Summerton et al.[34] From these studies it can be concluded that primary injuries are mainly related to traumas at the upper ureter and iatrogenic injuries to traumas at the lower ureter.

It can be stated, however, that reliable data on iatrogenic injuries are difficult to obtain due to restrained or moderate publication of these incidents. The occurrences of iatrogenic injuries vary from 0.5 to 30%, but it may be assumed that this value is even higher.[40]

In 1992, Moore et al. developed a classification to categorize the severity of ureteral injuries.[41] This 22-year-old classification is still used by the AAST and European Association of Urology (EAU) and provides the basis for the related groups of illnesses in the International Statistical Classification of Diseases and Related Health Problems (ICD). Table 3 shows the correlations between the AAST grading system, the ICD classifications of 1976 (ICD-9) and the recent 2014 classification (ICD-10-CM).

Table 3: Modified AAST grade of ureteral injuries according to EAU guidelines based on Moore et al. and the corresponding ICD codes.[34,41]

AAST grade	Type of injury	Ureteral injury	ICD-9 (1976)	ICD-10-CM (2014)
I	Hematoma	Contusion or hematoma without devascularisation	867.2/ 867.3	S37.10XAS31.001A
II	Laceration	<50% transection	867.2/ 867.3	S37.10XAS31.001A
III	Laceration	>50% transection	867.2/ 867.3	S37.10XAS31.001A
IV	Laceration	Complete transection with >2 cm devascularisation	867.2/ 867.3	S37.10XAS31.001A
V	Laceration	Avulsion with >2 cm devascularisation	867.2/ 867.3	S37.10XAS31.001A

Treatment planning for ureteral trauma is based on the cause, severity and location of the injury. There are at least 300 different surgical procedures available.[42] Basically, ureteral injuries from grades I to II (III) are supposed to be

drained by stenting, which may also prevent a collapse or a stricture, or with a nephrostomy tube.[34,35,41,43,44]

3.1.3 Aetiology and pathogenesis of ureteric injuries

Iatrogenic injuries often involve with symptoms like flank pain, incontinence, haematuria, fever, uraemia, hydronephrosis, fistula formation, urinoma, etc. Missing medical treatments may lead to further and more serious complications like infections, inflammation, fibrotic reactions and a total renal dysfunction.[17,34,38,45–47] Besides that, the replacement of ureters and the healing process become particularly complicated if the patient suffers from diseases like calculous disease, tuberculosis, endometriosis, diabetes, maldevelopment, bilharzial stricture and similar conditions.[17,34,48,49] In these cases, subsequent strictures may occur, which result in a dam of urine and the complications already mentioned.

Occurrence of iatrogenic injuries can be reduced by using correct and state-of-the-art instrumentation[50–52] as well as anatomical and surgical experience.[34,40,53]

3.2 Tissue engineering in urology

Tissue engineering in urology covers a wide range of biological tissue and organ substitutes from tissue-engineered bladders to urethras and ureters.

Nevertheless, there is just one company, UroTiss GmbH Germany, which has an approved and licensed tissue-engineered product on the market. The MukoCell compound is a complete autologous tissue equivalent which is used for urethral reconstructions.[54,55]

Reconstruction of ureters and urinary bladders are still being investigated and subject of clinical trials. Even though there are some promising results for the replacement of whole bladders, it is not yet a routine clinical application.[56,57]

3.2.1 Tissue engineering principles

Growing functional organs for transplantation is not yet trivial. Figure 7 shows many different factors belonging to at least one of three different categories has an important influence on a tissue engineering project. For the sake of clarity, these are reduced to three major factors for each category.

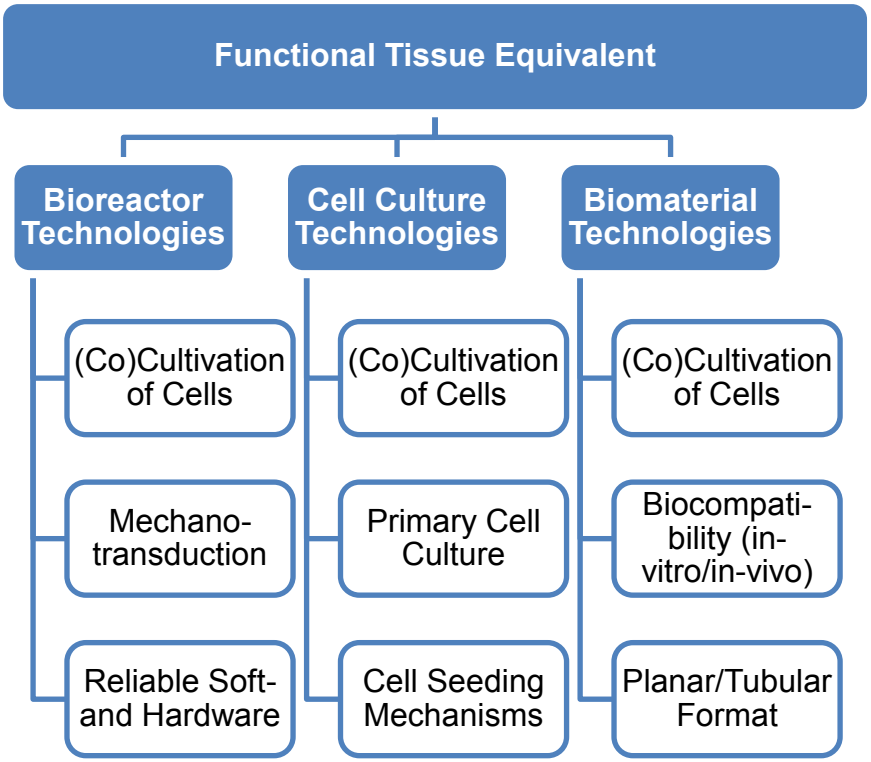

Figure 7: Functionalisation of a tissue requires three technologies that are dependent on each other.[6]

In Figure 7, all demands on a bioreactor system for growing functional tissues are reduced to the co-cultivation of cells, mechanotransduction and the need for reliable hard and software. Mechanical stimulation of the biohybrids used, is essential to the intended functionalization. Cell culture technologies include co-cultivation, primary cell culture and cell seeding mechanisms. In this context, the isolation of primary cells from the patient's tissue plays an important role for the personalised medical treatment with the generation of autologous tissues. Different seeding procedures need to be tested with the isolated cells in combination with the biomaterials to be used. Biomaterials are required to allow the co-cultivation of cells and they need to be biocompatible. At least tubular and planar material structures need to be available for initial in vitro tests.

All three technologies are dependent on each other. A lack in one component cannot be compensated by one of the others.

3.2.2 Bioreactors

Bioreactors can be defined as closed environmental vessels that provide a suitable culture environment to grow tissue. They enable highly precise control and measurement of parameters like pH, temperature, nutrient supply and waste removal, sterility and safety as well as pressure and gas supply. Continuous monitoring and sampling lead to high reproducibility, which is needed for biological, biochemical and chemical applications.[58–60]

Individualised bioreactors are used for various tissue engineering purposes like generated bone and cartilage[61–64], skin[65], trachea[66], intestine[67], heart valves[68] and more.

All these bioreactors serve the same purpose: they are used to generate three-dimensional (3D) tissue equivalents by providing optimal supply of nutrients, gases and mechanical stress. They are the key features in modern tissue engineering, which needs to be biomimetic by copying a physiological environment.[12,69,70]

Literature shows that mechanical conditioning with compression, elongation and pulsatile flow is important for growing tissue equivalents and their subsequent implantation. It enhances, cellular distribution, proliferation, differentiation and the mechanical properties of the tissue.[71–74] However, cellular effects like proliferation are cell-type specific and vary in depending on proliferative or contractile phenotypes.[61,73,75–77]

Literature on cell culture technologies indicates that mechanical conditioning leads to an orientation of cells. This effect is regarded to be stress level and cell type dependent.[78]

An overview of this literature with respect to applied stress magnitudes, frequencies and the consequences is given in Table 4. It can be observed that the obtained results are not consistent and difficult to compare, as not only the different cell types and passages used, but analytical and experimental setups (two or three-dimensional) as well. Nevertheless, it becomes clear that cells align themselves in the direction of low stress levels on two-dimensional substrates. This may be a reaction to reduce the applied stress.[78]

Table 4: Overview of literature dealing with cell culture technologies and mechanical stresses and the resulting orientation and proliferation of cells. NPS=not part of study, SIS=small intestine submucosa, BSM=bladder submucosa.

Strain [%]	Alignment in the direction of strain	Frequency [Hz]	2D/3D	Proliferation	Cell type/passage	Source
0 2 5	0° 90° 90°	0.0725	2D	significantly reduced proliferation (beginning from 5%)	porcine, oesophageal SMC; 4-10th passage	[78]
10	~70°	1	2D	NPS	human aortic vascular SMC; 4-8th passage	[79]
0-6.7	random (0%) to parallel (6.7%)	1	*3D bulb*	NPS	sheep aortic SMC; 4-8th passage neonatal rat cardiomyocytes	[80]
0 10	random 0°	1	*3D tube*	NPS	aortic rat SMC; 5-8th passage	[74]
0-7 7-24	random 90°	1	2D	significantly increased cell proliferation	bovine aortic SMC; < 5th passages	[81]
0-20	NPS	0.000152	2D	significantly reduced cell proliferation	human bladder SMC; 1-9th passage	[82]

Strain [%]	Alignment in the direction of strain	Frequency [Hz]	2D/3D	Proliferation	Cell type/passage	Source
0 6 20	NPS	0.1	2D	from 20% significantly increased proliferation	human bladder SMC 2-5th passage	[75]
NPS	NPS	0 0.167 0.667	*3D SIS*	significantly increased proliferation	human, urine derived stem cells; subsequent differentiation to UC/SMC	[83]
NPS	NPS	0 0.167 0.667	*3D BSM*	significantly increased proliferation	human UC/SMC	[84]

3.2.3 Cell culture technologies

The term cell culture technology includes all methods used for the in vitro cultivation of cells. This includes gaining of cells as well as evaluating cellular effects and responses as a result of an experiment. The experiments are performed outside the body, i.e. in vitro or ex vivo. It is important to differentiate between extracted organs that are used ex vivo and tissues or cells that are cultured in vitro. In vitro conditions are generally different to the situation in vivo, although organ baths for pharmacological applications are seen as in vivo situation. Nevertheless, the whole body system with its signalling molecules like hormones or cytokines is missing in these experiments. Due to its complexity, the in vivo system cannot be reproduced under laboratory conditions.

3.2.4 Biomaterials

In addition to the bioreactor technologies, there are biomaterials that are important for successful tissue engineering (TE). Biomaterials serve as a 3D scaffold for the generation of tissue equivalents. Therefore, these materials need to be biocompatible in vitro and in vivo. It is essential to the success of a TE project that the mimicking of a natural matrix is as accurate and precise as possible to enhance tissue growth and regeneration, avoiding side effects like fibrosis, inflammation and others. Figure 8 shows that biomaterials are divided into naturally derived (decellularised) and synthetically manufactured materials. Both groups are characterised by specific advantages as to their biocompatibility, reproducibility and controllability of (mechanical) features.[73,85]

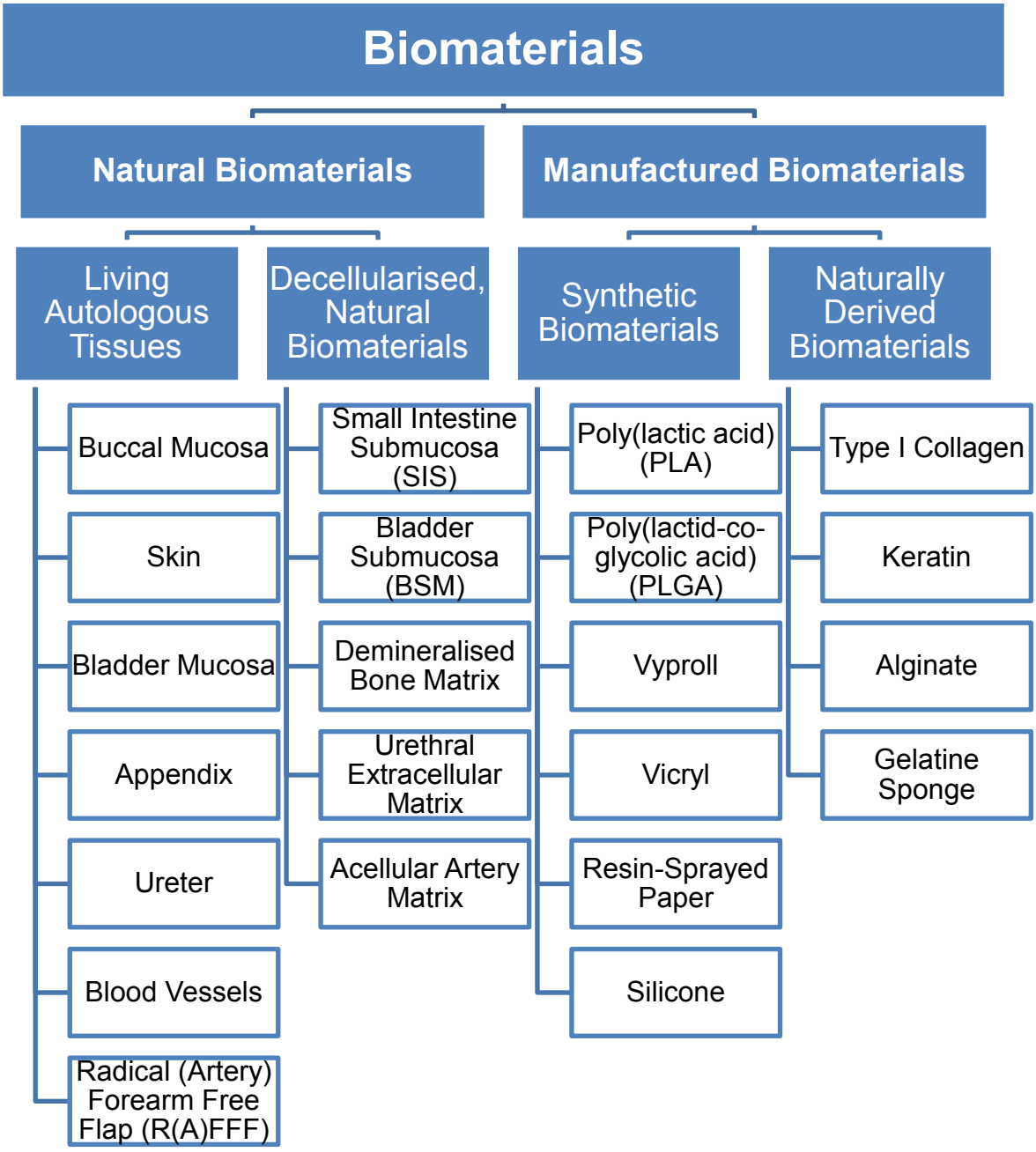

Figure 8: An assortment of biomaterials used in urological regenerative medicine according to [71,83,85–87]. The groups are divided into living autologous tissues (1), decellularised (2), natural biomaterials (3) synthetic and naturally derived biomaterials (4).[6]

At first sight, autologous tissues (Figure 8) seem to be the most suitable materials for the replacement of damaged organs. Nevertheless, there is still a high risk for negative implications. Bridging tissues for urological applications are often prone to necrosis, mucous production, inflammation and obstruction with frequent stricture formation and scarring at the sites of anastomosis.[88,89]

Decellularised matrices are natural 3D scaffolds, obtained by lysing and washing out of cells. This group is favoured for its high biocompatibility that is enhanced by biomimetic factors that are able to promote the tissue formation after recellularisation.[85,90,91] Exactly these residual heterogenic factors, however can also lead to negative side effects like immunological reactions, fibrosis or calcification.[83,92] Generally, physiochemical and mechanical characteristics depend on numerous variables like the location of extraction, donor age, manufacturing and sterilisation procedures and more. Thus, batch-to-batch variations impair the reproducibility.[83,90] Even so, a recellularisation can be enhanced by means of mechanical stimulation.[84]

Manufactured biomaterials are split up into synthetic and naturally derived biomaterials. Synthetic biomaterials are superior in their reproducibility ensuring a constant level of quality as well as their highly controllable characteristics like overall dimensions, pore sizes or degradation rates.[71] The application of pure synthetic materials like Vicryl® or Teflon® is often leads to mechanical failure or stone formation, abnormal fibroblast deposition and scarring.[86]

As a conclusion, it can be said that best functioning mechanical and biological bio-implants are still offered by combinations of synthetic and naturally derived biomaterials. This combination can increase mechanical and biological characteristics at the same time. The hollow structures in the body require the synthetic materials to keep their openings. Otherwise they will collapse. To increase the biocompatibility it is necessary to combine them with biological materials. These so called composites (temporarily) strengthen fragile and collapsible constructs with increased biocompatibility.[74,85–87] This method is biomimetic as it copies the basic structural setup of hollow organs. Different (bio-) mechanical properties are provided for tissue specific cell types.[85]

4 Materials and Methods

In this study, tissue engineering principles were used to prove and enhance a new bioreactor system for growing functionalised tubular organ structures for application in the genitourinary tract. To achieve this, biomedical skills i.e. cell culture technologies, mechanical engineering and material sciences were used. The following chapter shows materials and chemicals as well as classical methods and protocols used in this study.

4.1 Materials used in this study

Description	Company	Modell/Order Code	Parameter
Air Pump	Hagen	Elite 800	
Applicator	Medmix Systems AG	Double-Cartridge Delivery System (S)	Cartridge Volume 16 mL
Autoclave	Systec	2540EL	121 °C, 20 min
Battery	APC	Beck-UPS Pro 900	
Bottle	Schott Duran	1112627	GLS 80, 500 mL
Bottle	Schott Duran	21801245	GL 45; 100 mL
Cell Counter	BioRad	TC20™	
Cell Culture Flasks	Nunc	156499	75 cm²
Cell Culture Flasks	Nunc	159910	175 cm²
Cell Culture Flasks	Nunc	132913	500 cm²
Centrifuge	Heraeus	Biofuge 15R	290 g
Centrifuge Tubes	VWR	525-0156	50 mL
Centrifuge Tubes	VWR	525-0150	15 mL
Clean Bench	Heraeus	Hera Safe	

Description	Company	Modell/Order Code	Parameter
Counting Slides	BioRad	145-0011	
Critical point dryer	BAL-TEC/Leica Microsystems	CPD030	
Cuvettes	Hellma	115B-QS	200-2500 nm; 400 µL
Dialysis Membrane	CarlRoth GmbH + Co. KG	2711.1	Cut-Off 6000-8000 MW
Disposable Needle	CarlRoth GmbH + Co. KG	C630-1	0.8•120 mm, 21G•4 ¾"
Drape Sheet	Lohmann & Rauscher	33033	75•90 cm
Extension Pump head	Watson-Marlow	314X; 033.4431.000	
F-Fittings	BESTA-Technik GmbH	F-120	PEEK
Gauze Swabs	Fink & Walter	321063	10•10 cm
HPLC Starter Kit	Jasco		Fittings PEEK, tubing PEEK d_i = 0.5 mm
Incubator	HiTec Zang	Ramos	37 °C; 5% CO_2
Incubator	Heraeus	Hera Cell	37 °C; 5% CO_2
Instruments tray with lid	Bochem	8716	300•200•50 mm
Kyphoplasty Balloon Catheter	Allevo Joline	S9401	Balloon Ø16 mm; Balloon length = 10 mm
LabBox®2	HiTec Zang	LabBox®2	Serial: 020906599
LabDos	HiTec Zang	Vario4 P100	V4.1.2 V3.5.4

Description	Company	Modell/Order Code	Parameter
Light microscope	Leica	DM 6000B	Digital camera: JVC KY-S75U
Limit switch	Cherry	BB1C-A1LC	6 A, 250 V
Locating Pins	MISUMI	SPSS-D3.0-L10.0	Stainless steel
LUER to M6	Vieweg GmbH	990063-M6	Stainless steel
Male LUER to 10-32 Female	BESTA-Technik GmbH	P-656	PEEK
Microcentrifuge Tubes	Simport	T330-7N	1.5 mL
Microtome Blades	FEATHER	A35	
Mounting Stud	BESTA-Technik GmbH	P-645	PCTFE
Multiwell	Nunc	142475	24 wells
Neubauer Counting Chamber	Marienfeld	Cat.No.0640010	
O-Ring	Research Centre Jülich	311.01.043 311.01.011	2•24 mm; 1.5•8 mm
Osmomat	Gonotec	030	
Oven	Heraeus	T5060	125 °C
Pasteur pipettes	Hirschmann Laborgeräte GmbH	9250101	7•150 mm
Petri Dish	Nunc	172958	100•20 mm
pH - Electrode	Schott Instruments	SL 82-120 pHT	
pH - Meter	Mettler Toledo	Seven Multi	
Phase Contrast Microscope	Zeiss	Axiovert 25	

Description	Company	Modell/Order Code	Parameter
Pipette Filler	Hirschmann Laborgeräte	Pipetus	
Pipette Tips	Eppendorf	0030000.870 0030077.148 0030000.919 0030000.978	0.5 µL – 10 µL 10 µL – 100 µL 100 µL – 1000 µL 500 µL – 5000 µL
Pipettes	Eppendorf	Research variable	0.5 µL – 10 µL 10 µL – 100 µL 100 µL – 1000 µL 500 µL – 5000 µL
Precision Syringe Doser	HiTec Zang	SyrDos	Resolution: 48.000 steps
Pressure Sensor	Keyence	AP-13S#120327 AP-V80WP#1145669	1 MPa 4-20 mA
Scale	Sartorius Extend	ED 124S	
Screw Cap GLS 80	BOLA	XF072-110622	3•NTP ¼", 1•PG 13.5, 1•M14•1.5
Septum	VWR	548-0480	12.9 mm GL14, silicone-PTFE
Septum	VWR	11020115	11 mm; PTFE-silicone-PTFE
Serological Pipettes	CarlRoth GmbH + Co. KG	N236.1 N239.1 N242.1 N245.2	2 mL 5 mL 10 mL 25 mL
Shut-Off Valve	BESTA-Technik GmbH	P-732	PEEK

Description	Company	Modell/Order Code	Parameter
Single-Hand Quick-Connect	neoLab Migge Laborbedarf - Vertriebs GmbH	2-6306 2-6308 2-6315	Stainless steel; M5
Spectrophotometer	Jasco	V-550	
Sterile Gloves	Sempermed Supreme	822751721	
Sterile Syringe Filter	VWR	514-0073	PES, 0.2 µm
Suction Pump	IBS Integra Bioscience	Vacusafe comfort	
Syringe	CarlRoth GmbH + Co. KG	T549.1 0058.1 0057.1	50 mL 10 mL 5 mL
Tube	BOLA	S1810-38	d_i = 4 mm, d_a = 5 mm PTFE
Tube	Marprene	902.0032.016	d_i = 3.2 mm, d_a = 6.4 mm Marprene
Tube	VWR	228-1082	d_i = 3.2 mm, d_a = 6.4 mm Silicone
Ussing Chamber	Dipl.-Ing. K.Mussler		
Water bath	Huber	CC2	37 °C
Water bath	PolyScience	20-LM	37 °C
Wing Bolt	MISUMI	CHBS4-20	M4•20 mm, stainless steel

Description	Company	Modell/Order Code	Parameter
Wing Nut	MISUMI	CHNS4	M4, stainless steel
Y-Connector	BESTA-Technik GmbH	P-512	PEEK

4.2 Chemicals used in this study

Description	Company	Order Number	Trading Unit
Acetic Acid	CarlRoth GmbH + Co. KG	733.2	2.5 L
Acetone	CarlRoth GmbH + Co. KG	9372.1	1 L
Acheson Silver Dag 1415	Plano GmbH	G3692	25 g
Ammonium chloride	Sigma	A4514	500 g
Amphotericin	PAA	P11-001	100 mL
Calcium chloride	Merck	208290.1000	1 kg
Chloroform	CarlRoth GmbH + Co. KG	3313.1	1 L
Creatinine	Sigma	C4255	100 g
Cyklokarpron®/Tranexamic acid	Pfizer	6376165.00.00	1000 mg 10 mL^{-1}
Disodium hydrogen phosphate	Merck	6579.1000	1 kg
DMEM – with GlutaMAX™	Invitrogen	61965-026	500 mL
Ethanol 70%	CarlRoth GmbH + Co. KG	T868.1	1 L

Description	Company	Order Number	Trading Unit
Ethanol 99.8%	CarlRoth GmbH + Co. KG	9065.3	1 L
Fetal bovine serum	Gibco	25300-062	500 mL
Fibrinogen, human plasma	Calbiochem/ Merck Millipore	341576-1GM	1 g
Gentamicin	Sigma	G1272	100 mL
Glucose	Merck	8337.1030	1 kg
L-Ascorbic acid 2-phosphate sesquimagnesium salt hydrate	Sigma	A8960	5 g
Magnesium chloride	Sigma	M8266	100 g
Microscope	BioZero	BZ 8100E	
Penicillin/Streptomycin	Sigma	P4333	100 mL
Phosphate buffered saline	Invitrogen	14190-094	500 mL
Poly-Alcohol	Antiseptica	PZN 05905148	200 mL
Potassium chloride	Merck	4936.1000	1 kg
Potassium dihydrogen phosphate	CarlRoth GmbH + Co. KG	P018.1	500 g
Sodium bicarbonate	Sigma	56297	250 g
Sodium chloride	CarlRoth GmbH + Co. KG	3957.1	1 kg
Sodium citrate dihydrate	Merck	1.1200500.1000	1 kg
Sodium dihydrogen phosphate	Merk	6346.1000	1 kg
Sodium hydroxide	Roth	9356.1	1 kg

Description	Company	Order Number	Trading Unit
Sodium sulphate	CarlRoth GmbH + Co. KG	P032.1	500 g
Storage solution for pH electrodes	CarlRoth GmbH + Co. KG	9608.1	500 mL
Talcum powder	Drugstore		
Tris base	Sigma	252859	500 g
Tris HCl	CarlRoth GmbH + Co. KG	9090.2	500 g
Trypan blue	Sigma	T8154	100 mL
Trypsin/EDTA	Gibco	25300-054	100 mL
Uera	CarlRoth GmbH + Co. KG	7638.20	5 kg
Optimaix 3D Sponge1	Matricel GmbH		d_i = 6 mm; d_a = 14 mm
Polyvinylidenfluorid	ITA Aachen	Trickot E30 EAC 10	

4.3 Buffers and cell culture media used in this study

Buffers are also called balanced salt solutions (BSS). Different BSS were applied to cells to provide constant pH values as well as an isosmotic surrounding. For the preservation of the structural and functional integrity of proteins, the pH value is an important parameter.[93] Besides that, applying physiological salts with physiological concentrations ensures the control of the cells' water household.[94] Generally, a physiological plasma osmolality of 290 ± 10 mosmole kg^{-1} and a pH of 7.4 was desired and adjusted for the utilised buffers.[94,95] The only exception was synthetic urine, which had an higher osmolality (760 mosmole kg^{-1}) that was in the range of physiological urine as well as a lover pH value (5.6–5.8).

All components were weighed with an analytical scale (Sartorius) and were subsequently dissolved in distilled water.

4.3.1 Tris-buffered-saline (TBS)

Tris-buffered saline was used in this study for dialysing dissolved fibrinogen as well as for the fibrin preparation. The composition used is listed in Table 5.

Table 5: Composition of Tris-Buffered-Saline.

Tris-Buffered-Saline	
Substance	**Concentration [mmol L^{-1}]**
Potassium chloride	2.68
Sodium chloride	0,14
Tris Base	5.28
Tris HCl	27.66

4.3.2 Phosphate-buffered-saline (PBS)

The composition of phosphate-buffered-saline (PBS) can be traced back to 1954 and the scientists R. Dulbecco and M. Vogt. They developed the basic formulation of PBS, which is the most common balanced salt solution for general cell culture applications.[96] However, in this study calcium and magnesium free PBS was used with the following ingredients:

Table 6: Composition of Phosphate-Buffered-Saline.

Phosphate-Buffered-Saline	
Substance	**Concentration [mmol L^{-1}]**
Disodium hydrogen phosphate	8.06
Potassium chloride	2.67
Potassium dihydrogen phosphate	1.47
Sodium chloride	137.93

4.3.3 Artificial urine

Artificial urine was used for passive diffusion experiments in combination with an Ussing chamber to characterise the performance of the engineered prosthesis in

comparison to the natural material.[97] As mentioned in Chapter 3.1.1 the physiological urine osmolality can vary between 50 and 1200 mosmole L^{-1}. The applied buffer had an osmolality of 760 mosmole L^{-1} and a pH value of 5.8. The basic formulation can be traced back to Griffith et al. 1976[98]. In this study, the applied composition was adapted from Montzka et al. (2010)[97] and did not contain sodium oxalate.

Table 7: Composition of synthetic urine with its components and concentrations according to [98] and modification after [97].

Artificial Urine	
Substance	**Concentration [mmol L^{-1}]**
Ammonium chloride	18.69
Calcium chloride	5.86
Creatinine	9.72
Magnesium chloride	6.84
Potassium chloride	21.46
Potassium dihydrogen phosphate	20.57
Sodium chloride	78.7
Sodium sulphate	16.19
Tri-sodium citrate dihydrate	2.2
Urea	416.25

4.3.4 Krebs buffer

Krebs buffer was used for diffusion experiments in an Ussing chamber (see Chapter 4.4.1.4), too.[97] This buffer was adjusted to pH 7.4 and an osmolality of 290 ± 10 mosmole L^{-1}.

Table 8: Composition of the applied Krebs buffer solution.

Krebs buffer	
Substance	**Concentration [mmol L^{-1}]**
Calcium chloride	2.5
Glucose	11.5
Magnesium chloride	1.2
Potassium chloride	4.7
Sodium bicarbonate	25.0
Sodium chloride	117.0
Sodium dihydrogen phosphate	1.2

4.4 Cell culture technology

Cell culture technologies include all methods, principles and tools that are applied on tissues or cells under artificial environmental conditions (see Chapter 3.2.3). In the following chapter, the most important and used methods and protocols are presented.

4.4.1 Measurement of biochemical parameters

4.4.1.1 pH value

The pH value can be measured in various ways. Basically, there are two different methods: non-electrochemical and electrochemical.[99] Non-electrochemical methods, e.g. colorimetric methods, show great disadvantages, because of the subjective evaluation. For that reason, electrochemical methods and especially the use of pH glass electrodes are most common in scientific laboratories. Standard glass electrodes show the following setup within a measurement chain:

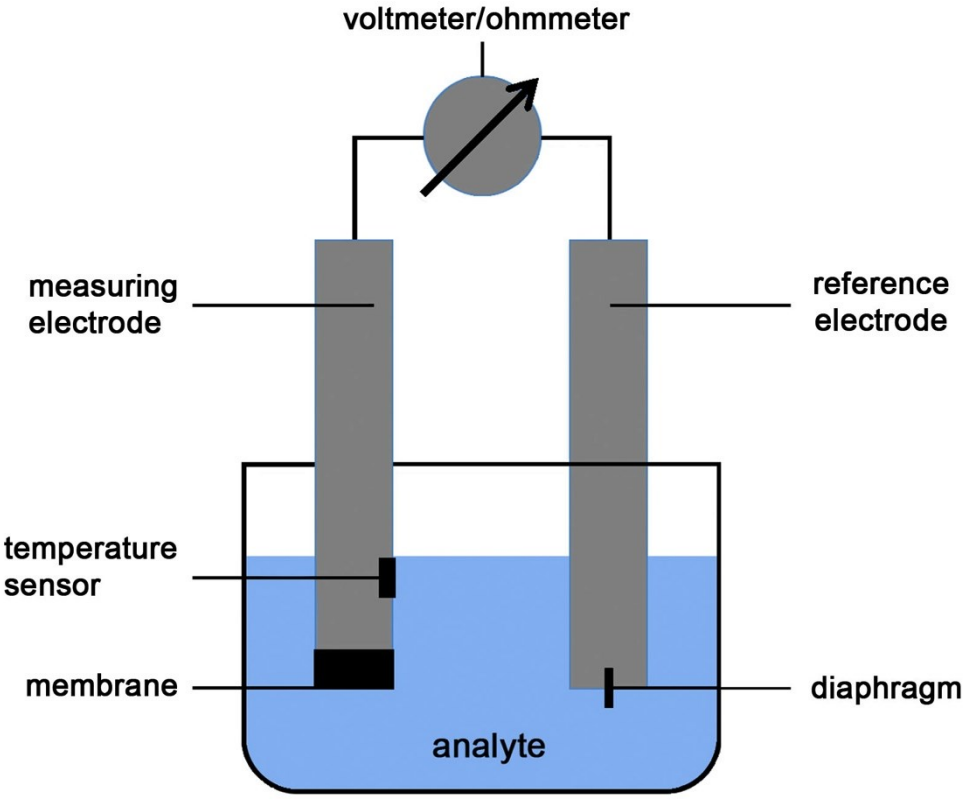

Figure 9: Schematic illustration of a measurement chain to evaluate the pH value in a liquid analyte. The chain consists of a measurement electrode that is equipped with a thin glass membrane and a temperature sensor. Like the measurement electrode, a reference electrode with its diaphragm is connected to a voltmeter or pH-meter, too.[6]

The objective is to measure a potential drop at the glass membrane of the measurement electrode to determine the pH value in the analyte. This potential can be read out with a voltmeter or pH meter. A pH meter is able to convert the potential into a pH value. The analyte's temperature needs to be followed because it influences the measurement. Reference electrodes have a constant potential and close the electrical circuit. Typically, this measurement chain is realised in a single-rod measuring cell.

Basically, potential drops and measured voltages correlate to a specific pH value and is described for optimal glass electrodes by the Nernst equation[99,100]:

$$U = U_0 - \frac{R \cdot T}{F} \cdot \log[H_3O^+] \qquad (1)$$

U = measured potential

U_o = standard electrode potential

R = gas constant

T = absolute temperature

F = Faraday constant

4.4.1.2 Temperature

Temperature measurements are important for in vitro cultivation processes because cell metabolism has a temperature optimum. For this study, a physiological temperature of 37 °C was kept constant during incubation processes. Measurements inside the bioreactor system were performed with Pt100 thermal sensors that had a typical electrical resistance of 100 Ω at 0 °C. Increasing temperatures lead to increasing resistances and were read out with a LabBox®2. The slope of this increase is described by temperature coefficients in specific temperature ranges. Coefficients are given from $3.86 \bullet 10^{-3}$ K^{-1} to $3.89 \bullet 10^{-3}$ K^{-1} at 20 °C and 40 °C or $3.85 \bullet 10^{-3}$ K^{-1} for the whole range.[99,101]

4.4.1.3 Osmolality

The two terms osmolality and osmolarity are related to each other by their basic definition, but differ with respect to the solvent. Both describe the osmotic pressure of a solution. They are defined as concentrations of molecules that contribute to the osmotic pressure.[102] Basically, there is just very little difference between osmolarity and osmolality when water is the solvent.[95,103] Osmolality refers to osmole kg^{-1} and osmolarity to osmole L^{-1} of the applied volume.

Generally, measurements are performed with an osmometer. The freezing point of the solution refers to pure water. One osmole kg^{-1} leads to a decrease of the freezing point by 1.85 °C.[104]

In this study, evaluations of the osmolality were performed with an Osmomat 030. Normally, buffer solutions were adjusted to 290 ± 10 mosmole kg^{-1}. Adding of distilled water reduced the osmotic pressure of prepared solutions, whereas physiological salts (i.e. sodium chloride) increased the osmotic pressure. There was just one exception with the synthetic urine, where the osmolality was in the range of 760 mosmole kg^{-1}.

4.4.1.4 Diffusion of molecules in an Ussing chamber

Tissue-engineered, fibrin-based prosthesis were characterised with respect to their tightness against urea and creatinine. Two Ussing chambers can be seen in Figure 10. An Ussing chamber consisted of two half shells.

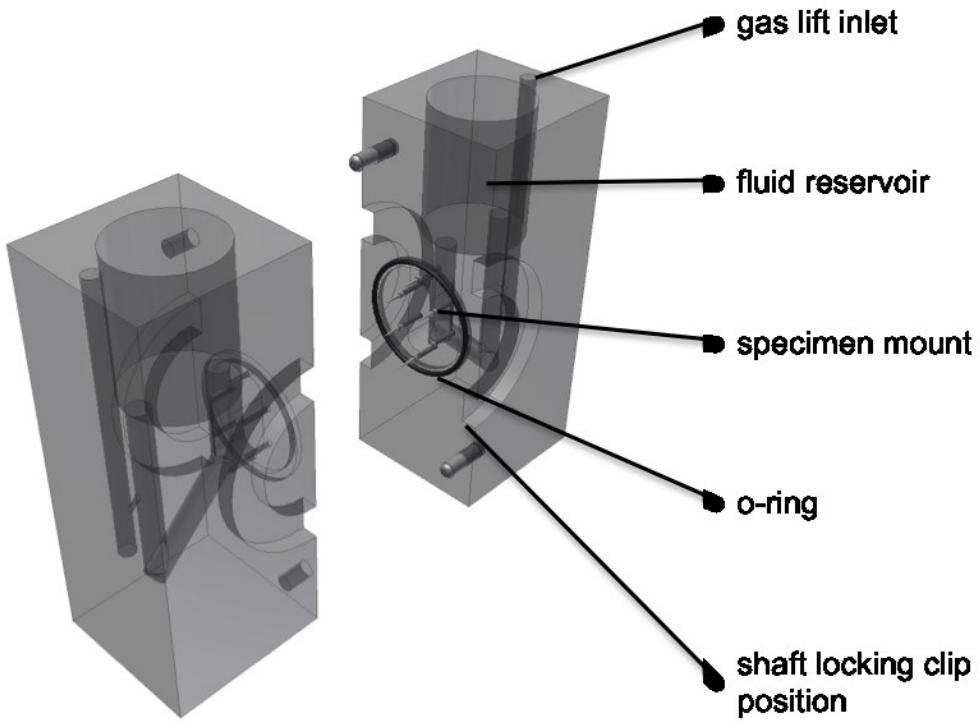

Figure 10: Scheme of an "Ussing" chamber used for passive diffusion experiments. For this study, the chamber consists of two half shells, where the tissue is clamped in between.[6]

The specimen to be characterised was put in between the two half shells, so that the tissue separated the two media reservoirs from each other. A specimen mount avoids a slipping of the tissue. Shaft locking clips on the two long sides of the chamber held both half shells together. The presented and applied model had a tissue-cross-section of 67.1 mm^2 (14.5•5 mm^2) and reservoirs contained 5 mL buffer solution. The gas lift for a homogenous mixture was operated with an aquarium pump. Valves located between the pump and the Ussing chamber were adjusted so as to insure an inflow of 5-10 bubbles per minute. Temperature was kept constant at 37 °C by placing the Ussing chamber into a water bath.

Figure 11 indicates the starting conditions that were used in this study. The Ussing chamber on the left contained 5 mL artificial urine (see Chapter 4.3.3) and 5 mL Krebs buffer (see Chapter 4.3.4). Specimens were placed in between the two chambers. In all cases, the luminal surface of the prostheses was arranged towards the synthetic urine. Regular sampling of 1 mL was performed after 0.5, 1, 1.5, 2, 3, 4, 5, 6, 7 and 8 hours to investigate the passive diffusion of urea and creatinine. Samples were taken from the Krebs buffer side. Sampling volumes

were replaced by fresh, preheated (37 °C) Krebs buffer solution. All samples were analysed in the veterinary laboratory of the RWTH Aachen University Hospital, Aachen.

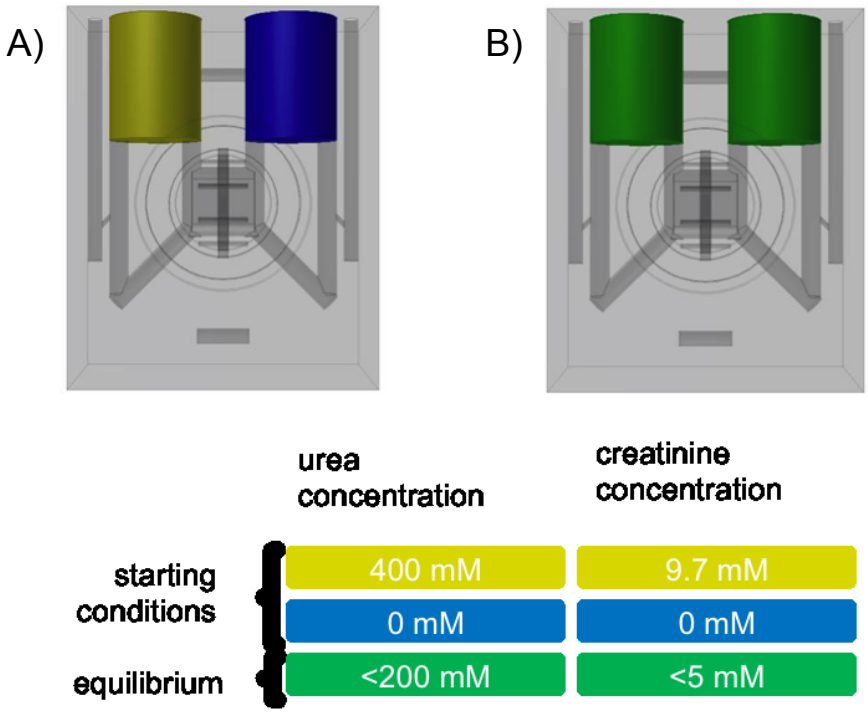

Figure 11: Starting conditions A) in the Ussing chamber with synthetic urine (yellow, left reservoir) and Krebs buffer (blue, right reservoir). Theoretical equilibrium B) conditions in the Ussing chamber, where both reservoirs (green) contain the same amounts of urea and creatinine.[6]

4.4.2 Cell culture medium preparation

In this study, three different cell culture media were applied for the following processes:

Medium I: Preparation of primary cell cultures

Medium II: Proliferation of primary cell cultures

Medium III: Application in the bioreactor system

Cell culture medium I consisted of Dulbecco's modified eagle's medium (DMEM) supplemented with 10% (V/V) fetal bovine serum (FBS), 1% (V/V) gentamicin and 1% (V/V) amphotericin.

Standard cell culture medium II was made up of DMEM supplemented with 10% (V/V) FBS. This medium did not contain any antibiotics and was applied during the cultivations and proliferations of isolated porcine smooth muscle cells (SMC).

Cell culture medium III was applied for the fibrin-based prosthesis, based on the formulation by [105,106] and contained DMEM, 1% (V/V) penicillin/streptomycin, 1 mM L-ascorbic acid-2-phosphate and 0.5 mg mL^{-1} Cyklokarpron®. L-ascorbic acid-2-phosphate was added to improve tissue generation.[107,108] The originally applied aprotinin was replaced by Cyklokarpron® to stabilise tissue constructs and regulate fibrin degradation.[109,110]

4.4.3 Passaging of cells

Splitting of cells followed standard cell culture technology protocols as described by[111,112]. Cells were washed twice with preheated (37 °C) PBS to remove disturbing ions that inhibit the Trypsin/EDTA solution. Trypsin/EDTA contained the serine protease trypsin and the ion chelator ethylenediaminetetraacetic acid to detach adhering cells. Cell culture flasks containing the cells and an appropriate amount of Trypsin/EDTA (see Table 9) were put into the incubator. The detachment process was monitored regularly using an inverted light microscope. When cells had detached, adding of preheated (37 °C) standard cell culture medium II, inhibited the digesting enzyme trypsin. Suspensions were pipetted into 50 mL centrifuge tubes and were centrifuged for 5 minutes at 280 g. A vacuum pump was used to remove supernatants before cell pellets were resuspended carefully with 1 mL cell culture medium II.

Table 9: Volumes of PBS, Trypsin/EDTA and cell culture medium that were added to cell culture flasks in accordance with [105].

Cell culture Flask	PBS [mL]	Trypsin/EDTA 0.05% [mL]	Cell culture medium [mL]
T75	5	3	10
T175	12	7	25
T500	30	15	60

This procedure is followed by the counting of the cells for a subsequent seeding them with a defined cell density. For primary porcine smooth muscle cells it could be observed that a seeding density of >2000 cells cm^{-2} was advisable to accelerate cellular proliferation.

4.4.4 Cell counting

All cells in this study were counted with the BioRad TC20™ cell counter. This automated device can be used to count cells and determine their viability by means of Trypan Blue staining. Cell counting was performed according to the manufacturer's instructions.[113] To this end, a 1:1 dilution was prepared and 10 µL of a cell suspension were mixed with 10 µL Trypan Blue in a micro centrifuge tube. Ten µL of this suspension were put into disposable counting slides (BioRad). The counting slides were inserted into the TC20™ device and results were read out. Cellular concentrations of $5 \bullet 10^4$-10^7 were not exceeded to obtain reliable measurements.[113] Results were checked again through evaluation of the particle sizes. Cell clots were made visible as big particles in the histogram and indicated on the front panel of the TC20™. A gating process allowed to exclude oversized particles from the evaluation process. The gates were set to 12-19 µm.

4.4.5 Isolation of primary cells

Isolation of primary cells was performed from porcine urinary bladders that were obtained from a local slaughterhouse. The bladders were transported in sterile glass containers with preheated (37 °C) cell culture medium, 1% (V/V) gentamicin and 1% (V/V) amphotericin.[97]

Urinary bladders were placed inside the laminar flow hood on a sterile drape sheet. Excessive tissue was removed with a set of scissors, tweezers and clamps. After cutting the urethra, the bladders were opened with another sterile scissor. Y-shaped incisions were performed medially to place bladders flat on the surgical drape. The luminal surfaces were directed to the topside.

For following steps, a new set of sterile scissors was used. The mucosal layer was removed completely by means of scissors and tweezers. Fine tweezers were used to lift the elastic mucosal layer (urothelium), which was then cut. Subsequently, it was possible to dissect the exposed smooth muscle cell layer.

Cutted smooth muscle tissue was collected in a petri dish, before it was minced into fragments of approximately 1 mm^3. About 20-25 fragments were placed in

close proximity in T75 cell culture flasks. A sterile 5 mL serological pipette was used to distribute the tissue inside the cell culture flask. Fragments were allowed to dry inside the flasks for 20 minutes before 15 mL cell culture medium I (see Chapter 4.4.2) were added at the side of the flasks. Care handling ensured the adhesion of the tissue fragments. Flasks were put into the cell culture incubator at 37 °C, 5% CO_2 and 100% humidity. Cell culture media was replaced by preheated (37 °C) standard medium II (see Chapter 4.4.2) after 1 week. Detached tissue fragments were removed by pipetting. Cells were allowed to grow for about 2-3 weeks before closely spaced cell population inside the flasks made passaging necessary. The passaging process was performed according to the description given in Chapter 4.4.3. For fibrin-based experiments cells were transferred into T175 flasks in passage 1 and in T500 flasks in passage 2.

4.5 Histology

4.5.1 Fixation and dehydration of tissues

For further evaluation, samples needed to be stabilised in a fixative. In this study, Carnoy's fluid was used to stop cellular activity and to fix cells. Carnoy's fixative consisted of 60 mL ethanol 99.9%, 30 mL chloroform and 10 mL acetic acid.[114,115] This fixative was used because of its advantages with respect to immunohistochemistry of tissue-engineered constructs. An application of Carnoy's fluid does not requires excessive antigen retrieval, which may impair the staining or visualisation of the samples.[115] Fibrin prostheses' samples were incubated for 4 hours, collagen based constructs for up to 8 hours.

To enable further classical staining methods and scanning electron microscopy, the fixative needs to be replaced by ethanol 99.9% or acetone 99.9%.[114]

Tissue-engineered samples were dipped in ethanol solution of different concentrations (70%, 80%, 90% and twice in 99.9%) for at least 20 minutes per solution. For classical histology, samples were stored in 99.9% ethanol. All other samples were dipped gradually into acetone (acetone/ethanol (v/v): 20/80; 40/60; 60/40; 80/20; 90/10; 100/0; 100/0).

4.5.2 Classical staining and light microscopy

Classical staining was carried out by the Aachen Interdisciplinary Centre for Clinical Research (IZKF). The samples were embedded in paraffin, cut into 5 µm slices and stained with Haematoxylin & Eosin (HE). HE is the most common staining and provides an overview of the sample after a very short period of time. It gives the opportunity to evaluate the structural setup of tissues with their cellular distribution. The typical dark blue/purple coloration results from the haematoxylin, whereas strong reddish/pink coloration is caused by the eosin. Generally, connective tissue and cytoplasm are stained by the eosin, while the haematoxylin stains the nucleus of cells.[114,116]

Classical light microscopy is limited to the visible light spectrum that needs to pass the analysed sample. The resolution of a light microscope is strongly related to the wavelength of the applied light and the numerical aperture of the optical system. Under normal conditions, the limit value for lateral resolution of a light microscope is approximately 0.2 µm.[114,117] This value expresses the distance between two objects that is necessary to identify them as two separate objects.

As this type of microscopy is not suitable for thick, lightproof tissues and for the evaluation of their outer surface, the scanning electron microscopy was used for this purpose.

4.5.3 Critical point drying (CPD) and scanning electron microscopy

Critical point drying (CPD) is a method to dry biological samples to prepare them for scanning electron microscopy. Other possibilities are drying them in environmental air or freeze-drying. However, CPD has the advantage that the risk of collapsing samples or damage due to ice crystal formation is reduced.[114,118]

First the samples were set into the CPD-device. The pressure chamber was closed tightly and the sample was cooled to 8 °C. Liquid carbon dioxide (CO_2) gradually replaced the acetone inside the chamber. The CO_2 and the sample were heated up to 40 °C, which resulted in an increasing pressure. Consequently, the critical point of CO_2 (74 bars, 31 °C) was exceeded.[114,118] This enables a borderless phase transition from liquid to a gaseous. The gas was vented and the samples were taken out of the pressure chamber.

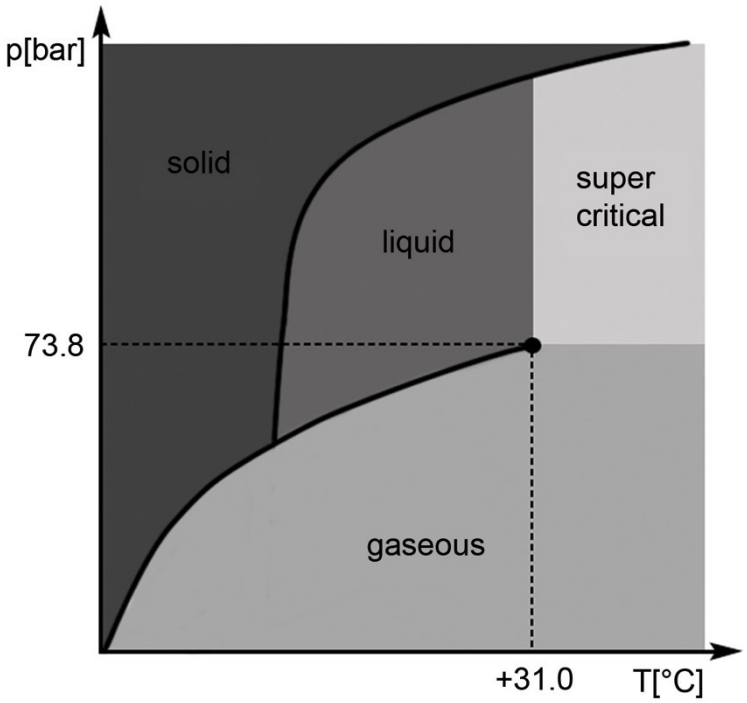

Figure 12: Phase diagram for CO_2, according to [119]. The critical point for CPD can be exceeded at pressures >73.8 bars and temperatures >31 °C. Both conditions need to be fulfilled at the same time for a prompt phase transition.[6]

After that, the samples were set onto holders for inserting them into the scanning electron microscope (SEM). The electrical connection between the holders and the samples were improved by applying Silver Dag 1415. Then, a gold-palladium (AuPd (80:20)) layer was added by sputtering. Collagen based scaffolds were sputtered for 1 minute, while fibrin-based prostheses were sputtered for 2 minutes. Subsequently, the samples were analysed with an ESEM Quanta 400 FEG.
Scanning electron microscopy is used to analyse the outer surface of objects. Additionally, modern SEMs are able to analyse the material composition of the surface. Both are dependent on electrons that are ejected from a glow filament. This filament forms a cathode and released electrons are accelerated through a circular anode. Magnetic fields guide and focus these electrons onto the specimen. A vacuum inside the microscope avoids interaction of the accelerated electrons with the ambient air. The electrons interact with the sample's surface, so that secondary and backscattered electrons can be used for imaging the sample's topography and for the image contrast. Secondary effects like characteristic x-rays give information about the composition of the specimen's upper layer.[120]
In such cases, the typical resolution is in the range of 2 nm.[118]

4.6 Application of scaffold materials

4.6.1 Optimaix 3D Sponge1

With a relative amount of 25%, collagen is the most abundant protein in the human body, and it appears in at least 27 different forms. This protein mostly consists of glycine, proline and hydroxyproline.[13]

Due to the high amount of collagen in the body and its availability there is the idea to use this extracellular matrix protein for tissue engineering purposes. Collagen type I is one of the most common extracellular matrix (ECM) proteins and its fibril structure is illustrated in Figure 13.

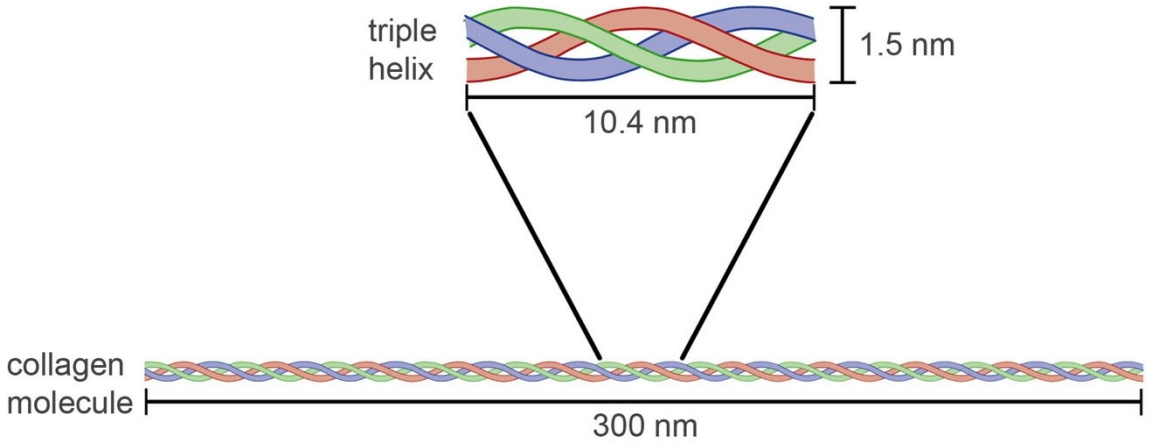

Figure 13: Structural setup of a fibril collagen according to [121].[6]

Figure 13 shows that collagen type I forms a super helical structure out of three polypeptide chains with a length of about 300 nm and a diameter of 1.5 nm. A single loop of the super helix has a length of 10.4 nm.[121,122]

Optimaix is a patented scaffold material based on type I collagen and low amounts of elastin. A specific freeze-drying manufacturing process results in its characteristic structure. Interconnected pores are parallel oriented with a width of 20-50 µm.[123] Thus, the cross-sectional area equals 1250-7850 µm^2, assuming circular pores.

The Optimaix 3D was tested by Montzka et al. (2010) with respect to its suitability for urological applications and showed useful results with respect to cellular proliferation and biocompatibility.[97] Based on these findings, a tubular matrix was developed with radially oriented pores. This new Optimaix 3D Sponge1 was used

in this study for the bioreactor system. Moreover, an in-vivo study (UroRepair) with this material in Göttinger Minipigs revealed an excellent performance in the urinary bladder. In this study, unseeded, with urothelial cells or smooth muscle cells seeded, and co-cultivated Optimaix 3D matrices with a size of up to 12 cm^2 were applied. Autologous, primary smooth muscle and urothelial cells were used to generate tissue for the replacement of injured bladders. No effects like stone formation, inflammation reaction or rejection were observable after about 6, 12, 18 and 26 weeks of implantation.[124–126]

4.6.1.1 Seeding procedures

The seeding procedure was adapted according to the manufacturer's instructions for the application of Optimaix 3D. With the "drop-on" and "dip-in" procedure, two different methods were available.[127]

The Optimaix 3D is able to take up fluid that equals 97% of the total scaffold volume. This volume was added onto Optimaix 3D Sponge1 scaffolds in the drop-on procedure. In contrast to that, scaffolds were immersed into a cell suspension for the dip-in procedure.[127]

4.6.2 Fibrin and polyvinylidenfluoride (PVDF)

Fibrin is the clotting factor I that is a systemic protein takes place in haemostatics processes.[128] Fibrinogen is a fibrin monomer and consists of subunits $(A\alpha, B\beta, \gamma)_2$ with a molecular weight of 338 kDa.[129,130] The structural setup of the molecule can be reduced to three components, depicted in Figure 14. Three subunits are straightly aligned and have a length of 450 ± 15 Å.[131]

Figure 14 also shows fibrinogen polymerisation; where the D and E domains are bound by electrostatic interactions. Factor XIIIa leads to a covalent bonding of the fibrin monomers between D and E subunits, which is indicated with red connecting lines in Figure 14. Fibrinolysis results in single subunits, not to intact fibrinogen.

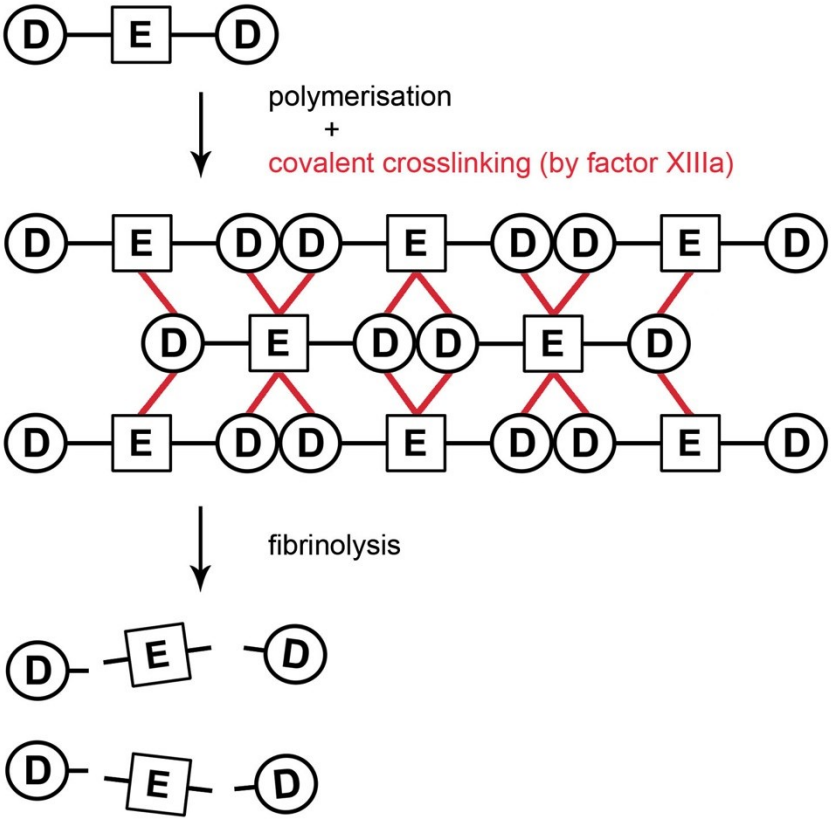

Figure 14: Structural setup of fibrinogen with its three subunits, 2●D and 1●E. Polymerisation and crosslinking of fibrinogen lead to a stable fibrin clot, while fibrinolysis results in single subunits.[6]

The clotting process as illustrated in Figure 14 and Figure 15 is actually the end of a whole blood clotting cascade and fibrinolysis.

Figure 15 shows both, the coagulation process and fibrinolysis. This overview illustrates the coagulation where prothrombin is converted to thrombin resulting in a fibrin clot. This clot is stabilised by factor XIIIa. The clot is the fibrinolysed. It can be seen in the figure that plasminogen is activated by the tissue plasminogen activator (tPA) or urokinase-type plasminogen activator (uPA), which results in the conversion to plasmin. Plasmin degrades fibrin clots at the binding sites of the D and E domains. This results in D-dimers and an E-subunit. However, competitive inhibition by tranexamic acid, antiplasmin or aprotinin can slow down this process.[128,130,132–135]

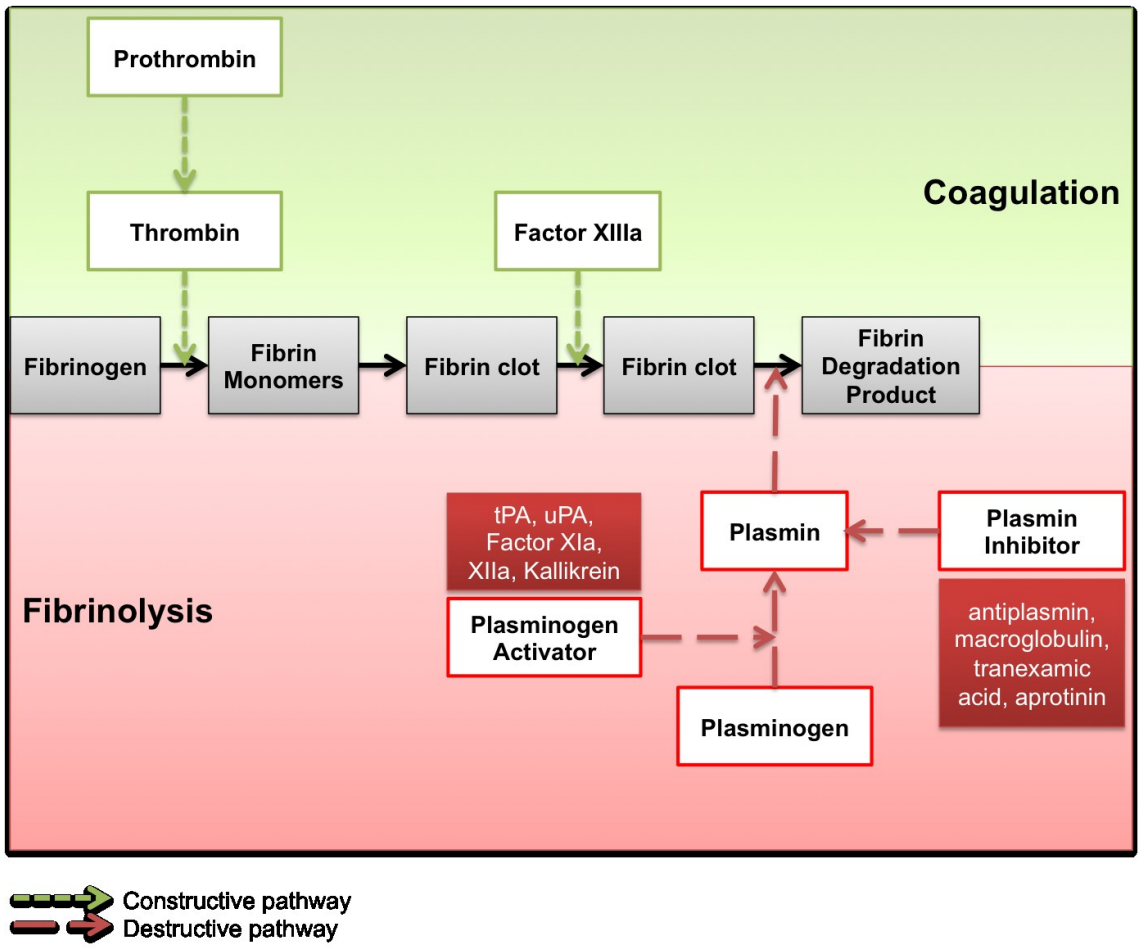

Figure 15: Simplified illustration of haemostasis that leads to natural blood clotting. Coagulation and fibrinolysis are schematised with focus on tissue engineering applications.[6,130,132–135]

For the composite biohybrids, the stabilising material was polyvinylidenfluoride (PVDF; $(CH_2\text{-}CF_2)_n$), which is a common material used in various (bio-) medical applications as scaffold material, mesh or suture. Its biocompatibility, chemical inertness, durability and the ability for surface modifications are appreciated for medical treatments.[136–139]

The institute for textile technology of the RWTH Aachen University (ITA) provided the applied PVDF mesh (Trickot E30 EAC 10). This mesh was manufactured in a melt spinning process, which produces a multifilament yarn consisting of 16 single filaments and was knitted into a tubular shape.

The PVDF mesh was sterilised by low temperature plasma sterilisation. In addition to sterility, this treatment leads to increased biocompatibility and surface tension. Thus, the adhesion of the applied fibrin and primary cell culture process can be improved.[140–142]

4.6.2.1 Fibrin preparation

Fibrin preparation started with the dissolving of the lyophilised protein in purified water. To this end, fibrinogen and purified water were placed separately in an incubator at 37 °C for at least 1.5 hours. Subsequently, 39 mL of the preheated water was transferred in a vial containing 1000 mg fibrinogen. The dissolution took 4-5 hours at 37 °C.

In a second step, the fibrinogen solution was split up (3•13 mL) and was dialysed against (3•) 4.5 L Tris-buffer (TBS) (see Chapter 4.3.1) overnight at room temperature. For this purpose, a cut-off membrane of 6000-8000 MW was used.[106,143,144] Thus, the TBS replaced the water. Sterile filtration was conducted prior to the determination of protein concentration by light spectrometry at 280 nm.[106,143]

The protein concentration was determined in a UV-VIS spectrophotometer in the ultra violet (UV) spectrum (<300 nm) using suitable cuvettes that do not absorb the UV-light.

Generally, the absorption of UV-light is based on the defined energetic difference between two energy orbitals. Electrons in the ground state are not excited, but they can be brought into higher energy orbital due to incident photons with a specific energy. The absorption maximum of proteins at a wavelength of 280 nm is characteristic for aromatic rings that are exclusively represented in phenylalanine, tryptophan, histidine and tyrosine. Variations in the total amount of these amino acids cause little differences in specific absorption coefficients. Further differences are caused by the influence of the buffer solution, which interacts, with the tertiary structure of proteins. To avoid this, parameters like pH values or ionic strength were kept constant.[145]

The Lambert Beer's law correlates the absorbance of light with specific (here: protein) concentrations:

$$c\ \left[\frac{mg}{mL}\right] = \frac{A}{\varepsilon \cdot d} \cdot \mu \qquad (2)$$

c = concentration

A = absorbance

ε = absorption coefficient

d = path length of light in the medium

μ = dilution

The specific absorption coefficient (ε) depends on the species and is given for human fibrinogen with a value of 1.55.[146]

Subsequent to the measurements, a fibrinogen concentration of 12.5 mg mL^{-1} was prepared with sterile TBS. Aliquots were arranged and stored at -80 °C.

For the prosthesis preparation, fibrinogen solution (50%), TBS with cells (35%), thrombin (40 U mL^{-1}) (7.5%) and 50 mM $CaCl_2$ (7.5%) were mixed with each other by means of a two-chamber applicator system.[106,143]

4.6.2.2 PVDF mesh preparation

Knitted PVDF meshes were cut into pieces of 9 cm length. Afterwards, these tubular segments were put onto Pasteur pipettes that had a diameter of 7 mm. They were then placed in an oven at 125 °C for 10 minutes. The meshes were washed with 99.9% ethanol and purified water for 15 minutes after a cooling phase at room temperature. They were dried in a laminar flow hood over night before plasma sterilisation was conducted at the RWTH Aachen University Hospital, Aachen.

4.7 The "UREPLACE" bioreactor system

The basis for this study was developed by Denis Schehl (2011)[147] and Volker Seifarth (2011)[148] a bioreactor system was designed comprising a tubular bioreactor for tissue engineering purposes. The bioreactor was separated from the incubation system to have an easy usage. Figure 16 shows the bioreactor with its modular setup, designed for the cultivation and growing of tubular constructs. It is characterised by two independent media circuits with two small inlets for the outer medium flux and one central inlet for the luminal support. Its equivalent diagram is depicted in Figure 17.

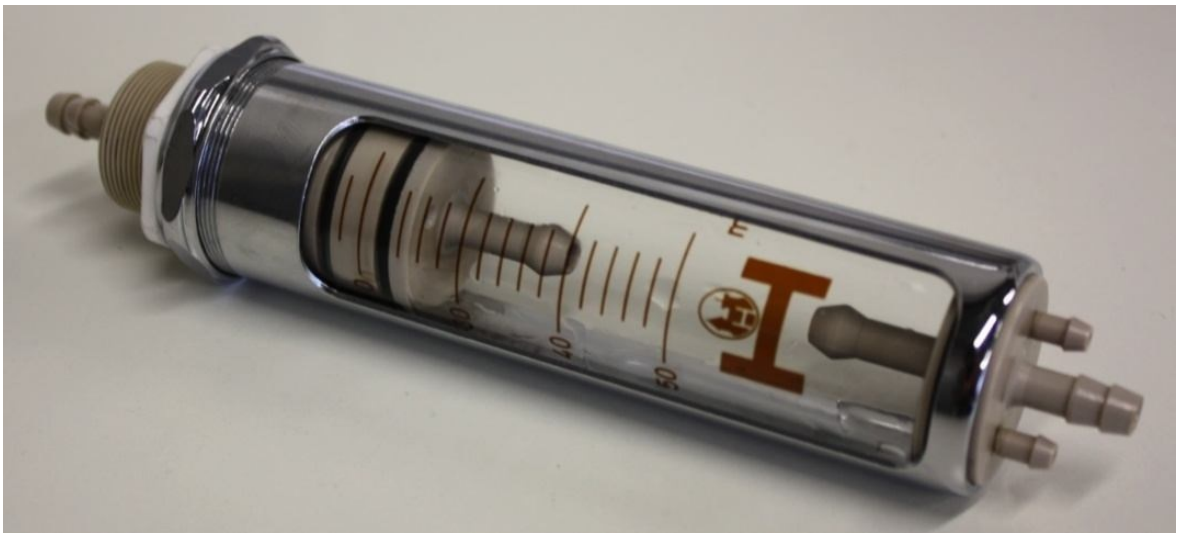

Figure 16: UREPLACE Bioreactor Prototype III.[149]

In the two studies mentioned before it was possible to show that the application of HiTec Zang components was useful for the transfer of cell culture media and that the LabBox®2 (HiTec Zang) was a suitable interface for controlling and recordinging incubation parameters. First test series lead an optimal adjustment of the controllers for the temperature and CO_2 fumigation system with respect to their step responses.[147,148] This means that the start-up process of the system was optimised to enable the setting of a specific temperature (37 °C) and CO_2 concentration (5%). Besides that, a prototype of a rotary unit was integrated that was supposed to make a homogenous distribution of cells in a collagen scaffold (Optimaix 3D Sponge1) possible. It was able to sway the bioreactor with a rotation angle of 270°. The pH value of the medium which is pumped from a reservoir through the system to the waste reservoir determined the media flow rate. The more the pH differed from 7.4,

the faster was the cell culture medium transfer.[147,148] Besides that, a first prototype of a catheter based peristaltic stimulation[150,151] was further developed by implementing an automated expansion and deflation of the catheter to achieve a physiological stimulation. Subsequent to the expansion, the catheter was supposed be pulled through the lumen of the tubular structure, before being deflated and pushed back again.[147,148]

Figure 17 schematises the setup for the application of the Bioreactor Prototype III. The unidirectional medium flow (M1, M2) was realised by peristaltic pumps (P1, P2) that were controlled by the measured pH value. Tubes and valves were connected to each other in such a way that both media circuits could be measured with one glass electrode. This electrode was washed with water in between the measurements.

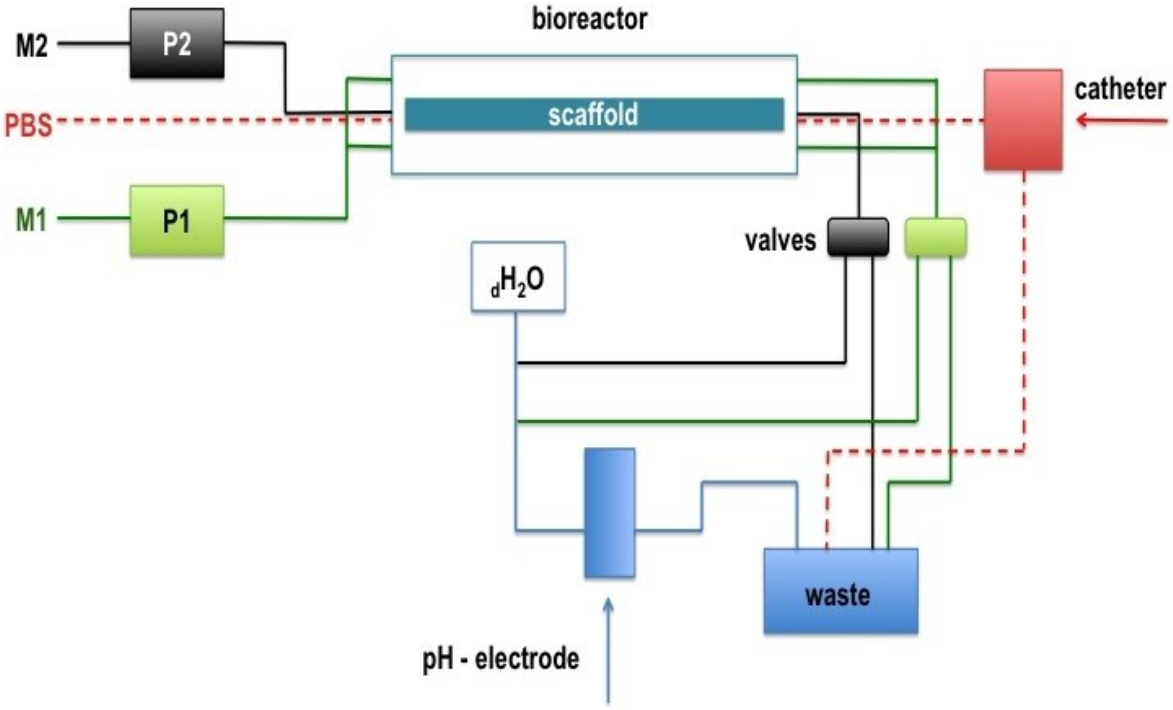

Figure 17: Schematic setup of the medium circulation in the Bioreactor Prototype III including peristaltic stimulation and PBS flushing to avoid contaminations.[147]

An inlet for the catheter was realised by the component seen in Figure 18 (left). Phosphate-buffered-saline (PBS) is directed through the central fitting of the bioreactor during peristaltic stimulation. Thus, contaminations were avoided by flushing out contaminating particles. There was no sealed connection between catheter and bioreactor. A catheter was attached to a linear actuator for the movement of the catheter was realised by the component seen in Figure 18 (right).

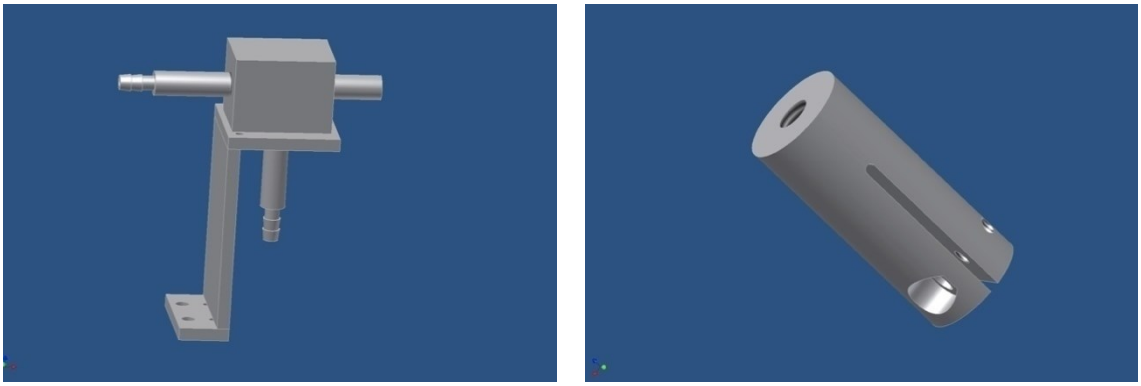

Figure 18: Components developed for access of the embolectomy catheter to the bioreactor (left) and for connection of the catheter to the linear actuator (right).[147]

4.8 Statistics

Statistical analyses were performed with Microsoft Excel, LabVIEW and Gnu R, where:

$$mean = \overline{x} = \frac{\sum_{i=0}^{n} x_i}{\mathrm{n}}, \tag{3}$$

$$standard\ deviation = \sigma = \sqrt{\frac{1}{n-1} \cdot \sum_{i=0}^{n} (x_i - \overline{x})^2}\,, \tag{4}$$

$$median = \tilde{x} = \begin{cases} x_{\frac{n+1}{2}} & for\ even\ datasets \\ \frac{1}{2} \cdot \left(x_{\frac{n}{2}} + x_{\frac{n}{2}+1} \right) & for\ odd\ datasets \end{cases}, \tag{5}$$

$$interquartil\ range = IQR = lower\ quartile - upper\ quartile = \tilde{x}_{0.75} - \tilde{x}_{0.25}. \tag{6}$$

n: number of data items

x_i: i[th] value in the dataset

Wilcoxon rank-sum test was used in Gnu R to determine significance.

5 Results and Discussion

During this thesis, several adaptions and improvements were a result from a constant learning curve. They were implemented in the bioreactor and the bioreactor system to improve the cultivation of different cell types in tubular structures. Improvements with respect to component design prior to the presented experiments lead to significant optimisations of the system and the bioreactor.

5.1 Adaptions to the "UREPLACE" bioreactor system

5.1.1 The graphical user interface (GUI)

HiTec Zang provided LabVision® and HiText™ as software packages that were used for customised control of laboratory equipment in combination with a LabBox®2. The panel configuration of the LabBox®2 was changed in comparison to (Schehl, 2011)[147]. A digital output was replaced by a digital input and two additional serial ports were added next to the BASCOM unit. The applied LabBox®2 served as interface between the actuators and sensors that were used for the bioreactor system. These actuators and sensors were driven and read out with LabVision® and HiText™. A graphical user interface (GUI) was designed in LabVision®. Preconfigured building blocks with predefined programs for the control of standard equipment, e.g. pH electrodes, allowed a fast and reliable setup of a user interface. Moreover, LabVision® was used to export all important measuring values as well as derived measurement values and parameters set by the operator. HiText™ was used in combination with LabVision® to code experimental sequences and monitoring systems.

The graphical user interface that can be seen in Figure 19 was based on the first draft by D. Schehl (2011) and was improved by adding tab pages for an advanced surface structure. The tab pages enable a clear division into three sections: A) the start-up of the bioreactor system, B) the "functional" units and C) the monitoring of the current measuring values.

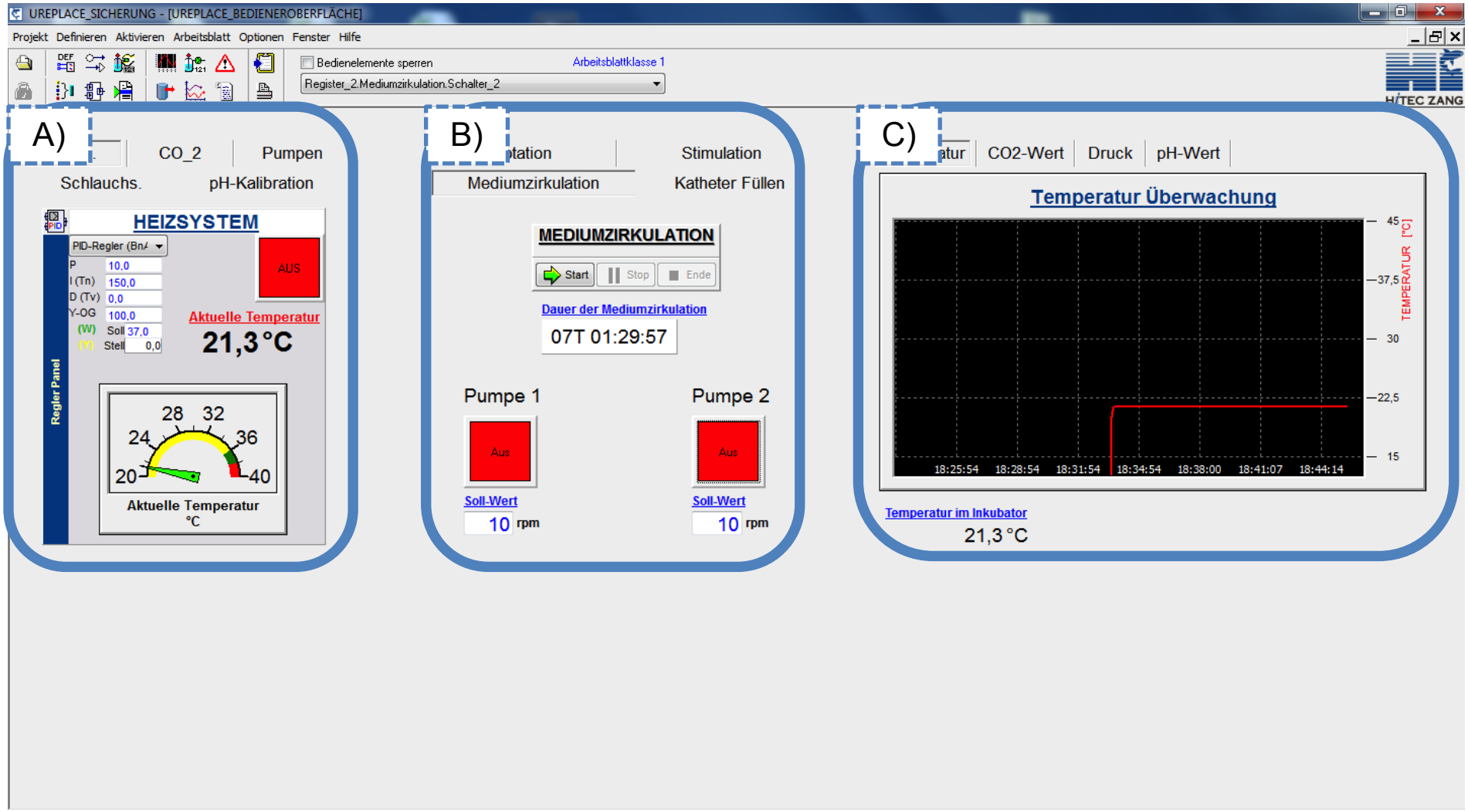

Figure 19: Improvement of the graphical user interface by a separation into a A) start-up, B) "functional" and C) monitoring section.[6]

Controlling and calibration units, e.g. temperature and pH electrodes, were arranged on tab pages, which resulted in fewer elements on the GUI even though elements were added. In addition to the previous version, a pH calibration unit ("pH-Kalibration"), a pump unit ("Pumpen") that was separated from the "Mediumzirkulation" and a tube-filling unit ("Schlauchs.") were added for easier start-up and control of the system. A pH calibration unit became necessary due to new pH electrodes that needed to be calibrated regularly.

The "functional" tabs were still placed in the centre of the interface to underline the importance of these elements. Instead of providing access to all functions on the page, which only required on click but made the surface appear confusing, the division into three sections still enabled direct access but also provided a much more structured surface. On the functional's unit tab a time panel was integrated that displayed the elapsed time for the active medium circulation system.

Extra information was added to the diagrams for monitoring the most important parameters. Current measurement value displays were added for the temperature in the incubator and the medium reservoirs, the CO_2 concentration, the pH values of the cell culture media and the pressure in the catheter pressure line.

All in all, the surface structure became clearer due to three defined sections so that the operating of the bioreactor system was improved further. The use of the system became intuitive, and even inexperienced operators to use the graphical user interface without much practice.

5.1.2 Redesign of the inputs and outputs of Prototype III

Further achievements were added to the bioreactor design. This design regarded new requirements resulting from e.g. cell seeding procedures. Figure 20 gives an overview of the different parts of the advanced bioreactor system. Prototype IV is presented there with several improvements compared Prototype III.

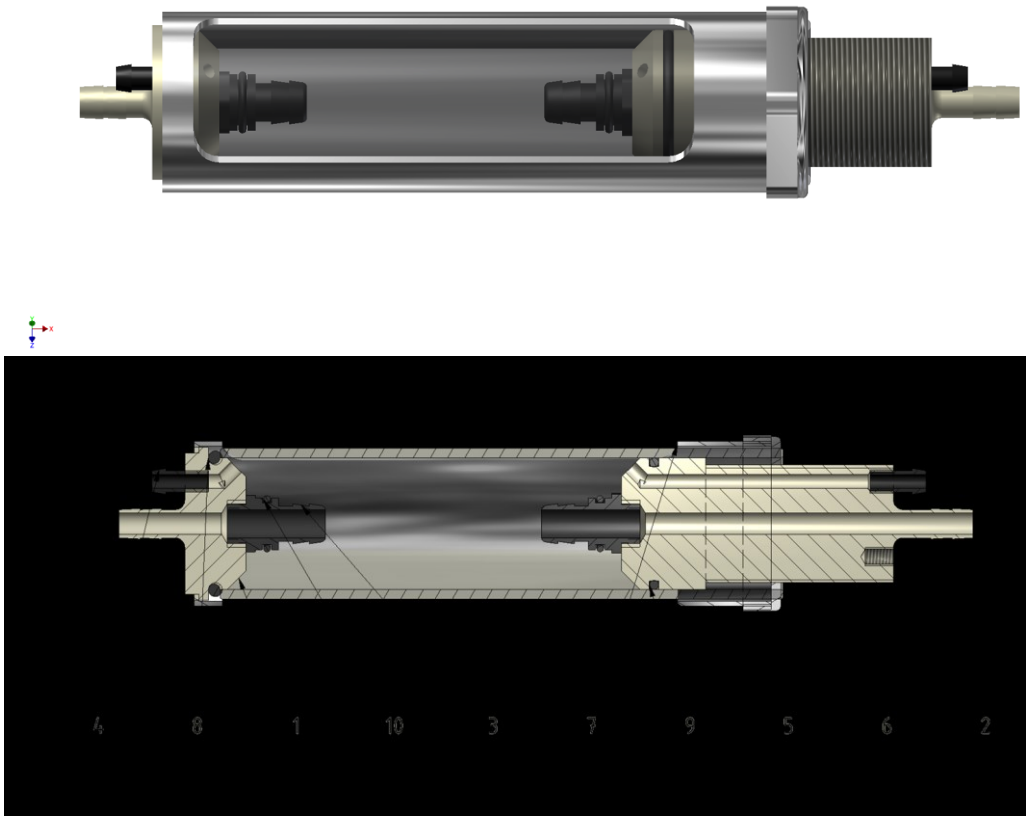

Figure 20: Bioreactor Prototype IV with angled medium inlets and outlets at the improved front plate (1) and piston (2), advanced central fittings (3) and fittings for the medium flow (4) covered in a glass cylinder (5) with a stainless steel housing (6), (7) and sealed with O-rings (8), (9) and (10).[6]

The redesign of the medium supply for the outer circuit was realised by increasing the diameters of the boreholes in front plate and piston from 2 mm to 4 mm. At the same time, the number of boreholes was reduced to one. **Thus, fewer tubes and fewer tube-connectors resulted in improved handling.**

Furthermore, angled inlets and outlets for the cell culture medium lead to fewer air bubbles inside the bioreactor compared to Prototype III. Nevertheless, except for the application in the rotatory unit, it needed to be ensured that the medium outlet was directed upwards. The bioreactor itself was still horizontally adjusted like in Figure 20. **Thus, an air bubble trap like in other systems became dispensable.**[67,152,153]

A further development can be seen regarding the sealing of the piston: the number of O-rings was reduced to one. As a consequence, it became much easier to insert and move the piston inside the glass cylinder. The distance between the central fittings could be adjusted more smoothly and the system stayed still without leakage.

Another improvements were the redesigned central fittings, on to which the scaffold material was placed. The previous Prototype III had fixed fittings at the front plate and at the piston with fixed dimensions. For the dip-in seeding procedure of cells in combination with the Optimaix 3D Sponge1 as scaffold material, it became necessary to detach the fittings. Screwable fittings were enabled to be attached to the front plate or the piston after an immersion of the scaffold in cell suspension. To achieve this, additional threaded boreholes were prepared at the attachment sites. These boreholes had the advantage that different types of fittings with different dimensions could be used in this Prototype IV.

The modular setup makes the bioreactor flexible and easy to handle. This results in cost effectiveness, which is an important factor in making bioreactor suitable for clinical application.[58,59,154]

The material of the redesigned parts (front plate, piston and fittings) was polyoxymethylene (POM), an inert plastic material with suitable characteristics for cell culture technologies. This material can be sterilised by autoclaving, shows a high biocompatibility and cells do not attach to it.[155]

All these parts were manufactured according to prepared technical drawings (see Chapter 8.3) in the workshop of the Aachen, University of Applied Sciences in Jülich.

5.1.3 Improvement of the central fittings

The redesigned central fittings for the fixation of the scaffold materials were a significant improvement that became necessary for the application of the Optimaix 3D Sponge1 as well as for the subsequent application of fibrin-based scaffolds. Figure 21 shows two different fitting configurations that were used in this study. These fittings provided a screw thread (M10) that could be attached to the front plate and piston of the bioreactor. A hexagon key was used to tighten the fitting. The opposite side of the fittings was characterised by smoothly rounded edges to reduce mechanical stress on the biohybrids.

A)

B)

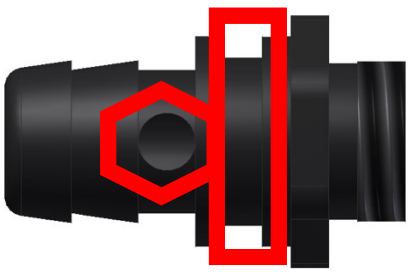

Figure 21: Central fittings for the application of Optimaix 3D Sponge1 and untrained fibrin-based prostheses A). And B) for the use in combination with trained prostheses in Bioreactor Prototype IV.[6]

The fitting design in Figure 21 A) was used for untrained Optimaix 3D Sponge1 and fibrin-based prostheses. This fitting was used for completely independent media circuits.

Cable ties were taken for both fitting configurations to fix the scaffold materials. A tight and reliable immobilisation was achieved in combination with two small barbs

(0.5 mm) that were added to these fittings. Moreover, it can be seen in Figure 21 B) that there was an additional notch (red rectangle), which was used as a seat for an O-ring. This O-ring was required for the use in the fibrin casting mould explained in Chapter 5.6.2.2 to avoid leakage. Dimensions of the notches were adapted to the diameter of the O-rings that were applied. Specialised table books gave a slot width of 2 mm and a depth of 1.1 mm.[156]

Configuration B) (Figure 21) was used exclusively for trained, fibrin-based prostheses. The reason for that was the missing central medium supply, because of the peristaltic stimulation that was performed with a kyphoplasty balloon catheter. Hence, the catheter needed to ensure the inner medium circulation. The catheter occluded the prosthesis and acted as a piston. Figure 22 illustrates the medium flux in stimulated fibrin-based biohybrids due to a moving balloon catheter. Cell culture medium was drawn through a borehole (red hexagon) in the fittings. This is a result of the lower pressure that is caused by the moving catheter ($p_1 < p_2$). On the other side of the balloon, excessive cell culture medium was pressed through the fitting. Consequently, there was a constant medium exchange in the lumen of the construct ensured by fresh medium from the outer medium circuit.

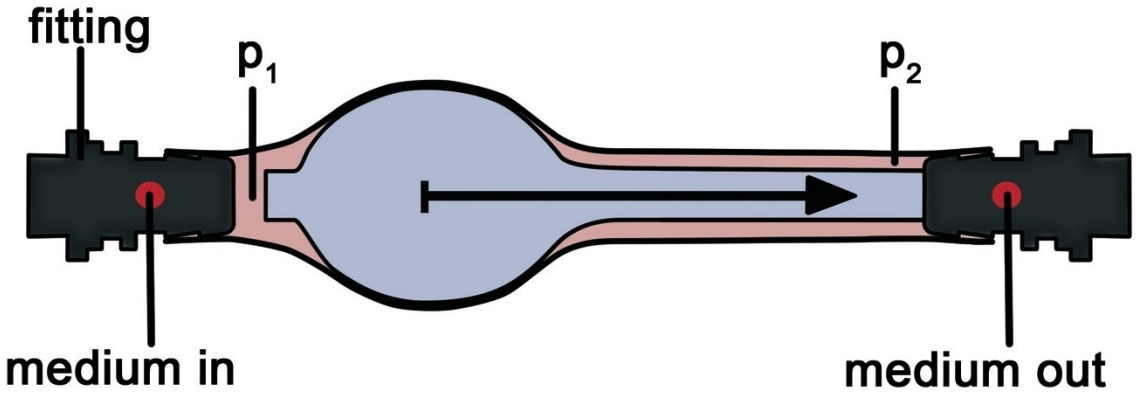

Figure 22: Schematic illustration of the inner medium circulation caused by mechanical stimulation with a balloon catheter. The movement of the catheter leads to a volume displacement, resulting in a medium transfer.[6]

5.1.4 The circulation of cell culture medium

The circulation of the cell culture medium was completely redesigned with a closed loop structure that ensured a contamination-free operation of the bioreactor system.

Figure 23 shows a scheme of the cell culture medium circulation for the bioreactor prototype IV. It can be seen that the medium circulations are separated from each other.

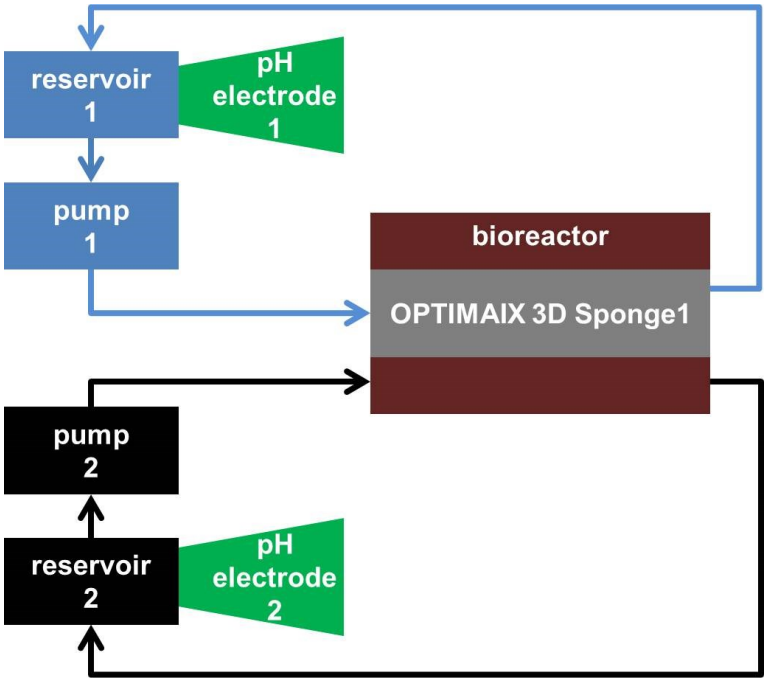

Figure 23: Flow chart of the redesigned medium circulation with a closed loop structure and separated circuits. Each circulation has its own reservoir, peristaltic pump and pH electrode.[6]

In this study, the closed loop structure was based on new medium reservoirs that were equipped with multifunctional customised lids (Bola). Screw caps for standard GLS 80 glass bottles (Schott Duran) were manufactured according to the requirements. They were sterilisable with damp heat and provided with:

- an inlet for a pH electrolyte electrode (Schott) with a PG 13.5 thread
- a tube inlet and outlet
- an opening for gas exchange
- a septum (VWR) for regular sampling

Figure 24: Customised GLS 80 screw cap made out of PTFE with 1•PG 13.5 for a pH electrode, 1•M14•1.5 for the integration of a septum and 3•NTP¼" for a cell culture medium inlet and outlet and for gas exchange.[6]

Figure 24 shows the screw cap developed to seal the medium reservoirs. The materials were polytetrafluorethylene (PTFE) and polyphenylene sulphide (PPS) so that it became possible to sterilised the caps by autoclaving at 121 °C and 2 bars.

The screw caps were equipped with openings for pH electrodes (1•PG 13.5), tubes and gas exchange (3•NTP¼") and a septum (1•M14•1.5).

The opening for the gas exchange at the screw cap was connected to an additional silicone tube and a sterile filter. Synthetic materials are gas permeable[157], but an additional opening to the atmosphere was provided to allow gas exchange. Medium that was transferred into the bioreactor was taken from the bottom of the reservoir that was filled with 550 mL of medium III (see Chapter 4.4.2) for fibrin-based prostheses. Medium II was chosen for collagen-based biohybrids. Returning cell culture medium dropped into the reservoir from a distance of about 5 cm above the fluid level. **This ensures a homogenous cell culture medium circulation inside the whole system.**

The medium quality was monitored with a gel electrolyte electrode that was sterilisable compared to standard glass electrodes that contain a standard 3 M KCl electrolyte.[158] Cell culture medium starts to get acidic during cultivation. Moreover,

the pH shows a metabolic lapse in case of a contamination. The applied pH electrode was equipped with a temperature sensor and attached to the LabBox®2 (HiTec Zang) to monitor and record the measured pH values. LabVision® provided a software component for the integration and calibration of the pH electrode. This made it possible to consider the current temperature in the calculation of the pH value (see Chapter 4.4.1.1).

The risk of a contamination during sampling was minimised by considering a place for an exchangeable septum instead of the T-connectors widely used as a "standard setup", because the surface that was susceptible was much smaller in such a septum. Another factor minimising the risk was the use of fewer components, further reducing the number of surfaces that can be contaminated.[63,159] Sterile syringes and needles were used to extract medium samples that may be used for further analysis.

The presented closed loop structure (see Figure 23) had the further advantage that no cell culture medium was wasted. During cultivation processes, the medium was changed regularly after 4-7 days. Moreover, there was no opening in the loop, which could lead to a contamination of the experimental setup. In this case, previous developments[147,150,151] had shown deficiencies. Additionally, the applied pH electrodes were not sterilisable.

During operation, the new medium circuit proved to be high reliable and sterile during application. More than 10 experiments were performed in combination with the Optimaix 3D Sponge1 without using antibiotics and no contaminations were observed. Even the first fibrin-based prostheses were applied without antibiotics. In literature it can be seen that similar medium circuits[153,160] were used, but they used antibiotics that was required by their system.

Peristaltic pump heads arranged in parallel, which were used in this study, allowed simultaneous operation of two bioreactors. This is an additional advantage with respect to a cost-effective operation of the tubular bioreactor system in a clinical setting.

The pump heads were combined with Marprene tubes and their flow rate was determined by the evaluation of the mass transfer of water in 30 minutes at a velocity of 20 rpms. Tubes were put into the pump heads one night prior to this investigation, so that the tubes could adapt to the pump. The mass transfer

amounted to 502 mL in 29.5 minutes. At 10 rpm, a general cell culture medium transfer rate of 8.6 mL min^{-1} was determined by the rule of proportion.

Additionally, single hand quick connectors were used to exchange the medium reservoirs faster. Thus two electrodes were necessary for one bioreactor. In this study, just two electrodes were connected to the LabBox®2. Consequently, this procedure was only possible in case of a single bioreactor application within the system.

A software (HiText™) was used to code an automatised program for the transfer of cell culture medium into the bioreactor system. A master program checked which medium circuit was selected on the graphical user interface. According to that, three subroutines were prepared for the control of medium circuit 1, 2 or both. The start-up and shut-down of the used peristaltic pumps were realised by an increasing or reducing of the pump head velocity with 0.5 rpm s^{-1}. This ensured a slow development of the flow rate.

All adaptions and improvements to Prototype III were performed to minimise outside influences, e.g. temperature decrease, unsuitable pH values or cell culture medium depletion.

Reducing negative outside influences, as shown for Prototype IV, and mimicking a natural surrounding as completely as possible increase the chance for successful tissue generation.[161,162]

5.2 Peristaltic stimulation

5.2.1 Catheters, pressure lines and sterility

Literature shows that mechanical stimulation of tubular constructs is based on pulsatile fluid flows that are generated by peristaltic pumps.[163–166] Moreover, it becomes apparent that the engineering of tubular tissue is mostly confined to vascular grafts.[163–166]

However, in this study several improvements were performed with respect to the design of the tools and components that were necessary for a physiologic peristaltic stimulation. Basic ideas from [147,148,150,151] that were presented in Chapter 4.7 were considered and served as a template **for the new mechanical stimulation procedure.**

A balloon catheter was used for the mechanical stimulation of the tubular, fibrin-based biohybrids (see Figure 22). This was done to achieve a local stimulation of the used primary smooth muscle cells that were isolated from porcine bladders (see Chapter 4.4.5). It was possible to show that the applied embolectomy catheter provided with a flexible guide wire, that was used by [147,150,151], was not useful for further application. This guide wire was unsuitable for the forwarding of the catheter. The distance between the attachment point at the linear actuator and the access to the bioreactor (see Figure 18) was so long that it lead to a sagging of the guide wire. In some cases, this resulted in curls in the wire due to the compression, when the catheter was pushed in toward the bioreactor. Additionally, it turned out that the balloon at the tip was too fragile. This balloon consisted of a thin layer of silicone. **New requirements specifying a rigid guidance and a suitable balloon material were defined.**

A kyphoplasty balloon catheter (Allevo Joline) showed the most suitable characteristics with a rigid guidance and a strong balloon made out of polyurethane. Normally, these catheters are applied for the reconstruction of vertebras, so that the balloons are extremely robust.[167–169]

The system for the inflation of the catheter was redesigned. Inflation of the catheter was reproducible with a peristaltic pump[147,148], but the period of time was long (about 20 seconds). Moreover when, peristaltic pumps were used, the catheter was filled in a pulsatile manner, which was not desired. A syringe pump replaced the peristaltic pump to achieve a constant, highly precise, accurate and

fast filling of the catheter (7.2-19.2 seconds for 150-400 µL). Nevertheless, the speed can be increased further.

The SyrDos syringe pump was operated with a stepper motor, where the volume of the attached syringe was divided into 48,000 single steps. For the characterisation, a HiText™ program was coded to transfer 1 mL of water. Then, a 1 mL syringe was attached to the pump and the transferred volume was determined by weighing three samples with an analytical scale. It was assumed that water has a density of 1 g cm^{-3}. Table 10 shows the results of the weighing procedure.

Table 10: Evaluation of the volume transferred by the SyrDos with 1 mL syringe cylinder attached.

Trial [n]	Weight [g]
1	0.9936
2	0.9946
3	0.9938

The average volume transferred was 0.994 mL. Thus, the deviation from the desired volume was 0.6% (0.006 mL).

Figure 25 illustrates the pressure line for the inflation of the kyphoplasty balloon catheter. Central elements were a syringe pump, a pressure sensor, a reservoir and a kyphoplasty catheter. Accessory parts, like connectors, adapters for the LUER connection, fittings etc. were obtained from the BESTA-Technik GmbH and matched the chosen tube material. The tube or capillary for the connection of the components was gained from an HPLC starter kit and had an inner diameter of 0.5 mm. This tube was chosen because of its pressure resistance, and small inner diameter and volume.

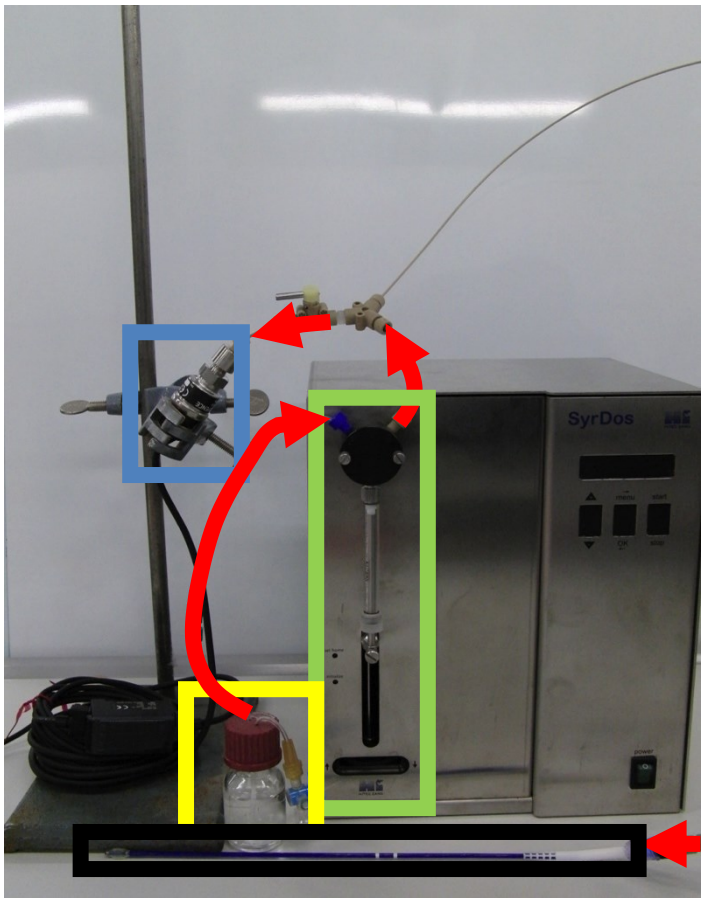

Figure 25: Pressure line (red arrows) with a SyrDos syringe pump (green) for the deflation of a balloon catheter (black). A reservoir (yellow), filled with distilled water, was attached to a pressure sensor (blue) and to the pressure line.[6]

Prior to each experiment, the water used to expand the catheter was degased and the pressure line was flushed several times to remove air bubbles. Flushing and filling of the pressure line was managed via program (“Schlauchs.”) that was integrated in the graphical user interface (see Chapter 5.1.1).

To characterise and map the deflation of the catheter, a HiText™ program was written. This was necessary to determine the diameter of the catheter required for different filling volumes that were added by the SyrDos. The pressure was evaluated in the pressure line. Two laser sensors were added that determined the diameter of the balloon catheter. The transparent catheter was made visible for the laser sensors with talcum powder. The distance of the sensors to the balloon was determined by triangulation methods. Figure 26 shows the measurement setup that was developed in the lab for cell biophysics at the Aachen, University of Applied Sciences.

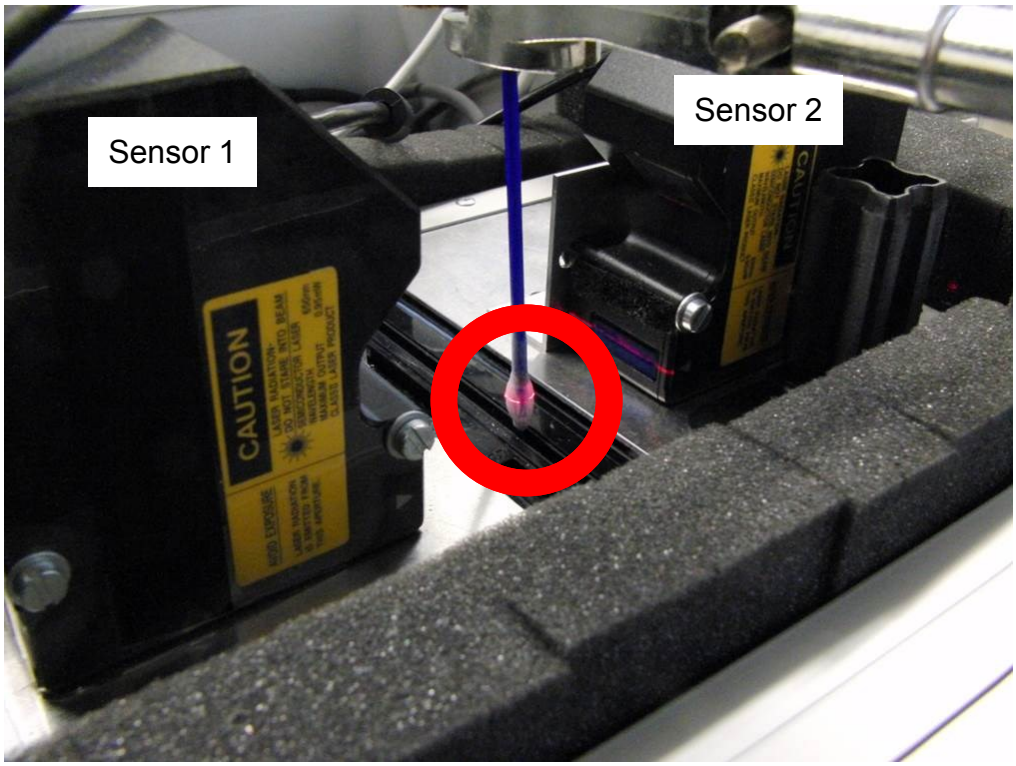

Figure 26: Measurement of the catheter diameter (red circle) with two laser sensors by means of laser triangulation.[6]

Figure 27 illustrates the development of the shape of the balloon during the filling procedure from left to right. It can be seen, the more volume was added, the more spherical the balloon became.

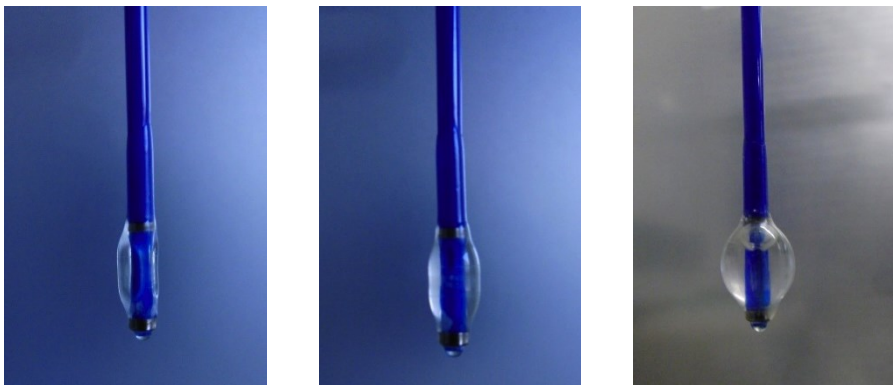

Figure 27: Filling process of a kyphoplasty balloon catheter. The diameter of the (blue) pole is 3 mm.[6]

The catheter was expanded gradually in steps of 20 µL to reach 300 µL (n=4). Diameters were read out from the Keyence user interface. Figure 28 shows a nonlinear dependence between the filling volume and the pressure in the PEEK tube system from the expansion and deflation of the catheter that was used for the peristaltic stimulation of tubular tissue matrices. The pressure is related to different catheter filling volumes.

Figure 29 illustrates the catheter filling volume versus to the measured balloon diameter. The line of best-fit was determined to be a straight line with:

$$balloon\ diameter\ [mm] = 0.0107x + 5.5938 \quad (7)$$

and a correlation coefficient (r^2) of 0.995.

The dependence on the expansion and the resulting stress on the prostheses were based on a luminal diameter of 6 mm, which was the same for collagen and fibrin-based prostheses. The following equation was used to determine the applied strain:

$$strain\ [\%] = \frac{x_i - d_i}{d_i} \cdot 100 \quad (8)$$

with:

d_i: luminal diameter (6 mm)

x_i: measured catheter diameter [mm]

In this study, a mechanical stress level of 20% was applied to all fibrin-based biohybrids. Regarding the relation between the catheter filling volume and diameter, a volume of 150 µL was required. The program with the syringe pump achieved 150 µL as catheter filling volume. Further, there was a radially directed reduction of the strain level, due to the thickness of the prostheses. Thus, the strain was reduced by 3.3%, when the diameter increased by 1 mm.

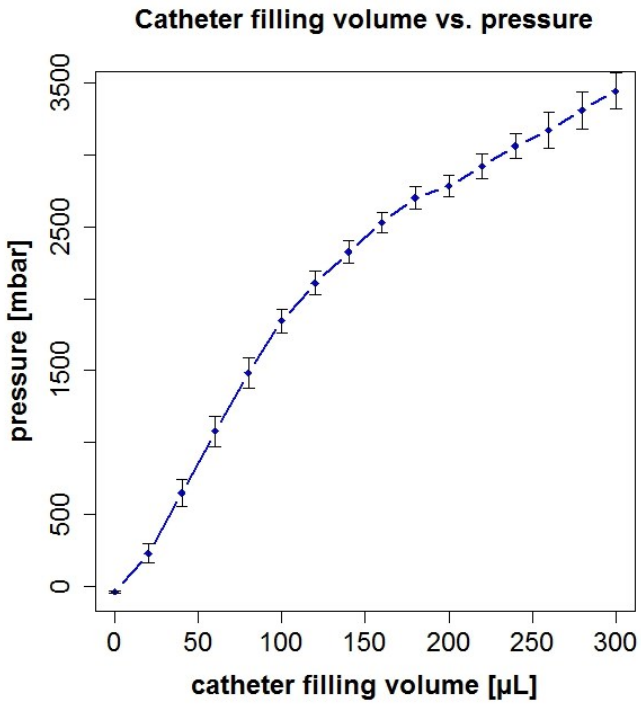

Figure 28: Catheter filling volume vs. pressure in the tube system for the expansion and deflation of the catheter.[6]

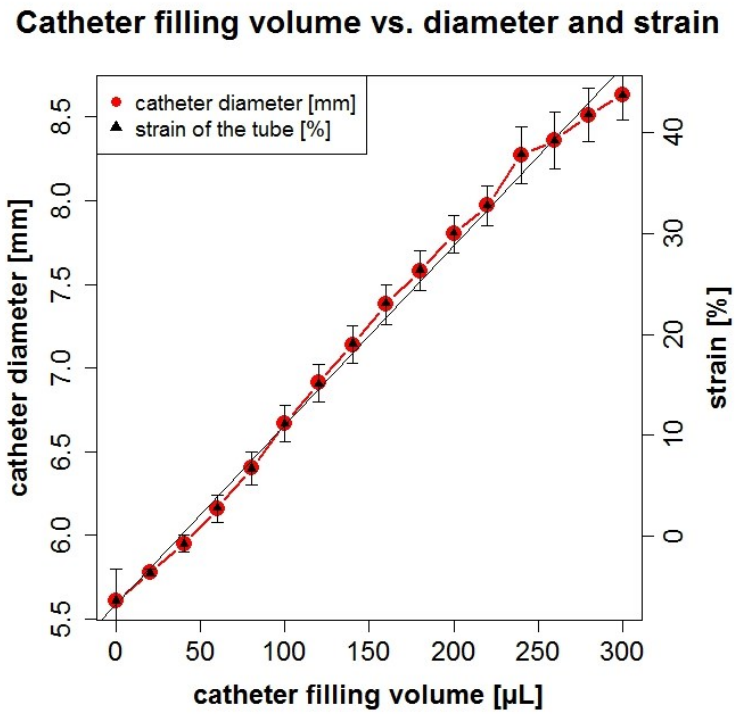

Figure 29: Catheter filling volume vs. diameter and strain. The basic luminal diameter of the prostheses was 6 mm.[6]

An improved component was used to ensure sterile access of the catheter to the bioreactor system and was called “contamination guard”. Figure 30 shows the contamination guard that was attached by a silicone tube to the bioreactor’s piston (see Figure 20). The distance between the bioreactor and the contamination guard was kept as short as possible.

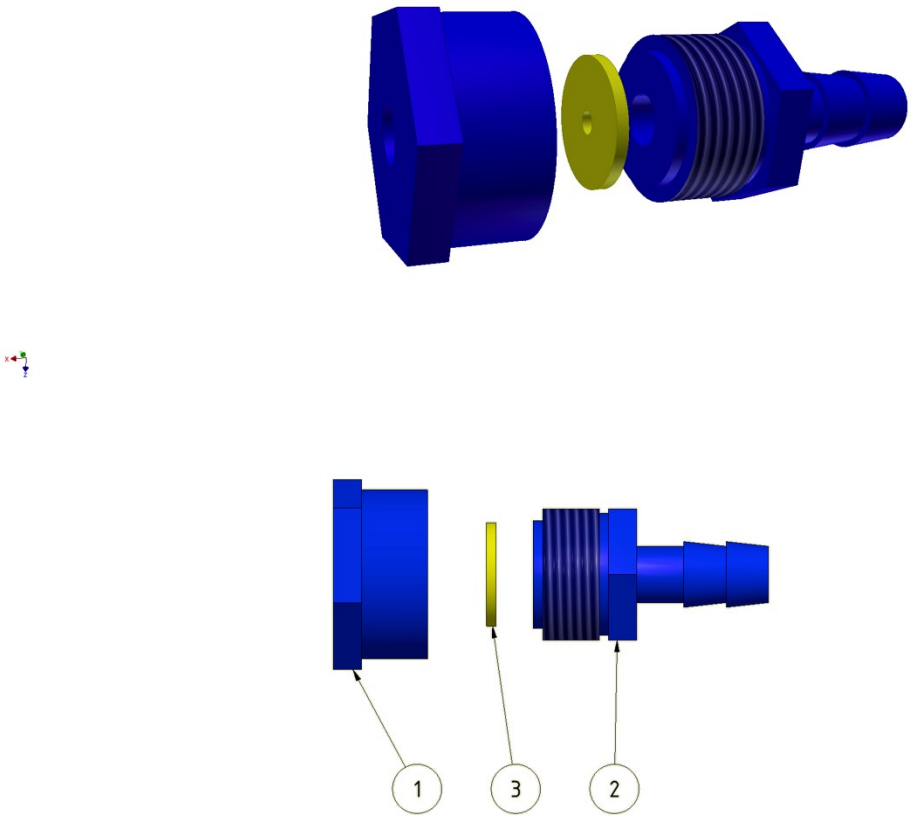

Figure 30: “Contamination guard” for sterile access of the kyphoplasty balloon catheter to the bioreactor, consisting of a septum (3) and two clamping components (1) and (2).[6]

This contamination guard consisted of a PTFE-silicone-PTFE septum (3) and two components (1) and (2) that were screwed together. The septum had a central hole of 2 mm that was stamped and that allowed the catheter to be introduced and slide smoothly. The hexagonal shape of components (1) and (2) allowed easy assembling and disassembling with a screw-wrench. These two parts clamped the septum tightly.

The whole bioreactor, the medium circulation and the inlet for the kyphoplasty balloon catheter provide a completely sealed and leakage-free system. This contamination guard had the advantage that there was no opening to the bioreactor. In comparison to the unit using PBS flushing for the removal of contaminants (see Chapter 4.7) it was more save, because there was no need to remove contaminating particles. Cost effectiveness was increased, because there was no PBS needed during the stimulation, which removed contaminating particles. Moreover, it was possible to reduce the application of antibiotics. **Test series revealed that an antibiotic-free application of the bioreactor was successful.**

In literature, there was no similar device was found. **This is due to the novelty of the system that is presented in this study.** A further improvement of this device could be achieved by adding a thread to the contamination guard and the piston at the bioreactor, leading to an enhanced, shorter and a stable connection.

Another important component for the presented mechanical stimulation/training is a linear actuator, which moves the catheter forward and backwards. Figure 31 depicts the linear actuator (1) that was attached to an engine mount (2), which was fixed with a base plate (3) in the incubator.[147,148] It was improved including modified with additional components (4) and (5) for the fixation of the kyphoplasty catheter. A covering plate above the stepping motor allowed additional guidance of the catheter and avoided a sticking/clamping of the catheter at the engine mount. Moreover, a bar (6) was attached and provided with a limit switch (not depicted) to calibrate the home position for the linear actuator. This device is important for regular calibration during the application.

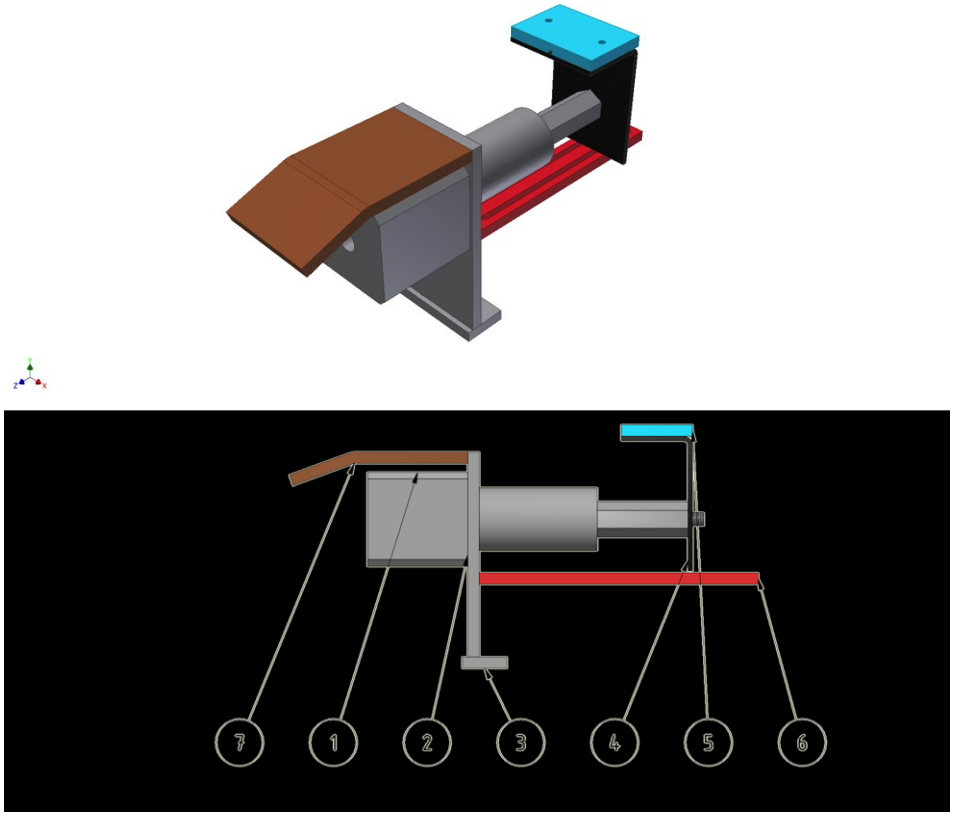

Figure 31: A linear actuator (1) was attached to an engine mount (2) on a base plate (3).[147] The kyphoplasty catheter was fixed with a clamping arrangement (4) and (5) that was attached to the linear actuator. A bar (6) was used for the installation of a limit switch and a covering plate (7) as an additional supporting area for the catheter.[6]

5.2.2 Software

The software that was used for the peristaltic stimulation was coded in HiText™ and consisted of a master program (“Peristaltik”) and 6 subroutines.

Routine sequences in the master program controlled the linear actuator and catheter expansion as well as the calibration steps. The program began with a start-up, activating subroutines, bringing the linear actuator and the catheter into the starting conditions. The catheter was driven slowly with 0.2 mm s^{-1} into the home position and the catheter was deflated gradually in steps of 20 µL, resulting in neutral pressure in the pressure line.

Next, the catheter was moved forward by the distance and with the velocity that were adjusted on the graphical user interface (see Chapter 5.1.1). The path length was 45 mm and the velocity was 2.5 mm s^{-1} for fibrin-based prostheses. Subsequently, the catheter was expanded following a sigmoidal filling capacity.

$$filling\ volume\ [\mu L] = \frac{G}{1+e^{-k\cdot G\cdot\left(\left(\frac{\Delta t}{86400}\right)-C\right.}}$$

G: maximal filling volume [µL]
k: slope
C: day of the turning point [d]
Δt: duration of the peristaltic stimulation [s]

(9)

A sigmoidal adaption of the catheter filling volume lead to a slow increase of the exerted mechanical stress on the prostheses. In any experiment with a peristaltic stimulation, the slope (*k*) was set to 0.005, the inflection point to the third day and the maximal filling volume to 150 µL, which corresponds to a strain of 20%. Figure 32 shows the relation of the catheter filling volume from the time of incubation and the resulting diameter of the kyphoplasty balloon catheter. This diameter lead to specific mechanical strains for prostheses with an initial diameter of 6 mm.

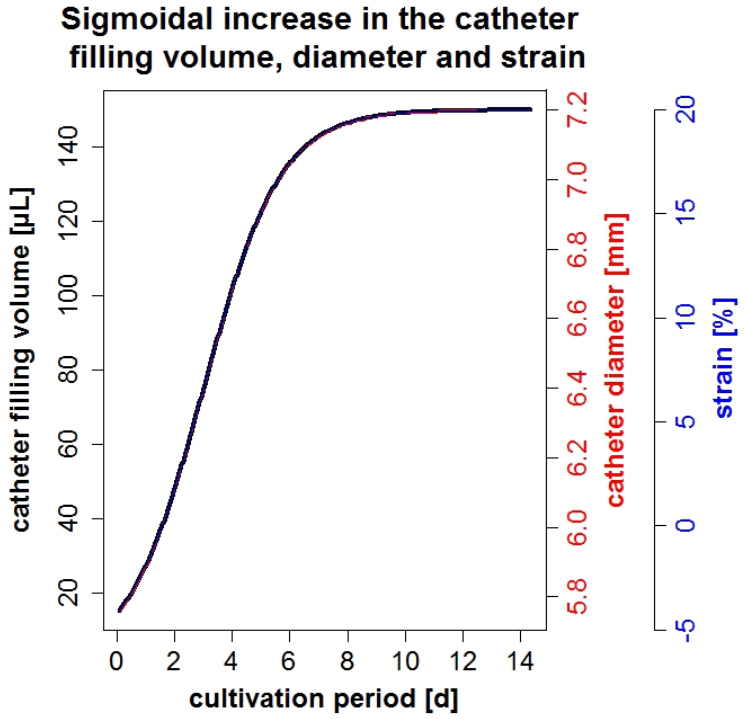

Figure 32: Sigmoidal filling of the kyphoplasty catheter followed during incubation. It results in a maximum diameter of 7.2 mm and 20% strain.[6]

Subroutines were also used to monitor the system. In case of failure, e.g. pressures exceeding 8 bar or a delay time of more than 20 minutes, an emergency

sequence was initiated. Then, the catheter was deflated gradually in steps of 20 µL until neutral pressure was reached and was driven into the starting position. The procedure was similar to the start-up sequence. Subsequently, it became possible to begin the routine sequence again to continue mechanical conditioning. Regular calibrations were performed in the course of incubation, where the pressure line and the position of the linear actuator were adjusted to intervals of 20 stimulations. In the end, a mean stimulation frequency of 0.015 Hz was achieved for mechanically stimulated fibrin-based prostheses. Figure 33 shows a sample of a mechanical stressed prosthesis, where a kyphoplasty catheter was pulled through the lumen of the tubular structure. It can be seen that the stimulation lead to a weak ablation of fibrin at the contact surface. Nevertheless, this did not result in a separation of the fibrin-matrix and PVDF mesh or in a negative influence for surrounding cells.

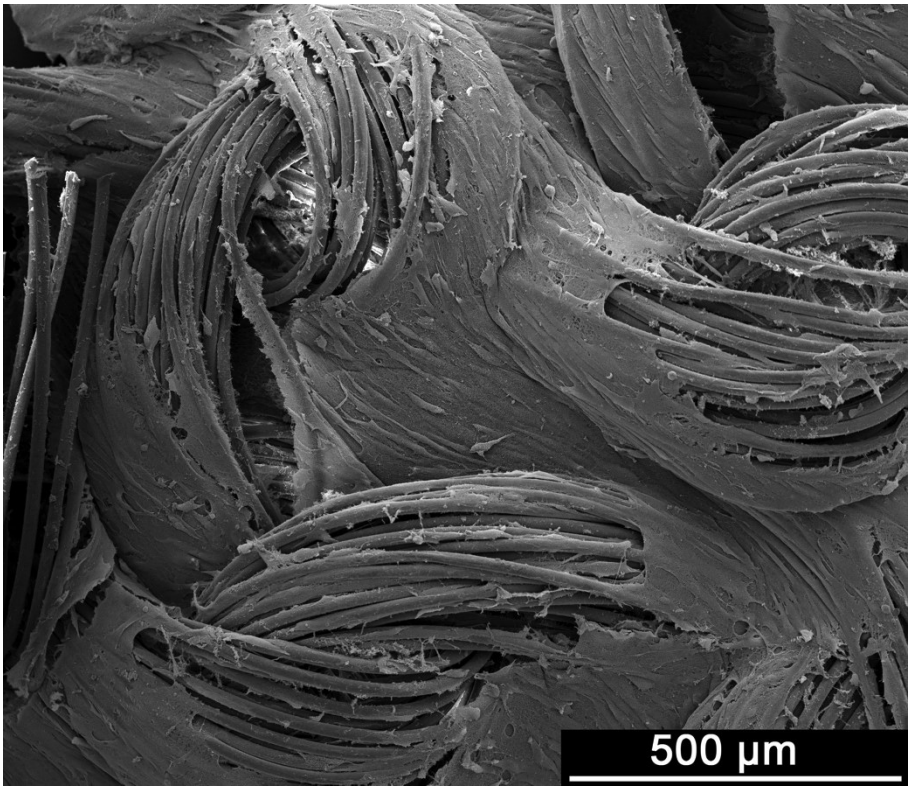

Figure 33: Luminal surface of a fibrin-based prosthesis that was stimulated for 1 week with a kyphoplasty catheter.[6]

5.2.3 First test series

First tests on the catheter in combination with cells were done with an established cell line (C2C12 myoblasts), primary smooth muscle cells and the Optimaix 3D

Sponge1. Additionally, a combination with fibrin and Optimaix 3D Sponge1 was tested.

Table 11 summarizes the experimental parameters and differences with respect to cell types, fibrin applications and durations of the experiments and the resulting quantity of stimulations. Control samples were treated equally to mechanically stressed (trained) biohybrids disregarding the application of the catheter.

Table 11: Experimental setup to test a mechanical stimulation with a kyphoplasty catheter. An established cell line (C2C12) and primary smooth muscle cells were applied on the Optimaix 3D Sponge1 with and without fibrin.

Experiment	Cellcount	Duration	Cell culture medium (see Chapter 4.4.2)
Fibrin + SMCs + Optimaix 3D Sponge1	5000 cells μL^{-1} in 1 mL	6 days 17 hours/ 8057 stimulations	medium III
C2C12 + Optimaix 3D Sponge1	5000 cells μL^{-1} in 1 mL	9 days 18 hours/ 18069 stimulations	medium II

Optimaix 3D sponge1 fragments with a length of 1 cm were seeded with 1 mL cell suspension using the drop-on procedure (see Chapter 4.6.1.1). On each sample, $5 \bullet 10^6$ cells were applied. Primary smooth muscle cells were seeded with fibrin to fix the cells inside the sponge matrix. The application of fibrin is explained in Chapter 4.6.2.1.

Figure 34 shows the experimental setup based on a Schott Duran bottle (GL 45). It was equipped with the contamination guard to introduce the catheter into the bottle that contained cell culture medium II or III (80 mL). Additionally, there was a silicone tube covered with a sterile filter to allow gas exchange with the ambient air in the incubator.

The catheter was introduced into the bottle and the seeded scaffolds were placed at the catheter tip before the periodical expansion and deflation started. In this experiment, the catheter was expanded to about 10 mm with a filling volume of 400 µL. It was not moved throughout the seeded collagen scaffold. Thus, mechanical stress was applied exclusively in circular direction. The whole setup was placed inside the incubator at 37 °C and 5% CO_2.

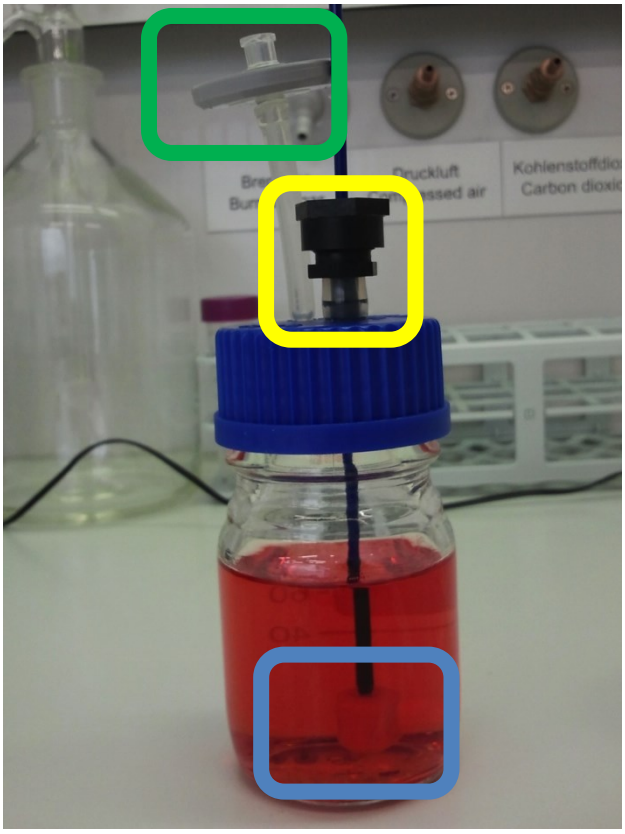

Figure 34: Experimental setup for the application of circular mechanical stress on cells that were seeded onto the Optimaix 3D Sponge1 (blue). A kyphoplasty catheter was introduced into a glass bottle which the screw cap was equipped with the contamination guard (yellow) and an opening to the outside (green).[6]

Samples were fixed in Carnoy's fluid and prepared for further histological analysis (see Chapter 4.5). Scanning electron microscopic pictures were prepared to analyse the effect of the mechanical stimulation on cellular orientation.

The following scanning electron microscopic pictures (Figure 35 and Figure 36) indicate the effect on circularly stretched tubular structures that were seeded with different cell types. Figure 35 A) and Figure 36 A) show unstimulated (untrained) samples i.e. samples that were not exposed to mechanical stress (training). Primary smooth muscle cells (Figure 35 A)) and C2C12 myoblasts (Figure 36 A)) were distributed homogeneously on the outer surface of the tubular, sponge-like collagen scaffold. In contrast to that, it can be seen in Figure 35 B) and Figure 36 B) that the cells preferred a certain orientation. In both cases, this orientation was circular around the tubular structure. These results are comparable to [74,80], where **the stretching of a three dimensional structure lead to a cellular orientation towards the applied strain.**

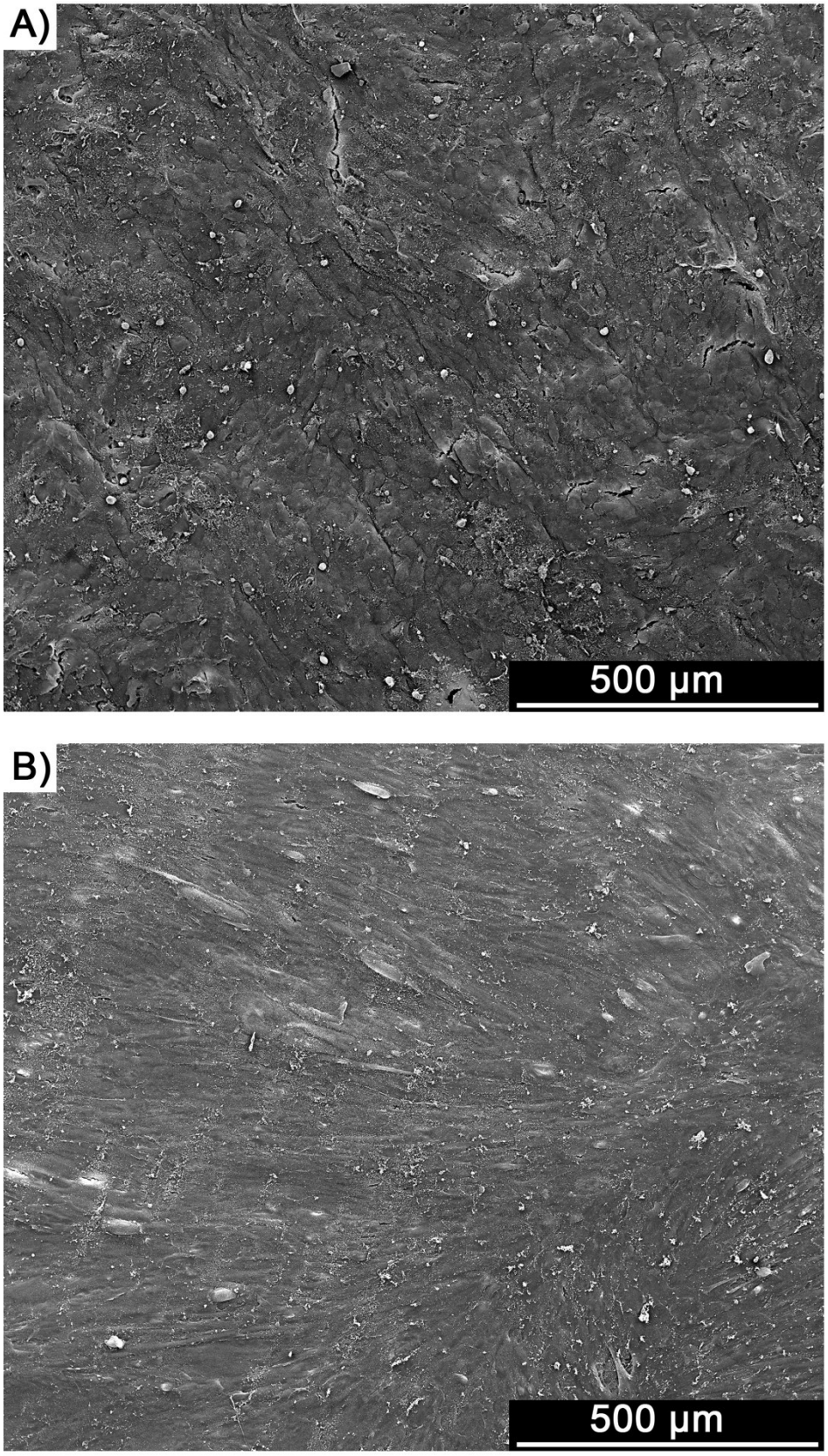

Figure 35: Scanning electron microscopic pictures of mechanically unstimulated A) and stimulated B) porcine primary smooth muscle cells that were seeded onto the Optimaix 3D Sponge1.[6]

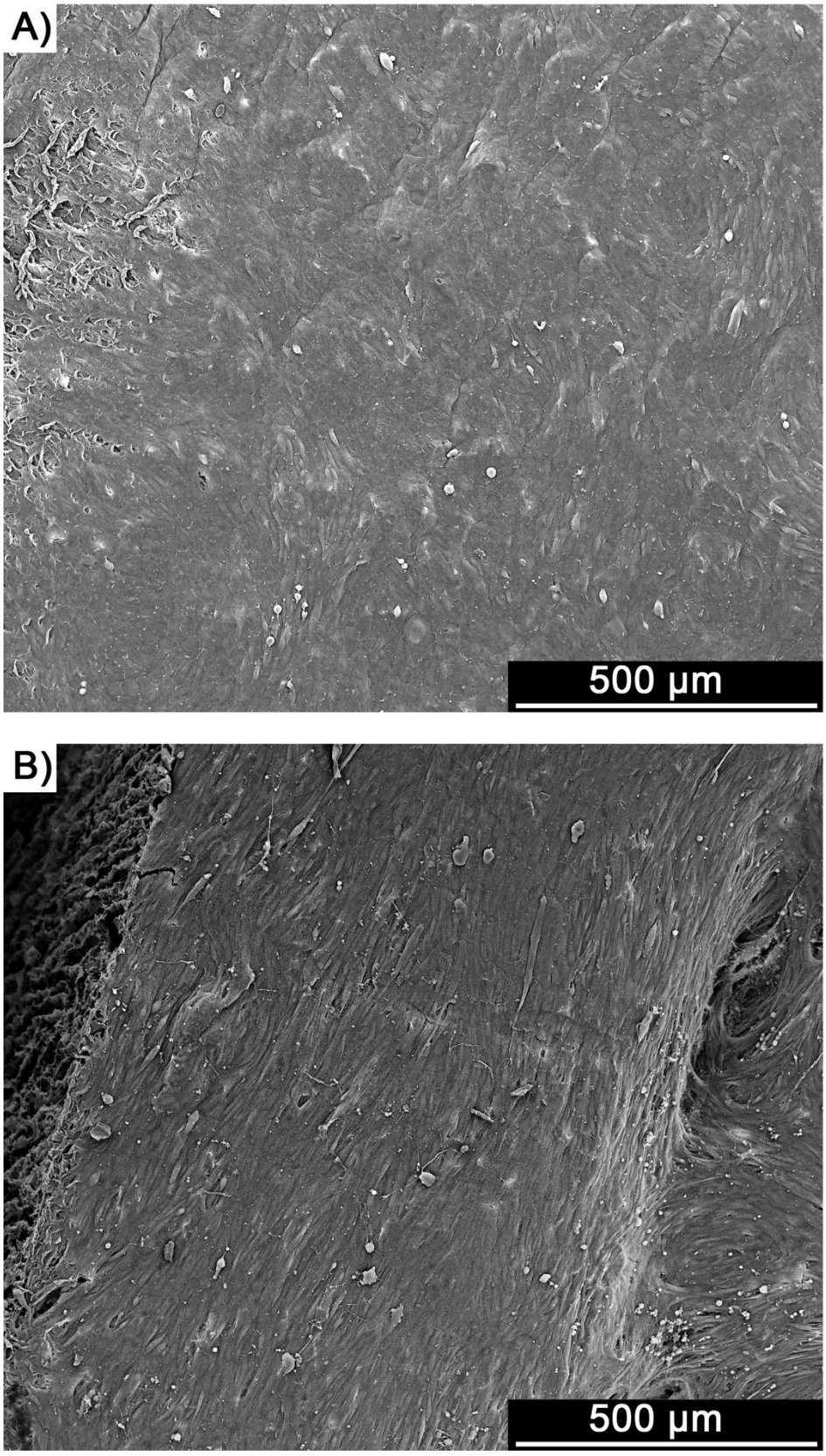

Figure 36: Scanning electron microscopic pictures of mechanically unstimulated A) and stimulated B) C2C12 myoblasts that were seeded onto the Optimaix 3D Sponge1.[6]

5.3 Long-term stability of the bioreactor system

Long-term stability of the bioreactor system was monitored during the use of Bioreactor Prototype IV for 1 week (n=4) and for 2 weeks (n=4). The incubation system was started prior to cell seeding (see Chapter 0) and was initiated at the same time as temperature and CO_2 system. Both were part of the start-up section (see Chapter 5.1.1) displayed on the graphical user interface.
All data were recorded with 1 Hz from the beginning of the experiment and exported in comma-separated values (CSV) at the end of the incubation phase.
Table 12 shows the results of the evaluation as mean values with their standard deviation (SD). Additionally, the deviation is given in %.

Table 12: Evaluation of the incubation parameters in long-term experiments for 1 week (n=4) and 2 weeks (n=4) for the application of Prototype IV in the incubation system, with SD = standard deviation.

	1 week			2 weeks		
	Mean	SD	Deviation [%]	Mean	SD	Deviation [%]
Temperature in the incubator [°C]	37.0	0.2	0.4	36.9	0.9	2.4
Temperature in the medium [°C]	36.9	0.2	0.6	36.9	0.7	1.8
pH in the cell culture medium	7.5	0.3	3.4	7.6	0.2	3.2
CO_2 [%]	5.0	0.3	6.0	5.0	0.30	6.0

It can be concluded that the incubation system was working reliably. The temperature inside the incubator and media reservoirs were nearly identical and differed from the nominal value (37 °C) by less than 1 °C (≤ 2.4%). This was caused by the fact that the media reservoirs were placed inside the incubator. All sensors (Pt100) were calibrated at the same time and showed just little variations. Greater temperature differences in experiments lasting 2 weeks were caused by a maloperation. In a single case, the temperature dropped subsequently to a planned exchange of medium reservoirs. A telemetric alert sent by the system via

e-mail or short message could be used in the future to avoid such incidents. LabVision® is able to detect if parameters deviate from a defined range. In emergency cases, the system could contact the operator.

Furthermore, pH values were kept in the range of 7.4 with deviations of less than 3.4%. This range could be narrowed in the future by using new electrodes that have a shorter response time.

CO_2 concentrations were in the range of 5.0 ± 0.3 in all experiments. A 6% deviation happened as the daily sampling was performed. Sampling involved opening the incubator completely, which changed the 5% CO_2 concentration and consequently lead to greater standard deviations. Nevertheless, it could be shown that the correction time required to get back to 5% was in the range of 10 minutes.[148]

Besides that, all other programs (mechanical stimulation, cellular distribution or the start-up of the system) were functioning properly.

5.4 Rotation unit and cellular distribution

To distribute seeded cells homogeneously, it was required that the bioreactor was swayed around its longitudinal axis. The rotation unit[147] was redesigned to enable increased rotation angles from 270° to 380°.

Figure 37 depicts the rotation unit with an attached bioreactor is attached. The support (blue) was connected to a stepper motor. This bearing was an improvement to the previous version because it made operation more comfortable. It became easier to place the bioreactor into this unit, even when tubes were connected. Additionally, the increased bearing area lead to a more stable fixation of the bioreactor.

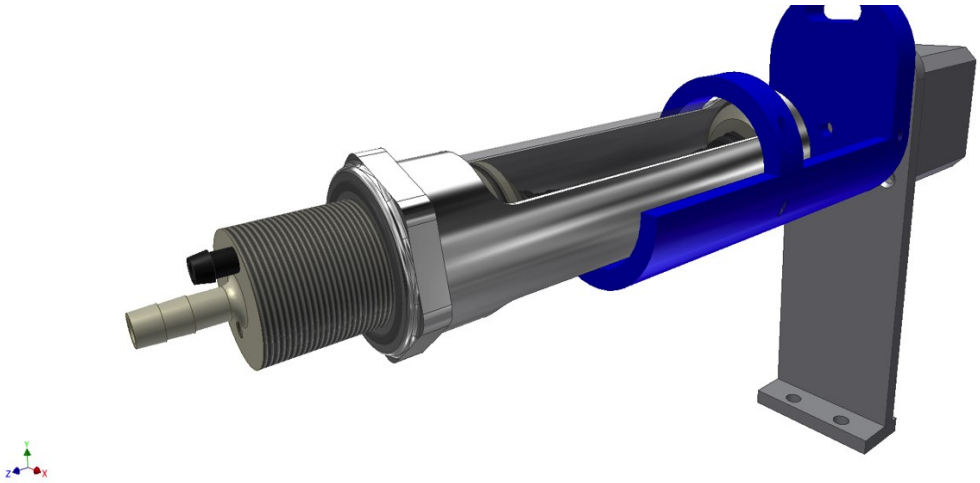

Figure 37: Redesigned rotation unit with an improved bearing for a homogeneous distribution of cells on Optimaix 3D Sponge1 scaffolds.[6]

It was possible to demonstrate that this rotation unit lead to a homogeneous distribution of applied cells. Figure 38 shows a DAPI staining photographed with a fluorescence microscope. NIH-3T3 fibroblasts were applied on the Optimaix 3D Sponge1 scaffolds and incubated for 21 days. This incubation process resulted in a circular, homogeneous distribution of the cells on the outer surface of the scaffold material.

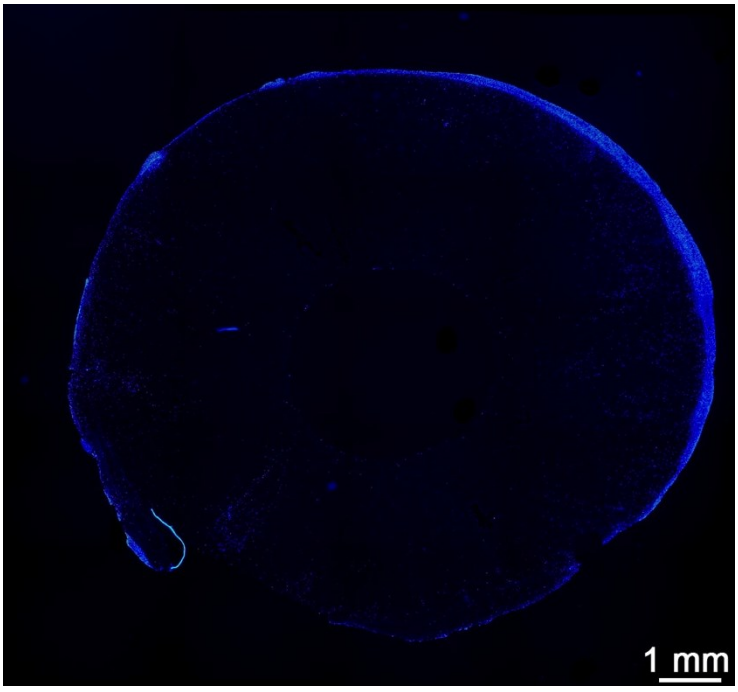

Figure 38: DAPI staining of NIH-3T3 fibroblasts applied on Optimaix 3D Sponge1 and incubated for 21 days.[6]

5.5 Isolation and cultivation of primary smooth muscle cells

The isolation of primary smooth muscle cells was performed according to the protocol that was described in Chapter 4.4.5. This protocol was applied for all fibrin-based tubular constructs. Prepared T75 cell culture flasks were put into the cell culture incubator at 37 °C, 5% CO_2 and 100% humidity and were not moved for a week. Thus, tissue fragments were not displaced, resulting in less stress and violent detachment of cells. Cells grew out of tissue fragments and attached to the cell culture flasks. After 1 week, cell culture medium I was replaced by cell culture medium II, which did not contain antibiotics (see Chapter 4.4.2). After that, the cell culture medium was changed regularly every 4 to 5 days.

Cell clusters grew circularly and got denser in their centre. When these centres started to get necrotic and when contact inhibition started, the cells were sub-cultivated to reduce cellular density. For fibrin-based experiments, cells were passaged into T175 flasks in passage 1 and into T500 flasks in passage 2. Passage 3 was 7 times used and passage 5 only once for preparation of fibrin-based prostheses (n=8).

Viability of the cells was determined with a BioRad cell counter TC20™. **Mean cell viability was determined to be 97% and the average time from cell isolation to the application in a prosthesis was 57 ± 17 days.**

Cell viability was greater than 90% in all cases, which shows the cells were treated gently and compliant to the rules of cell culture technologies. Nevertheless, it became apparent that the proliferation of the cells isolated from different pigs differed, which resulted in preparation periods in the range of 1 to 2 months. This period of time was required from the isolation of the cells to the application in the Bioreactor Prototype IV in order to achieve high initial cell counts in the biohybrids.

5.6 Scaffold materials – application and characterisation

5.6.1 Optimaix 3D Sponge1

Optimaix 3D Sponge1 was analysed with respect to its biocompatibility, pore sizes and suitability for cell culture application. To achieve that, different cell types (NIH 3T3 fibroblast, Urotsa, C2C12) were applied on the scaffold with varying seeding procedures. Co-cultivations were tested, using C2C12 myoblasts and Urotsa cells. Both proved the bioreactors performance and suitability. Pore sizes were analysed by means of scanning electron microscopy and a specially coded LabVIEW program that measures pores randomly selected by the operator.

In addition to the results presented in Chapter 4.6.1, it could be shown, that tubular Optimaix 3D Sponge1 behaves similar to planar Optimaix 3D. To test that, Optimaix 3D was implanted into the porcine bladder wall, between the serosa and the smooth muscle. Test animals were sacrificed after 12, 16 and 26 weeks and were inter-individually compared. The results showed decreasing amounts of intact collagen scaffold between 12 and 16 weeks and after 26 weeks there was no scaffold detectable. Due to the fact, that there were no negative side effects e.g. inflammation or encapsulation, it was concluded that this configuration is biocompatible in vivo in pigs, too.

5.6.1.1 Optimaix 3D Sponge1 dimensions

For scanning electron microscopy, collagen scaffolds were cut into sections as depicted in Figure 39. Scaffolds were cut with microtome blades (Feather), which allowed to prepare adequate cutting areas. The use of scissors and scalpels had lead to squeezed materials and surfaces, which rendered the sample useless. The analysed fragments had a thickness of about 1-2 mm and were fixed on specimen mounts. Pore sizes were measured on the outer surface (n=4) and inner matrix. To analyse pores inside the sponge, two additional sections were prepared: the modified surfaces (n=3), where just the top (outer) layers were removed, and central surfaces (n=4) in the middle of the collagen sponge. Besides that, samples were set showing the luminal surface (n=3).

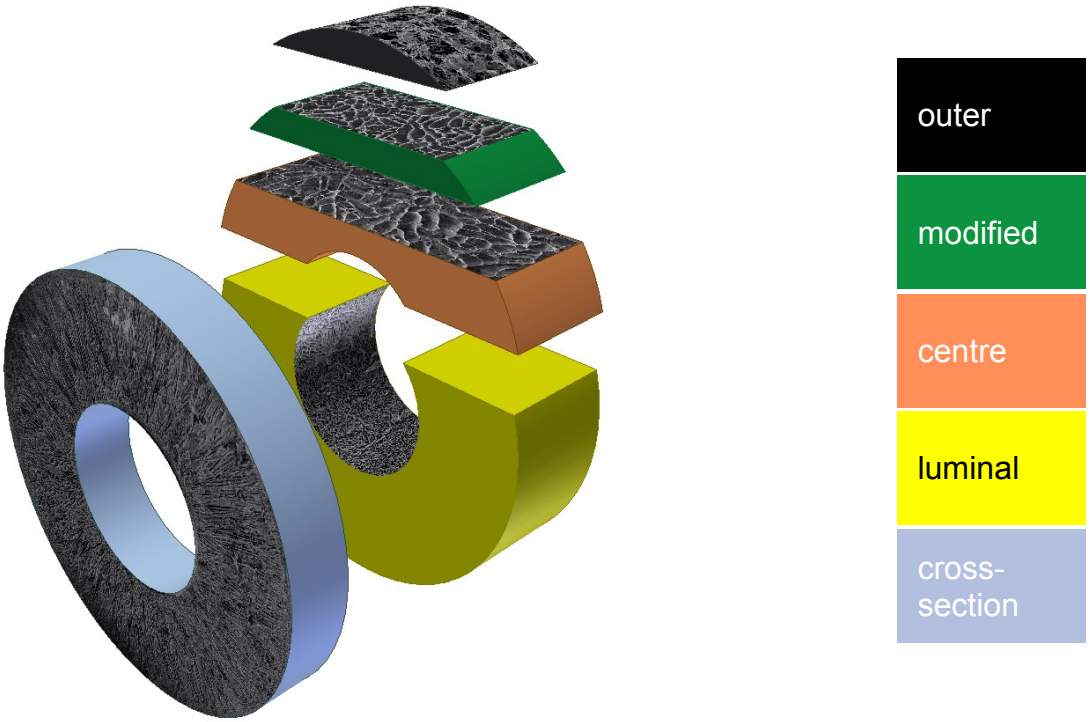

Figure 39: Schematic illustration of prepared sections for the scanning electron microscope to determine pore sizes. Different colours code for different surface positions that were analysed.[6]

A LabVIEW program was designed, which was able to load scanning electron microscopic pictures and enabled the definition of regions of interest (n=20) by hand of the operator. The program analysed the size of encircled particles or pores. The data were exported as a cross-sectional surface area into an EXCEL sheet and statistically analysed. Figure 40 and Table 13 summarize pore sizes on and in Optimaix 3D Sponge1.

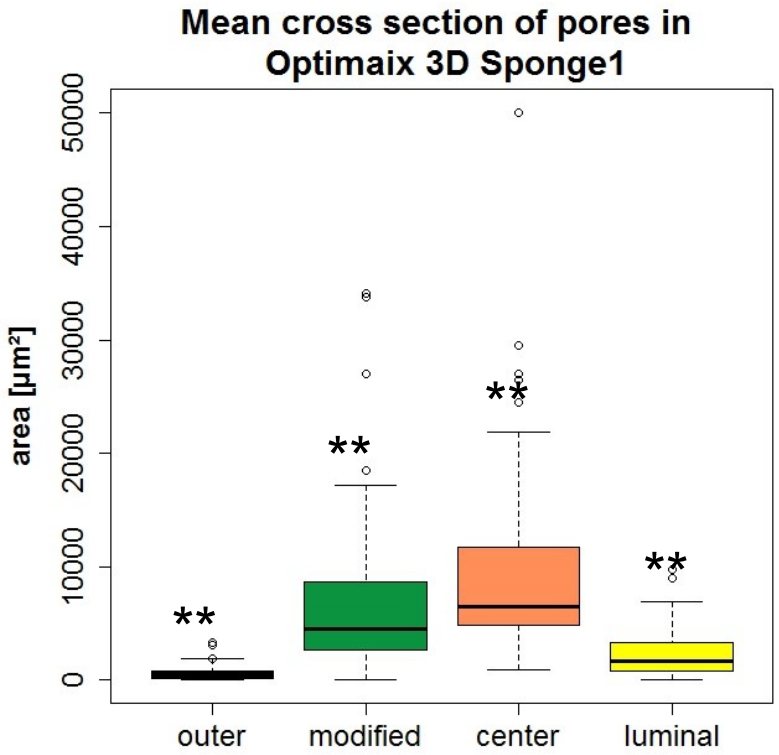

Figure 40: Evaluation of pore sizes of Optimaix 3D Sponge1. Colours correspond to Figure 39. Differences between any two groups are significant (p<<0.01).[6]

Table 13: Cross-sectional surface areas of pores detected in and on the Optimaix 3D Sponge1.

	Outer	Modified	Centre	Luminal
Mean pore size [µm²]	590	6910	9650	2350
Standard deviation	650	7210	7790	2180
Median pore size [µm²]	340	4460	6440	1640

Table 13 summarizes the results that are presented in Figure 40. The table and graphical illustration show that the **pore sizes increased from the outer surface to the central matrix of the Optimaix 3D Sponge1.** On average, diameters increased from 13.6 µm to 55.4 µm and reduced to 27.4 µm at the luminal site. Moreover, high standard deviations became apparent, caused by great variations in the cross-sectional area and diameter of the pores. The boxplot illustrates several statistical outliers that had an impact on the standard deviation. Nevertheless, differences between any two segments were significant (p<<0.01).

The Optimaix 3D Sponge1 showed interconnected, radially oriented pores, but these pores do not have a constant cross-section. From the results it has to be concluded that the outer and luminal pores were smaller, which may lead to a reduced cellular penetration depth.

5.6.1.2 Application of cells to Optimaix 3D Sponge1

Cell seeding onto the collagenous Optimaix 3D Sponge1 was performed either in a drop-on or dip-in procedure (see Chapter 4.6.1.1). Provided scaffolds had a length of about 8 cm, were dry and γ-sterilised. Test series with Optimaix 3D Sponge1 in combination with the Bioreactor Prototypes III and IV were done with shortened scaffolds (4 cm). Scaffolds with an initial length of 8 cm were cut into two halves with damp heat sterilised microtome blades, which were best suitable for slicing without damaging the material.

In all cases, the bioreactor was sterilised with its components and tubes placed in an instruments tray with lid in an autoclave. Figure 41 shows both cell seeding procedures that were used to seed cells after to the fixation of the scaffold on two central fittings of the Bioreactor Prototype III and Prototype IV. Fixing the scaffold required high attention, because the dry collagen sponge tended to rupture in case of high shear stresses, caused by the cable ties. Therefore, the Optimaix 3D Sponge1 was carefully pushed over the fittings and cable ties were fixed. The cable ties were tightened slowly and carefully, while the scaffold was squeezed by hand at the position of the fitting. Compressed collagen sponges returned to their initial shape with a narrowing at the position of the cable ties, when they were wetted by cell culture medium or buffer solutions.

Figure 41 A) shows the drop-on method where an adequate amount of cell suspension was added by pipetting. It can be seen that the scaffold was fixed on both central fittings inside the bioreactor. The applied cell suspension had a concentration of $5 \bullet 10^3$-$10 \bullet 10^3$ cells μL^{-1}, which was in the range of the manufacturer's instructions ($1 \bullet 10^3$-$40 \bullet 10^3$ cells μL^{-1}).

For the dip-in procedure, the scaffold was immersed into a cell suspension with $5 \bullet 10^3$ cells μL^{-1} for 2-5 minutes. In Figure 41 B) shows that the scaffold material was attached to the bioreactor's piston (see Figure 20) on one side and to a sealed piston on the other side. The immersed fitting was sealed with a silicone plug to ensure that an undesired cell type (muscle cells) did not get into the lumen of the prosthesis.

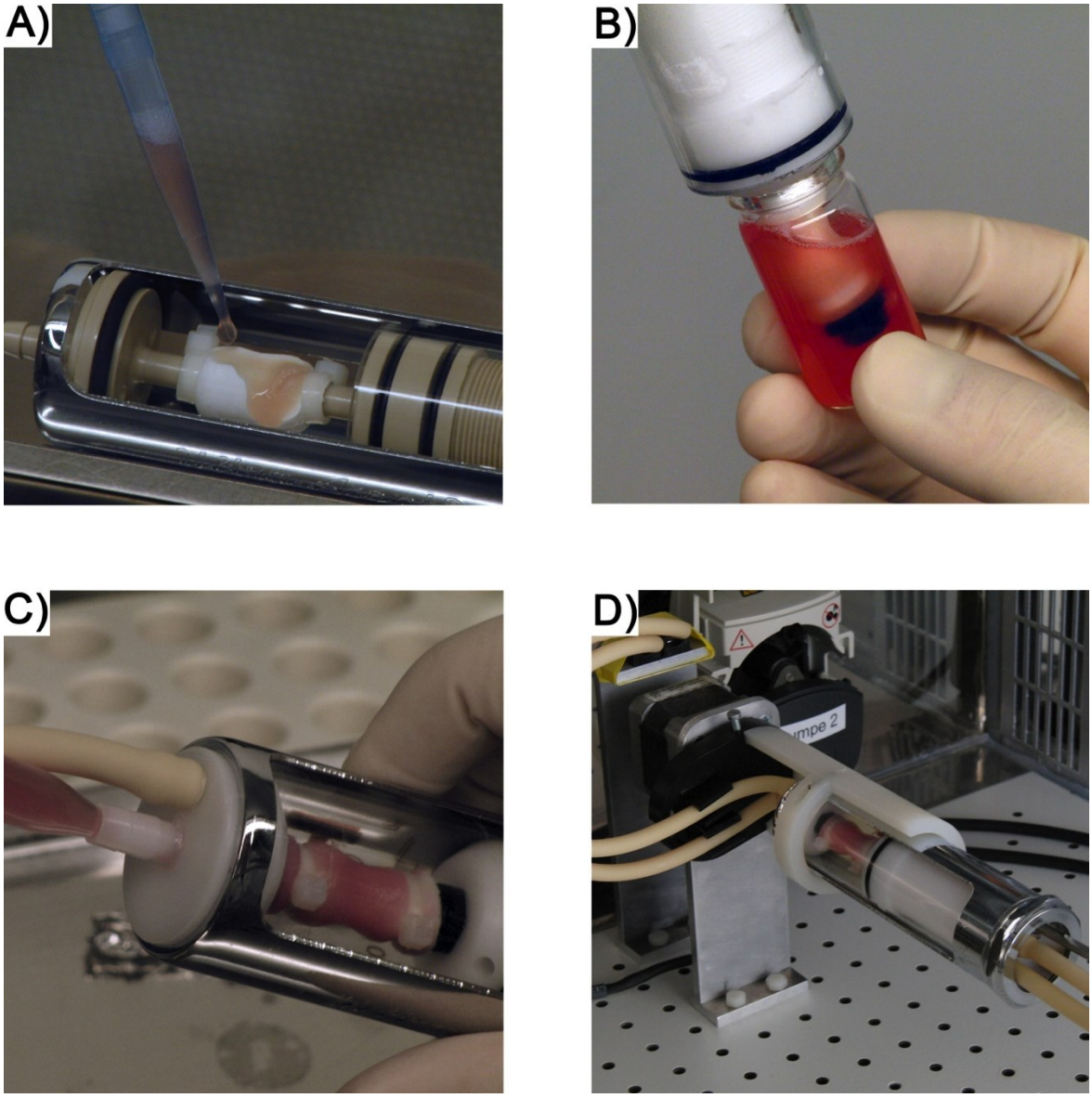

Figure 41: Seeding mechanisms for the Optimaix 3D Sponge1. The drop-on A) and dip-in B) procedure could be followed by a luminal seeding C). Homogenous cellular distribution was achieved by a rotatory unit D).[6]

The luminal seeding of epithelial cells (Urotsa) is indicated in Figure 41 C). A cell suspension with $1 \bullet 10^3$-$5 \bullet 10^3$ cells μL^{-1} was injected through the central fitting with a serological pipette. This was done slowly so that the cell suspension in the collagen matrix was not pressed out. Moreover, the tubes at the front plate and at the piston were closed after to the injection to keep the cell suspension in its position.

Then, the bioreactor was placed and fixed in a rotatory unit (see Figure 41 D)). In this study, a rotation angle of 380° at a rotating speed of 0.05 rpm was applied.

The angle of more than 360° was chosen to ensure a homogenous distribution of the cells. A smaller rotation angle might lead to the fact that the cells cannot cover the tipping point. This setup and principle were similar to the "Slow Turing Lateral Vessel" described by Freed and Vunjak-Novakovic[170] as well as the reactor presented by Sodian et al.[60], where the bioreactors were turned around their longitudinal axis. In addition to that, literature shows that dynamic cultivations lead to improved reseedings of porous materials e.g. decellularised SIS or BSM, where the penetration depth was significantly increased.[83,84] Moreover, this cellular distribution has a direct influence on the development of the tissue replacement and cannot be neglected.[58]

Experiments (n=3) were performed to investigate the period of time cells require to attach to a flat surface. It was demonstrated that this process took at least 6 hours. Primary cells were observed with the BioZero microscope to which an incubation chamber was attached. Nevertheless, long lasting rotations lead to an acidic environment for the cells. Cell metabolism leads to a pH drop in the cell culture medium and its environment. The ratio of cell culture medium referred to the cell count is significantly lower in these experiments compared to standard cultivations. This lead to a fast consumption of the medium. Therefore, a balance needed to be found between cell attachment, rotating speed and pH value.

5.6.1.3 Co-cultivation on Optimaix 3D Sponge1

A co-cultivation of at least two cell types was desired in the Bioreactor Prototypes III and IV. To that end, two independent medium circuits were established. Test series on co-cultivations were performed with C2C12 myoblasts that were seeded onto the outer scaffold and Urotsa, which were placed in the lumen of the prostheses. Independent experiments revealed that the seeding procedures were working well. It can be seen in Figure 42 that there were homogenous cell layers in the lumen and on the outer surface of the prostheses. A mixture of the cell types was not observed, because the outer surface still shows typical morphologic characteristics with spindle shaped cell bodies. Cells on the luminal surface show a cobblestone-like appearance, which is typical for epithelial tissues.

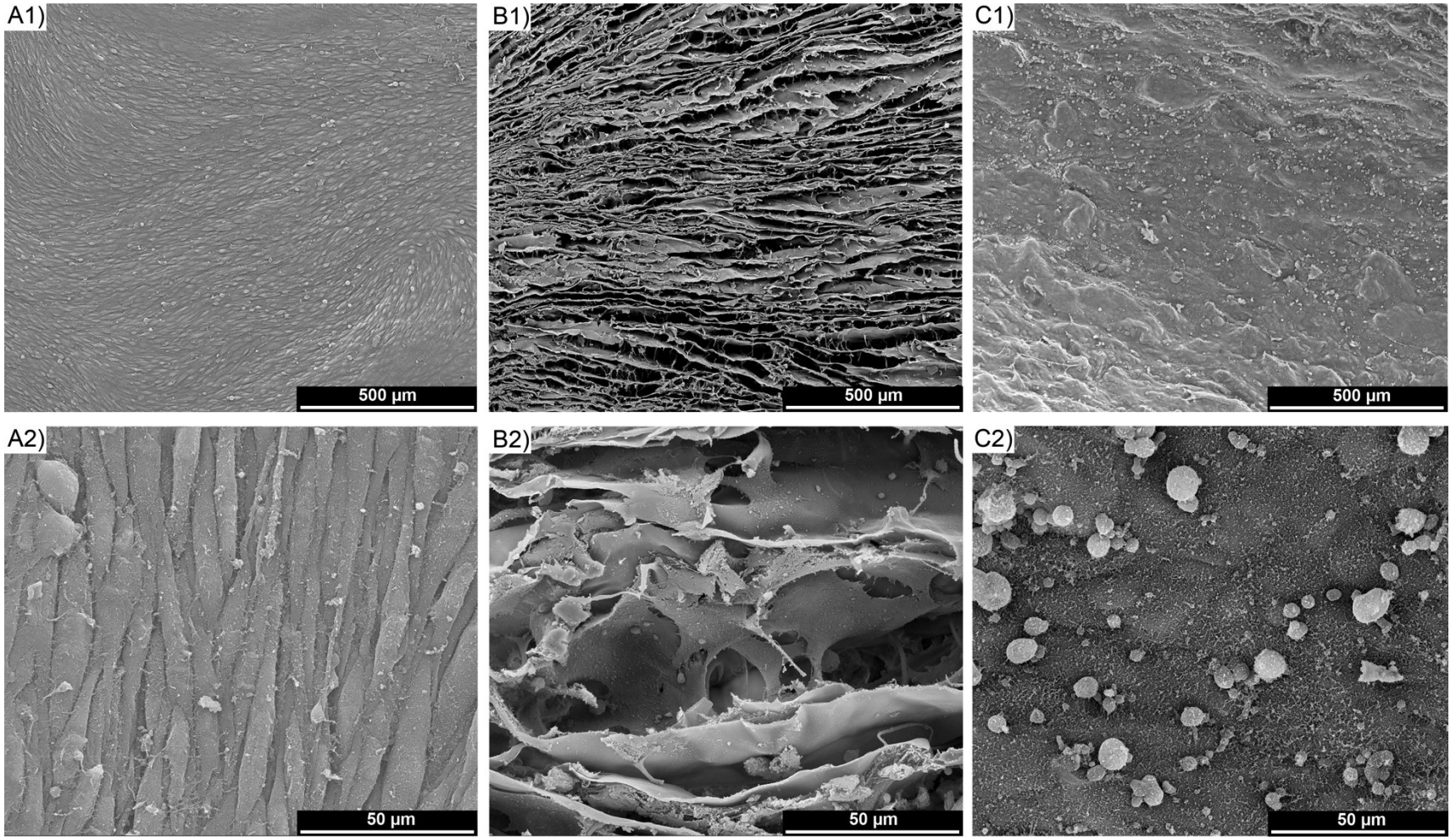

Figure 42: Co-cultivation of C2C12 myoblasts (spindle-shaped) and Urotsa (flat/cobblestone-like) on the outer surface A1)/A2), in the matrix B1)/B2) and lumen C1)/C2).[6]

These experiments (cf. Figure 42) showed that a basic application of two cell types on Optimaix 3D Sponge1 was possible. Nevertheless, it was noticed in the scanning electron microscopic pictures that no confluent seeding of the sponge matrix was possible. Cells were distributed in the matrix as depicted in the picture, but strong decreasing gradients (cf. Figure 38) were seen in any experiment that was performed.

5.6.2 Fibrin and PVDF as matrix for a peristaltic stimulation

As described in Chapter 3.2.4, composite biomaterials are better physiologic copies than single materials. This is based on the fact that tissues are made up of different layers that have different biomechanical properties, so composite materials offer a better chance to realise more of these properties and thus get closer to the original.

5.6.2.1 The composite material used

In this study, polyvinylidenfluoride and fibrin were combined as it had been done in previous studies by others (see Chapter 4.6.2). Figure 41 depicts the setup that was used in this study. It differed from other studies, e.g. from Tschoeke et al. (2011)[171], who covered the mesh with fibrin on both sides.

The setup that can be seen in Figure 43 was chosen in order to ensure a stabilisation for the mechanical stimulation of the prostheses developed as ureteral interposition graft. This mechanical stabilisation supported the fibrin matrix and protected it against rupture during the stimulation.

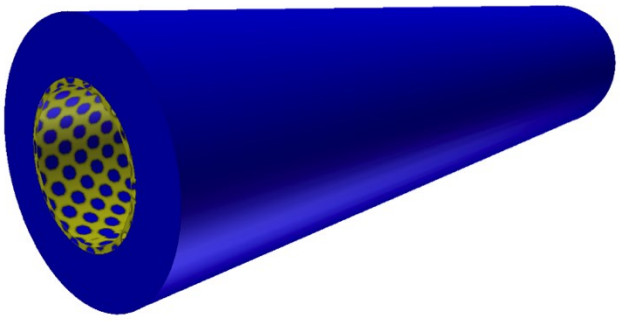

Figure 43: Schematic illustration of the two-component tubular structure consisting of fibrin (blue) as three-dimensional matrix and PVDF mesh (yellow with holes) as stabilising structure.[6]

5.6.2.2 Fibrin application – first test series

Fibrinogen solution needed to be prepared prior to fibrin-matrix production according to the protocol that was presented in Chapter 4.6.2.1. Subsequent to the dissolution of the lyophilised fibrinogen, it was analysed by the spectrophotometer at 280 nm. A dilution series were prepared (V/V) of 1:10, 1:20, 1:40 and 1:80 in Tris-buffer to achieve measureable concentrations with moderate absorptions up to 3. Two independent preparations were used in this study. Their measurement values are shown in Figure 44. The correlation coefficients (r^2) of the lines of best-fit were determined to be 0.999 and 0.997.

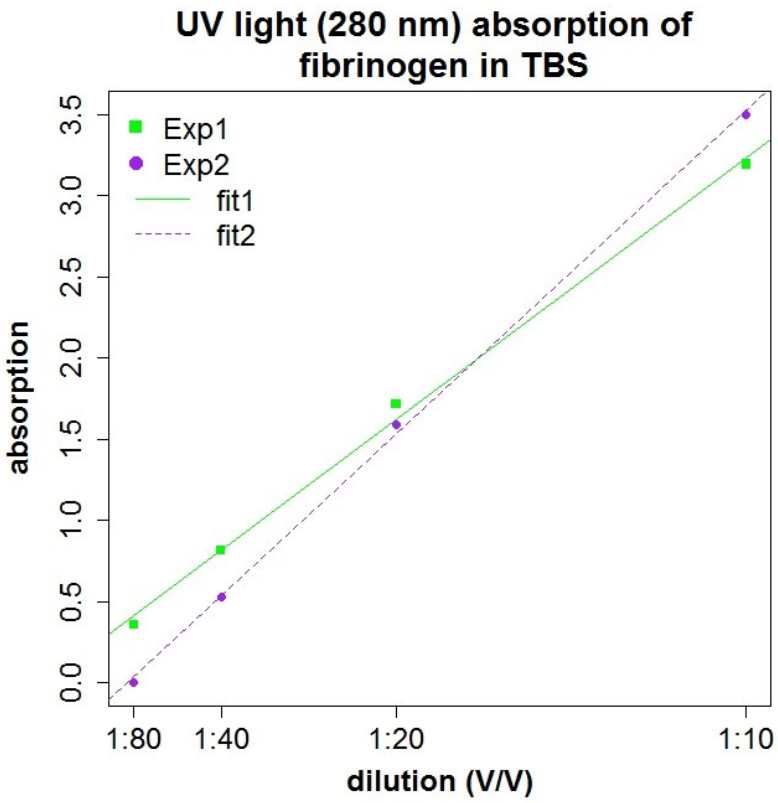

Figure 44: Fibrinogen concentration in Tris-buffer measured at 280 nm in dilutions (V/V) of 1:10, 1:20, 1:40 and 1:80.[6]

The measured results were used to calculate the protein concentration according to equation (2). Mean concentrations of 20.7 ± 0.6 mg mL^{-1} and 20.5 ± 1.6 mg mL^{-1} were calculated. Aliquots were prepared and stored at -80 °C.
First test series on fibrin preparation were done in combination with primary smooth muscle cells or NIH-3T3 fibroblasts that were poured in 24 well plates (Nunc) up to a level of 2.8 mm thickness. Figure 45 shows a fibrin matrix that was

prepared according to the protocol (see Chapter 4.6.2.1). The initial cell concentration was 100 cells μL^{-1}.

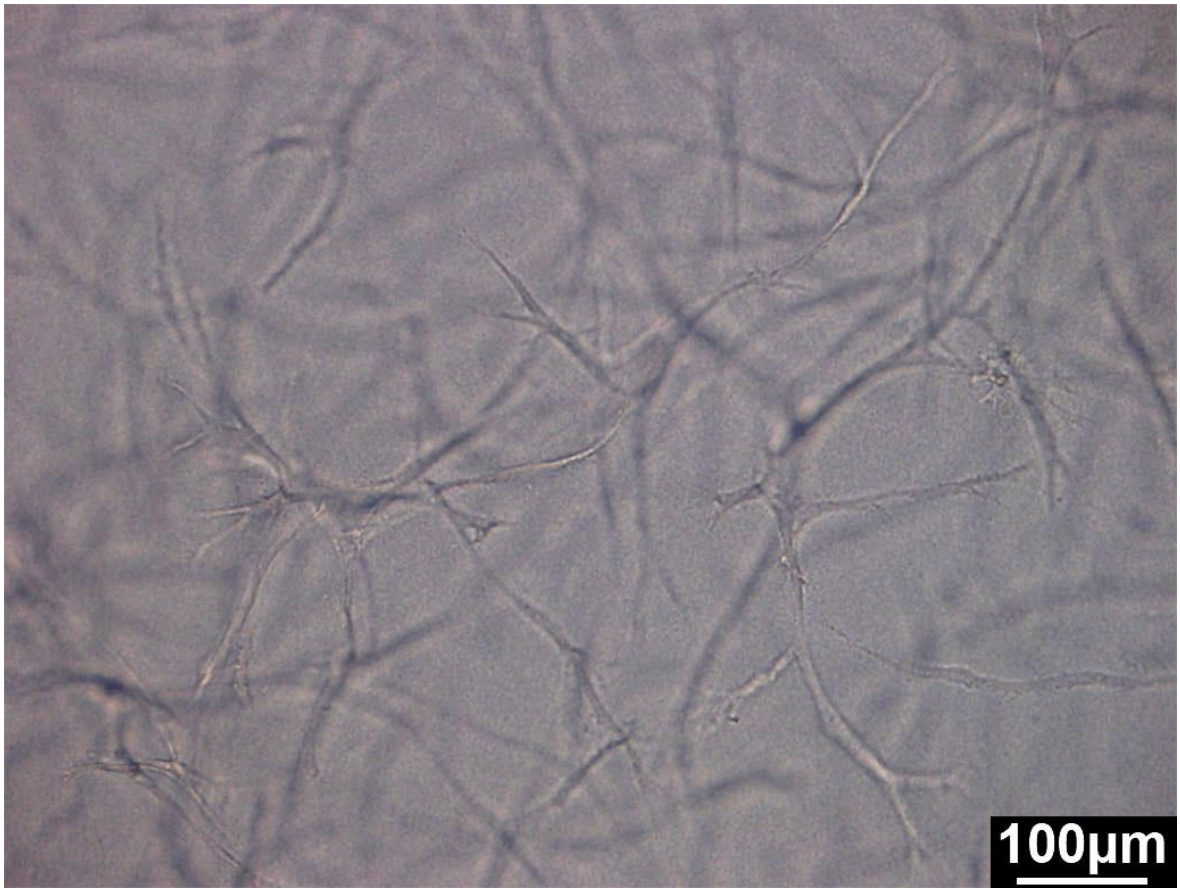

Figure 45: NIH-3T3 fibroblasts in fibrin gel with an initial concentration of 12.5 mg mL^{-1} and 100 cells μL^{-1} after 7 days of incubation. Scale bar: 100 µm.[6]

Subsequent to the cell seeding process it was observed that the cells started to grow into the fibrin matrix, where elongated/stretched cells were seen. After 7 days of incubation, it became apparent that there was a homogenous distribution of the cells in all spatial directions inside the matrix, which was proven with z-stack-recordings. Moreover, NIH-3T3 fibroblasts showed the typical morphology, having developed several pseudopodia for cellular communication.[172] The low initial cell count was chosen to allow monitoring with light microscopy. Too high concentrations would have lead to optical opaque constructs.

5.6.2.3 Casting of fibrin into a tubular structure

A casting mould was developed for the application of fibrin, cells and a PVDF mesh. First evaluations of the plastic material's performance in combination with fibrin were achieved by applying of a fibrinogen-thrombin solution onto polished plastic surfaces. Effects became directly visible as it is shown in Figure 46, where fibrin was applied on polished PTFE A) and polished POM B). The fact that drops on the PTFE showed much steeper contact angles than on POM was clearly visible by the naked eye; therefore no contact angle measurements were performed. After an hour, it was noticed that it was possible to remove the polymerised fibrin more easily from PTFE. It was concluded that PTFE is much more hydrophobic and that there was less adhesion. This is based on lower surface tensions leading to fewer interactions between the material and the liquid.[173]

A)

B)

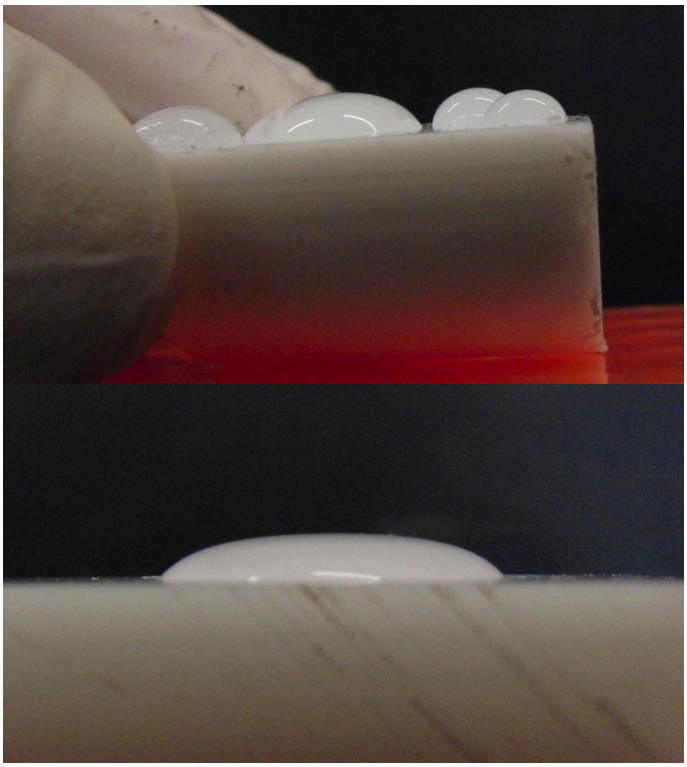

Figure 46: Fibrin applied on A) PTFE and B) POM to select a suitable material for a casting mould.[6]

The fibrin casting mould developed for this thesis was prepared out of PTFE. It was manufactured in the workshop of the Aachen, University of Applied Sciences in Jülich according to the technical drawing shown in the Appendix. A schematic illustration is given in Figure 47. The mould, (except bolts, nuts, fittings, pins and the LUER adapters) consisted of PTFE. Its fittings were manufactured from POM and bolts, nuts, pins and LUER connectors consisted of stainless steel.

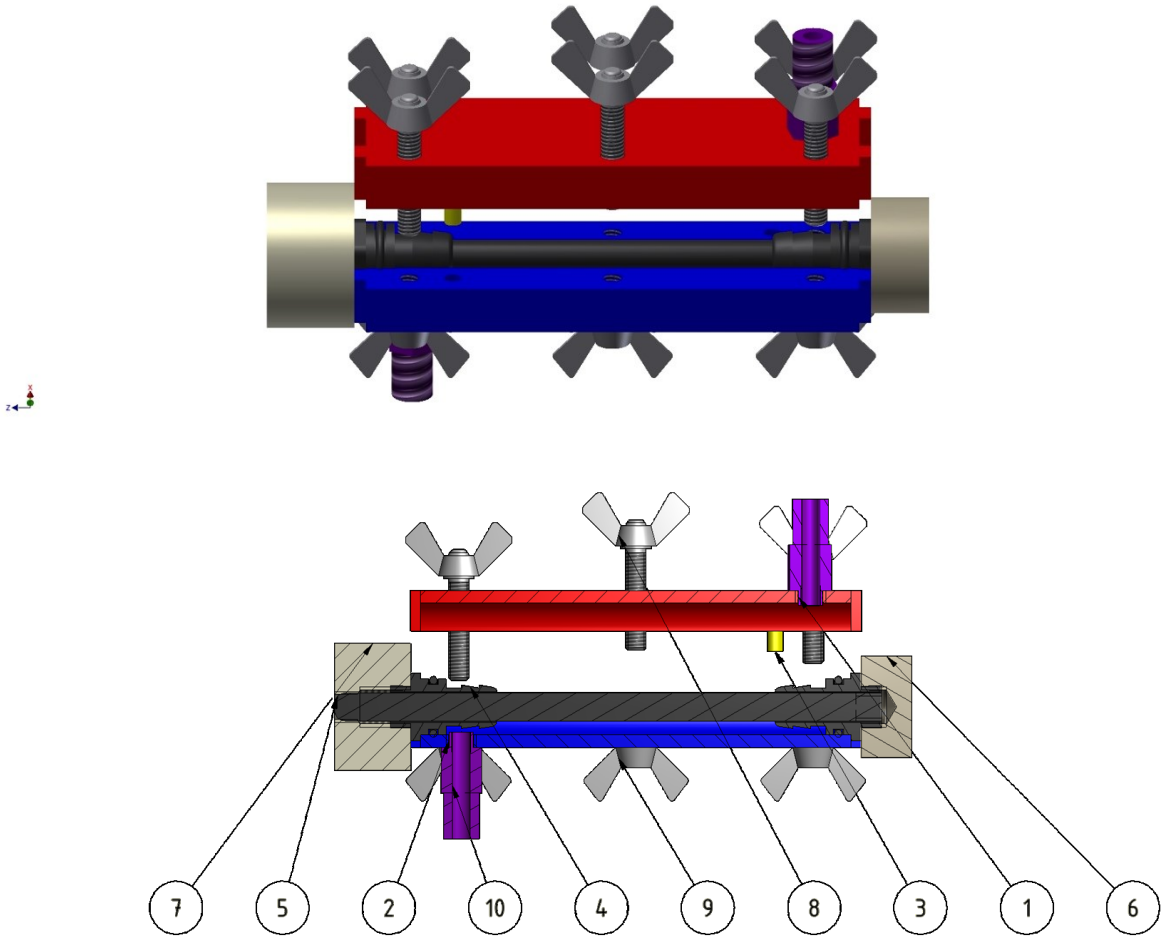

Figure 47: Fibrin casting mould consisting of: top (1), bottom (2), pins for positioning (3), fittings (4), central rod (5), front cap (6), end cap (7), wing bolts/nuts (8)/(9) and LUER adapters (10).[6]

The casting mould was assembled completely, prior to the application of the fibrin, cells and PVDF mesh. A fitting (4) (cf. Figure 21) was screwed down into the end cap (7), which has been already attached to the central rod (5). A prepared piece of mesh was pulled over the rod and fitting, before the second fitting was added.

This combination was then set onto the bottom plate (2). The top (1) was adjusted in a way that the LUER adapters (10) (VIEWEG) arranged in an antiparallel manner. Stainless steel pins (3) (MISUMI) supported a correct adjustment. Subsequently, the wing bolts and nuts (8)/(9) were attached to close the casting mould tightly, before the front cap was screwed down. In this case, additional bars at the short sides of the casting mould fixed the fittings that had a wrench size of 12 mm. Thus, no twisting of the scaffold was avoided, which could have lead to inhomogenities, e.g. wrinkles.

Afterwards, cells were applied to the assembled casting mould. To achieve that, cells were detached from cell culture flasks with Trypsin/EDTA (see Chapter 4.4.3). Then, they were resuspended with cell culture medium II and were counted with the cell counter (see Chapter 4.4.4). For one experiment with two prostheses, a total cell count of $6 \bullet 10^7$ cells was required. This lead to a final cell concentration of $5 \bullet 10^6$ cells mL^{-1}. The cells were centrifuged at 280 g again to be resuspended in TBS-buffer to a total amount of 2.1 mL. The two-chambered applicator was used with 3 mL fibrinogen solution (12.5 mg mL^{-1}), which was separated from the 2.1 mL cell suspension, 450 µL thrombin (40 U mL^{-1}) and 450 µL $CaCl_2$ (50 mM) (see Chapter 4.6.2.1). The suspension needed to be injected with consistent speed to achieve a prosthesis with a homogenous shape, as shown in Figure 48. Moreover, the casting mould was arranged vertically to avoid bubbles/holes in the tubular construct. Thus, the filling level kept constantly moving upwards.

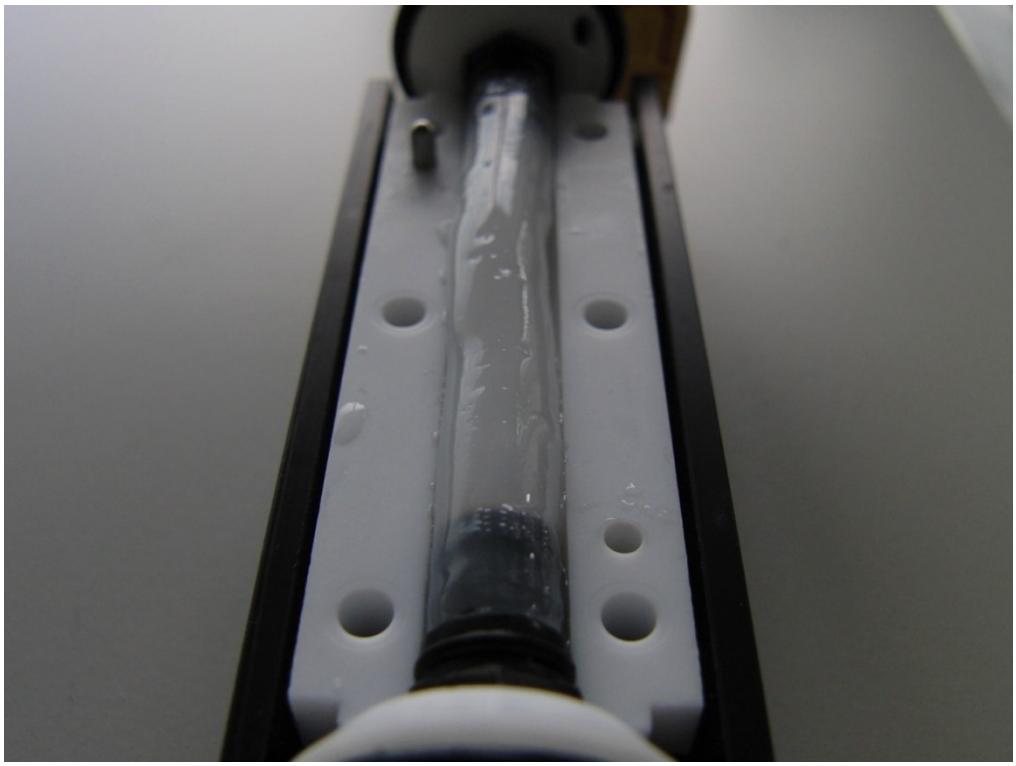

Figure 48: Homogeneously casted fibrin prosthesis with a length of 75 mm in the developed casting mould.[6]

The fibrin was allowed to polymerise for 45 minutes before the casting mould was opened. To open the mould, the front and end cap were removed and the piston and front plate of the Bioreactor Prototype IV were attached. The piston had been already introduced in the glass cylinder. Subsequently, a stainless steel rod (3•20 cm) was driven through the central fittings to ensure a support of the prosthesis. Then, the topper and bottom were removed carefully and cable ties were applied to fix the prosthesis on the fittings.

When fitting configuration B) (cf. Figure 21) was used, boreholes were cleared by cutting holes into the mesh in the direction of the piston or front plate. These fittings were required for the central cell culture medium support. Then, the piston was pulled through the glass cylinder till the front plate closed the bioreactor. The metal housing was attached to achieve tight sealing before the central metal rod was removed and before the tubes from the reservoirs were attached to the bioreactor. For stimulated prostheses, the contamination guard was connected to the bioreactor's piston to introduce the kyphoplasty catheter that had been cleaned with an antiseptic agent and sterilised at 90 °C for at least 12 h. Additionally, the front plate was sealed with a silicon plug.

Untrained/unstimulated prostheses were placed in the incubation system and the tubes for the medium supply were put into the peristaltic pump heads. Cell culture medium III (see Chapter 4.4.2) was transferred with 10 rpm (8.6 mL min^{-1}).

Trained/mechanically stimulated samples were placed in the bioreactor system and only the outer medium circuit was attached. The pressure line had been filled with degased water before it was connected to the catheter.

For the preparation of the fibrin prostheses it was shown that homogeneous tubular structures were prepared with a wall thickness of 2 mm. The casting mould was tightly sealed and had a total volume of nearly 6 mL, leading to a total scaffold length of 75 mm. The length between the fittings was 55 mm. Fibrin did not attach to the PTFE resulting in an easy removability of the prostheses. Potential for improvements can be seen with respect to the location of the fittings. The wall thickness was just 1 mm at the position of the fittings. At this position, however, the prostheses were most fragile.

5.6.2.4 Observations during the incubation period

Incubation procedures with fibrin-based prostheses were conducted for 1 (n=4) and 2 (n=4) weeks. Every day during this period of time, cell culture medium samples of 3 mL were taken and the outer appearance of the prostheses was examined.

The first test series revealed that the Cyklokarpron® concentration in cell culture medium III needed to be increased from 0.16 mg mL^{-1} to 0.5 mg mL^{-1} to slow down fibrin degradation (see Chapter 4.6.2). Its concentration was adapted to levels found in literature where Cyklokarpron® was used in combination with other cell types.[174] This was necessary because the urothelium produces tissue-type plasminogen activator (tPA) and urokinase-type plasminogen activator (uPA) that lead to the degradation of fibrin (see Chapter 4.6.2). It may be assumed that, this secretion prevents fibrin clots from obstructing the urine guiding system.[175] In this study, SMCs were isolated from porcine bladders which lead to cellular cross contaminations in any case.

In the future, this prosthesis will need to be seeded on the luminal surface to improve tissue tightness (see Chapter 2.1.1). To achieve that, an additional seeding step is required. In this case, an additional layer of fibrin might be attached to the luminal PVDF, so that there is a more homogenous and smooth surface. The procedure may be adopted in accordance with Tschoeke B. et al.

(2008)[171]. A casting mould with a central cylinder (d_i <6 mm) could be used to add the inner layer of fibrin. Subsequently, the luminal seeding with urothelial cells may be performed.

Moreover, the connection between PVDF mesh, fibrin and cells could be improved further with covalent bonding of extracellular matrix (ECM) proteins, e.g. fibronectin[136], or different ECM cell adhesion domain frequencies (RGDs)[176].

During the incubation and stimulation, no prostheses were lost because of failure at the PVDF mesh. However, the PVDF meshes used in this study were knitted, which had the advantage of providing very high variability regarding mechanical and structural characteristics.[140] Different knitting patterns have a direct influence on the cellular behaviour. Thus, additional experiments should be performed comparing altered weaving patterns to unwoven patterns.[177]

5.6.3 Porous sponge vs. compact extracellular matrix

Significant differences between the scaffold materials became apparent when the bioreactor was opened directly after the incubation. When the bioreactor was emptied, a thin biofilm became visible on the inside of the glass cylinder only in cases where Optimaix 3D Sponge1 had been used. This film was not seen in experiments with fibrin-based scaffolds. Light microscopy identified the cell type that was seeded onto the Optimaix 3D sponge1. Figure 49 shows two glass cylinders subsequent to the incubation with Optimaix 3D Sponge 1 A) and fibrin-based scaffolds B).

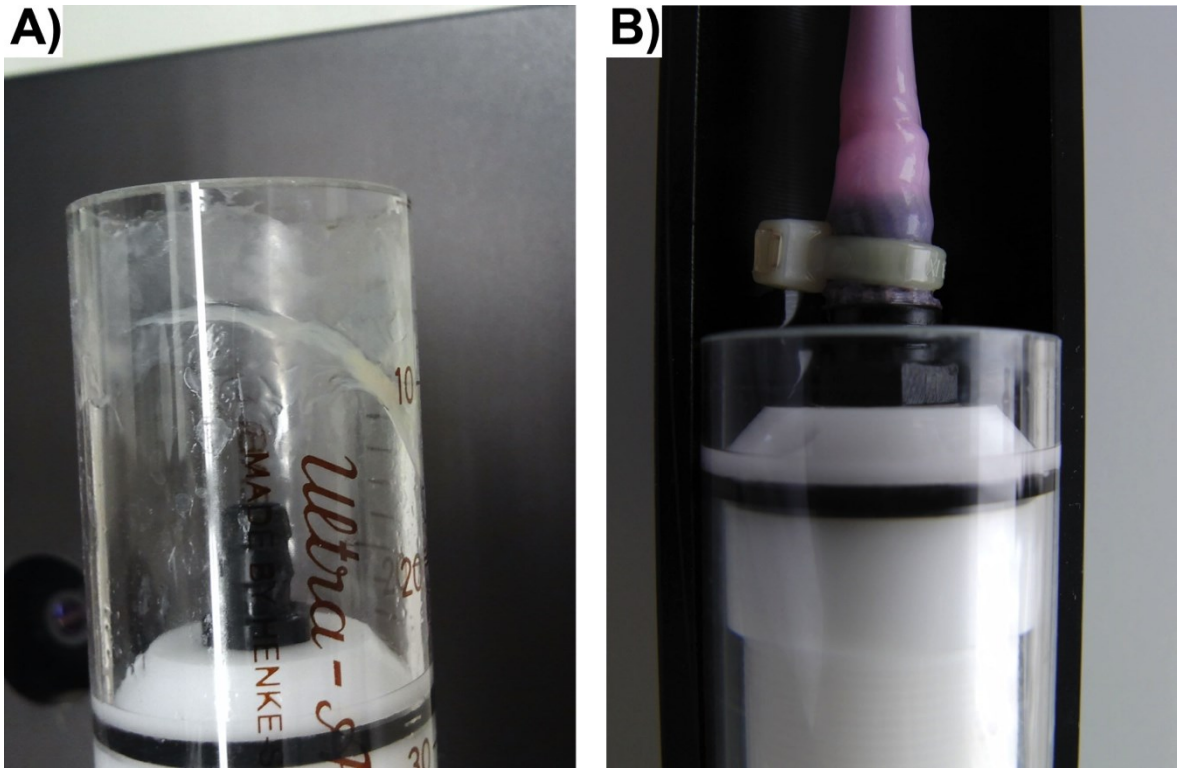

Figure 49: Comparison of the situation in Bioreactor Prototype IV after the incubation with Optimaix 3D Sponge1 and fibrin.[6]

These photographs illustrate that cells that were seeded onto the sponge like matrix dropped out of the pore system. Obviously, not all cells were tightly attached to the collagen sponge. That lead to a loss of cells after the bioreactor had been flushed with cell culture medium and to cells attaching to the inner surface of the glass cylinder. Cells proliferating inside the bioreactor but not in/on the scaffold resulted in an unnecessary consumption of cell culture medium. Moreover, this may contribute to failures in cell culture medium analysis with respect to any parameters that might be used for quantitative or qualitative examinations. This effect was not observed for fibrin-based prostheses (Figure 49 B)), where cells were casted into their position inside the matrix. Subsequent to the casting, the cells grew into the matrix by reorganising it. However, no cells were flushed out of this scaffold.

Figure 50 shows a control scaffold. It did not contain cells but was treated in the same way as an unstimulated prosthesis. In this picture, the fine fibrin meshwork becomes apparent and leads to the conclusion that entrapped cells cannot be flushed out of the matrix, even if they have not yet attached to the fibrin mesh.

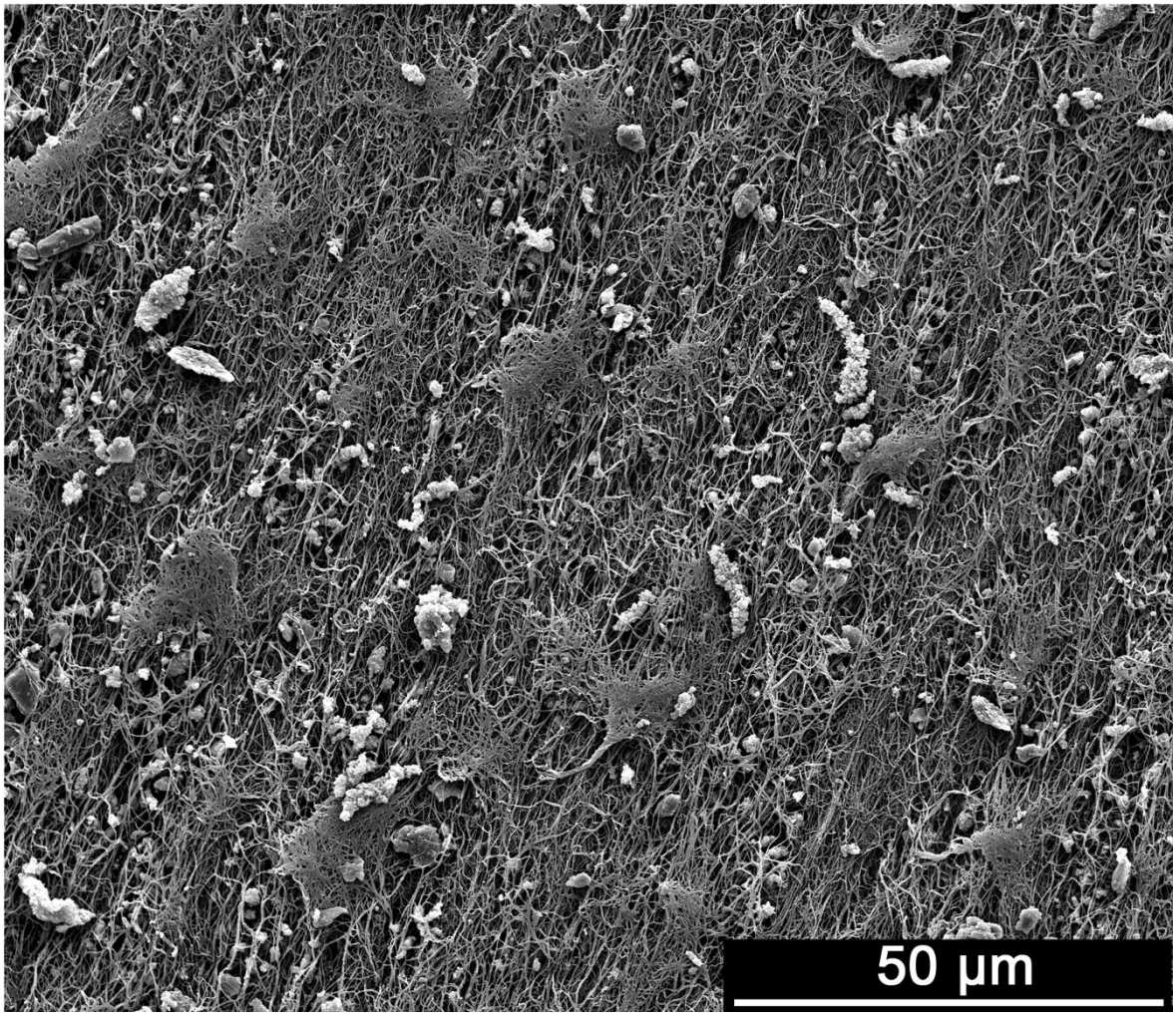

Figure 50: Control scaffold prepared out of fibrinogen without cells incubated with medium III in the Bioreactor Prototype IV for 1 week. Protein agglomerations as well as fibrin filaments can be identified.[6]

As a conclusion it can be stated, that tissue engineering with Optimaix 3D Sponge1 has not been yet successful, even though results of in vivo and classical in vitro experiments were suitable and encouraging for further investigations. It was demonstrated that the seeding of cells did not lead to a homogeneous cellular distribution and confluency inside the matrix. Strong gradients were seen from surface layers into the matrix. Problems may be traced back to the dimensions and pore sizes of the matrix and/or the combination of material and bioreactor system. The conclusion is that this matrix **in combination with Prototypes III and IV**, and the structural setup of the sponge-like material were not applicable for tissue engineering purposes.

5.7 Ussing chamber

The Ussing chamber was used to examine the tissue's tightness against the diffusion of urinary excreted substances (see Chapter 4.4.1.4). Urea and creatinine were analysed in the veterinary laboratory of the RWTH Aachen University Hospital. Generally, these molecules are common renal markers that can be found and quantified in the urine.[178]

Urea (CH_4N_2O; 60.06 g mol^{-1}) is a degradation product of amino acids and can be used to determine the integrity of the urothelium.[13,14,179]

Creatinine ($C_4H_7N_3O$; 113.12 g mol^{-1}) is nearly twice as heavy as urea. It is a metabolic waste compound from creatine to creatinine in muscles.[178]

First, native porcine ureters (n=7) were prepared to be analysed in the Ussing chamber. The preparation of porcine ureters for the application in the Ussing chamber can be seen in Figure 51.

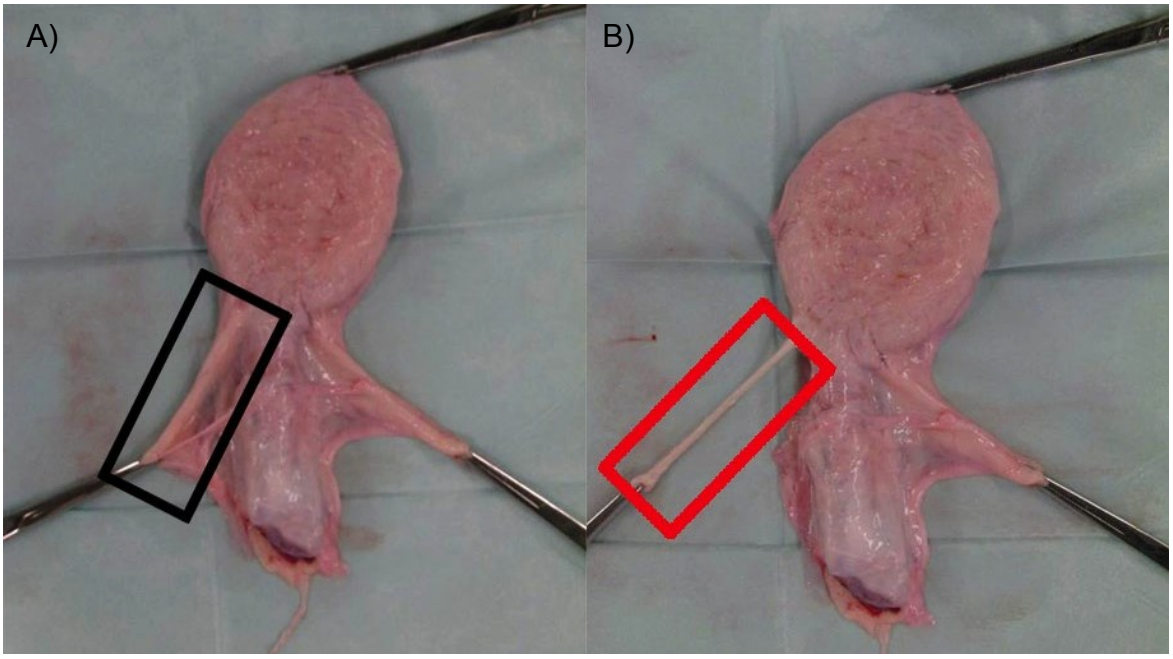

Figure 51: Preparation of native porcine ureters to prior to analysis of passive diffusion of urine-excreted substances. Connective tissue at the native bladder and ureter (black) A) was removed with scissors to obtain a pure ureter (red) B). Clamps at the top mark the urachus.[6]

Marks in this figure, indicate that excessive fatty connective tissue was removed from the native bladder and ureter A) in order to get a ureter samples without disturbing tissue B). Any tissue up to the adventitia was dissected with sharp

scissors and fine tweezers. It was ensured that the adventitia was still intact after the preparation, because any damage may have a direct influence on the diffusion experiments.

Ureters were cut into fragments with a length of about 2 cm and were opened in longitudinal direction. Subsequently, the samples were fixed on the specimen mounts before the chambers were closed and the reservoirs were filled with 5 mL of the specific buffer solutions each (see Chapter 4.4.1.4).

The same procedure was performed with tissue-engineered fibrin-based prostheses. After the bioreactor has been opened, prostheses were cut into fragments with a length between 0.5 cm and 1 cm. Then, a sample was randomly chosen before it was sliced longitudinally.

In every case, the luminal/urothelial layer was directed towards the synthetic urine, i.e. in the physiologic diffusion direction.

Figure 52 shows measurement curves for native and tissue-engineered structures with respect to the diffusion of urea. Mean values were calculated for native samples (green) as well as for trained (blue) and untrained (red) prostheses. Additionally, the overall statistical mean (black) of tissue-engineered structures was introduced for comparison.

It can be seen that urea was much better able to penetrate tissue-engineered constructs than native ureteral tissues. The difference was significant. After 8 hours, there was a mean difference of 140 mmol L^{-1} between native and tissue-engineered samples. This was based on the fact that tissue-engineered constructs did not have a luminal urothelium, which is one of the tightest tissues in the human body (see Chapter 3.1.1). Besides that, histological staining revealed that cellular densities are lower in tissue-engineered matrices, which may have contributed to the increased diffusion rates.

Moreover, a difference can be seen between trained and untrained prostheses, which are separated from each other in the picture by the overall mean value of all fibrin-based prostheses. That means trained prostheses seem to be slightly more leaky than untrained constructs. Nevertheless, this effect is not significant.

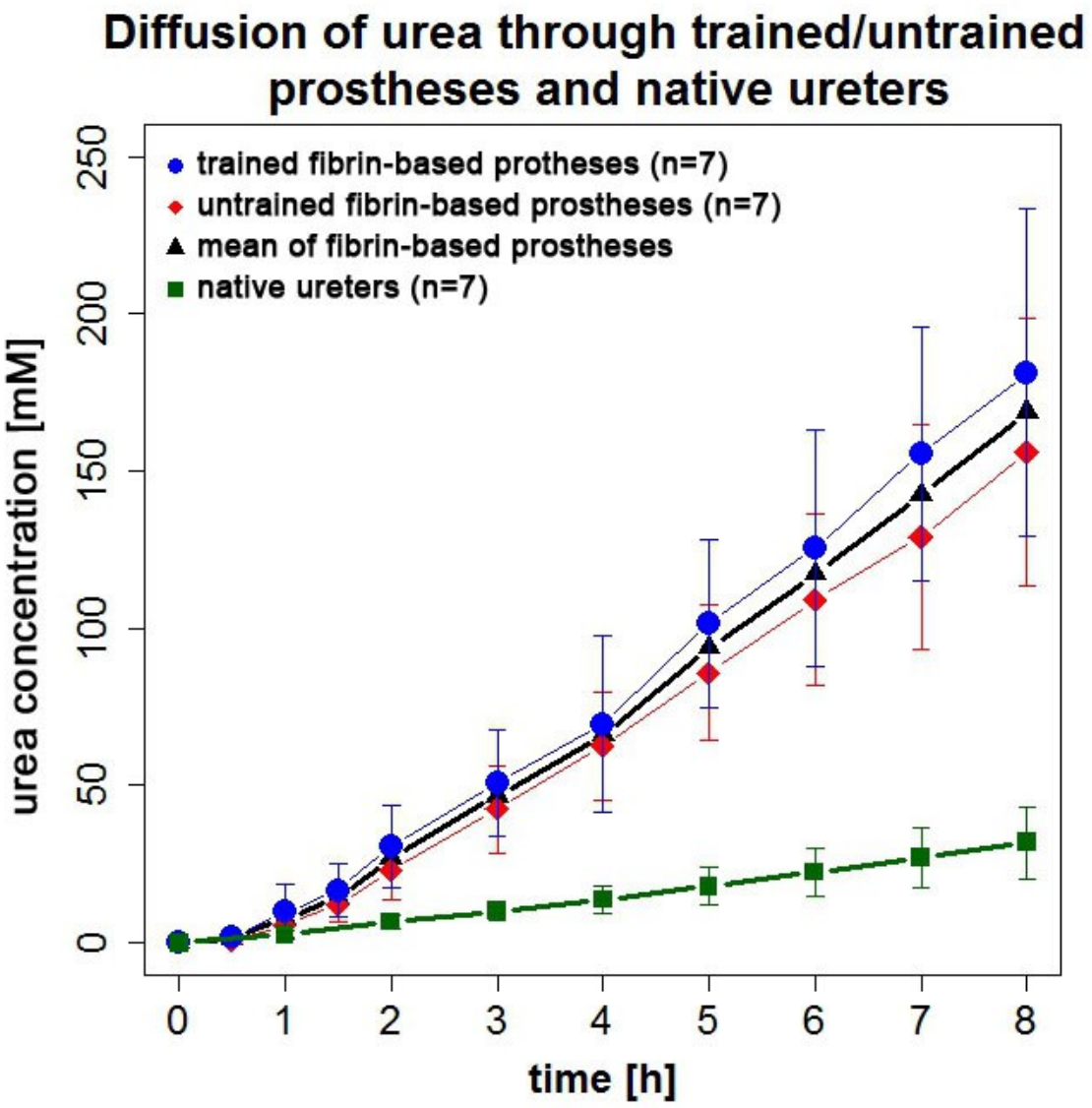

Figure 52: Diffusion of urea through tissue-engineered, trained and untrained prostheses (n=14) and mean tissue-engineered constructs in comparison to native ureters. TE=tissue-engineered.[6]

Creatinine diffusion is illustrated in Figure 53. It becomes apparent that the diffusion characteristic was comparable to the diffusion of urea. Colour coding of the samples is the same as in Figure 53. The permeation of creatinine was significantly higher for tissue-engineered constructs after 8 h; the difference amounted to 1940 µmol L^{-1}. Moreover, the statistic mean of trained prostheses (blue, n=7) lies above the overall mean (black, n=14). Untrained prostheses (red, n=7) were slightly denser than the overall mean.

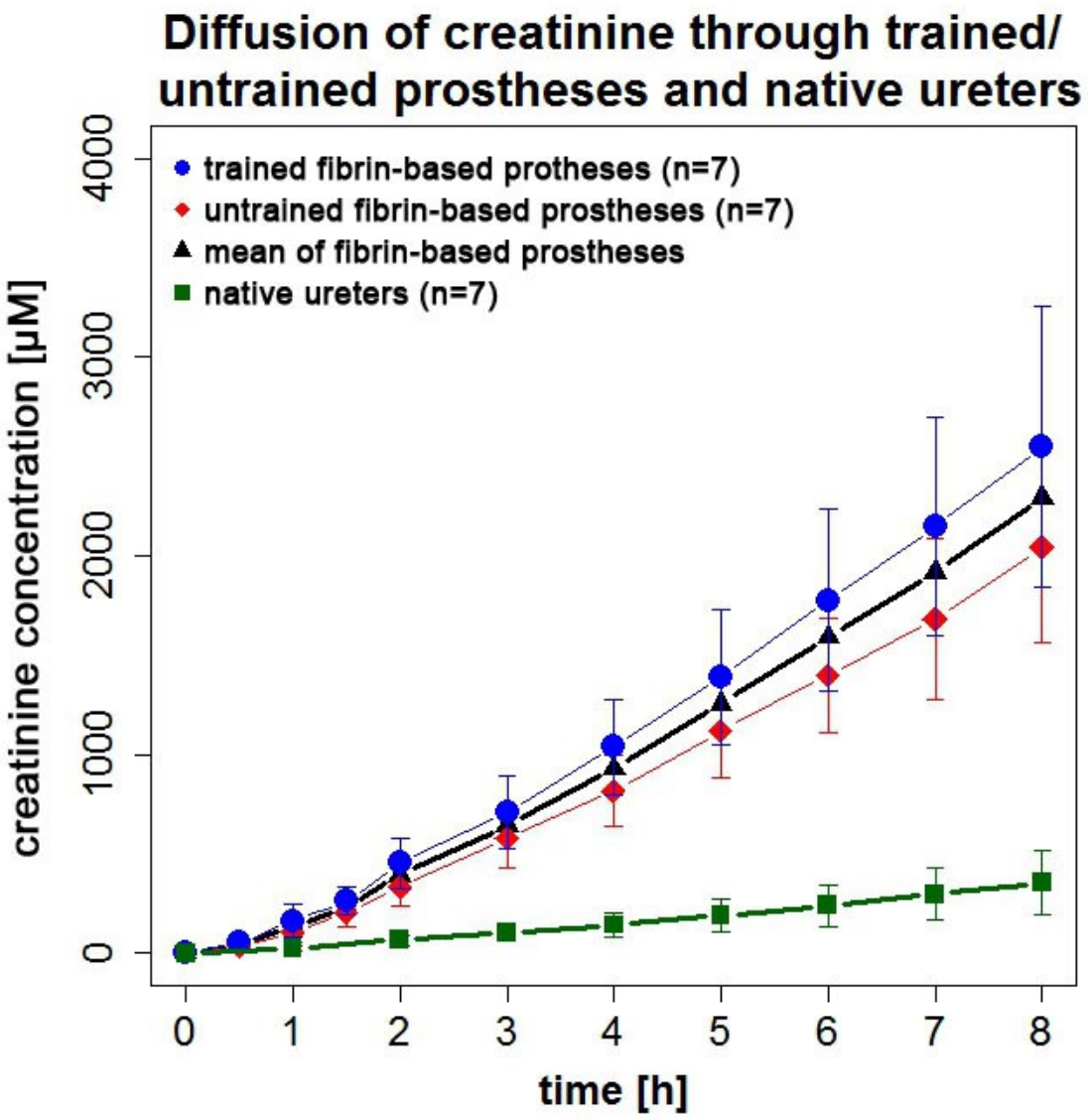

Figure 53: Diffusion of creatinine through native ureters (n=7), trained and untrained prostheses (n=14) and mean tissue-engineered constructs. TE=tissue-engineered.[6]

Both experiments reveal that untrained prostheses are not significantly denser with respect to diffusion than trained prosthesis. The low number of experiments with n≤8 may explain a merging of the curves. In case of single evaluations, where one trained and one untrained prosthesis comprising primary cells from one donor were compared it was observed that the trained prostheses showed higher leakage of urea in 5 of 8 experiments. With respect to creatinine, 6 of 8 experiments showed higher leakage in trained prostheses.

Once, an evident failure was observed during the experiments, when air bubbles got stuck at the tissue. This reduced the surface area available for diffusion and

the results were affected negatively. For that reason, this experiment was excluded from the analysis.

Another influencing factor m be seen in different donors. No data were available on the age of the pigs that were used. No differentiation was made between the pigs' genders. Moreover, differences between races might matter.

It was suggested that creatinine diffuses more slowly than urea. This was based on the assumption that the molecular size of creatinine is bigger than that of urea and that its concentration gradient is lower from synthetic urine to Krebs buffer. The diagrams showed that the average diffusion per hour was 290 µmol L^{-1} h^{-1} for creatinine and 22 mmol L^{-1} h^{-1} for urea. Consequently, the relative diffusion is higher for urea, which may be a result of its molecular size and concentration gradient.

In fact, no significant difference of tissue-engineered constructs was observable with respect to the diffusion of urea or creatinine. Differences between trained and untrained prostheses were too little to be significant. Additionally, an incubation period of two weeks could not increase tissue impermeability in comparison to one week incubation periods.

Literature gives little information on the diffusion of urea both in the genitourinary tract and in tissue-engineering constructs. Only a few scientists are working with diffusion chambers. Nevertheless, a comparison is difficult because media as well as experimental setups were different.[180,181]

However, Cattan V. et al. (2011)[180] showed the influence of the urothelium at tissue-engineered constructs for the genitourinary tract regarding the tightness against diffusion of urea. It was shown that the urothelium stratified due to mechanical stress, which has a significant influence on urea permeation.

5.8 Bursting pressure

In order to compare mechanical properties of tissue-engineered prostheses, the burst pressure of fibrin-based constructs was examined. For that reason, an experimental setup was designed that is schematised in Figure 54.

It can be seen that a tube connected a syringe with a cube-shaped pressure chamber, which was developed for this purpose. It was manufactured in the workshop of the Aachen, University of Applied Sciences, Jülich, according to the technical drawings contained in the Appendix. The massive cube was equipped with a central borehole (d_i= 4 mm). To clamp the specimen, it was possible to attach a plate with a thickness of 1 cm to the cube. The plate was fixed with four screws. To enable proper sealing and clamping, a seat for an O-Ring (1.5•8 mm) was milled into the cube. Basically, this pressure chamber replaced the kyphoplasty catheter that was used for peristaltic stimulation of fibrin-based constructs (see Chapter 5.2.1). The SyrDos syringe pump was used to apply a constantly increasing pressure onto the specimens by adding a volume of 2 µL s^{-1}. Pressure was monitored by the pressure sensor that was attached parallel to the pressure line. Hence, a qualitative comparison of the results became possible.

The measurement was done after Bioreactor Prototype IV had been opened and fibrin-based prostheses had been sliced into pieces between 0.5 cm and 1 cm length. Tubular structures were cut twice in longitudinal direction to obtain two tissue fragments of the same size. Furthermore, the chamber was flushed so that there was no air left in the system. Samples were chosen randomly for analysing their rupture pressure. The outer surface of a specimen was directed to the pressure line in the direction of the junction. Thus, pressure was acting on the fibrin which was then pressed against the PVDF mesh. Four screws fixed the covering plate.

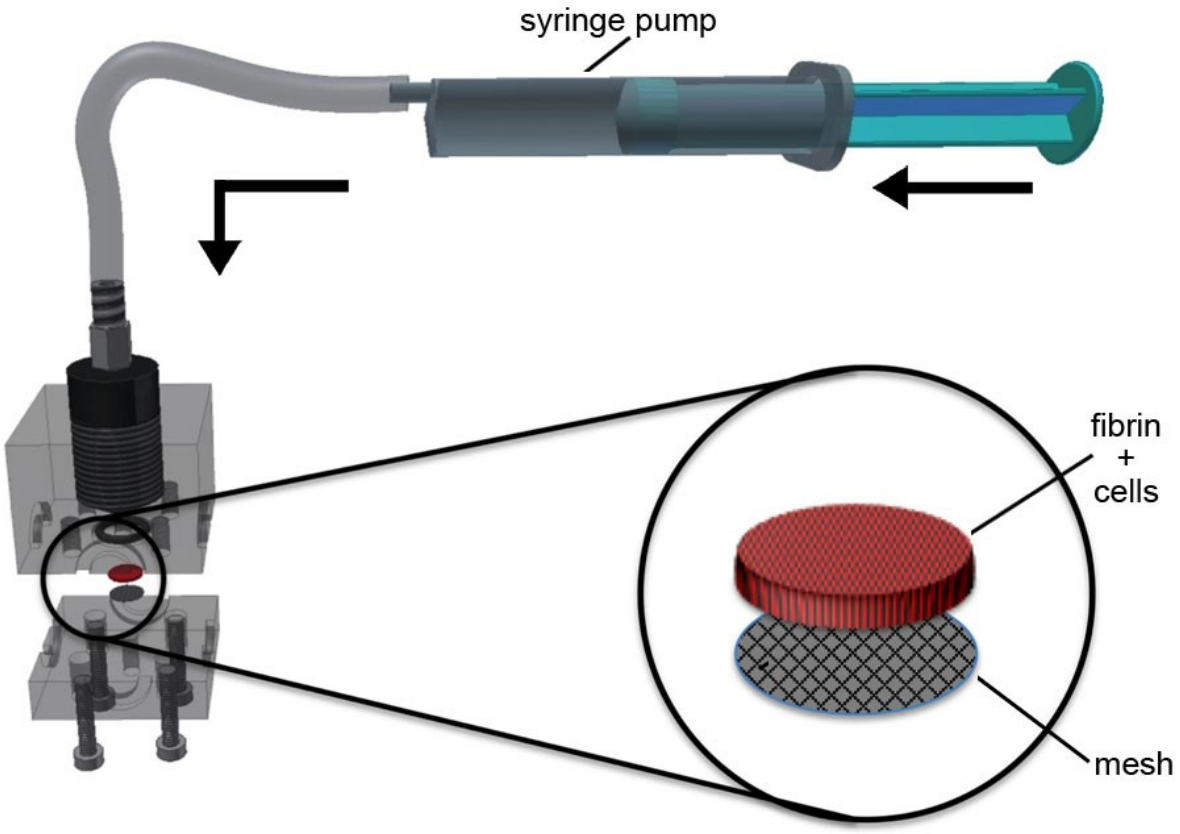

Figure 54: Bursting pressure test setup with a syringe pump and a specially designed chamber to attach a pressure line. The fibrin layer (red) is directed to the top and the underlying PVDF mesh (grey) is in contact with the atmosphere.[6]

This measurement was directly started in HiText™. The syringe pump was filled with water and released it continuously with 100 steps s^{-1}. Pressure values were recorded with 10 Hz. Generally, the amount of analysed fragments of a prosthesis varied between two and five. A typical burst pressure curve is illustrated in Figure 55. This figure shows that the pressure was constantly increasing from atmospheric pressure to a maximum, where the tissue ruptured. Then, the pressure decreased to atmospheric pressure again.

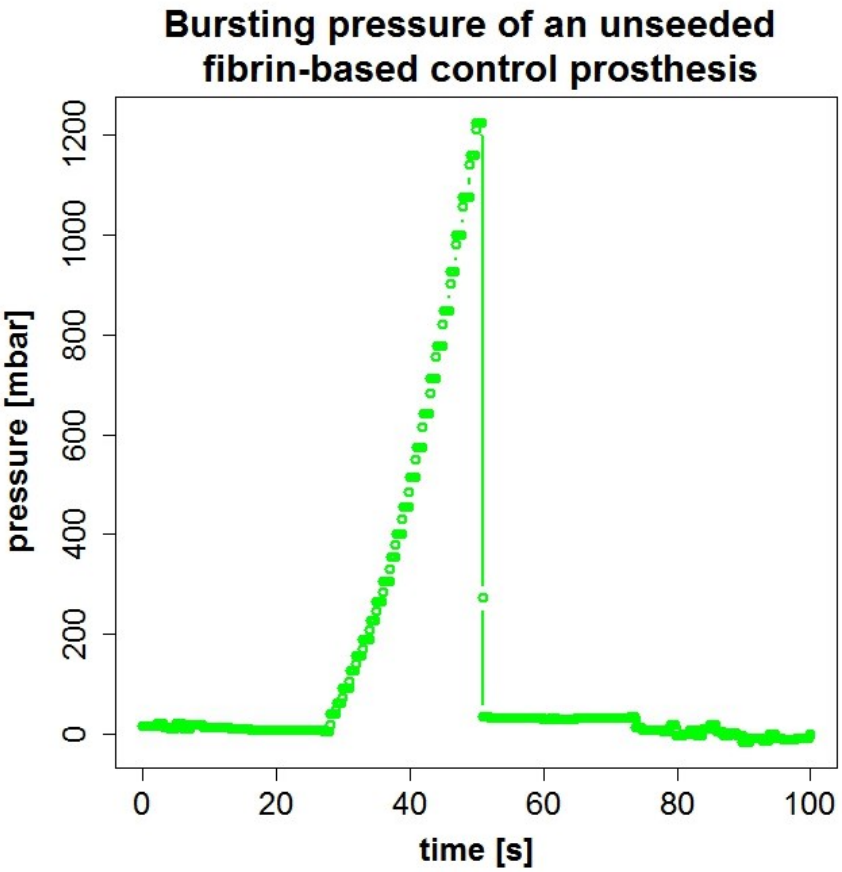

Figure 55: Typical progress of a burst pressure experiment using the example of an unseeded fibrin-based control sample.[6]

The rupture pressure for a fibrin-based control sample was determined to be 1280 ± 130 mbar. Pure PVDF meshes were not able to retain the liquid in any way, resulting in maximum pressures <20 mbar, which may be a result of the capillary resistance.

Figure 56 illustrates the overall results that were achieved regarding fibrin-based prostheses that were seeded with primary porcine smooth muscle cells and incubated for 1 week or 2 weeks with and without peristaltic stimulation. Red coloured boxplots untrained prostheses and blue boxes indicate trained prostheses. Both colours allow a further differentiation between the donor pigs. Primary smooth muscle cells from one donor were used for each experiment (i.e. 8 donors were used) and marked with an alphabetic character. One prosthesis was prepared for mechanical stimulation (blue) and one without training (red). Experiments lasting 1 week range from A1 to D2, whereas prostheses from E1 to H2 were incubated for 2 weeks.

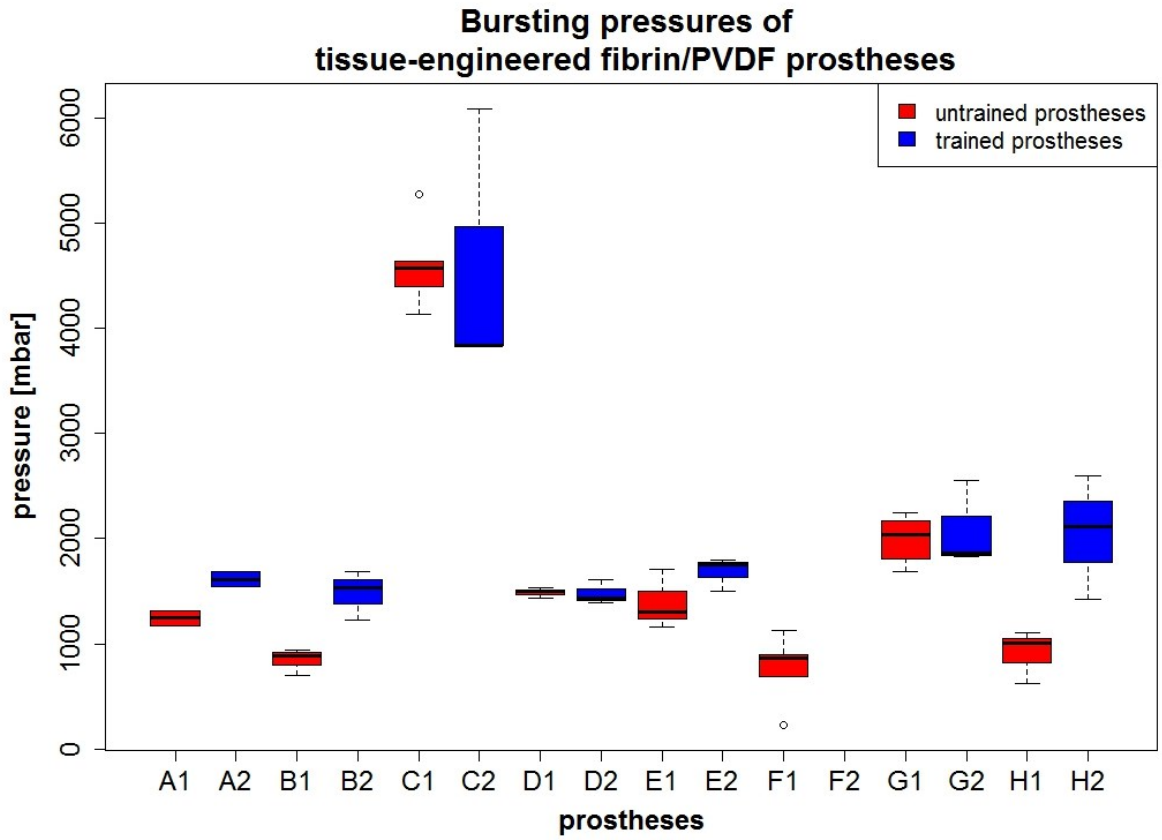

Figure 56: Bursting pressures of tissue-engineered tubular structures based on fibrin-PVDF prostheses incubated for 1 week (A-D) and 2 weeks (E-H).[6]

Figure 56 shows two spikes for C1 and C2. These samples show a significantly increased mechanical stability in comparison to all other prostheses. Their mean values were at least twice as high as the others. For that reason, these two samples (C1 and C2) were excluded from further analysis. Moreover, no measurement was possible for F2 due to fibrinolysis. This might be caused by a high contamination with urothelial cells that were found as cell clusters after HE histological staining.

Corrected charts are shown in Figure 57 with the samples C1/C2 and F1/F2 removed. These diagrams differentiate between one week and two weeks of incubation as well as trained (blue) and untrained (red) prostheses.

An analysis of the median bursting pressure in intraindividual experiments using from one donor shows that the median bursting pressure of trained prostheses was greater than the rupture pressure of untrained prostheses in 4 of 6 experiments. The differences between A1/A2, B1/B2 and H1/H2 cannot be proven to be significant because of the low number of measurement values in one experiment (n≤5).

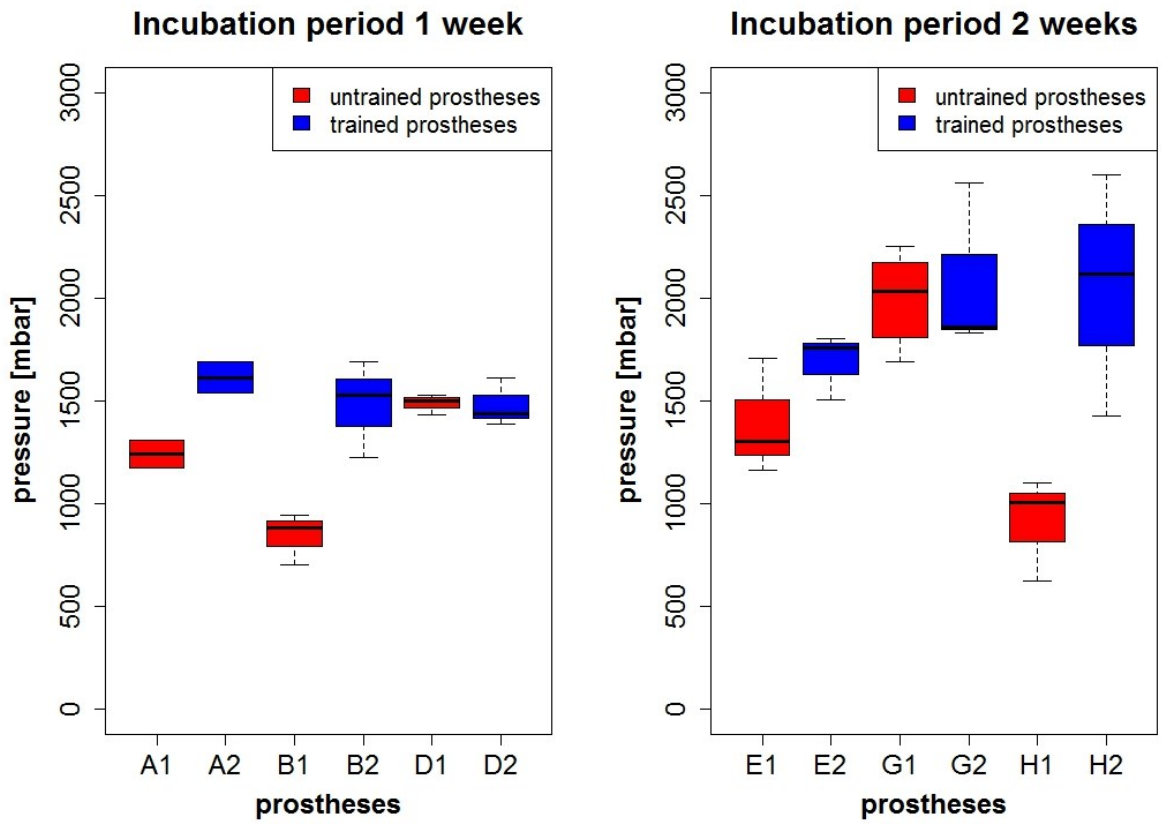

Figure 57: Bursting pressures of fibrin-based prostheses differentiated according to their incubation periods.[6]

Additionally, Table 14 shows the mean values of the medians of trained and untrained prostheses for 1 and 2 weeks of. **It becomes apparent that trained prostheses show a higher rupture pressure and a standard deviation that is at least half of the standard deviation of untrained prostheses.** This may show a greater homogeneity in trained constructs with respect to cellular distribution, extracellular matrix secretion and strengthening or orientation.

Table 14: Mean of the median bursting pressures according to experiments shown in Figure 57.

Incubation period	Median bursting pressure untrained [mbar]	Median bursting pressure trained [mbar]
1 week	1210 ± 310	1530 ± 50
2 weeks	1450 ± 530	2120 ± 200

Figure 58 summarises the measurements that are shown in Figure 57. The same trend becomes apparent that was shown in Table 14. The boxes, or the interquartile range, of trained prostheses (blue) are smaller than to those of the untrained constructs (red). Thus, 50% of the measurement values were distributed in a smaller range.

Nevertheless, it can be seen that the whiskers that are based on the one and a half times the interquartile range were greater for experiments with an incubation period of two weeks. Statistical outliers, that would be indicated by circles, were not observed.

All in all, **a positive trend may be seen in Figure 58 for increasing bursting pressures over time for trained and untrained prostheses.** This tendency is not yet significant and needs to be proven by further experiments.

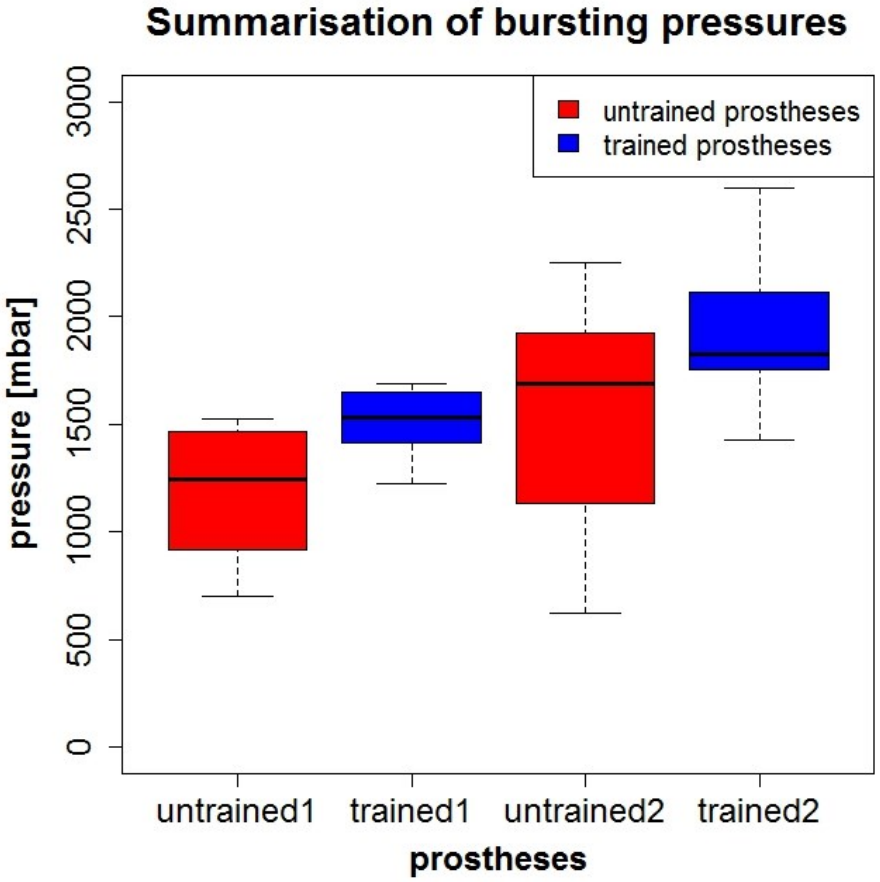

Figure 58: Boxplot of bursting pressures of samples shown in Figure 57. Differentiation is made with respect to the incubation periods: 1 week (untrained1/trained1) and 2 weeks (untrained2/trained2).[6]

The amount of analysed samples per prosthesis varied because of the loss of specimens. Insufficient fixation/clamping due to slipping out of the position where the central borehole was covered completely, lead to the loss of tissue fragments. This could be reduced during the experimental phase so that just one experiment (A1/A2) contained n=2 measurement values per prostheses. For that reason, a specimen mount with pin points is suggested as a further optimisation.

All in all, the achieved results correspond to literature that deals with tubular tissue engineering at the urinary tract and that considers mechanical stability of grown prostheses. It can be stated that the rupture pressure or the mechanical stability of prostheses increases with time and dynamic incubation.[182] Similar effects can be observed for vascular tissue engineering.[112] A comparison to these studies is difficult, however, due to different approaches with different cell types, geometries and biomaterials.

5.9 Evaluation of cellular orientation

The orientation of smooth muscle cells both along the ureter and circularly around the ureter are key features required for peristaltic forwarding of urine from the kidneys toward the urinary bladder (see Chapter 3.1.1). For that reason, cellular orientation in and on the tissue-engineered fibrin-based tubular structures were analysed.

5.9.1 Outer surface and scanning electron microscopy

Generally, the outer surface of the tubular structures was analysed by means of scanning electron microscopic pictures.

The outer surface of the tissue-engineered tubular structure made up of fibrin and primary smooth muscle cells was evaluated with the help of a computer program written in LabVIEW. An individualised graphical user interface (GUI) was designed in the lab with the support of Peter Linder, M.Sc., in order to find the alignment of pictorial elements in the raster electron microscopic pictures. Figure 59 shows the GUI with the different steps of the image processing. A) indicates the selection of a survey image. The major part of the sample and its cutting edges are visible for the identification of the sample position. All orientations of particles and cells are referred to a reference line that was placed in this survey (Figure 59 B). In C), a second image with an effective magnification factor of 400 was loaded and a Gaussian filter applied to smoothen this image to remove speckles. In this display, it was possible to define a region of interest (ROI), where disturbing elements, e.g. the image annotation, were excluded. Subsequently, two further images (Figure 59 D) and E) were prepared. Image D) was strongly smoothed with a low pass filter that had a grid of 20•20 pixels and a tolerance of 10%. The second photo, E), was smoothed weakly with a grid of 10•10 pixels and a tolerance of 5%. Subsequently, the figures were subtracted from each other and the absolute subtraction image was analysed with the LabVIEW particle detection tool using the parameters indicated in Figure 59 F). Data containing the orientation of identified particles and structures G) were put into the histogram H) and exported into an Excel sheet. In this example, the mean orientation of structural elements was 140° compared with the reference line. That means that these elements were shifted by 50° with regard to the longitudinal axis of the tubular structure. Moreover, this example showed an interquartile range of 30°, which indicates that 50% of all investigated orientations

were in the range the median orientation. The narrower this interquartile the more aligned the structural elements and cells. Widely distributed structures show interquartile ranges of around 90°. An interquartile range of 180° indicates an orientation along the reference line. In all images, the reference line equalled a circular arrangement of objects. Thus, a mean value of 90° indicates a longitudinal arrangement of the cells on the outer surface.

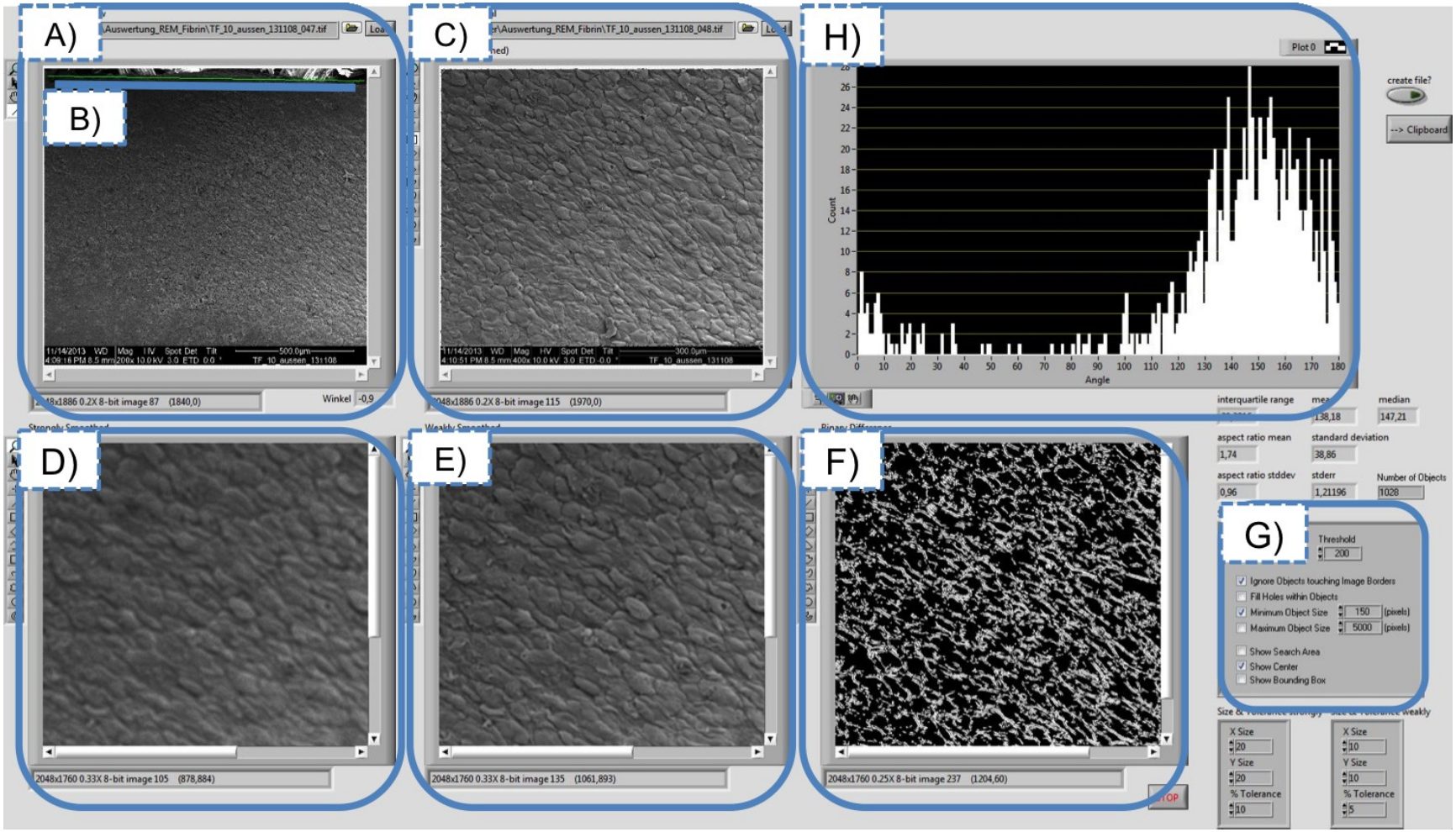

Figure 59: LabVIEW GUI for the evaluation of the structural alignment on the outer surface of the tissue-engineered prosthesis. Labels indicate different steps for image processing with filters and standardised analysing tools.[6]

Figure 60 and Figure 61 show test patterns for strongly aligned elements and a homogenous distribution. In the first example, the analysing software revealed an interquartile range of 0°, which indicates that there was no variation in the orientation of the test elements. In contrast to that, Figure 61 shows a homogeneous distribution of the elements. 50% of all particles were in the range of 90° around the virtual “centre” orientation. Hence, 50% had to be distributed in the remaining 90°. This shows a homogenous distribution over all possible orientations in the range of 180°. Consequently, there was no preferred alignment of objects was detected.

Both situations are displayed in the histogram. Strong orientations lead to a high and narrow peak, while broad distributions indicate arrangements spread over a wide range.

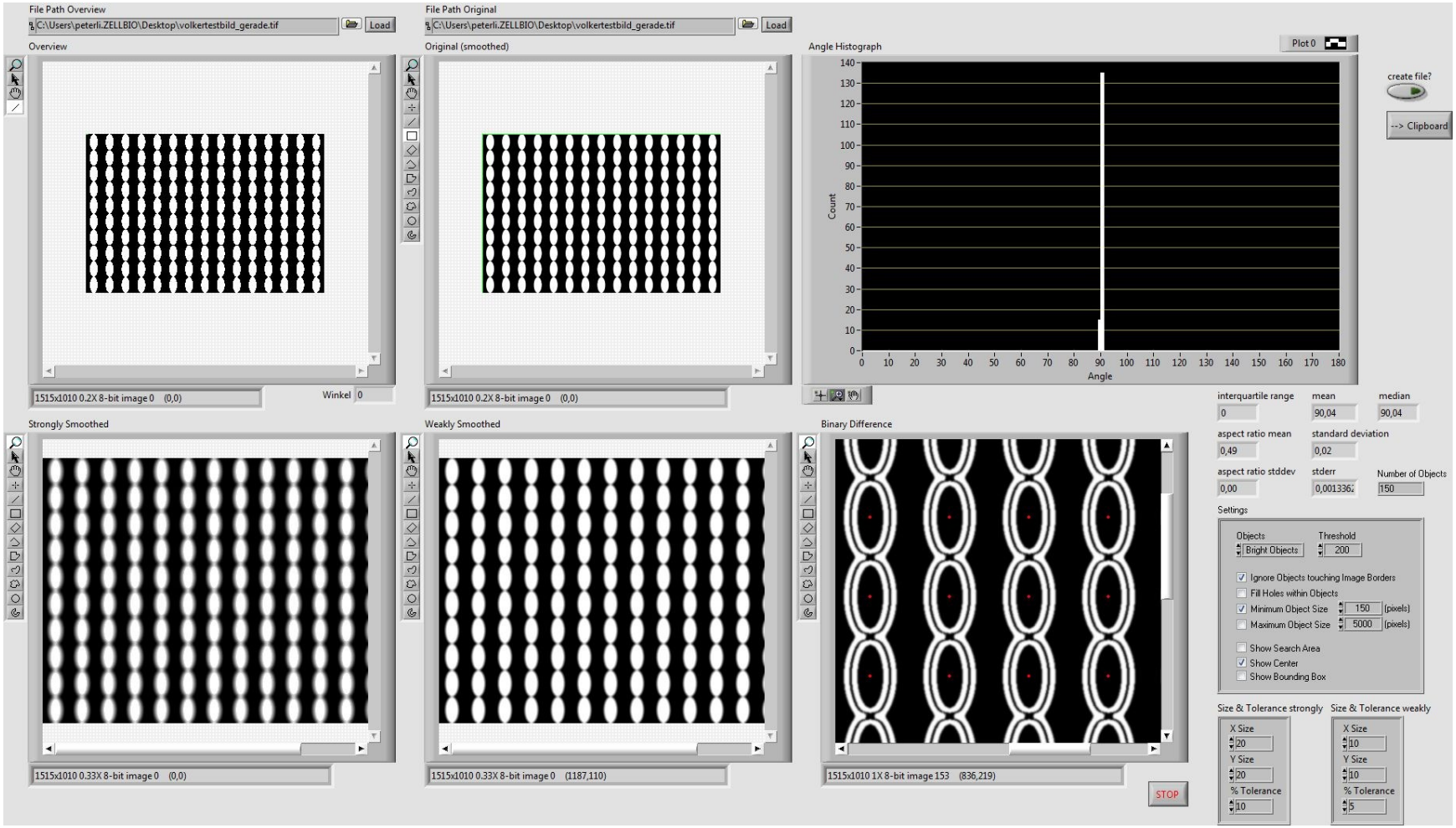

Figure 60: Test pattern for the illustration of strongly aligned elements. The analysis reveals an interquartile range of 0, a mean orientation of 90° and a standard deviation of 0.[6]

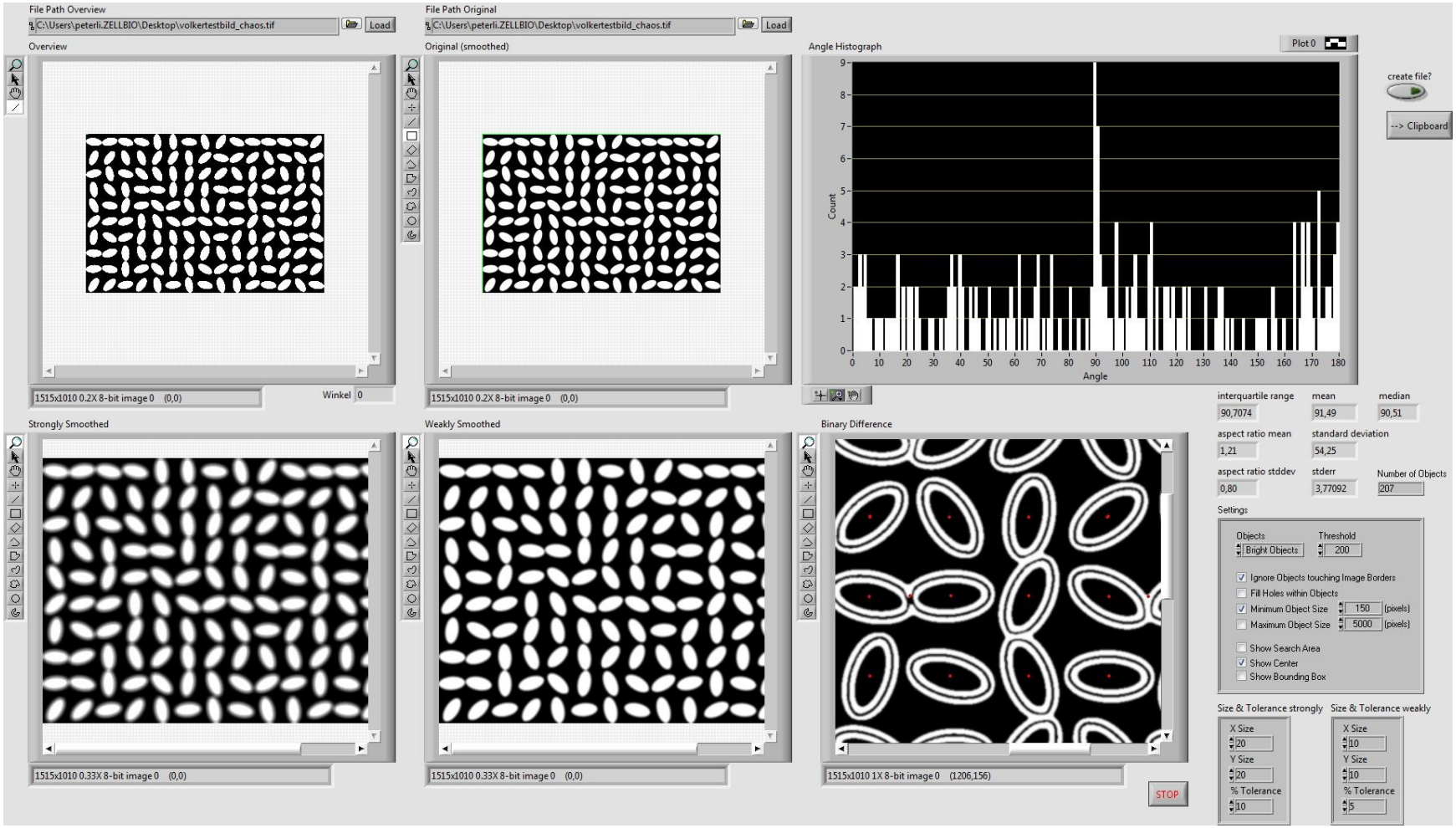

Figure 61: Test pattern for the illustration of strongly aligned elements. The analysis reveals an interquartile range of 91, a mean orientation of 92° and a standard deviation of 54.[6]

Difficulties with this evaluation occurred with pictures that had a low contrast and where probably a urothelial cell contamination was prominent. In this case, pictures looked similar to Figure 42 C1), where Urotsa was applied on Optimaix 3D Sponge1. Moreover, it was observed that high numbers of round particles, e.g. protein fragments, impair the evaluation as well as the view onto the sample. Possible consequences are optical distortion and preferential orientations.

Figure 62 shows the resulting orientations of fibrin-based prostheses in a boxplot. It can be seen that generally all possible directions (0°-180°) were seen on the outer surface of trained and untrained prostheses; this is indicated by the whiskers (dotted lines; one and a half times the interquartile range) and outliers (circles). Nevertheless, just trained prostheses (blue) presented to outliers, resulting in a narrower distribution of measured angles around a mean value.

All in all, untrained prostheses show bigger boxes (red) covering a range from 69° to 134°. In contrast to that, the interquartile ranges of the blue boxes (trained constructs) lay between 24° and 44°.

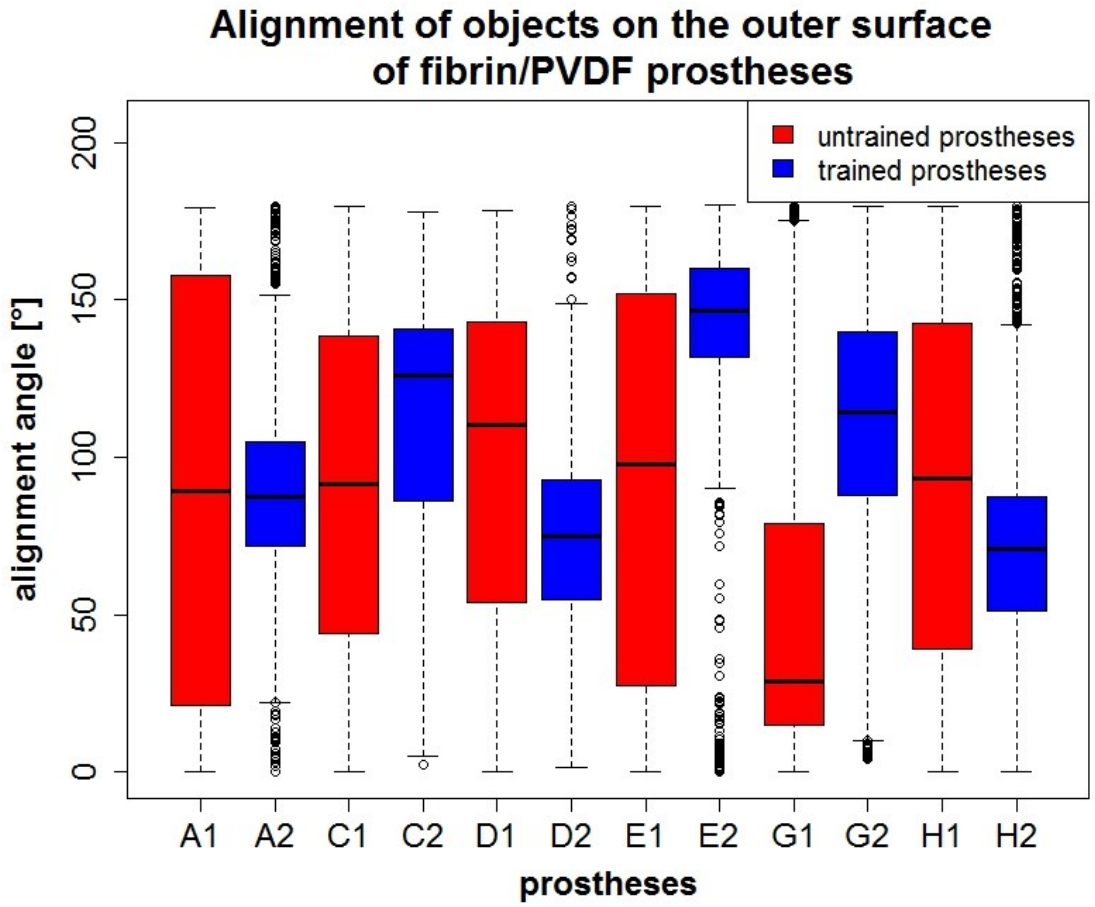

Figure 62: Evaluation of the alignment of all structural elements in a scanning electron microscopic picture of the outer surface of fibrin-based prostheses. Trained prostheses are coloured in blue, untrained in red.[6]

The interquartile ranges seen in Figure 62 were summarised for each group (trained and untrained prostheses). The means of the interquartile ranges with their standard deviations are shown in a bar plot in Figure 63. **The mean interquartile range for untrained prostheses was 95 ± 12°, compared to 34 ± 6° that were determined for trained prostheses.** The null hypothesis of the Wilcox rank-sum test, where both groups are the same, was rejected with p=0.002.

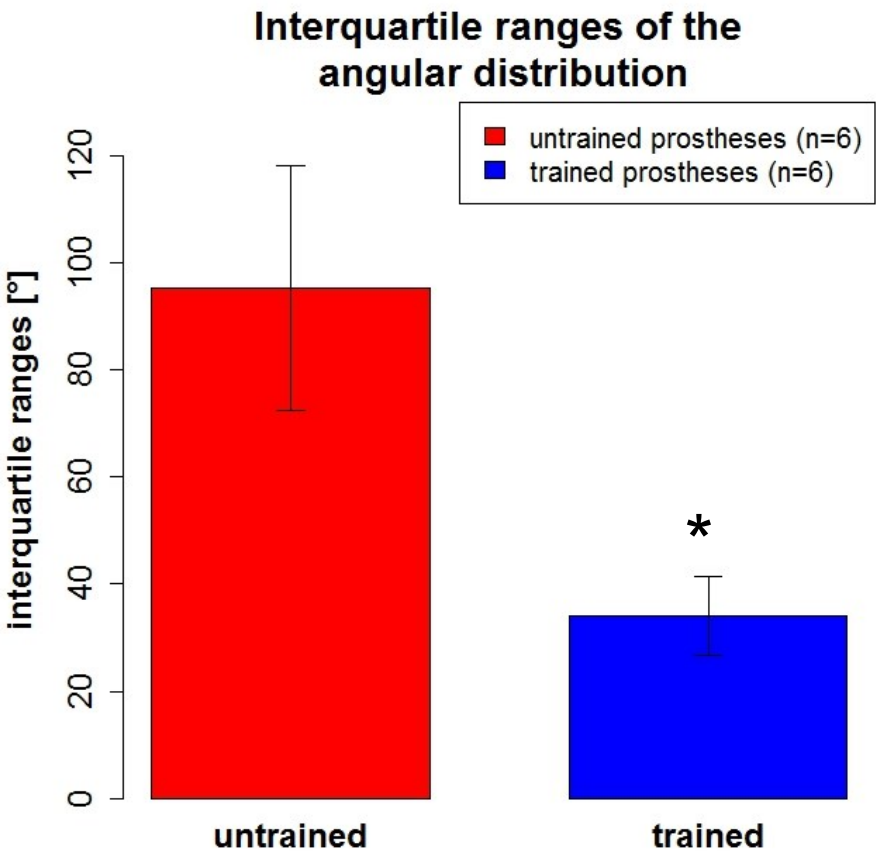

Figure 63: Size of the interquartile ranges showing the orientation of structural elements on the outer surface of untrained (red) and trained (blue) prostheses. The difference between the groups is significant ($p<0.05$) according to the results of the Wilcoxon rank-sum test.[6]

From these experiments and based on this examination it can be concluded that there was a preferred orientation of structural elements that became visible in scanning electron microscopic pictures of trained prostheses. A mean interquartile range of 95° for untrained prostheses leads to the conclusion that there is no prominent arrangement of elements in this group. In contrast to that, it can be seen that the mean angular distribution of trained prostheses was 34°. **Moreover, trained prosthesis show a mean orientation of structural elements and cells of 93° in a longitudinal direction.**

5.9.2 Cross-section and classical histology

Evaluations on cellular orientation in cross-sectional pictures were performed with microscopic pictures, taken with a light microscope, after the cells had been stained with haematoxylin & eosin (HE staining). A computer based GUI (cf. Figure 65) was prepared in LabVIEW with the support of Peter Linder, M.Sc. It was similar to the program that was described in Chapter 5.9.1. Significant differences to the previous program can be seen in the structure that is analysed in the corresponding pictures. Scanning electron microscopic pictures were analysed with respect to the orientation of particles. The main focus was put on the orientation of cellular borders that create high contrast regions in the picture. Therefore, cellular orientation was determined indirectly. In contrast to that, histological pictures analysed cellular orientation directly. This is based on the fact that single cells could be identified more easily than in scanning electron microscopy pictures, where the identification of single cells was challenging.

Figure 64 shows an example of an HE stained cross section of a trained fibrin prosthesis with a higher magnification than used for analysis. This was done in order to make the elements stand out to make further evaluation easier. In this figure, elongated cell bodies become apparent that were used for analysis. Such histological cross sections allow an automatised identification of cells, which was not possible with scanning electron microscopic pictures.

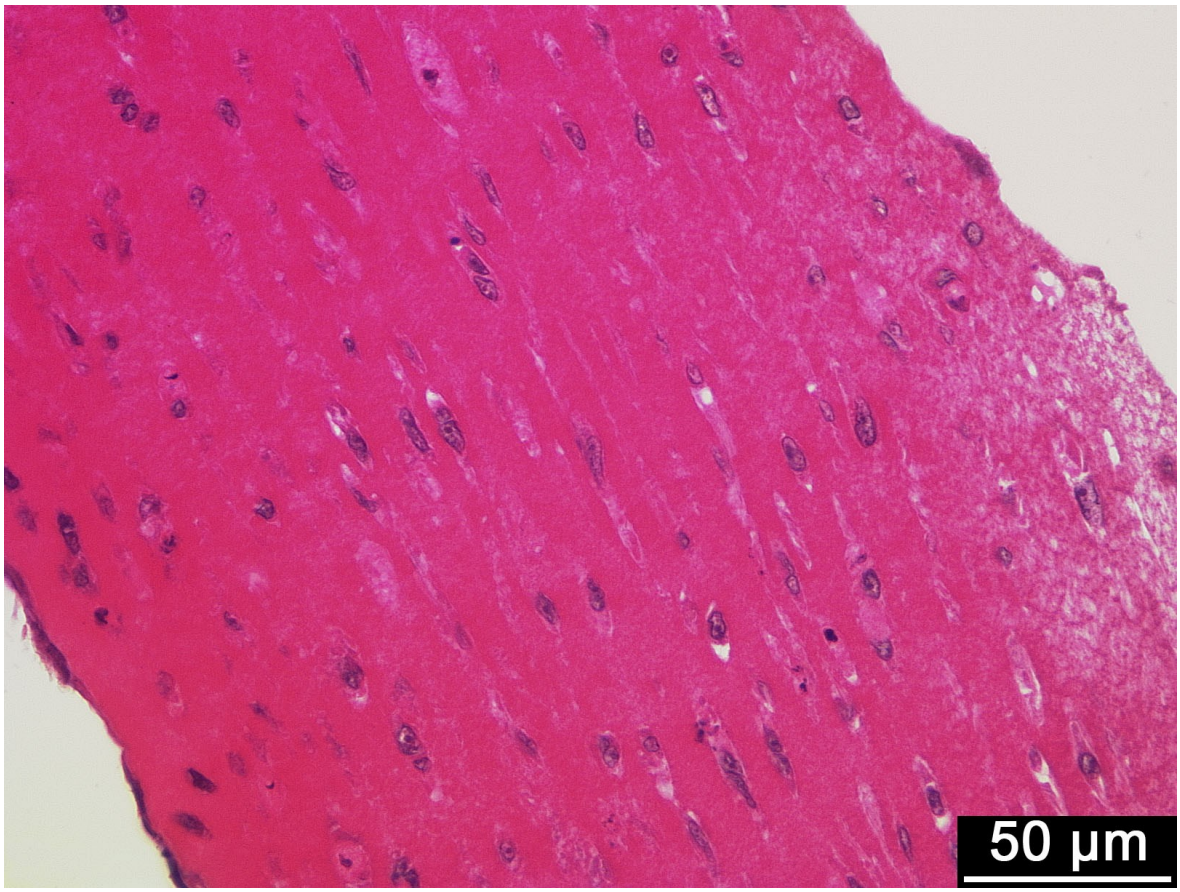

Figure 64: Cross section of a tissue-engineered and trained sample stained with haematoxylin & eosin. Scale bar: 50 µm.[6]

Pictures selected for analysis were loaded into the program and the fragments of the tubular samples were horizontally adjusted to the angle entered manually (see Figure 65 A). The pictures were then horizontally adjusted and displayed on the GUI, where a region of interest (ROI) was defined for the prostheses B). After that, the red image plane was subtracted C). Speckles were extracted according to a filter that was included in LabVIEW (Nth-order), where the nth value (30) of a defined region (10•10 pixels) was used to smooth the picture. After that, the particle (here: cell) detection was carried out according to the settings (F). The detected particles were displayed in E) and analysed according to their orientation F). To achieve that, their longitudinal axes were evaluated with respect to the horizontal orientation of the sample (cf. Figure 65 A)).

It was possible to demonstrated that inhomogeneity of the sample's density and thus in the coloration of the histological pictures lead to problems in the analysis of the cellular orientation. In these cases, holes or loose tissue segments were identified as cells and included in the statistics, even if they were artefacts. This

effect was reduced by defining the ROI as well as by setting a minimum object size of 300 pixels. Moreover, embedded cell clusters (urothelial cells) impair the analysis due to their round morphological appearance.

For further improvement, an additional weighting of the cellular orientation could be performed with respect to the aspect ratio of the cellular shape. This means that elongated, spindle shaped cells would have a stronger impact in statistics compared to rounder cells.

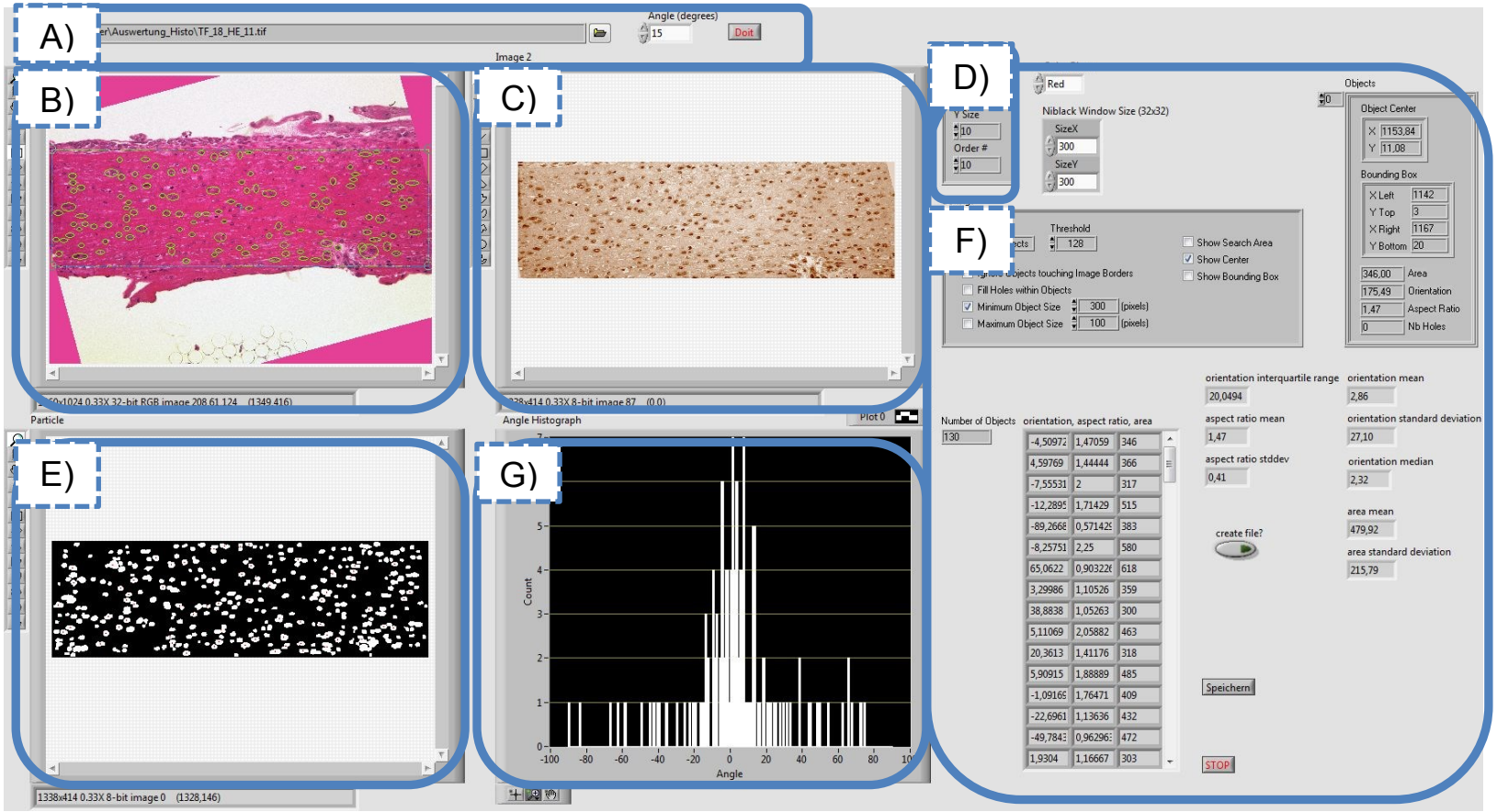

Figure 65: Graphical user interface for the analysis of histological pictures to evaluate cellular orientations. Labels indicate the evaluation process beginning with the loading and horizontal alignment of the picture/sample (A). A ROI was defined (B), before the red image plane was subtracted (C). Speckles were filtered (D) and a local threshold for the pixels' colour was set, before the particles/cells were identified (E) according to the settings (F). Results were evaluated (F) and were indicated in a histogram (G).[6]

Figure 66 shows the angular distribution of cells in a fibrin matrix referred to a horizontally arranged sample. Thus, an angle of 0° was equal to a circular arrangement of the cells. It can be seen that cells were distributed in all possible directions from 90° to -90°. All medians were in the range of 26°. Moreover, they were distributed around 0°, showing that there were preferred orientations in a circular direction.

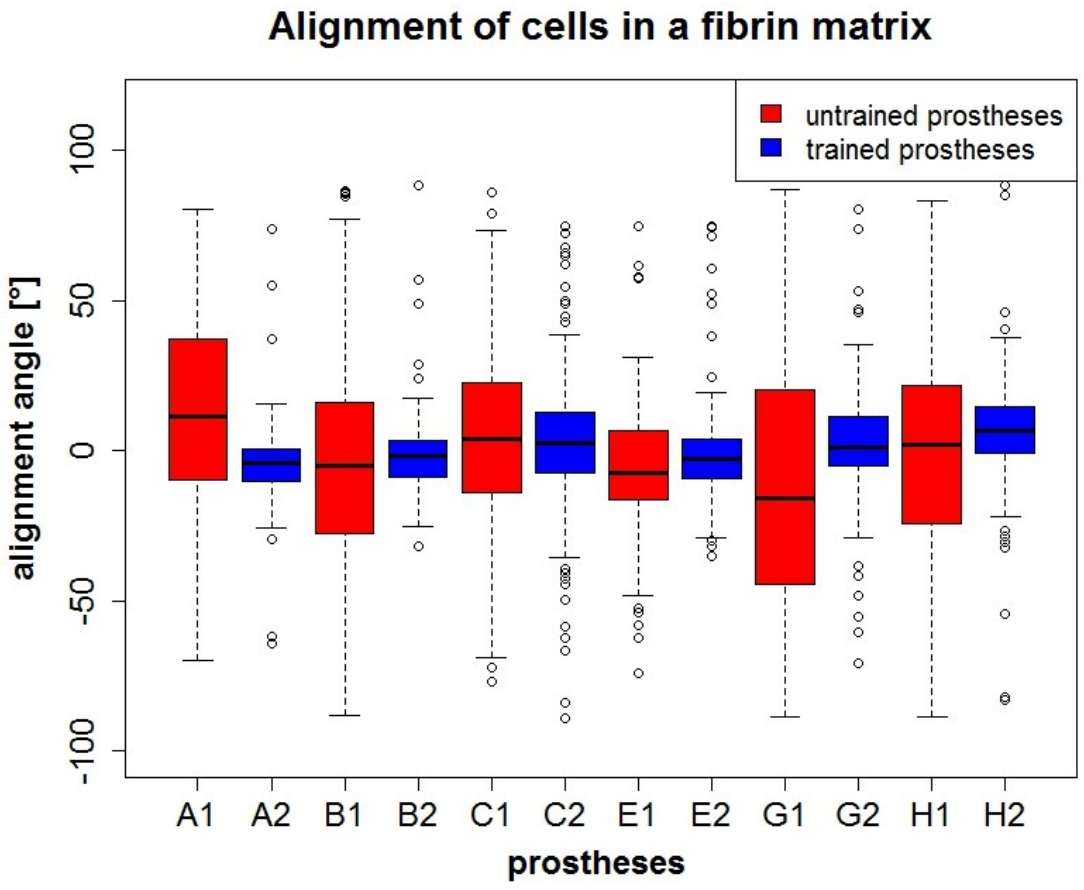

Figure 66: Cellular alignments in untrained (red) and trained (blue) fibrin matrices.[6]

Figure 67 analyses the size of the interquartile ranges of the angular distribution of cells inside the fibrin matrices. It can be seen that the mean of the interquartile ranges of untrained prostheses (red) was 45 ± 10° and 15 ± 3° for trained (blue). **Both groups differ significantly indicating a narrower distribution of cellular orientation with mechanically stressed prostheses.**

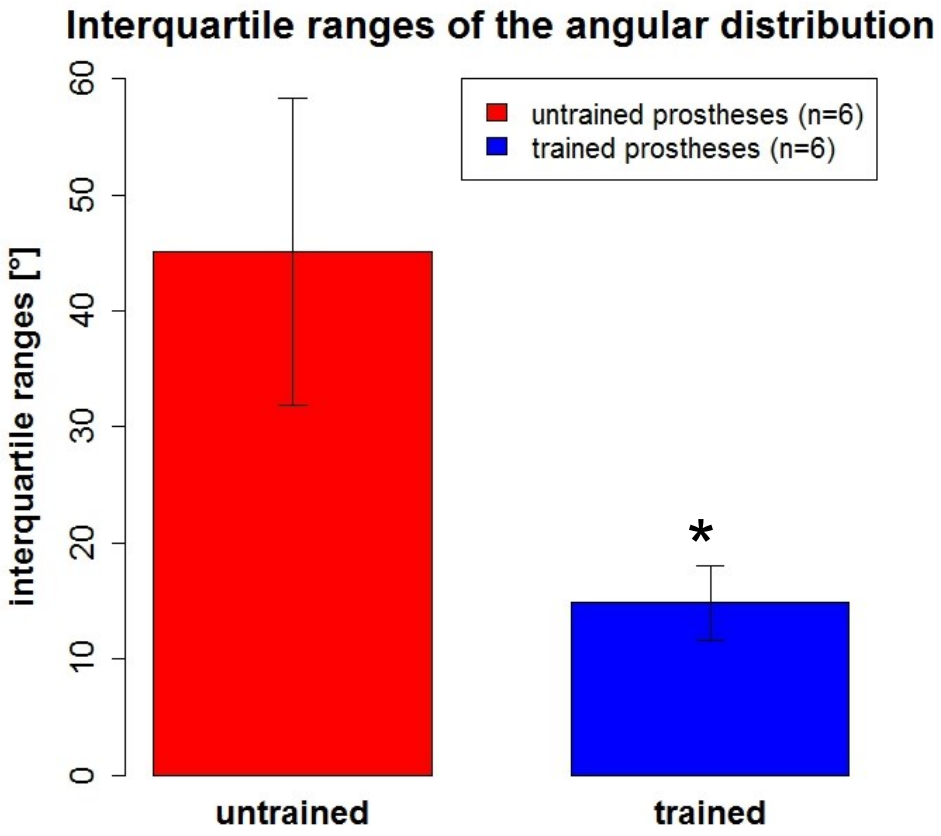

Figure 67: Size of the interquartile ranges showing the orientation of cells in a fibrin matrix of untrained (red) and trained (blue) prostheses. The difference between the groups is significant ($p<0.05$) according to the results of the Wilcoxon rank-sum test.[6]

The analysis of the cellular orientation inside the fibrin matrix reveals that even untrained cells showed a preferred direction. This might be based on the fact that peristaltic pumps ensured the cell culture medium supply. Even slow turning (10 rpm) pump heads could caused a pulsatile flow which might have contributed to a preferred orientation of the cells. Nevertheless, this stimulation was not as effective as for trained prostheses (cf. Figure 67).

During the work on this thesis, no other literature was found that deals with the alignment of primary, porcine bladder smooth muscle cells in a tubular 3D matrix. In this study, special focus was placed on the orientation of cells in different layers. All in all, it was concluded from the analyses carried out after a peristaltic stimulation with a catheter, that there was a certain preferred growth direction on the outer surface of tubular fibrin-based prostheses. The orientation inside the matrix was found as it had been expected for stimulated constructs. This alignment of cells was often found in literature for mechanically stressed structures, especially for vascular tissue engineering.[74,183]

It became apparent, that cells reacted to the applied mechanical stimulation with bidirectional growth. Angles were shifted by 90°. Nevertheless, the achieved structural setup was reversed, with a stratum circulare followed by a stratum longitudinale that was observed on the outer surface. Moreover, it could be seen that this layer had a thickness of only few (<5) cell layers.

For further experiments, numerous variables could be diversified, e.g. the stimulation frequency, intensity, incubation period, cell count or even the matrix composition.

6 Summary

This study is placed in the field of tissue engineering, which comprises several technical and medical engineering disciplines dealing with the generation of tubular constructs as replacements damaged parts of the genitourinary tract. Numerous primary and iatrogenic diseases affect the ureters, leading to severe injuries. A reliable bridging of ureters is not yet trivial. Even though bridging with small intestine is the gold standard, it still involves negative side effects, e.g. mucous production. Generally, it can be seen that tissue engineering is performed in various medical fields. Nevertheless, genitourinary tissue engineering and especially tubular tissue formation is not in focus. This is probably due to the fact that tissue-engineered constructs have to withstand a very complex natural milieu.

The few publications on tubular tissue engineering of the urinary tract are based on experiments in bioreactors, where no physiologic mechanical stimulation is applied. Most bioreactors that were utilised, create pulsatile flows for stimulation. Obviously, a lot of attention is paid to the urothelium that plays a crucial role in tissue tightness in the urinary tract. Reducing its role merely to its barrier function, however, would underrate the importance of the urothelium. Further, it excretes signalling molecules and to protects against infection. Additionally, the studies mentioned neglect the function of the smooth muscle cell layer and the fact that an application of muscle cells inside the matrix is necessary to reduce shrinkage. Shrinkage and fibroblast incorporation are seen as major hindrances leading to postoperative complications. The presented study is intended to contribute to the bridging of the gap.

The bioreactor system used was developed in the labs for Cell Biophysics and Medical & Molecular Biology of the Aachen, University of Applied Sciences, Jülich. It was developed to enable temperature and carbon dioxide regulation during cultivation periods of at least 2 weeks. It was demonstrated that the system worked reliably over the whole time.

One main part of this thesis shows the improvements that were achieved with the bioreactor system placing the focus on the mechanical stimulation of tubular prostheses. It was shown that several changes to the initial system were required to enable a successful imitation of peristaltic stimulation. A kyphoplasty catheter

mimicked the physiologic urine drop and a syringe pump inflated and deflated the balloon.

Further experiments lead to an advanced bioreactor design with an improved cell culture medium inlet and outlet to eliminate air bubbles inside the bioreactor. Moreover, the central fittings became screwable allowing different cell seeding mechanisms as well as providing high flexibility with respect to the dimensions and material of the applied scaffolds. The Bioreactor Prototype IV is easy to manage and it is reusable due to its heat resistance. This makes it ideally suited for efficient use in a clinical setup in future. Its suitability is further boosted by the possibility to operate at least two bioreactors in parallel (an achievement of this study).

Another achievement was accomplished by restructuring the graphical user interface of the system. Visualising current measurement values in numbers in combination with diagrams as well as arranging the setting options in tab pages lead to a clearly organised graphical user interface.

The combination of all these elements enabled a mechanical stimulation/training with a stretch of 20% and a frequency of 0.015 Hz.

Efficient cell culture media circuits and a contamination guard developed in this study ensured sterile and effective operation Bioreactor Prototype IV. The reduction of components achieved by the development of customised screw caps for use on the top of the media reservoirs made the use of antibiotics during the process dispensable. Sterilisable pH electrodes were introduced into the system to enable suitable monitoring of the media condition. Thus, the screw caps developed for this study supported the high flexibility of the bioreactor system by allowing several monitoring methods.

Two different biomaterials were tested in combination with various cell types, e.g. C2C12 or primary smooth muscle cells. Optimaix 3D Sponge1 was selected because of its suitable characteristics shown in first in-vitro and in-vivo studies. Nevertheless, it was concluded that this material with its huge wall thickness was not applicable in combination with this bioreactor system. Different seeding procedures and cultivation under dynamic conditions did not increase cellular penetration depth and cellular density, which were required for a mechanical stimulation. For that reason, Optimaix 3D Sponge1 was not used for further investigations.

Fibrin matrices in combination with a stabilising PVDF mesh proved to be convenient proper composite materials. Cells were directly casted into their position in a homogenous distribution. Incubation periods of 1 week (n=4) and 2 weeks (n=4) were achieved. Elongated incubation periods require higher amounts of Cyklokarpron® to avoid fibrinolysis and failure of the prosthesis. This is based on the tPA and uPA producing urothelium of the urinary tract. For that reason, it seems reasonable to test other material combinations using e.g. collagen, gelatine or alginate.

Grown tubular constructs were examined with respect to their tightness against urine-excreted substances, their mechanical strength, cellular distribution and orientation. It became apparent that classical histological analysis could not be performed on the Optimaix 3D Sponge1, whereas these methods were useful for fibrin-based prostheses. Scanning electron microscopy was useful for both types, leading to analysable surface images. LabVIEW-based programs with image processing tools revealed preferred directions of cellular orientation subsequent to mechanical stimulation. On the outer surface, a thin layer of longitudinally arranged cells could be proven, whereas cells inside the fibrin matrix were arranged circularly. Even untrained samples showed preferred cellular orientation, which might be traced back to the peristaltic perfusion with cell culture medium. Nevertheless, the orientation for trained prostheses was significantly increased. It can be summarised that two cell layers were detected with different orientations that were shifted by 90°, even if this specific setup is more likely to be expected in the intestine. Similar observations were not yet found in literature.

This study was able to show that an Ussing chamber can be used for further characterisation of tissue-engineered structures. For this study, the chamber was used for monitoring the passive diffusion of urea and creatinine through the tissue constructs as well as through native ureters. Similar experiments were shown in sed literature and demonstrate that the urothelium plays an important role in the diffusion of molecules through the ureters. Results that were achieved in this study showed in 5 of 7 (for urea) and 6 of 7 (for creatinine) analysable intraindividual experiments that there were differences in passive diffusion based on a mechanical stimulation and the use of primary smooth muscle cells. Mechanically stressed structures were more permeable for urea and creatinine than untrained prostheses. Taken in a whole, the differences were not significant.

Mechanical strength of the prostheses was determined based on their bursting pressures. An automatised measuring setup was developed with a pressure line for catheter inflation and deflation and a pressure chamber. Water was consistently pressed towards the sample with the syringe pump and generated increasing pressure onto the prostheses until they ruptured. Bursting pressures were analysed intraindividually and showed in 4 of 6 analysable experiments increased bursting pressures for mechanically trained prostheses. A tendency which was not yet significant may be observed with respect to the incubation periods and mechanical training. It seems that longer incubation periods as well as mechanical stress lead to more stable prostheses.

The novelty and main conclusion of this study is that a mechanical stimulation exerted by a catheter in a tubular bioreactor that mimics physiologic conditions leads to a bidirectional arrangement of smooth muscle cells. The application and mechanical stimulation of primary smooth muscle cells, which were isolated from porcine bladder, was intended to be used as ureter replacement. Presented results are encouraging to proceed investigations on this system with various biomaterial combinations to further enhance the grown tissues to achieve an even more physiologic tissue.

7 List of Literature

[1] D. Leon, *Int. J. Epidemiol.* **2011**, *40*, 271–277.

[2] K. Barnett, S. W. Mercer, M. Norbury, G. Watt, S. Wyke, B. Guthrie, *Lancet* **2012**, *380*, 37–43.

[3] A. Rahmel, Ed., *Annual Report 2012 Eurotransplant International Foundation*, Netherlands, **2012**.

[4] "German Organ Transplantation Foundation - DSO: Zahlen zur Organspende und - transplantation," can be found under http://www.dso.de/servicecenter/fachpublikum/zahlen-zur-organspende-und-transplantation.html, **2014**.

[5] "Anzahl der postmortalen Organspender in Deutschland bis 2013," can be found under http://de.statista.com/statistik/daten/studie/70873/umfrage/anzahl-der-postmortalen-organspender-in-deutschland/, **2014**.

[6] Graphics/technical drawings and photographs prepared by Volker Seifarth, **2014**.

[7] R. Skalak, C. F. Fox, in *Tissue Eng. Proc. a Work. Held Granibakken* (Eds.: R. Skalak, C.F. Fox), Alan R. Liss Inc. New York, **1988**.

[8] M. S. Chapekar, *J. Biomed. Mater. Res.* **2000**, *53*, 617–620.

[9] R. Langer, J. P. Vacanti, *Science* **1993**, *260*, 920–926.

[10] E. Lavik, R. Langer, *Appl. Microbiol. Biotechnol.* **2004**, *65*, 1–8.

[11] R. E. Guldberg, H. a Awad, G. Vunjak-Novakovic, H. Donahue, A. Das, *IBMS Bonekey* **2013**, *10*, 13–14.

[12] D. E. Ingber, V. C. Mow, D. Butler, L. Niklason, J. Huard, J. Mao, I. Yannas, D. Kaplan, G. Vunjak-Novakovic, *Tissue Eng.* **2006**, *12*, 3265–3283.

[13] Benninghoff, Drenckhahn, *Anatomie - Makroskopische Anatomie, Embriyologie, Zellbiologie*, Urban & Fischer, **2003**.

[14] W. S. McDougal, A. J. Wein, L. R. Kavoussi, A. C. Novick, A. W. Partin, C. A. Peters, P. Ramchandani, *Campbell-Walsh Urology 10th Edition Review*, Elsevier Health Sciences, **2011**.

[15] V. W. Nitti, *Rev. Urol.* **2005**, *7 Suppl 6*, 14–21.

[16] Figures by the Department of Urology, RWTH Aachen, **2014**.

[17] X. D. Jin, Z. D. Chen, S. L. Cai, S. W. Chen, *Scand. J. Urol. Nephrol.* **2009**, *43*, 73–75.

[18] G. Aumüller, G. Aust, A. Doll, *Duale Reihe Anatomie*, Thieme, **2010**.

[19] G. J. Tortora, B. H. Derrickson, *Principles of Anatomy and Physiology: Maintenance and Continuity of the Human Body. Volume 2*, John Wiley & Sons, Incorporated, **2009**.

[20] M. Lazzeri, *Urol. Int.* **2006**, *76*, 289–295.

[21] H. O. Negrete, J. P. Lavelle, J. Berg, S. Lewis, M. L. Zeidel, *Am. J. Physiol.* **1996**, *271*, 886–894.

[22] H. Lippert, *Lehrbuch Anatomie*, Elsevier Health Sciences Germany, **2011**.

[23] X. R. Wu, X. P. Kong, A. Pellicer, G. Kreibich, T. T. Sun, *Kidney Int.* **2009**, *75*, 1153–1165.

[24] P. Murray, H. Brady, J. B. Hall, *Intensive Care in Nephrology*, Taylor & Francis, **2005**.

[25] D. Jocham, K. Miller, *Praxis Der Urologie: Band I*, Thieme, **2007**.

[26] S. N. Cheuvront, R. W. Kenefick, K. R. Heavens, M. G. Spitz, *J. Clin. Lab. Anal.* **2014**, *6*, 1–6.

[27] J. I. Friedlander, D. M. Moreira, C. Hartman, S. E. Elsamra, A. D. Smith, Z. Okeke, *J. Endourol.* **2014**, *28*, 871–876.

[28] J. Hannappel, *Motorik Des Harntraktes - Physiologische Grundlagen Und Pharmakologie*, Habilitationsschrift Der RWTH-Aachen, **1983**.

[29] C. E. Constantinou, M. A. Silvert, J. Gosling, *Invest. Urol.* **1977**, *14*, 440–441.

[30] P. Santicioli, C. Maggi, *Pharmacol. Rev.* **1998**, *50*, 683–722.

[31] D. J. Griffiths, C. Notschaele, *Neurourol. Urodyn.* **1983**, *2*, 155–166.

[32] D. J. Griffiths, *J. Biomech. Eng.* **1989**, *111*, 206–211.

[33] A. Shafik, *Scand. J. Urol. Nephrol.* **1998**, *32*, 14–19.

[34] D. J. Summerton, N. Djakovic, N. D. Kitrey, F. Kuehhas, N. Lumen, E. Serafetinidis, *EAU Guidelines on Urological Trauma.*, **2013**.

[35] N. A. Armenakas, in *Urol. Emergencies* (Eds.: H. Wessells, FACS, J.W. McAninch), Springer, **2005**, pp. 25–38.

[36] J. M. Preston, *BJU Int.* **2000**, *86*, 313–317.

[37] J. R. Wagner, P. Russo, *Semin. Surg. Oncol.* **2000**, *18*, 216–228.

[38] S. P. Elliott, J. W. McAninch, *Urol. Clin. North Am.* **2006**, *33*, 55–66.

[39] Z. Dobrowolski, J. Kusionowicz, T. Drewniak, W. Habrat, W. Lipczyñski, P. Jakubik, W. Wêglarz, *BJU Int.* **2002**, *89*, 748–751.

[40] M. P. Gangai, R. E. Agee, C. R. Spence, *Urology* **1976**, *8*, 22–27.

[41] E. E. Moore, T. H. Cogbill, G. J. Jurkovich, J. W. McAninch, H. R. Champion, T. A. Gennarelli, M. A. Malangoni, S. R. Shackford, P. G. Trafton, *J. Trauma* **1992**, *33*, 337–339.

[42] S. Corvin, G. Feil, A. Stenzl, *Der Urologe Ausg. A* **2004**, *43*, 1213–1216.

[43] L. Martínez-Piñeiro, N. Djakovic, E. Plas, Y. Mor, R. A. Santucci, E. Serafetinidis, L. N. Turkeri, M. Hohenfellner, *Eur. Urol.* **2010**, *57*, 791–803.

[44] R. Santucci, J. M. Bartley, *Nat. Rev. Urol.* **2010**, *7*, 510–519.

[45] R. Lee, R. E. Symmonds, T. J. Williams, *Obstet. Gynecol.* **1988**, *72*, 313–319.

[46] J. Lee, M. Darcy, *Semin. Intervent. Radiol.* **2011**, *28*, 380–391.

[47] S. Ito, M. Ikeda, H. Asanuma, S. Shishido, H. Nakai, M. Honda, *Pediatr. Nephrol.* **2000**, *14*, 831–832.

[48] J. H. Naude, *BJU Int.* **1999**, *83*, 751–754.

[49] A. Woolf, S. Welham, *Maldevelopment of the Human Kidney and Lower Urinary Tract: An Overview*, Academic Press, **2003**.

[50] Y. Ono, S. Ohshima, T. Kinukawa, O. Matsuura, S. Hirabayashi, S. Yamada, *J. Urol.* **1989**, *142*, 958–960.

[51] R. Hofmann, *Der Urologe Ausg. A* **2006**, *45*, 637–647.

[52] P. Geavlete, D. Georgescu, G. Niţă, V. Mirciulescu, V. Cauni, *J. Endourol.* **2006**, *20*, 179–185.

[53] J. J. Weinberg, K. Ansong, A. D. Smith, *J. Urol.* **1987**, *137*, 384–385.

[54] D. Fahlenkamp, *Dtsch. Zeitschrift für Klin. Forsch. Innov. und Prax.* **2012**, 53–54.

[55] S. B. Kukarni, G. Barbagli, *Art of Urethral Reconstruction*, Elsevier, **2012**.

[56] A. Atala, *Br. Med. Bull.* **2011**, *97*, 81–104.

[57] H. Orabi, S. Bouhout, A. Morissette, A. Rousseau, S. Chabaud, S. Bolduc, *ScientificWorldJournal.* **2013**, *2013*, 1–13.

[58] I. Martin, D. Wendt, M. Heberer, *Trends Biotechnol.* **2004**, *22*, 80–86.

[59] R. Pörtner, S. Nagel-Heyer, C. Goepfert, P. Adamietz, N. M. Meenen, *J. Biosci. Bioeng.* **2005**, *100*, 235–245.

[60] R. Sodian, T. Lemke, *Tissue Eng.* **2002**, *8*, 863–874.

[61] M. J. Jaasma, N. a Plunkett, F. J. O'Brien, *J. Biotechnol.* **2008**, *133*, 490–496.

[62] A. B. Yeatts, J. P. Fisher, *Bone* **2011**, *48*, 171–181.

[63] F. W. Janssen, J. Oostra, A. Oorschot, C. A. van Blitterswijk, *Biomaterials* **2006**, *27*, 315–323.

[64] Z. Chunqiu, D. Xin, W. Han, Z. Weimin, Z. Dong, *Biosci. Hypotheses* **2008**, *1*, 319–323.

[65] T. Sun, D. Norton, J. W. Haycock, A. J. Ryan, S. MacNeil, *Tissue Eng.* **2005**, *11*, 1824–1831.

[66] C. H. Lin, S. H. Hsu, C. E. Huang, W. T. Cheng, J. M. Su, *Biomaterials* **2009**, *30*, 4117–4126.

[67] S. S. Kim, R. Penkala, P. Abrahimi, *J. Surg. Res.* **2007**, *142*, 327–331.

[68] Z. H. Syedain, R. T. Tranquillo, *Biomaterials* **2009**, *30*, 4078–4084.

[69] S. Bhumiratana, J. Bernhard, E. Cimetta, G. Vunjak-Novakovic, in *Princ. Tissue Eng.*, **2014**.

[70] P. Lenas, F. P. Luyten, M. Doblare, E. Nicodemou-Lena, A. E. Lanzara, *Artif. Organs* **2011**, *35*, 656–662.

[71] S. V. Murphy, A. Atala, *Bioessays* **2013**, *35*, 163–172.

[72] M. Nishi, R. Matsumoto, J. Dong, T. Uemura, *J. Biomed. Mater. Res. A* **2013**, *101*, 421–427.

[73] R. M. Nerem, D. Seliktar, *Annu. Rev. Biomed. Eng.* **2001**, 225–243.

[74] D. Seliktar, R. Black, R. P. Vito, R. M. Nerem, *Ann. Biomed. Eng.* **2000**, *28*, 351–362.

[75] A. Orsola, R. Adam, C. Peters, M. Freeman, *Urology* **2002**, *59*, 779–783.

[76] B. S. Kim, D. J. Mooney, *J. Biomech. Eng.* **2000**, *122*, 210–215.

[77] S. W. Liao, K. Hida, J. S. Park, S. Li, *Conf. Proc. IEEE Eng. Med. Biol. Soc.* **2004**, *7*, 5024–5027.

[78] C. Ritchie, S. Wijaya, W. F. Ong, S. P. Zhong, K. S. Chian, *Biotechnol. Bioeng.* **2009**, *102*, 1703–1711.

[79] J. H. Zhu, C. L. Chen, S. Flavahan, J. Harr, B. Su, N. Flavahan, *Am. J. Physiol. Heart Circ. Physiol.* **2011**, *300*, 1770–1780.

[80] M. Gonen-Wadmany, L. Gepstein, D. Seliktar, *Ann. N. Y. Acad. Sci.* **2004**, *1015*, 299–311.

[81] I. Mills, C. R. Cohen, K. Kamal, G. Li, T. Shin, W. Du, B. E. Sumpio, *J. Cell. Physiol.* **1997**, *170*, 228–234.

[82] U. Hubschmid, A. Basset-Dardare, S. Ruault, P. Frey, *Tissue Eng.* **2005**, *11*, 161–171.

[83] S. Wu, Y. Liu, S. Bharadwaj, A. Atala, Y. Zhang, *Biomaterials* **2011**, *32*, 1317–1326.

[84] Y. Liu, S. Bharadwaj, S. J. Lee, A. Atala, Y. Zhang, *Biomaterials* **2009**, *30*, 3865–3873.

[85] D. Eberli, L. Freitas Filho, A. Atala, J. J. Yoo, *Methods* **2009**, *47*, 109–115.

[86] A. Atala, S. B. Bauer, S. Soker, J. J. Yoo, A. B. Retik, *Lancet* **2006**, *367*, 1241–1246.

[87] P. Geutjes, L. Roelofs, H. Hoogenkamp, M. Walraven, B. Kortmann, R. Gier, F. Farag, D. Tiemessen, M. Sloff, E. Oosterwijk, et al., *J. Urol.* **2012**, *188*, 653–660.

[88] J. Dabernig, O. P. Shelley, G. Cuccia, J. Schaff, *Eur. Urol.* **2007**, *52*, 547–553.

[89] G. Garaffa, D. J. Ralph, N. Christopher, *BJU Int.* **2010**, *106*, 1206–1210.

[90] D. Raghavan, B. P. Kropp, H. K. Lin, Y. Zhang, R. Cowan, S. Madihally, *J. Biomed. Mater. Res. A* **2005**, *73*, 90–96.

[91] Y. Xu, W. Fu, G. Li, J. Shi, H. Tan, K. Hu, F. Cui, Q. Lin, X. Zhang, *J. Mater. Sci. Mater. Med.* **2012**, *23*, 1119–1128.

[92] M. H. Zheng, J. Chen, Y. Kirilak, C. Willers, J. Xu, D. Wood, *J. Biomed. Mater. Res. B. Appl. Biomater.* **2005**, *73*, 61–67.

[93] S. Ozturk, W. S. Hu, *Cell Culture Technology for Pharmaceutical and Cell-Based Therapies*, Taylor & Francis, **2005**.

[94] B. M. Martin, *Tissue Culture Techniques: An Introduction*, Birkhäuser Boston, **1994**.

[95] G. Gstraunthaler, T. Lindl, *Zell- Und Gewebekultur*, Springer Berlin Heidelberg, Berlin, Heidelberg, **2013**.

[96] R. Dulbecco, M. Vogt, *J. Exp. Med.* **1954**, *99*, 167–182.

[97] K. Montzka, T. Läufer, C. Becker, J. Grosse, A. Heidenreich, *BJU Int.* **2011**, *107*, 1974–1981.

[98] D. P. Griffith, D. M. Musher, C. Itin, *Invest. Urol.* **1976**, *13*, 346–50.

[99] E. Hering, G. Schönfelder, *Sensoren in Wissenschaft Und Technik*, Vieweg+Teubner Verlag, **2012**.

[100] S. E. Manahan, *Fundamentals of Environmental Chemistry, Second Edition*, Taylor & Francis, **2000**.

[101] H. Lindorf, *Technische Temperaturmessung*, Girardet, **1970**.

[102] S. Parsons, *Pharmaceutical Calculations*, Parsons Printing Press, **2012**.

[103] M. A. Harrison, I. F. Rae, *General Techniques of Cell Culture*, Cambridge University Press, **1997**.

[104] H. J. Boxberger, *Leitfaden Für Die Zell- Und Gewebekultur: Einführung in Grundlagen Und Techniken*, Wiley, **2013**.

[105] Stefan Wilhelm Hasken, Pädiatrische Tissue Engineerte Herzklappen Auf Basis Einer Fibringelmatrix – Optimierung Des Herstellungs- Und Konditionierungsprozesses, Rheinisch-Westfälische Technische Hochschule Aachen (RWTH Aachen University), **2012**.

[106] S. Koch, T. C. Flanagan, J. S. Sachweh, F. Tanios, H. Schnoering, T. Deichmann, V. Ellä, M. Kellomäki, N. Gronloh, T. Gries, et al., *Biomaterials* **2010**, *31*, 4731–4739.

[107] Q. Ye, G. Zünd, S. Jockenhoevel, S. P. Hoerstrup, A. Schoeberlein, J. Grunenfelder, M. Turina, *Eur. J. Cardiothorac. Surg.* **2000**, *17*, 449–454.

[108] R. I. Hata, H. Senoo, *J. Cell. Physiol.* **1989**, *138*, 8–16.

[109] E. Cholewinski, M. Dietrich, T. C. Flanagan, T. Schmitz-Rode, S. Jockenhoevel, *Tissue Eng. Part A* **2009**, *15*, 3645–3653.

[110] C. M. Pipan, W. P. Glasheen, T. L. Matthew, S. L. Gonias, L. J. Hwang, J. Jane, W. D. Spotnitz, *J. Surg. Res.* **1992**, *53*, 402–427.

[111] P. S. Bisen, *Laboratory Protocols in Applied Life Sciences*, Taylor & Francis, **2014**.

[112] S. P. Hoerstrup, G. Zünd, R. Sodian, a M. Schnell, J. Grünenfelder, M. I. Turina, *Eur. J. Cardiothorac. Surg.* **2001**, *20*, 164–169.

[113] *TC20™ Automated Cell Counter - Instruction Manual*, **2011**.

[114] M. Mulisch, U. Welsch, *Romeis Mikroskopische Technik*, Spektrum Akademischer Verlag GmbH, **2010**.

[115] S. Koch, N. Stappenbeck, C. G. Cornelissen, T. C. Flanagan, P. Mela, J. Sachweh, B. Hermanns-Sachweh, S. Jockenhoevel, *Tissue Eng. Part C. Methods* **2012**, *18*, 976–983.

[116] G. Lang, *Histotechnik: Praxislehrbuch Für Die Biomedizinische Analytik*, Springer-Verlag KG, **2012**.

[117] R. Heintzmann, G. Ficz, *Brief. Funct. Genomic. Proteomic.* **2006**, *5*, 289–301.

[118] J. J. Bozzola, L. D. Russell, *Electron Microscopy: Principles and Techniques for Biologists*, Jones And Bartlett, **1999**.

[119] D. C. Giancoli, *Physik: Lehr- Und Übungsbuch*, Pearson Studium, **2010**.

[120] L. Reimer, G. Pfefferkorn, *Raster-Elektronenmikroskopie*, Springer Berlin Heidelberg, Berlin, Heidelberg, **1977**.

[121] A. El Sherif, F. Yano, S. Mittal, C. J. Filipi, *Hernia* **2006**, *10*, 511–520.

[122] K. E. Kadler, D. F. Holmes, J. Trotter, J. Chapman, *Biochem. J.* **1996**, *316*, 1–11.

[123] V. Kroehne, I. Heschel, F. Schügner, D. Lasrich, J. W. Bartsch, H. Jockusch, *J. Cell. Mol. Med.* **2008**, *12*, 1640–1648.

[124] D. Leonhäuser, V. Seifarth, K. Strick, C. Fera, N. Gaisa, I. Heschel, R. H. Tolba, A. (Temiz) Artmann, J. Grosse, in *4. Symp. Urol. Forsch. Der DGU*, Springer, Berlin, **2012**, p. 126.

[125] D. Leonhäuser, K. Strick, V. Seifarth, N. Huppertz, C. Fera, N. Gaisa, I. Heschel, A. Woitok, I. Zraik, Y. He, et al., in *Kongress Der Dtsch. Gesellschaft Für Urol. e.V.*, Dresden, **2013**, p. 96.

[126] D. Leonhäuser, V. Seifarth, K. Strick, N. Gaisa, I. Heschel, R. H. Tolba, A. Artmann, J. Grosse, *Eur. Urol. Suppl.* **2013**, *12*, e871.

[127] *Instructions for Use - Optimaix-3D^{TM} Scaffolds*, **2010**.

[128] N. Beck, *Diagnostic Hematology*, Springer London, London, **2009**.

[129] J. McDonagh, H. Messel, R. P. McDonagh, G. Murano, B. Blombäck, *Biochim. Biophys. Acta - Protein Struct.* **1972**, *257*, 135–142.

[130] M. W. Mosesson, *J. Thromb. Haemost.* **2005**, *3*, 1894–1904.

[131] L. Bachmann, W. W. Schmitt-Fumain, R. Hammel, K. Lederer, *Die Makromol. Chemie* **1975**, *176*, 2603–2618.

[132] H. Fritz, G. Wunderer, *Arzneimittelforschung.* **1983**, *33*, 479–494.

[133] S. Jockenhoevel, T. Flanagan, in *Tissue Eng. Tissue Organ Regen.* (Ed.: Eber), InTech, **2011**, pp. 35–48.

[134] R. W. Busuttil, *J. Am. Coll. Surg.* **2003**, *197*, 1021–1028.

[135] D. Green, C. Wong, P. Twardowski, *Transfus. Med. Rev.* **1996**, *10*, 171–182.

[136] D. Klee, Z. Ademovic, A. Bosserhoff, H. Hoecker, G. Maziolis, H. J. Erli, *Biomaterials* **2003**, *24*, 3663–3670.

[137] E. Urban, M. W. King, R. Guidoin, G. Laroche, Y. Marois, L. Martin, A. Cardou, Y. Douville, *ASAIO J.* **1994**, *40*, 145–156.

[138] P. Lynen Jansen, U. Klinge, M. Anurov, S. Titkova, P. R. Mertens, M. Jansen, *Eur. Surg. Res.* **2004**, *36*, 104–111.

[139] C. D. Klink, K. Junge, M. Binnebösel, H. P. Alizai, J. Otto, U. P. Neumann, U. Klinge, *J. Invest. Surg.* **2011**, *24*, 292–299.

[140] E. Wintermantel, S. W. Ha, *Medizintechnik: Life Science Engineering*, Springer, **2009**.

[141] M. Noeske, J. Degenhardt, S. Strudthoff, U. Lommatzsch, *Int. J. Adhes. Adhes.* **2004**, *24*, 171–177.

[142] P. Chu, J. Y. Chen, L. P. Wang, N. Huang, *Mater. Sci. Eng. R Reports* **2002**, *36*, 143–206.

[143] Q. Ye, G. Zünd, P. Benedikt, S. Jockenhoevel, S. P. Hoerstrup, S. Sakyama, J. a Hubbell, M. Turina, *Eur. J. Cardiothorac. Surg.* **2000**, *17*, 587–591.

[144] S. Jockenhoevel, G. Zund, S. P. Hoerstrup, K. Chalabi, J. S. Sachweh, L. Demircan, B. J. Messmer, M. Turina, *Eur. J. Cardio-thoracic Surg.* **2001**, *19*, 424–430.

[145] C. M. Stoscheck, *Methods Enzymol.* **1990**, *182*, 50–68.

[146] R. J. Dellenback, S. Chien, *Proc. Soc. Exp. Biol. Med.* **1970**, *134*, 353–355.

[147] Schehl, UREPLACE – Ureter Prosthesis: Progression to a New Ureter Bioreactor Prototype III System and a Preliminary Test Run with Its Evaluation, FH Aachen University of Applied Sciences, **2011**.

[148] Seifarth, UREPLACE - Ureter Prothesis: Optimization and First Application of the Ureplace Prototype III, FH Aachen University of Applied Sciences, **2011**.

[149] V. Seifarth, D. Schehl, P. Linder, M. Gossmann, I. Digel, G. M. Artmann, D. Porst, C. Preiß, P. Kayser, O. Pack, et al., *Al-Farabi Kazakh Natl. Univ. Bull. Biol. Ser.* **2011**, *2*, 56–58.

[150] R. Jauregui, UREPLACE: Ureter Replacement Bioreactor, FH Aachen University of Applied Sciences, **2010**.

[151] C. Stöck, Weiterentwicklung Eines Bioreaktors Für Eine Biohybride Harnleiterrekonstruktion, FH Aachen University of Applied Sciences, **2010**.

[152] M. A. Brown, R. K. Iyer, M. Radisic, *Biotechnol. Prog.* **2008**, *24*, 907–920.

[153] M. Radisic, A. Marsano, R. Maidhof, Y. Wang, G. Vunjak-Novakovic, *Nat. Protoc.* **2008**, *3*, 719–738.

[154] I. Martin, T. Smith, D. Wendt, *Trends Biotechnol.* **2009**, *27*, 495–502.

[155] K. J. Penick, L. Solchaga, J. Berilla, J. F. Welter, *J. Biomed. Mater. Res. A* **2005**, *75*, 168–174.

[156] Eriks, *Technisches Handbuch O-Ringe*, **2014**.

[157] H. Saechtling, E. Baur, S. Brinkmann, T. A. Osswald, N. Rudolph, E. Schmachtenberg, *Saechtling Kunststoff Taschenbuch*, Carl Hanser Verlag GmbH & Company KG, **2013**.

[158] S. Intruments, “Prozesselektroden - Sensoren für die Analytik im Prozess,” can be found under http://www.labo.de/upload_hoppenstedt/Prozesselektroden_Katalog_865975.pdf, **2014**.

[159] J.-P. Chen, C.-T. Lin, *J. Biosci. Bioeng.* **2006**, *102*, 41–45.

[160] D. Pazzano, K. a Mercier, J. M. Moran, S. S. Fong, D. D. DiBiasio, J. X. Rulfs, S. S. Kohles, L. J. Bonassar, *Biotechnol. Prog.* **2000**, *16*, 893–896.

[161] Y. Martin, P. Vermette, *Biomaterials* **2005**, *26*, 7481–7503.

[162] H. C. Chen, Y. C. Hu, *Biotechnol. Lett.* **2006**, *28*, 1415–1423.

[163] L. E. Niklason, R. S. Langer, *Transpl. Immunol.* **1997**, *5*, 303–306.

[164] A. D. McCulloch, A. B. Harris, C. E. Sarraf, M. Eastwood, *Tissue Eng.* **2004**, *10*, 565–573.

[165] S. I. Jeong, J. H. Kwon, J. I. Lim, S.-W. Cho, Y. Jung, W. J. Sung, S. H. Kim, Y. H. Kim, Y. M. Lee, B.-S. Kim, et al., *Biomaterials* **2005**, *26*, 1405–1411.

[166] K. Iwasaki, K. Kojima, S. Kodama, A. C. Paz, M. Chambers, M. Umezu, C. Vacanti, *Circulation* **2008**, *118*, 52–57.

[167] R. Bornemann, E. M. W. Koch, M. Wollny, R. Pflugmacher, *Eur. J. Orthop. Surg. Traumatol.* **2014**, *24 Suppl 1*, 131–143.

[168] R. Buchbinder, R. H. Osborne, P. R. Ebeling, J. D. Wark, P. Mitchell, C. Wriedt, S. Graves, M. P. Staples, B. Murphy, *N. Engl. J. Med.* **2009**, *361*, 557–568.

[169] R. S. Taylor, P. Fritzell, R. J. Taylor, *Eur. Spine J.* **2007**, *16*, 1085–1100.

[170] L. E. Freed, G. Vunjak-Novakovic, *In Vitro Cell. Dev. Biol. Anim.* **1997**, *33*, 381–538.

[171] B. Tschoeke, T. C. Flanagan, A. Cornelissen, S. Koch, A. Roehl, M. Sriharwoko, J. S. Sachweh, T. Gries, T. Schmitz-Rode, S. Jockenhoevel, *Artif. Organs* **2008**, *32*, 800–809.

[172] H. Lippert, *Wundatlas: Kompendium Der Komplexen Wundbehandlung*, Thieme, **2012**.

[173] G. Krüger, *Haftklebebänder, Selbstklebende Folien Und Etiketten: Entwicklung, Verarbeitung Und Industrieller Einsatz*, Carl Hanser Verlag GmbH & Company KG, **2012**.

[174] J. Meinhart, M. Fussenegger, W. Höbling, *Ann. Plast. Surg.* **1999**, *42*, 673–678.

[175] F.-M. Deng, M. Ding, R. M. Lavker, T.-T. Sun, *Proc. Natl. Acad. Sci. U. S. A.* **2001**, *98*, 154–9.

[176] J. Heuts, J. Salber, A. M. Goldyn, R. Janser, M. Möller, D. Klee, *J. Biomed. Mater. Res. A* **2010**, *92*, 1538–1851.

[177] A. Schellenberg, R. Ross, G. Abagnale, S. Joussen, P. Schuster, A. Arshi, N. Pallua, S. Jockenhoevel, T. Gries, W. Wagner, *PLoS One* **2014**, *9*, e94353.

[178] C. Ronco, R. Bellomo, J. A. Kellum, *Critical Care Nephrology*, Saunders/Elsevier, **2008**.

[179] C. Hick, A. Hick, *Intensivkurs Physiologie*, Elsevier, Urban & Fischer, **2009**.

[180] V. Cattan, G. Bernard, A. Rousseau, S. Bouhout, S. Chabaud, F. A. Auger, S. Bolduc, *Eur. Urol.* **2011**, *60*, 1291–1298.

[181] S. Bouhout, E. Perron, R. Gauvin, G. Bernard, G. Ouellet, V. Cattan, S. Bolduc, *Tissue Eng. Part A* **2010**, *16*, 1539–1548.

[182] M. Magnan, P. Lévesque, R. Gauvin, J. Dubé, D. Barrieras, A. El-Hakim, S. Bolduc, *Tissue Eng. Part A* **2009**, *15*, 197–202.

[183] K. Kanda, T. Matsuda, T. Oka, *ASAIO J.* **1993**, *39*, 686–690.

8 Appendix

8.1 Abbreviations

Abbreviation	Meaning
3D	Three dimensional
AAST	American association for surgery of trauma
BSM	Bladder submucosa
BSS	Balanced salt solution
C2C12	Mouse myoblast cell line
cf.	confer
CO_2	Carbon dioxide
CPD	Critical point drying
DAPI	4′,6-diamidin-2-phenylindol
d_i	Inner diameter
DMEM	Dulbecco's modified eagle's medium
e.g.	Exempli gratia (for example)
EAU	European association of urology
ECM	Extracellular matrix
FBS	Fetal bovine serum
GUI	Graphical user interface
HE	Haematoxylin & Eosin
i.e.	id est (meaning)
ITA	Institute for textile technology of the RWTH Aachen University
IZKF	Interdisciplinary Centre for Clinical Research
n	Number of data items
NPS	Not part of study
PBS	Phosphate buffered saline

Abbreviation	Meaning
PCTFE	Polychlortrifluorethylene
PEEK	Polyether ether ketone
PES	Polyethersulfone
POM	Polyoxymethylene
PPS	Polyphenylene sulphide
PTFE	Polytetrafluoroethylene
PVDF	Polyvinylidenfluorid
ROI	Region of interest
SEM	Scanning electron microscope
SIS	Small intestine submucosa
SMC	Smooth muscle cell
TBS	Tris buffered saline
TE	Tissue Engineering
tPA	Tissue-type plasminogen activator
uPA	Urokinase-type plasminogen activator
UV	Ultraviolet
$\mathbf{x_i}$	I^{th} value in the dataset

8.2 Medical dictionary

Term	Meaning
Adventitia	Connective tissue layer covering of a hollow organ (e.g. blood vessels) for the integration into the surrounding tissue.
Anastomosis	Surgical connection of two separated hollow tubular structures (intestine/blood vessel/ureter/urethra) to form a continuous pipe.
Avulsion	Violent tearing off body parts of tissues by accidents or surgery.
Bilharzial	Tropical disease with an infection by schistosomes (small worms), leading to the damage of genitourinary tract tissues and other organs.
Calculus	Concentration of mineral salts, forming stones for example in the kidney or urinary bladder.
Caudal	Directed/related to the tail.
Collapse	Fall down/break down/cave in of a tissue structure, losing tissue's function.
Contusion	Injury that does not rupture the skin, resulting in a swelling and discoloration.
Cranial	Directed/related to the skull.
Diabetes	Chronic disorder of the glucose household. The patient is lacking an adequate insulin production, resulting in abnormal concentrations of sugar in the blood and urine.
Endometriosis	Painful periods with abnormal endomaterial tissue that is located outside the uterus.
Fistula	Tunnel/passage/duct that connects (abnormal) body cavities and hollow organs to other hollow organs or to the body surface.
Hematoma	Damage of a blood vessel resulting a swelling of the tissue due to blood inflow.
Hydronephrosis	Distension of the renal pelvis and calyces because of an obstructed urinary tract impairing the drainage of urine.
Iatrogenic injury	Unintentional/undesired injury of patient by a medical intervention.
Incontinence	Uncontrolled/involuntary excretion of urine or fecal matter.

Term	Meaning
Intravenous	Given/applied into a body's vein.
Kyphoplasty	Spinal procedure, where a fractured vertebra is reconstructed by the injection of bone cement. Vertebrae are inflated in balloon kyphoplasty procedures.
Laceration	Irregular/jagged/open wound or cut by for example blunt trauma.
Lamina propria	Thin connective tissue layer beneath the epithelium (here: urothelium).
Lumen/luminal	Open space/cavity/volume of a hollow organ like blood vessels, intestine, ureter or urethra.
Medial	Situated in/directed to the middle.
Mucosa	Membrane lining a hollow organ, excreting mucous.
Mucous	Viscous body secretion produced by moist membranes.
Myogenically/myogenic	Arising from the muscles/myocytes
Necrosis	Dying of cells/tissue due to injury/disease/negative outer influences.
Nephrostomy tube	A tube that is placed throughout the skin in the renal pelvis to drain the urine.
Parasagittal	Off/shifted from the medial/sagittal plane that divides the body symmetrically into a left and right section.
Primary injury	Injury/trauma of a patient caused by an accident or disease or malformation.
Retrospective	Contemplating the past. Looking back on s.th.
Serosa	Serous membrane covering the outer walls of an organ or lining body/peritoneal/pleural or pericardial cavities.
Stent/stenting	A tubular mesh that is placed in a tunnel/passage to keep the luminal cross section open. Body fluids can be drained.
Stratum	One of several tissue layers that follow one after another in a complex organ system.
Stricture	Narrowing of the luminal cross section of a tunnel/passage or duct.
Transection	Separation of a tissue by cutting transversally.

Term	Meaning
Trauma	Serious injury/wound externally caused by accidents or violence.
Tuberculosis	Infective disease caused by the tubercle bacillus/mycobacterium tuberculosis, forming tubercles in the lungs and other tissues.
Tunica	Tissue layer (e.g. muscle) covering other anatomical structures.
Urinoma	A volume/cyst containing urine outside the physiological urine guiding system as a result from trauma or obstruction.
Urogram	Radiographic illustration of the urinary tract.

8.3 Technical Drawings

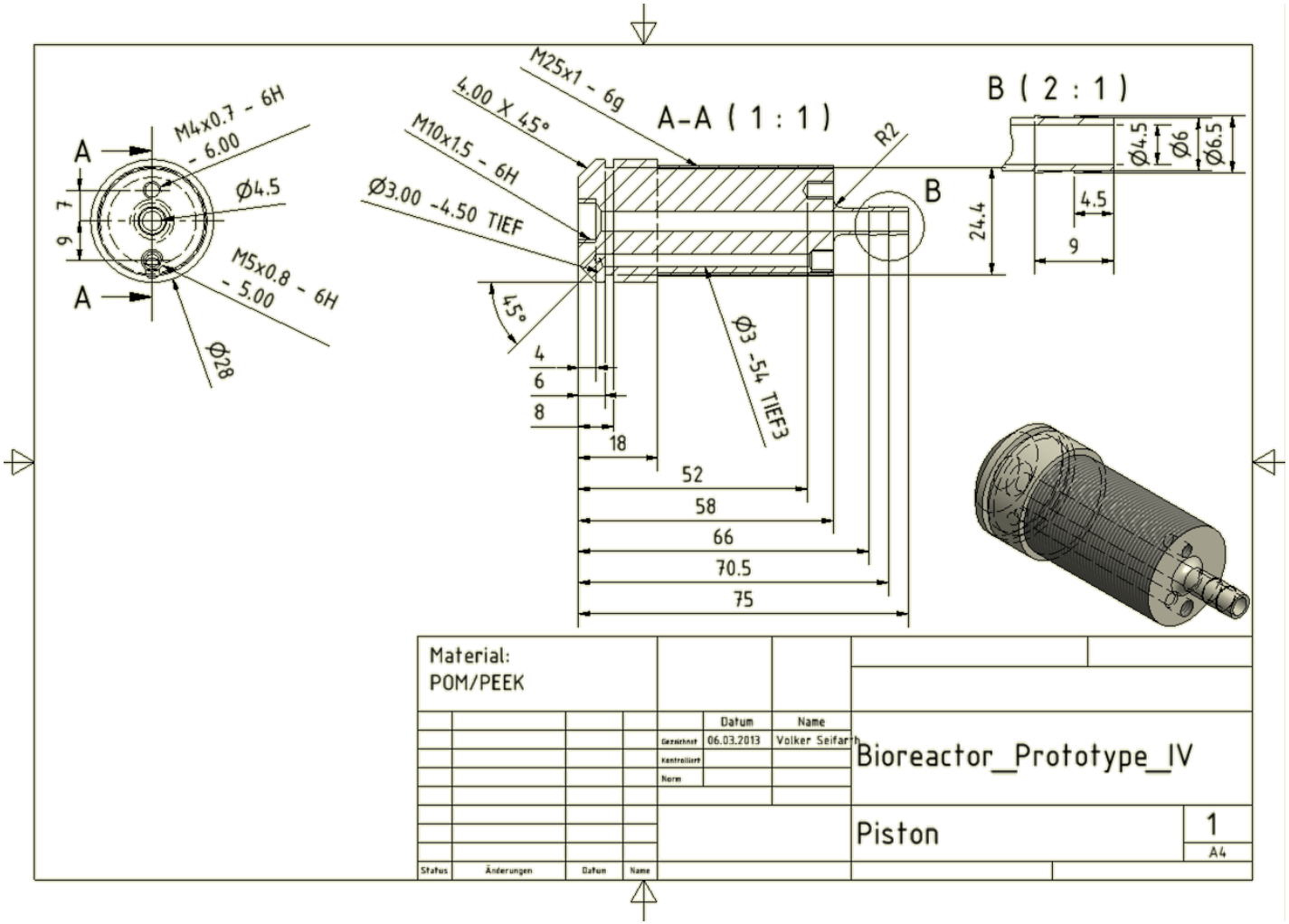

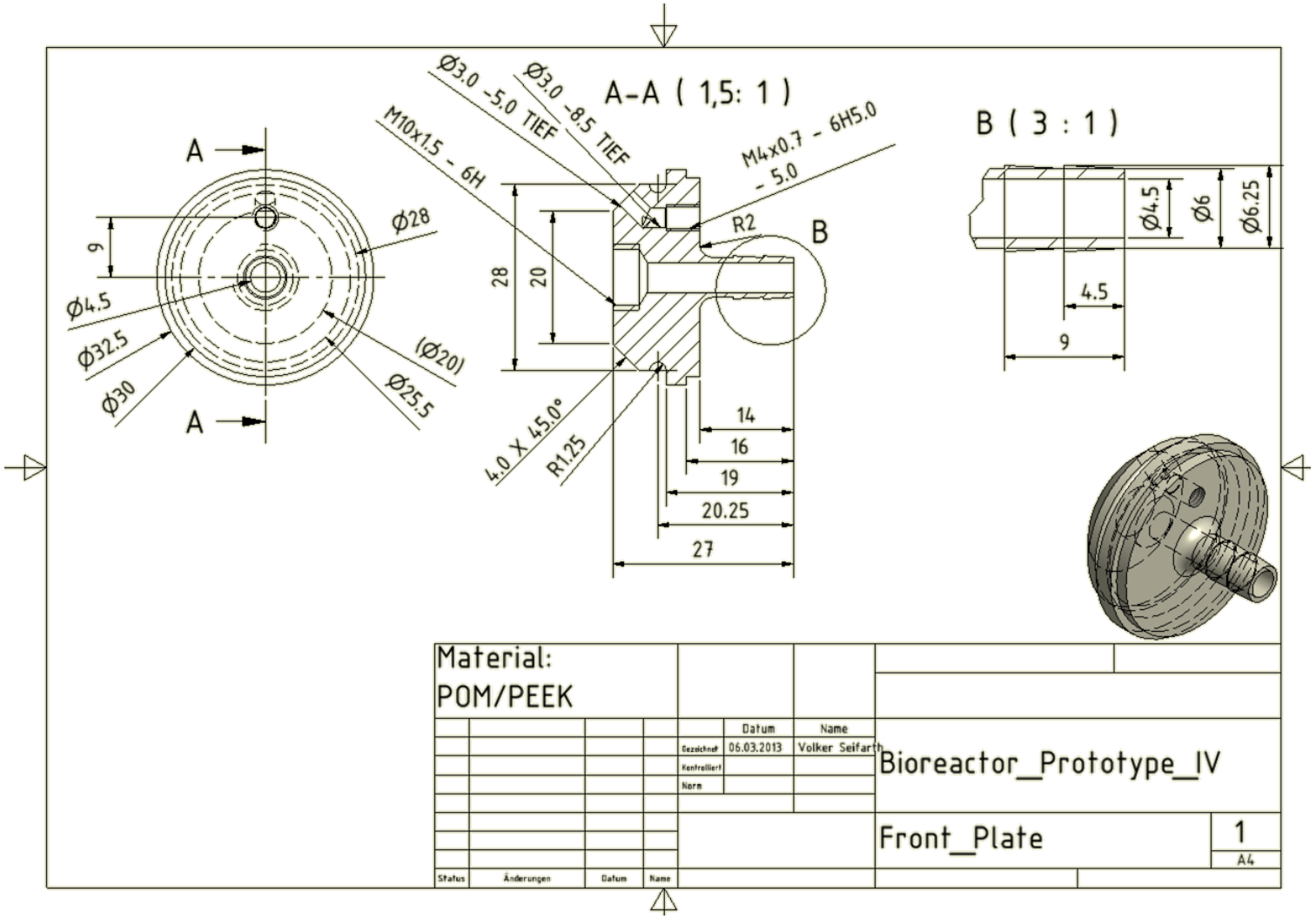
A-A (1,5: 1)
B (3 : 1)
Ø3.0 -5.0 TIEF
Ø3.0 -8.5 TIEF
M10x1.5 - 6H
M4x0.7 - 6H5.0 - 5.0
R2
B
A
Ø28
9
Ø4.5
Ø32.5
Ø30
(Ø20)
Ø25.5
28
20
4.0 X 45.0°
R1.25
14
16
19
20.25
27
Ø4.5
Ø6
Ø6.25
4.5
9
Material:
POM/PEEK
Datum
Name
Gezeichnet
06.03.2013
Volker Seifarth
Kontrolliert
Norm
Bioreactor_Prototype_IV
Front_Plate
1
A4
Status
Änderungen
Datum
Name

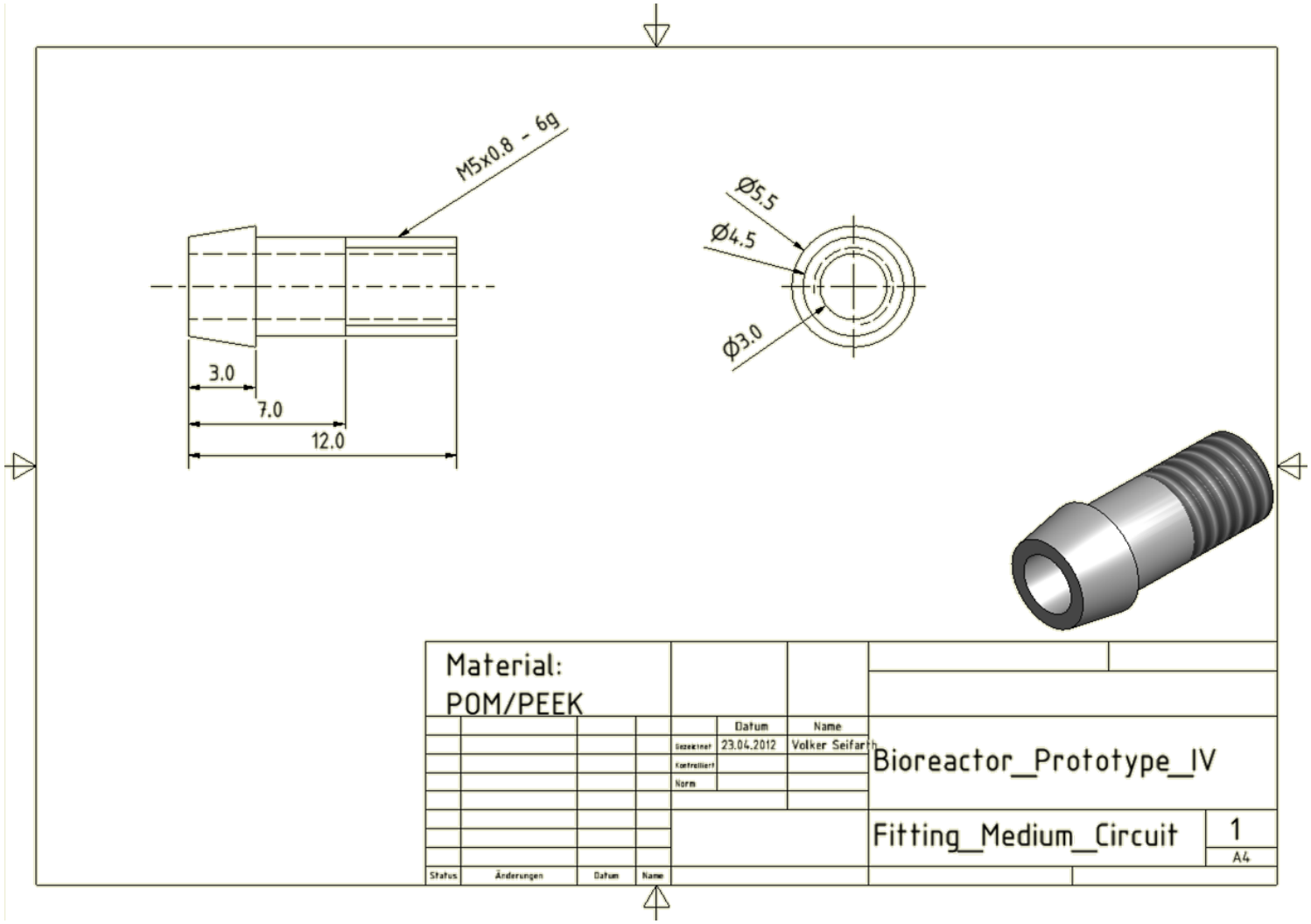
M5x0.8 - 6g
Ø5.5
Ø4.5
Ø3.0
3.0
7.0
12.0
Material:
POM/PEEK
Datum
Name
Gezeichnet
23.04.2012
Volker Seifarth
Kontrolliert
Norm
Bioreactor_Prototype_IV
Fitting_Medium_Circuit
1
A4
Status
Änderungen
Datum
Name

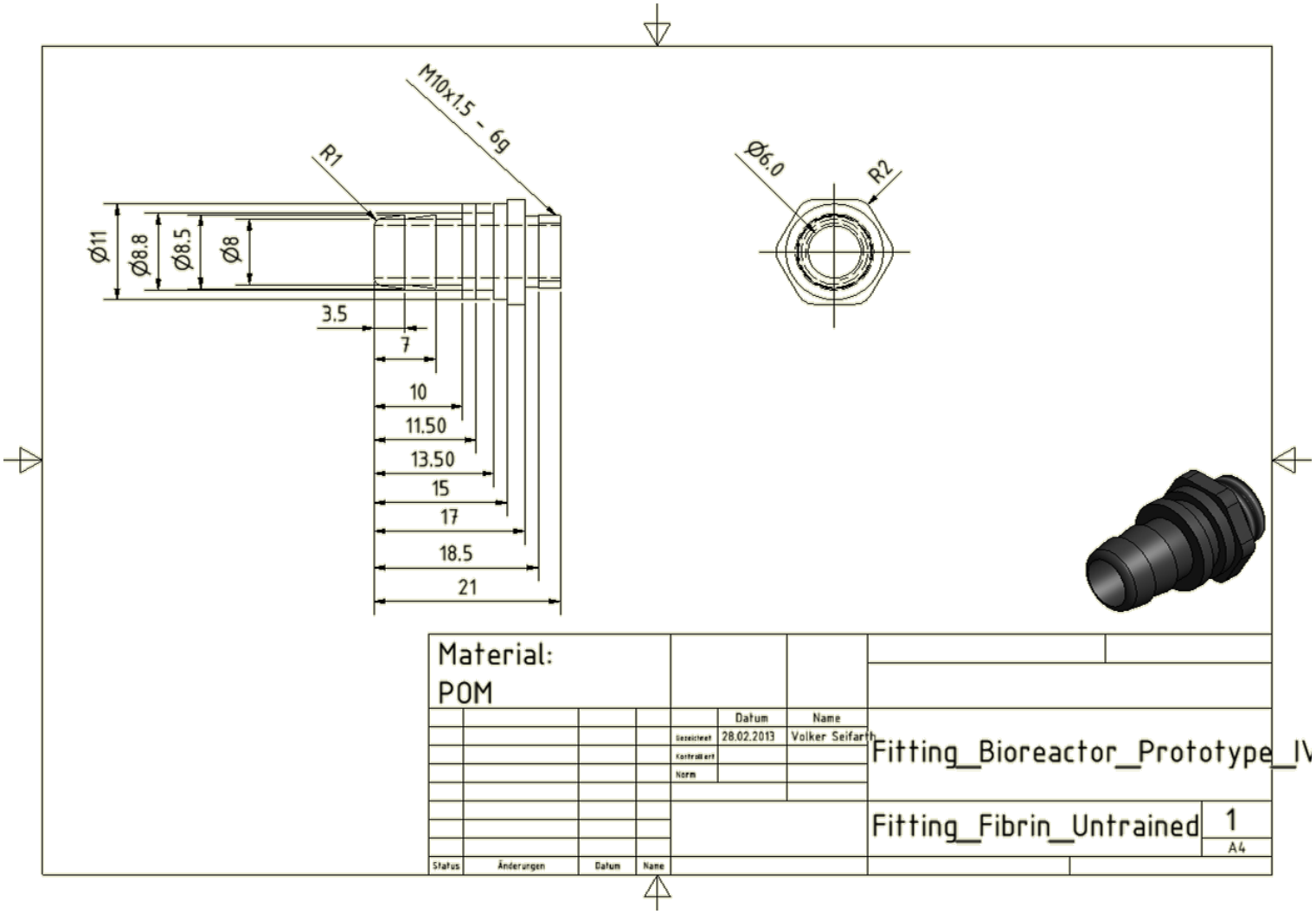
M10x1.5 - 6g
R1
Ø11
Ø8.8
Ø8.5
Ø8
3.5
7
10
11.50
13.50
15
17
18.5
21
Ø6.0
R2
Material:
POM
Datum
Name
Gezeichnet
28.02.2013
Volker Seifarth
Kontrolliert
Norm
Fitting_Bioreactor_Prototype_IV
Fitting_Fibrin_Untrained
1
A4
Status
Änderungen
Datum
Name

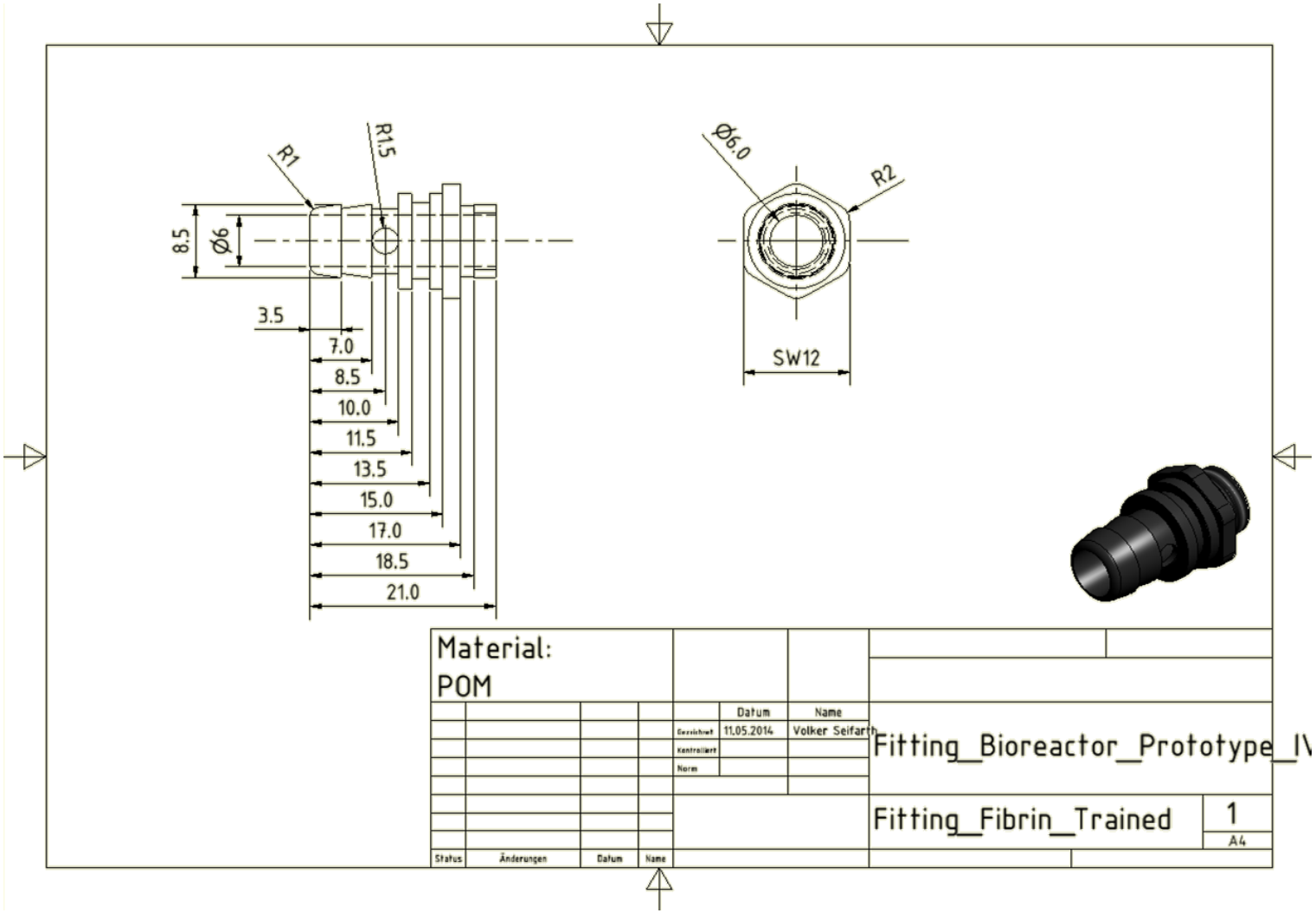
R1
R1.5
8.5
Ø6
3.5
7.0
8.5
10.0
11.5
13.5
15.0
17.0
18.5
21.0
Ø6.0
R2
SW12
Material:
POM
Datum
Name
Gezeichnet
11.05.2014
Volker Seifarth
Kontrolliert
Norm
Fitting_Bioreactor_Prototype_IV
Fitting_Fibrin_Trained
1
A4
Status
Änderungen
Datum
Name

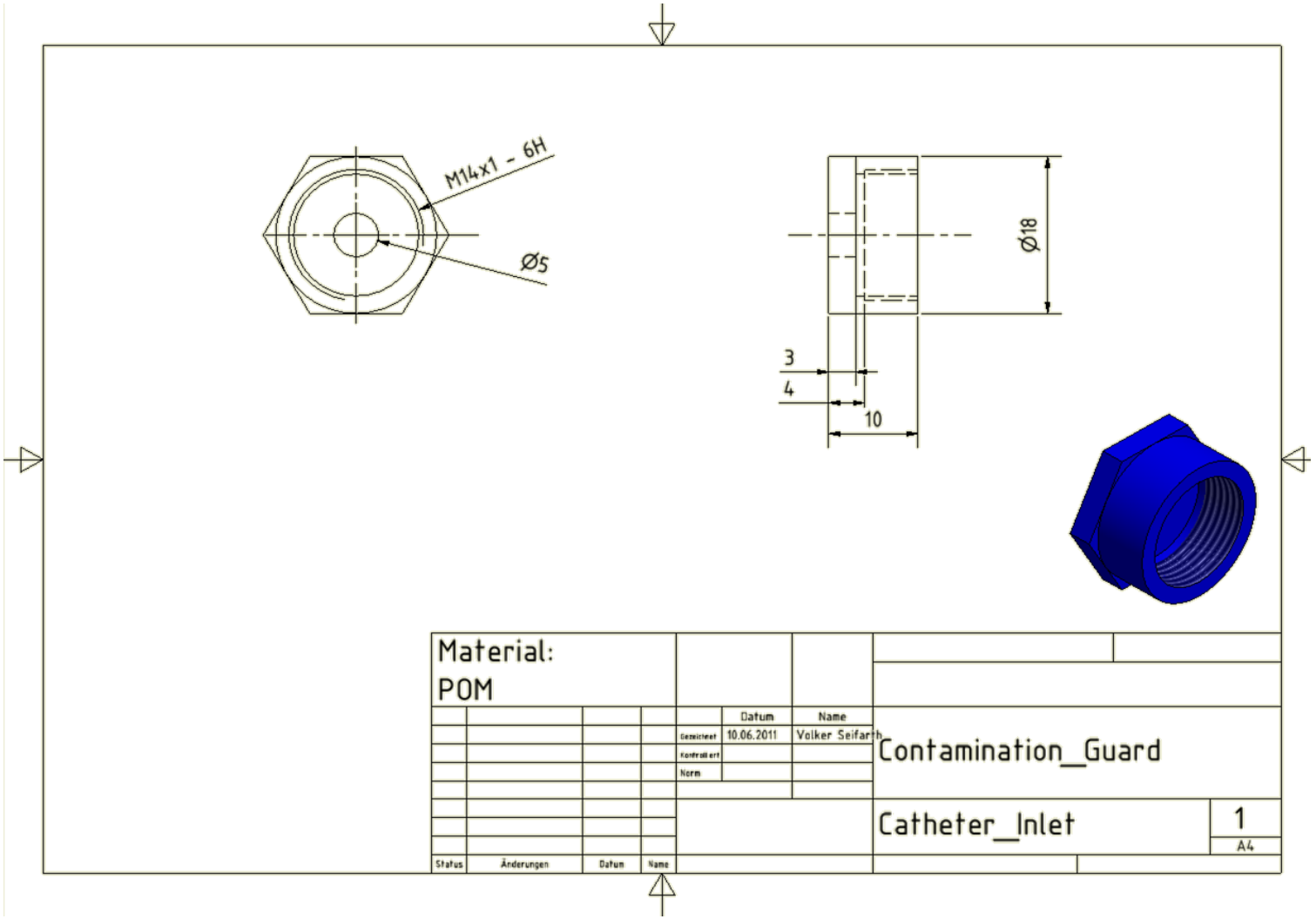
M14x1 - 6H
Ø5
Ø18
3
4
10
Material:
POM
Datum
Name
Gezeichnet
10.06.2011
Volker Seifarth
Kontrolliert
Norm
Contamination_Guard
Catheter_Inlet
1
A4
Status
Änderungen
Datum
Name

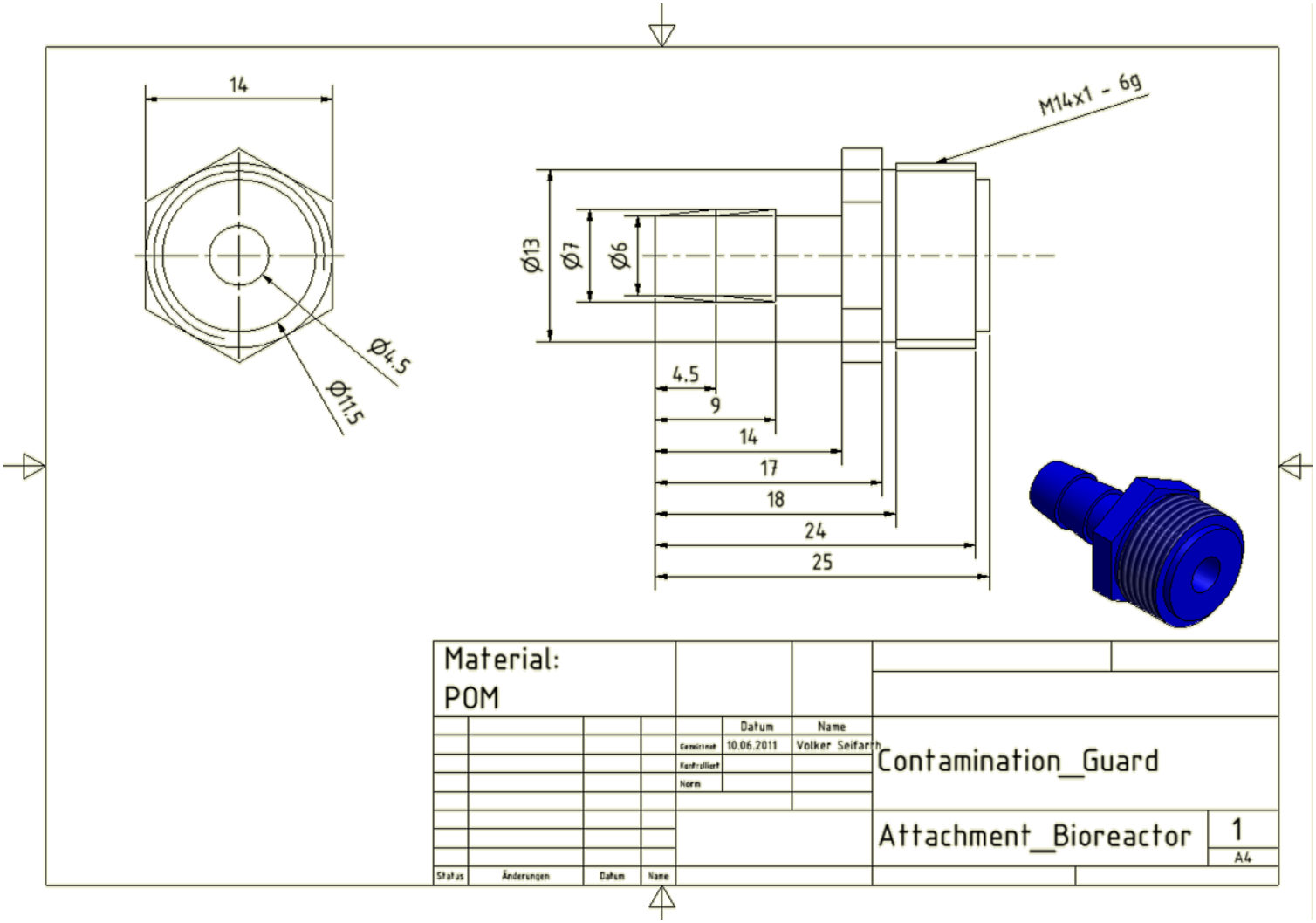
14
M14x1 - 6g
Ø13
Ø7
Ø6
Ø4.5
Ø11.5
4.5
9
14
17
18
24
25
Material:
POM
Datum
Name
10.06.2011
Volker Seifarth
Contamination_Guard
Attachment_Bioreactor
1
A4
Status
Änderungen
Datum
Name

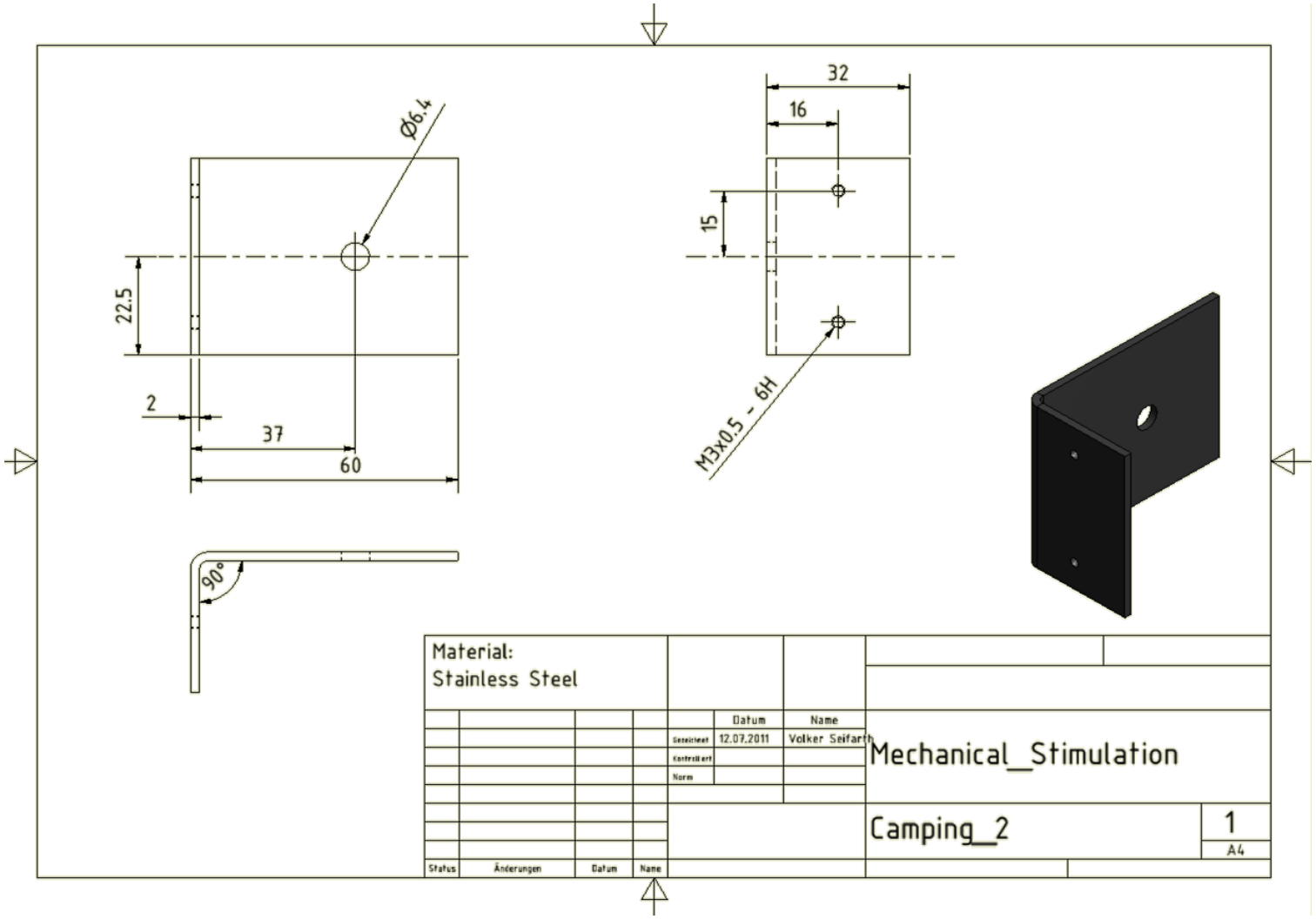
Ø6.4
22.5
2
37
60
32
16
15
M3x0.5 - 6H
90°
Material:
Stainless Steel
Datum
Name
Gezeichnet
12.07.2011
Volker Seifarth
Norm
Mechanical_Stimulation
Camping_2
1
A4
Status
Änderungen
Datum
Name

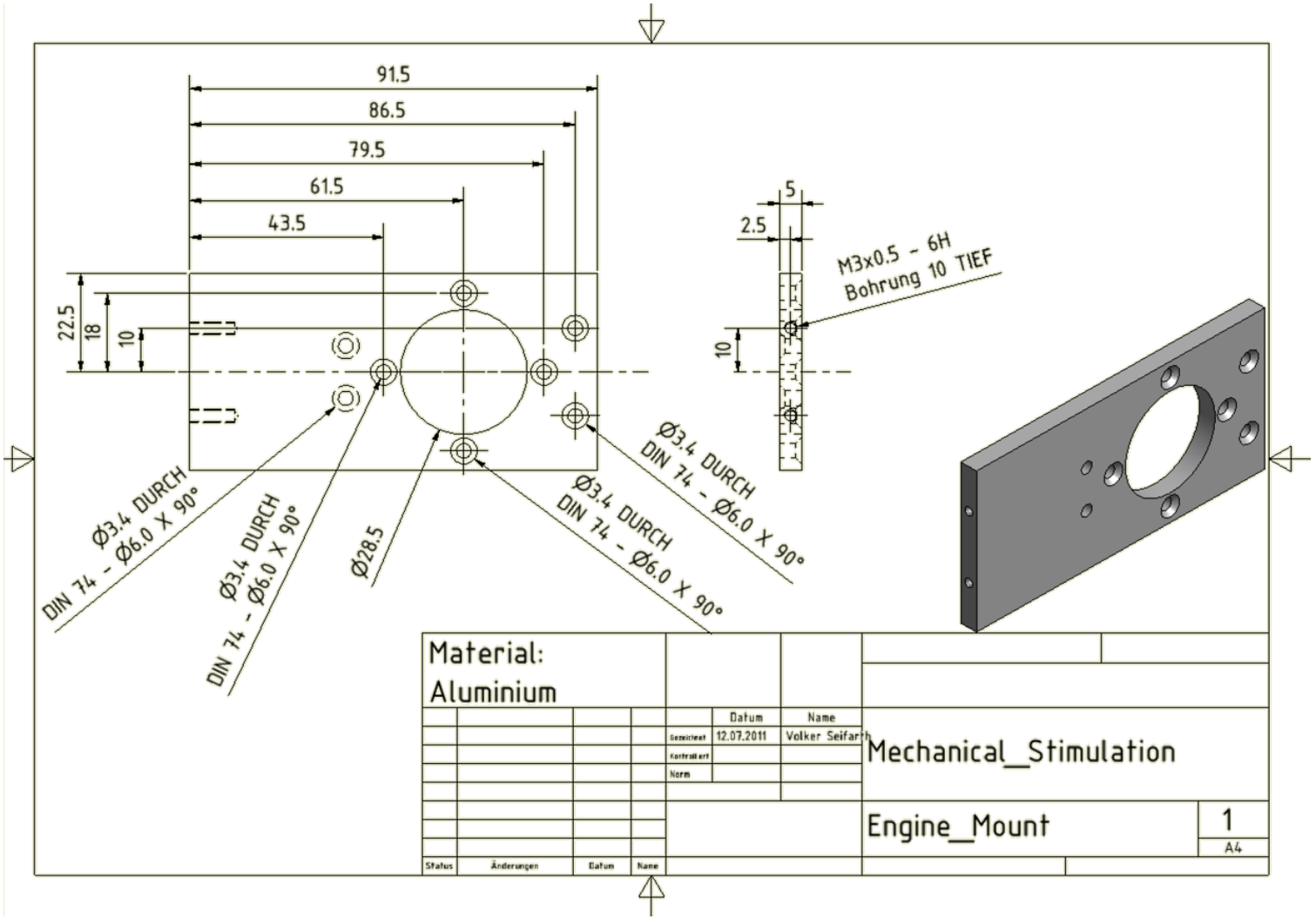
91.5
86.5
79.5
61.5
43.5
22.5
18
10
5
2.5
M3x0.5 - 6H
Bohrung 10 TIEF
10
Ø3.4 DURCH
DIN 74 - Ø6.0 X 90°
Ø3.4 DURCH
DIN 74 - Ø6.0 X 90°
Ø28.5
Ø3.4 DURCH
DIN 74 - Ø6.0 X 90°
Ø3.4 DURCH
DIN 74 - Ø6.0 X 90°
Material:
Aluminium
Datum
Name
Gezeichnet
12.07.2011
Volker Seifarth
Kontrolliert
Norm
Mechanical_Stimulation
Engine_Mount
1
A4
Status
Änderungen
Datum
Name

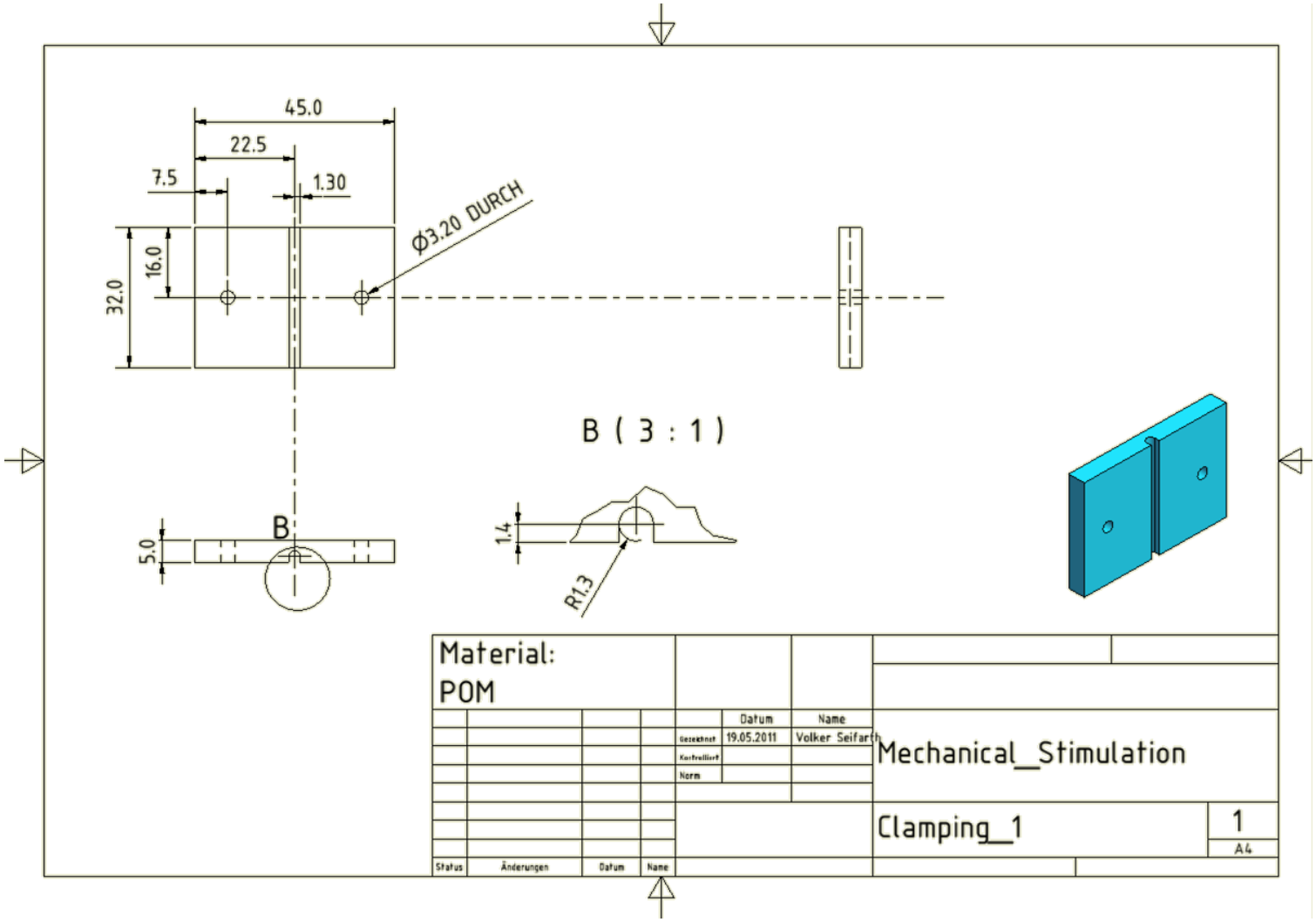
45.0
22.5
7.5
1.30
Ø3.20 DURCH
16.0
32.0
B (3 : 1)
B
5.0
1.4
R1.3
Material:
POM
Datum
Name
Gezeichnet
19.05.2011
Volker Seifarth
Norm
Mechanical_Stimulation
Clamping_1
1
A4
Status
Änderungen
Datum
Name

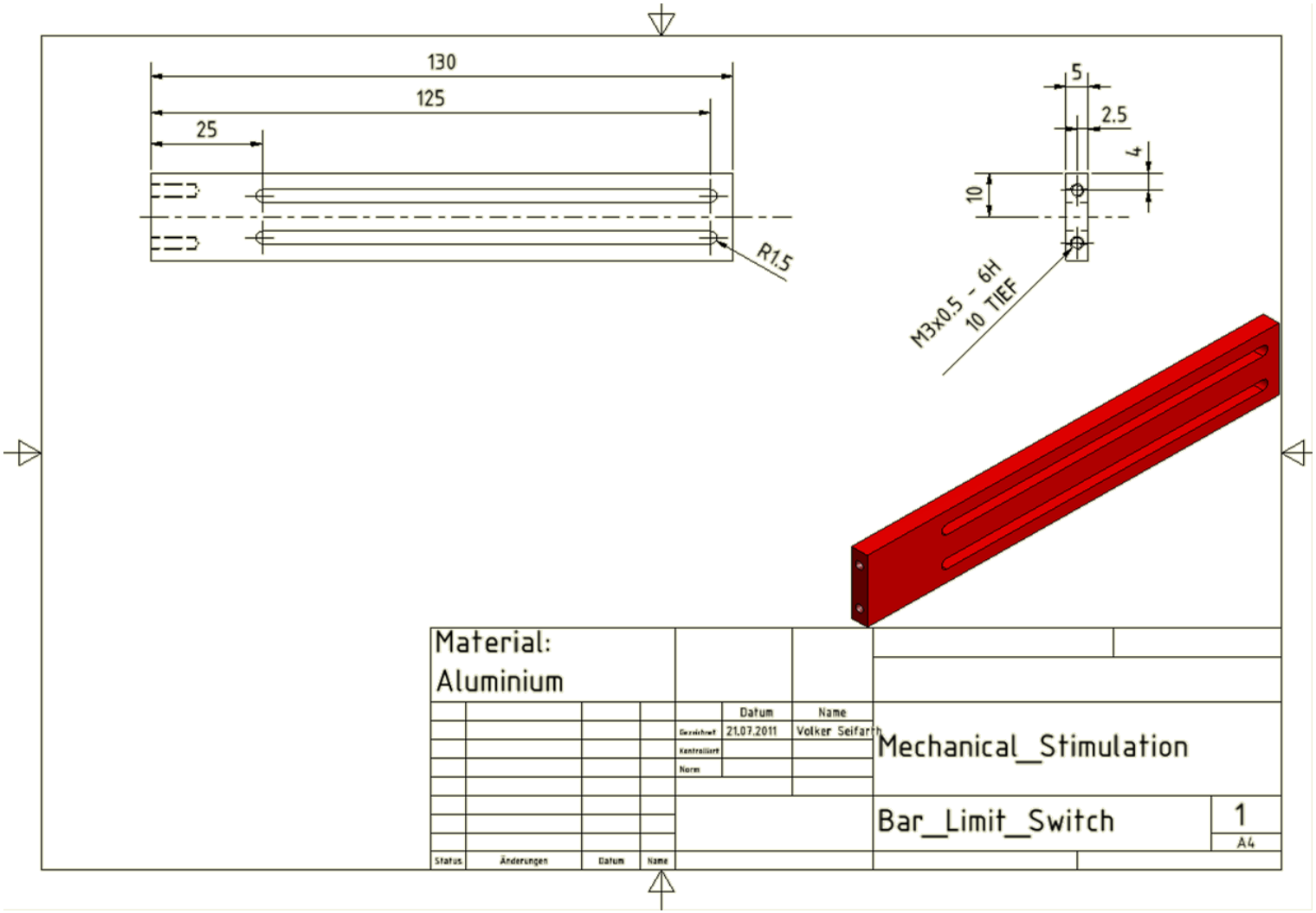
130
125
25
R1.5
5
2.5
4
10
M3x0,5 - 6H
10 TIEF
Material:
Aluminium
Datum
Name
Gezeichnet
21.07.2011
Volker Seifarth
Kontrolliert
Norm
Mechanical_Stimulation
Bar_Limit_Switch
1
A4
Status
Änderungen
Datum
Name

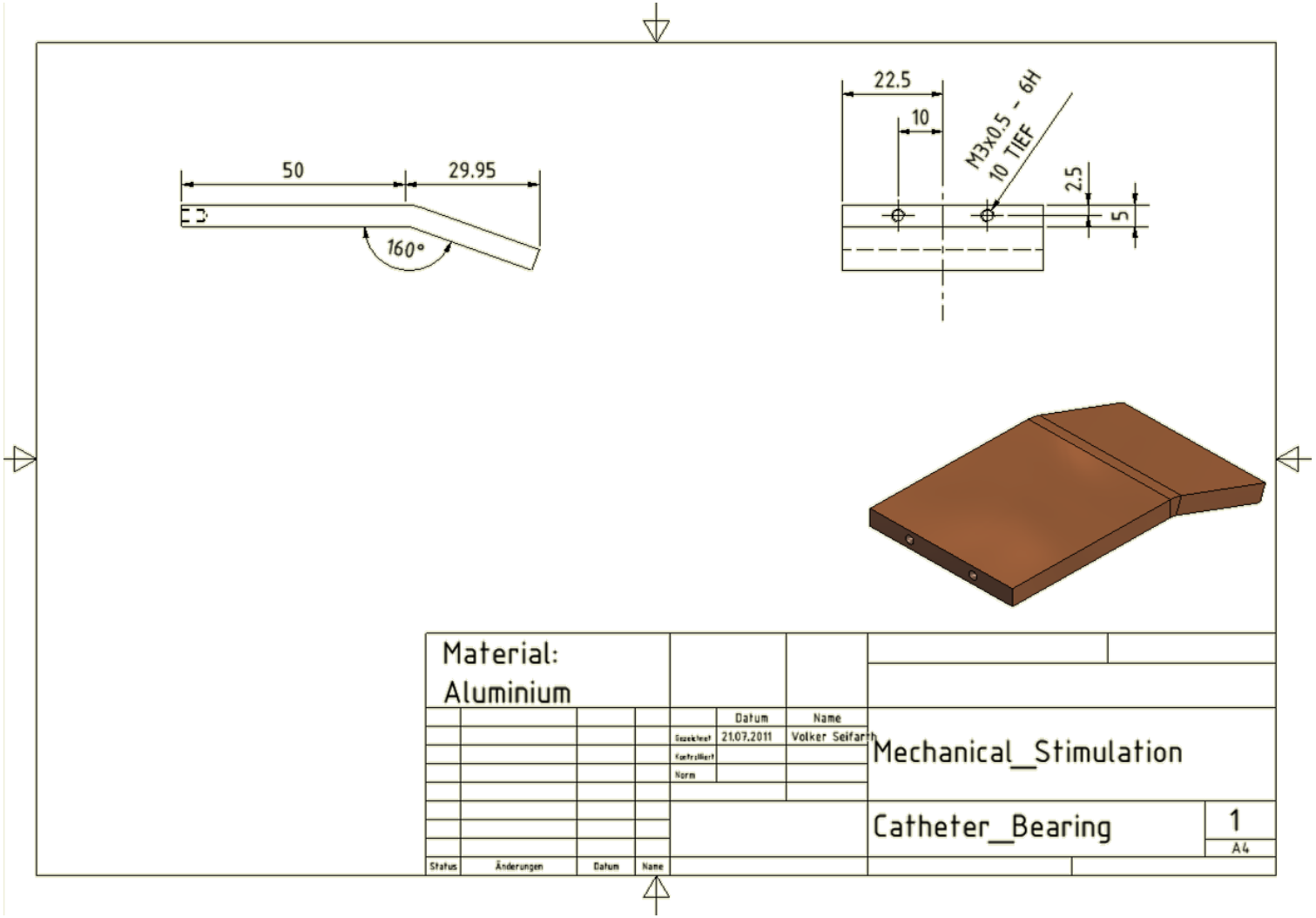
50
29.95
160°
22.5
10
M3x0.5 - 6H
10 TIEF
2.5
5
Material:
Aluminium
Datum
Name
Gezeichnet
21.07.2011
Volker Seifarth
Geprüft
Norm
Mechanical_Stimulation
Catheter_Bearing
1
A4
Status
Änderungen
Datum
Name

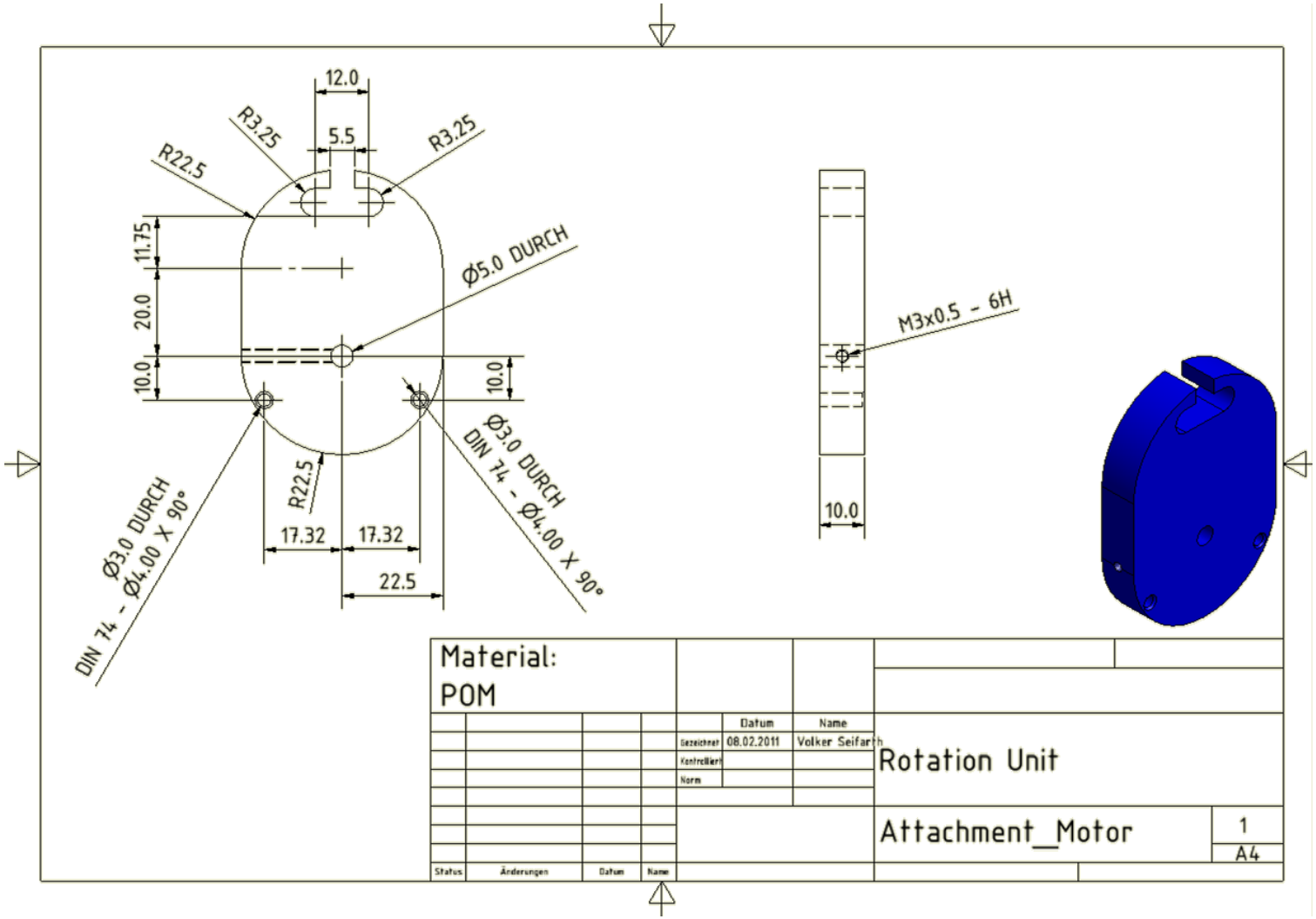
12.0
5.5
R3.25
R3.25
R22.5
11.75
20.0
10.0
Ø5.0 DURCH
10.0
R22.5
17.32
17.32
22.5
Ø3.0 DURCH
DIN 74 - Ø4.00 X 90°
Ø3.0 DURCH
DIN 74 - Ø4.00 X 90°
M3x0.5 - 6H
10.0
Material:
POM
Datum
Name
Gezeichnet
08.02.2011
Volker Seifarth
Kontrolliert
Norm
Rotation Unit
Attachment_Motor
1
A4
Status
Änderungen
Datum
Name

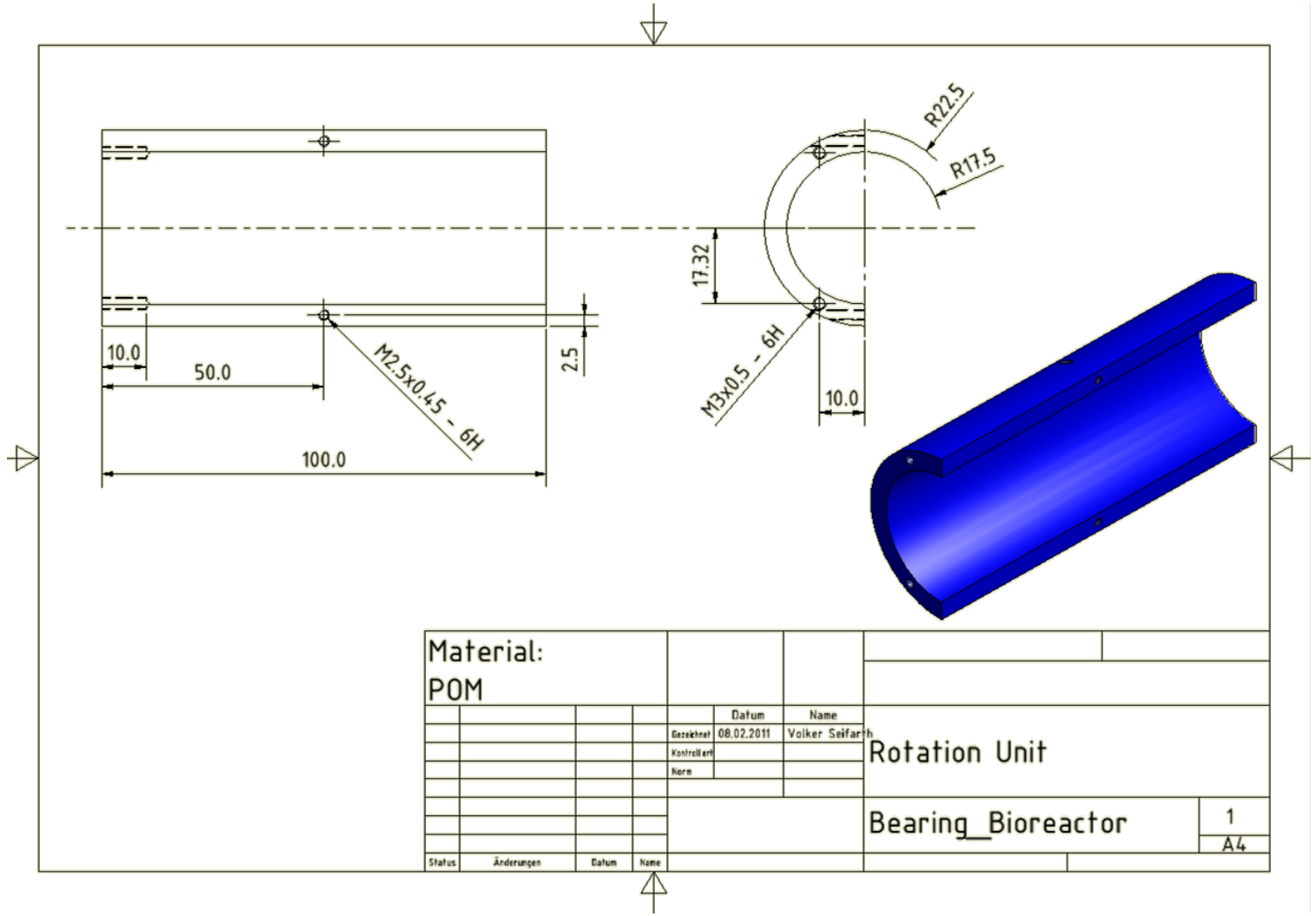
R22.5
R17.5
17.32
M3x0.5 - 6H
10.0
10.0
50.0
M2.5x0.45 - 6H
2.5
100.0
Material:
POM
Datum
Name
Gezeichnet
08.02.2011
Volker Seifarth
Kontrolliert
Norm
Rotation Unit
Bearing_Bioreactor
1
A4
Status
Änderungen
Datum
Name

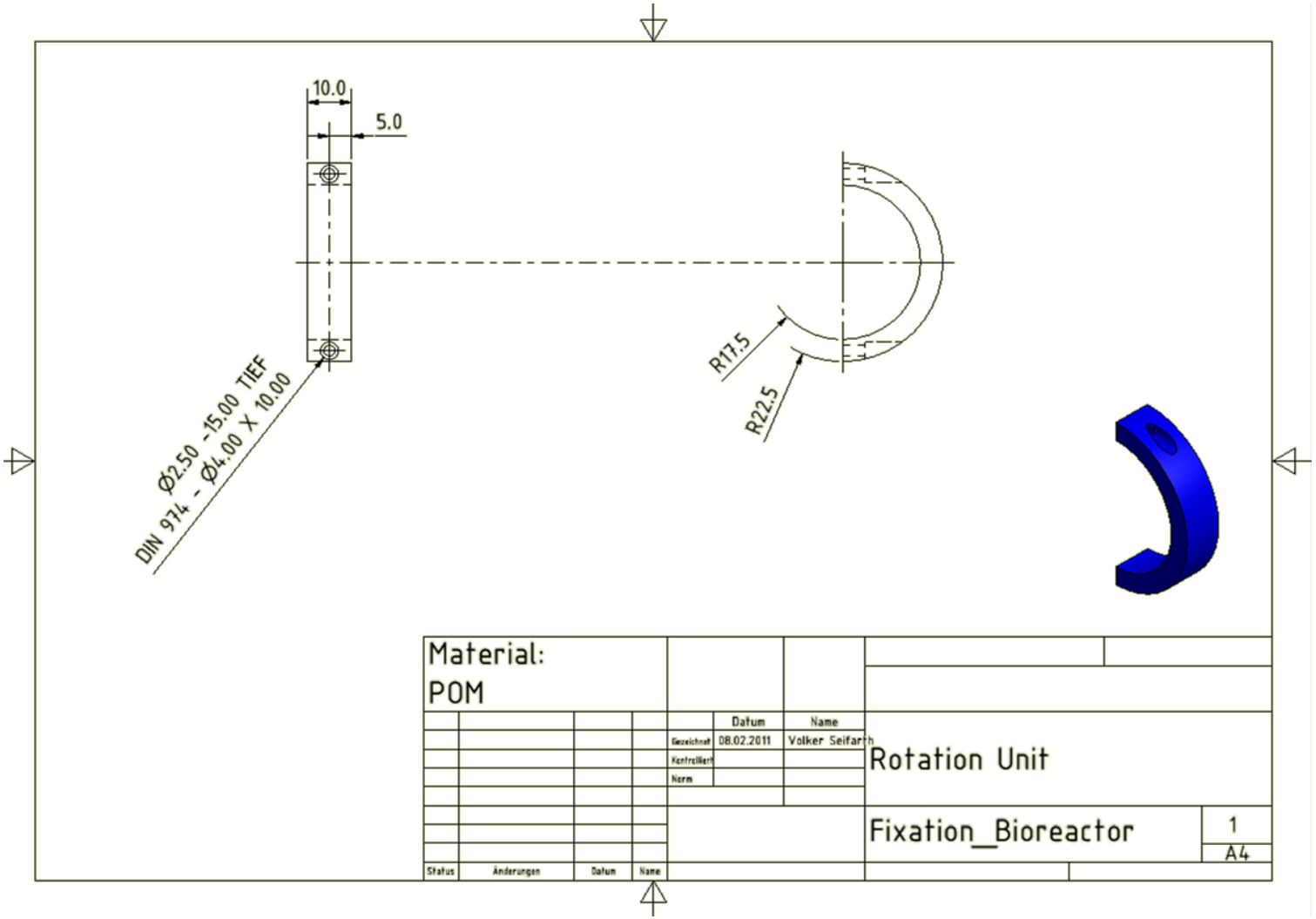
10.0
5.0
Ø2.50 -15.00 TIEF
DIN 974 - Ø4.00 X 10.00
R17.5
R22.5
Material:
POM
Datum
Name
Gezeichnet
08.02.2011
Volker Seifarth
Kontrolliert
Norm
Rotation Unit
Fixation_Bioreactor
1
A4
Status
Änderungen
Datum
Name

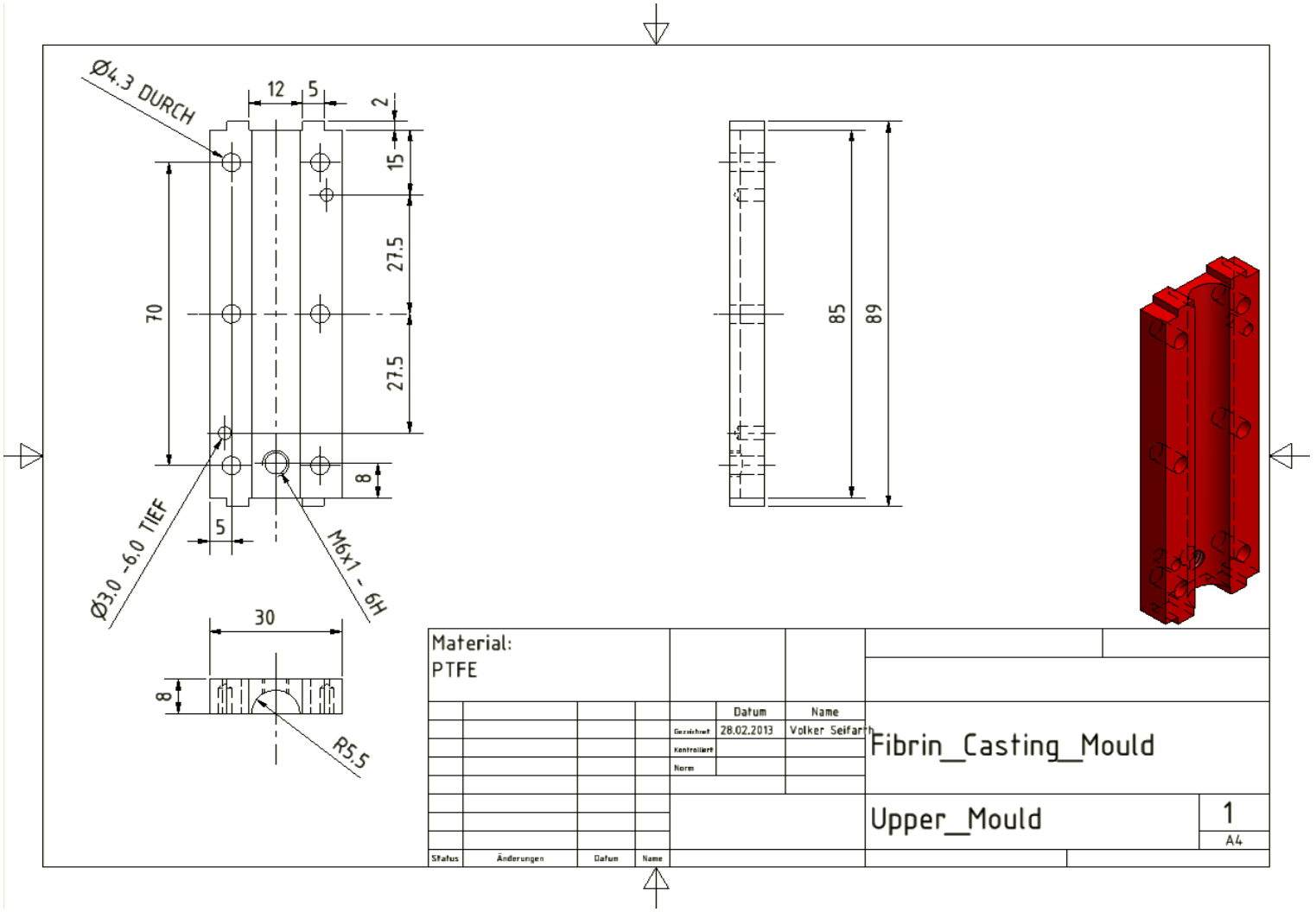
Ø4.3 DURCH
12
5
2
15
27.5
27.5
70
8
5
Ø3.0 -6.0 TIEF
M6x1 - 6H
30
8
R5.5
85
89
Material:
PTFE
Datum
Name
Gezeichnet
28.02.2013
Volker Seifarth
Kontrolliert
Norm
Fibrin_Casting_Mould
Upper_Mould
1
A4
Status
Änderungen
Datum
Name

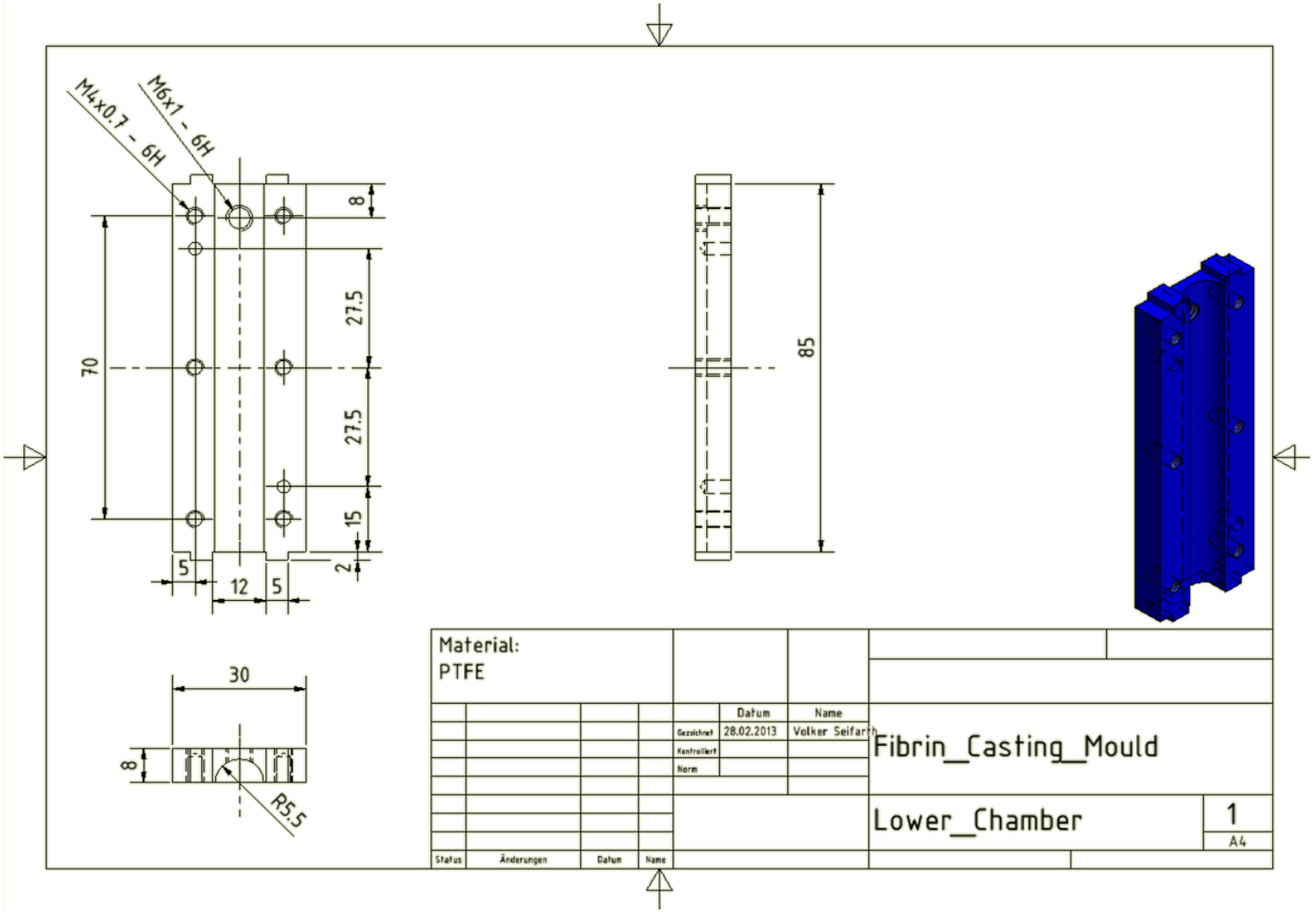
M4x0.7 - 6H
M6x1 - 6H
8
27.5
27.5
15
2
70
5
12
5
85
30
8
R5.5
Material:
PTFE
Datum
Name
Gezeichnet
28.02.2013
Volker Seifarth
Kontrolliert
Norm
Fibrin_Casting_Mould
Lower_Chamber
1
A4
Status
Änderungen
Datum
Name

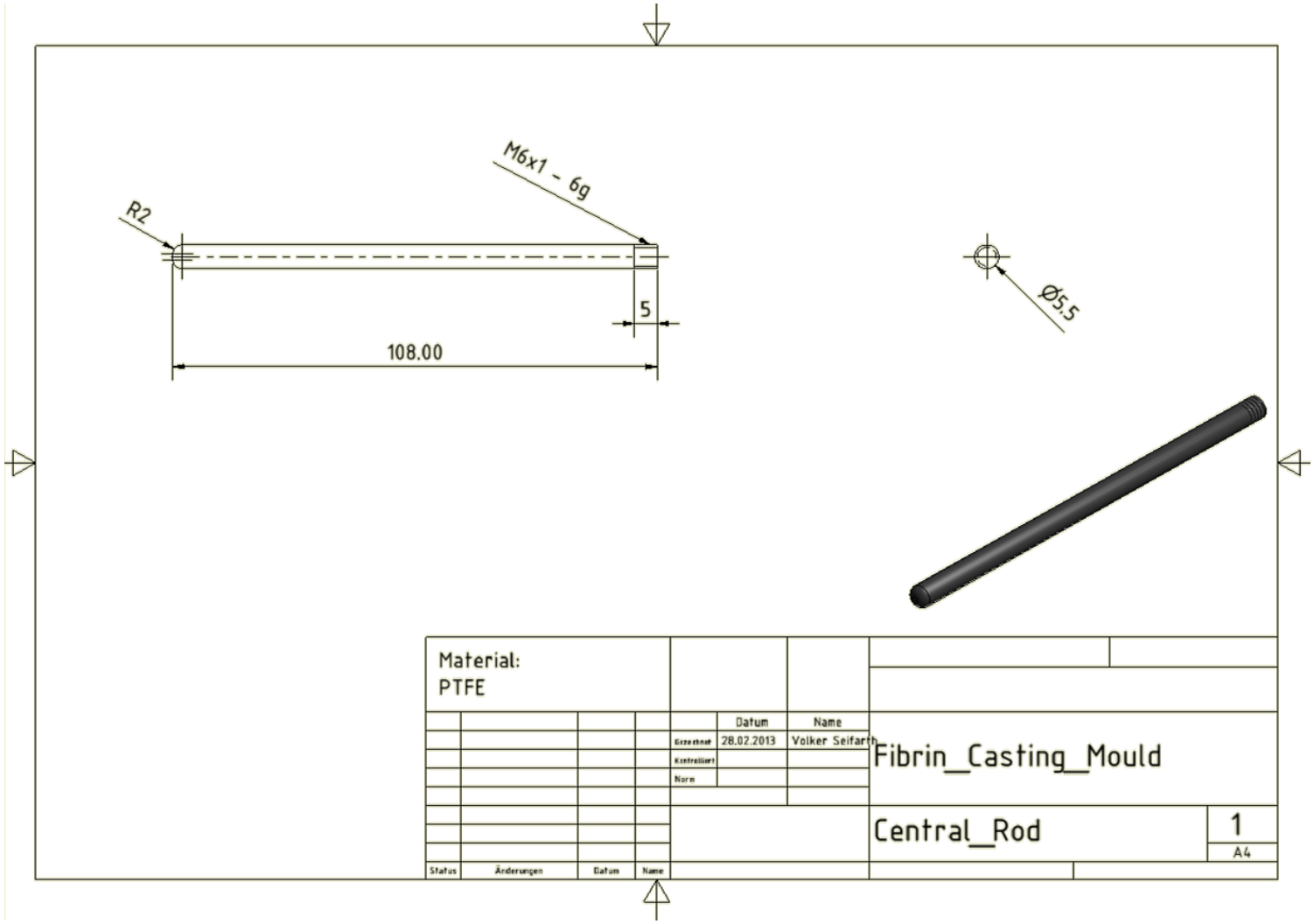
M6x1 - 6g
R2
5
108.00
Ø5.5
Material:
PTFE
Datum
Name
28.02.2013
Volker Seifarth
Fibrin_Casting_Mould
Central_Rod
1
A4
Status
Änderungen
Datum
Name

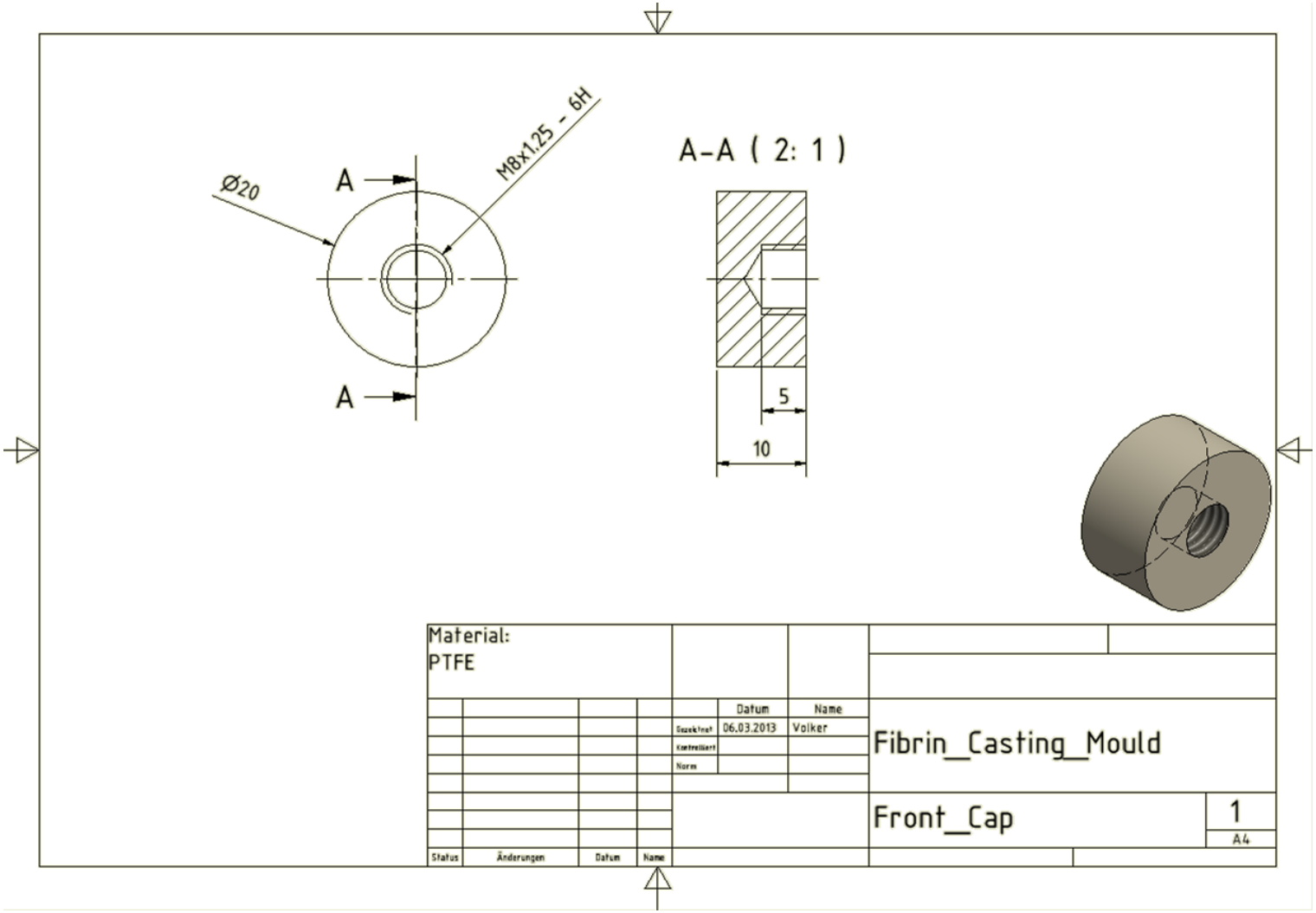
Ø20
A
M8x1.25 - 6H
A
A-A (2: 1)
5
10
Material:
PTFE
Datum
Name
Gezeichnet
06.03.2013
Volker
Kontrolliert
Norm
Fibrin_Casting_Mould
Front_Cap
1
A4
Status
Änderungen
Datum
Name

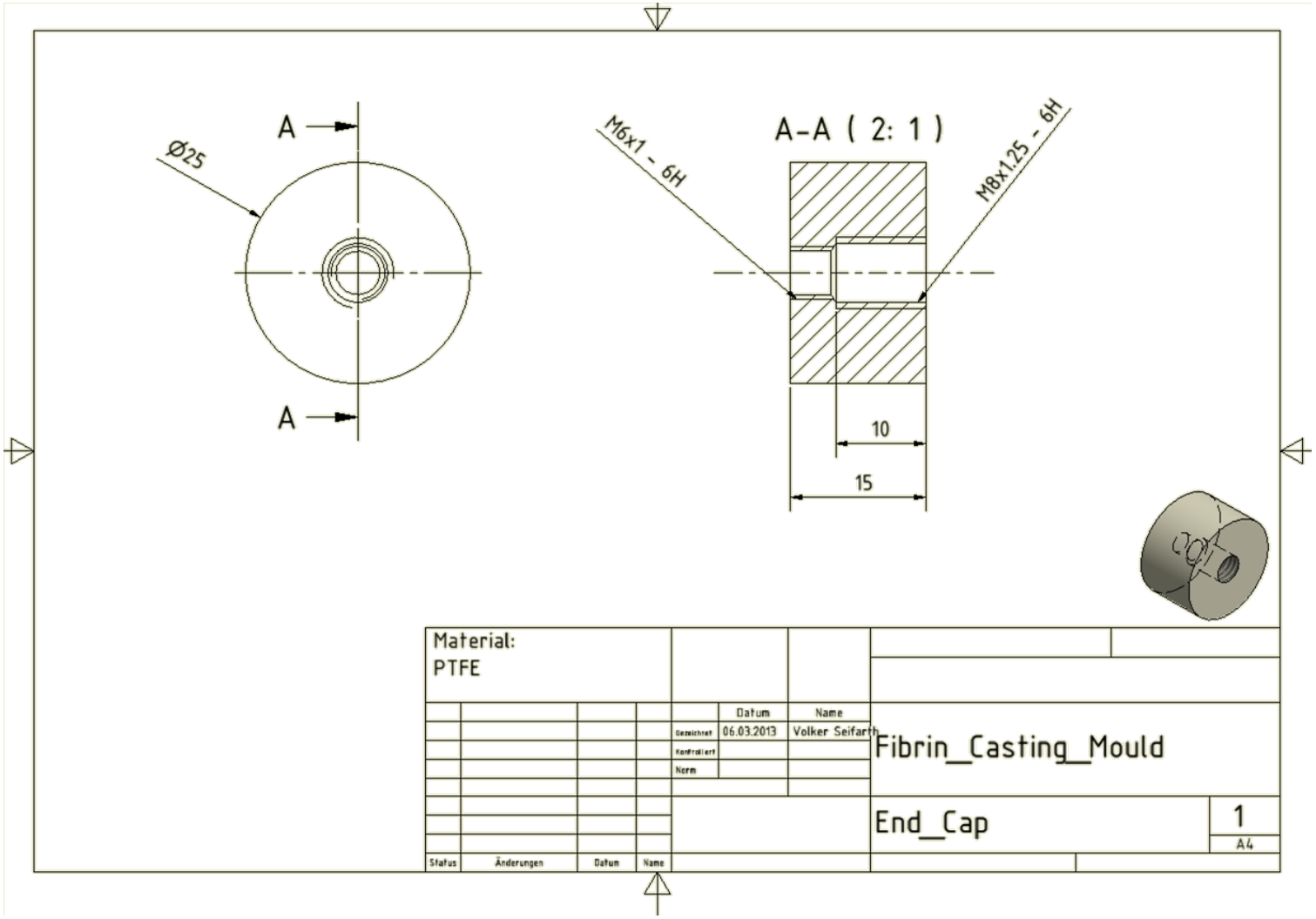
A
Ø25
A
A-A (2: 1)
M6x1 - 6H
M8x1.25 - 6H
10
15
Material:
PTFE
Datum
Name
Gezeichnet
06.03.2013
Volker Seifarth
Kontrolliert
Norm
Fibrin_Casting_Mould
End_Cap
1
A4
Status
Änderungen
Datum
Name

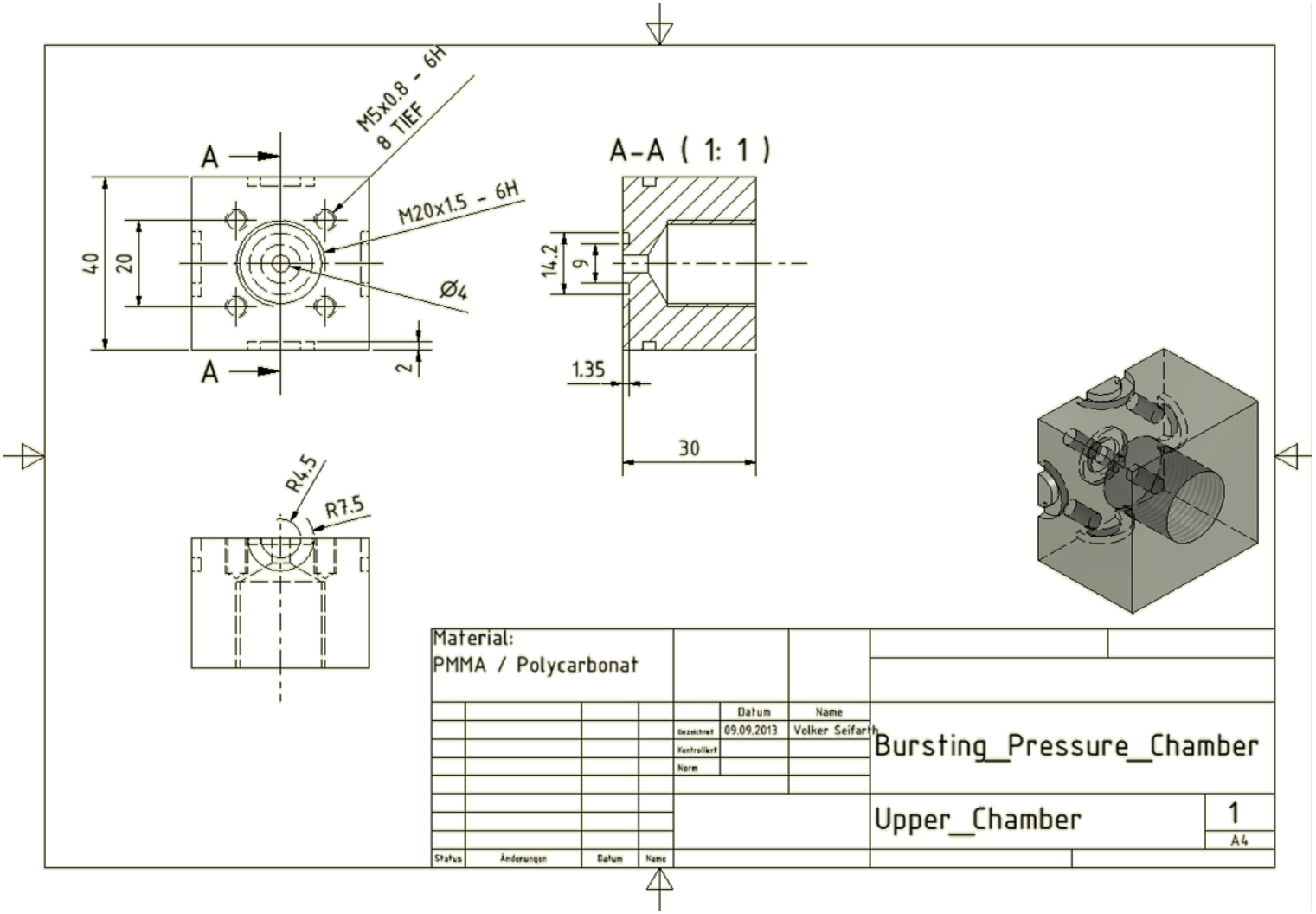
M5x0.8 - 6H
8 TIEF
M20x1.5 - 6H
Ø4
A
A
40
20
2
A-A (1: 1)
14.2
9
1.35
30
R4.5
R7.5
Material:
PMMA / Polycarbonat
Datum
Name
gezeichnet
09.09.2013
Volker Seifarth
Kontrolliert
Norm
Bursting_Pressure_Chamber
Upper_Chamber
1
A4
Status
Änderungen
Datum
Name

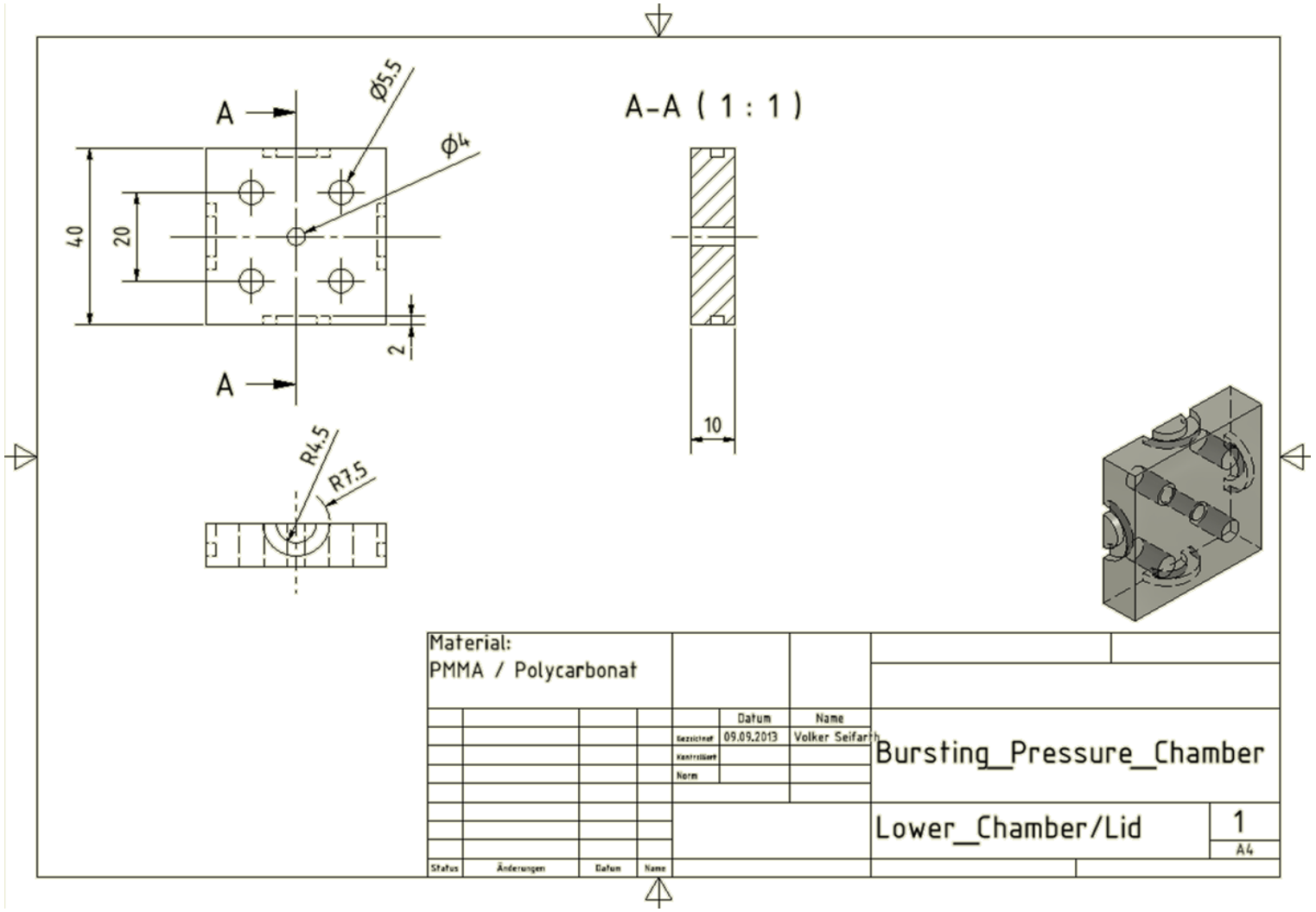
A
Ø5.5
Ø4
40
20
2
A
A-A (1 : 1)
10
R4.5
R7.5
Material:
PMMA / Polycarbonat
Datum
Name
Gezeichnet
09.09.2013
Volker Seifarth
Kontrolliert
Norm
Bursting_Pressure_Chamber
Lower_Chamber/Lid
1
A4
Status
Änderungen
Datum
Name

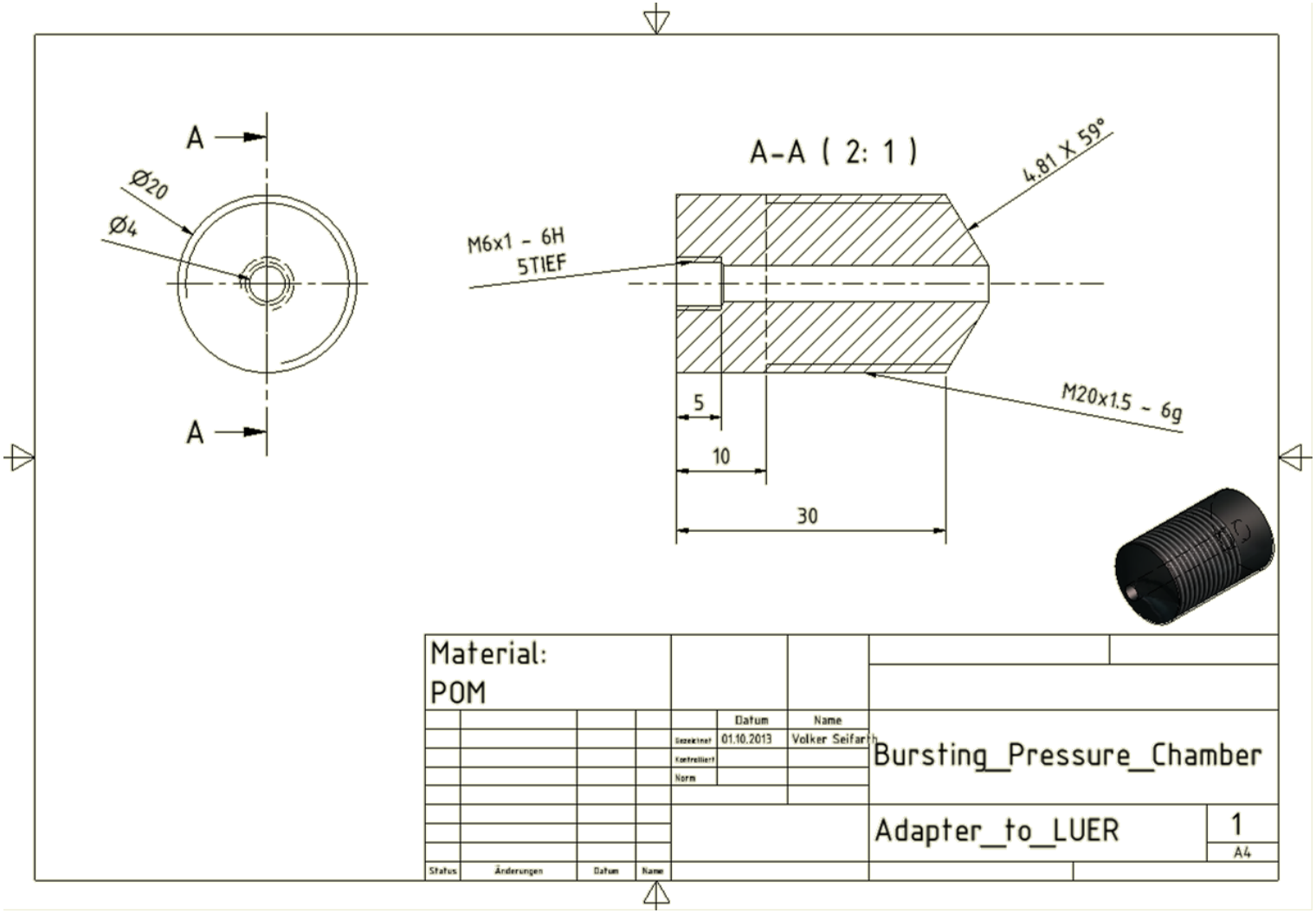
A
Ø20
Ø4
A
A-A (2: 1)
4.81 X 59°
M6x1 - 6H
5TIEF
M20x1.5 - 6g
5
10
30
Material:
POM
Datum
Name
Gezeichnet
01.10.2013
Volker Seifarth
Kontrolliert
Norm
Bursting_Pressure_Chamber
Adapter_to_LUER
1
A4
Status
Änderungen
Datum
Name

8.4 Curriculum Vitae

Der Lebenslauf ist in der Onnline-Version aus Gründen des Datenschutzes nicht enthalten.

8.5 List of Publications

8.5.1 Regular scientific publications

Seifarth, V., Schehl, D., Linder, P., Goßmann, M., Digel, I., Artmann, G. M., Porst, D., Preiß, C., Kayser, P., Pack, O., (Temiz) Artmann, A.: UREPLACE: Development of a bioreactor for in vitro culturing of cell seeded tubular vessels on collagen scaffolds, Kazakh National University Bulletin (biological series), 2 (2011) 48-49.

Seifarth, V., Gossmann, M., Janke, H. P., Grosse, J., Zang, W., Heschel I., Artmann G. M., Temiz Artmann, A.: Development of a Bioreactor to Culture Tissue Engineered Ureters based on the Application of Tubular OPTIMAIX 3D Scaffolds, Urologia Internationalis, accepted

Seifarth, V., Grosse, J., Gossmann, M., Janke, H. P., Koch, S., Epple, M., Artmann, G.M., Temiz Artmann, A.: Mechanical stimulation of primary porcine bladder smooth muscle cells in a tubular fibrin-PVDF scaffold, to be submitted

Seifarth, V., Grosse, J., Digel, I., Rohrmann, D., Artmann, A.: Ureteric Reconstruction – Is Tissue Engineering an Option in the near Future?, to be submitted

8.5.2 Scientific posters

9-11 May 2012, 4th International Symposium Interface Biology of Implants, Warnemünde, Goßmann, M., Seifarth, V., Linder, P., Digel, I., Kettenhofen, R., Artmann, G.M., (Temiz) Artmann, A.: Simultaneous Control and Measurement of Mechanical Properties of Ultra-thin Tissue Equivalents.

26-29 September 2012, 64th Kongress der Deutschen Gesellschaft für Urologie e.V., Seifarth, V., Schehl, D., Grosse, J., Zang, W., Tholl, S., Koch, S., Artmann, G.M., (Temiz) Artmann, A.: An automatized bioreactor system based on tubular collagen matrices.

8-10 November 2012, 4th Symposium Urologische Forschung of the DGU, Berlin, Seifarth, V., Grosse, J., Goßmann, M., Heschel, I., Zang, W., (Temiz) Artmann, A.: Tubular collagen matrices for ureteral transplants.

8-10 November 2012, 4th Symposium Urologische Forschung of the DGU, Berlin, Leonhäuser, D., Seifarth, V., Strick, K., Fera, C., Gaisa, N., Heschel, I., Tolba, R.H., (Temiz) Artmann, A., Grosse, J.: Potential of collagen matrices "Optimaix" as bladder wall substitute – preliminary study in a Göttingen Minipig model.

15 November 2012, 5th Graduate Symposium, Jülich, Seifarth, V., Schehl, D., Grosse, J., Zang, W., Heschel, I., Artmann, G.M., (Temiz) Artmann, A.: Development of a tubular bioreactor system for the generation of biohybrids.

15 November 2012, 5th Graduate Symposium, Jülich, Goßmann, M., Linder, P., Seifarth, V., Artmann, G.M., Epple, M., (Temiz) Artmann, A.: Measurement of the contractile forces of autonomously beating cardiomyocytes.

15-19 March 2013, 28th Annual European Association of Urology Congress, Mailand, Seifarth, V., Grosse, J., Goßmann, M., Heschel, I., Zang, W., Artmann, G.M., (Temiz) Artmann, A.: 250 Tubular matrices for biohybrids.

15-19 March 2013, 28th Annual European Association of Urology Congress, Mailand, Leonhäuser, D., Seifarth, V., Strick, K., Gaisa, N., Heschel, I., Tolba, R.H., (Temiz) Artmann, A., Grosse, J.: 871 Bladder wall substitution with autologously seeded collagen scaffolds "Optimaix" in a Göttingen minipig model.

11-12 April 2013, 59th Kongress der Nordrhein-Westfälischen Gesellschaft für Urologie, Düsseldorf, Leonhäuser, D., Seifarth, V., Strick, K., Fera, C., Huppertz, N., Gaisa, N., Heschel, I., Woitok, A., Zraik, I., He, Y., Tolba, R., (Temiz) Artmann, A., Grosse, J.: Blasenwandersatz aus autolog besiedelten Kollagenscaffolds „OPTIMAIX" - Studie an Göttinger Minipigs.

25-28 September 2013, 65th Kongress der Deutschen Gesellschaft für Urologie e.V, Dresden, Leonhäuser, D., Strick, K., Seifarth, V., Huppertz, N., Fera, C., Gaisa, N., Heschel, I., Woitok, A., Zraik, I., He, Y., Tolba, R., (Temiz) Artmann, A., Grosse, J.: Vergleich zweier biodegradierbarer Kollagenscaffolds „OPTIMAIX" als möglicher Blasenwandersatz im Göttinger Minipig Modell.

3-4 April 2014, 60th Kongress der Nordrhein-Westfälischen Gesellschaft für Urologie, Düsseldorf, Seifarth, V., Zang, W., Artmann, G.M., (Temiz) Artmann, A., Grosse, J.: Ein automatisiertes Bioreaktorsystem zur Kultivierung von tubulären Strukturen. (Posterprice)

Eidesstattliche Erklärung

Hiermit versichere ich, die vorliegende Arbeit mit dem Titel
„Ureteral Tissue Engineering: Development of a Bioreactor System and subsequent characterization of the generated Biohybrids“
selbst verfasst und keine außer den angegebenen Hilfsmitteln und Quellen verwendet zu haben.
Zudem erkläre ich, dass ich die Arbeit in dieser oder einer ähnlichen Form bei keiner anderen Fakultät eingereicht habe.

Köln, den 06.10.2014

Volker Seifarth

Acknowledgement

First of all, I would like to thank Mr Epple, Mr Artmann and Mrs Artmann, who made this thesis possible. I am very thankful for the opportunity to work in your labs for Inorganic Chemistry, Medical & Molecular Biology and Cellbiophysics. I thank you both for the constructive support and discussions during the experimental phase. It was a pleasure for me to present achieved results on congresses and seminars. The atmosphere in the group was really great and I appreciated your engagement.

Thank goes to Mrs Loza for the great support at the scanning electron microscopy.

I would like to thank all people in the lab that supported me. For that reason I would like to thank Mrs Föckler, Mr Porst, Mr Linder, Mr Kayser and all other colleagues in Jülich. Especially, I would like to thank Mr Gossmann working and living with me for several weeks in Essen.

The great support from Mr Jockenhövel's working group was very important for this thesis. I thank you and your group for the support with further suggestions.

Special thank goes to Mr Grosse, who supported this thesis with material and know how. I really appreciate your commitment.

Moreover, I would like to thank Mr and Mrs Meinberger for the great support during my education and this thesis.

Thank goes to family Fichert for help and support in any case even if it was not always related to this thesis.

Additionally, I would like to thank my parents.

Special thank goes to my wife. I thank you for the great support during this thesis and my studies.

In the end, my thank goes to all people that took part in this study, who supported me and who were not mentioned.